

Cover Page



Universiteit Leiden



The handle <http://hdl.handle.net/1887/23252> holds various files of this Leiden University dissertation.

Author: Bijkerk, Roel

Title: MicroRNAs in kidney health and disease

Issue Date: 2014-01-29

MicroRNAs in Kidney Health and Disease

Roel Bijkerk

MicroRNAs in Kidney Health and Disease
© Roel Bijkerk, 2013

All rights are reserved. No part of this publication may be reproduced, stored, or transmitted in any form or by any means, without permission of the copyright owners.

ISBN: 978-90-8891-794-3

Cover: Adapted from “white matter fibers, brainstem and above” from the Human Connectome Project of the Laboratory of Neuro Imaging, UCLA (www.humanconnectomeproject.org).

Layout: Roel Bijkerk

Printed by: Proefschriftmaken.nl || Uitgeverij BOXpress

Published by: Uitgeverij BOXpress, 's Hertogenbosch

The research presented in this thesis was performed at the Department of Nephrology of the Leiden University Medical Center, the Netherlands, and at the Renal Division of the Brigham and Women’s Hospital, Harvard Medical School, Boston, USA.

MicroRNAs in Kidney Health and Disease

Proefschrift

ter verkrijging van
de graad van doctor aan de Universiteit Leiden,
op gezag van de Rector Magnificus Prof. mr. C.J.J.M. Stolker,
volgens besluit van het College voor Promoties
te verdedigen op woensdag 29 januari 2014
klokke 15.00 uur

door

Roel Bijkerk
geboren te Maassluis
in 1983

Promotiecommissie

Promotores	Prof. Dr. A.J. van Zonneveld Prof. Dr. A.J. Rabelink
Overige leden	Prof. Dr. P.M.T. Deen <i>Radboud University Nijmegen Medical Centre, Nijmegen, the Netherlands</i> Prof. Dr. M.J. Goumans Prof. Dr. R.A. Bank <i>University of Groningen, Groningen, the Netherlands</i> Prof. Dr. P.H. Reitsma Prof. Dr. C. van Kooten

The research described in this thesis was supported by a grant from the Dutch Kidney Foundation (C07.2227) and a grant from the Dutch Heart Foundation (2006B145).

Financial support by the Dutch Kidney Foundation and the Dutch Heart Foundation for the publication of this thesis is gratefully acknowledged.

Publication of this thesis was further supported by Astellas Pharma B.V., Amgen B.V., Life Technologies, Roche Nederland B.V. and sanofi-aventis Netherlands B.V.

“Y’a pas d’lapin dans mon chapeau”
Gilbert Becaud

Contents

Chapter 1	General introduction	9
Chapter 2	MicroRNA-155 functions as a negative regulator of RhoA signaling in TGF- β -induced endothelial to mesenchymal transition <i>MicroRNA 2012, 1: 2-10.</i>	29
Chapter 3	MicroRNA-126 modulates endothelial SDF-1 expression and mobilization of Sca-1+/Lin- progenitor cells in ischemia <i>Cardiovasc Res. 2011, 92(3):449-55.</i>	49
Chapter 4	Hematopoietic microRNA-126 protects against renal ischemia/reperfusion injury by promoting vascular integrity <i>J Am Soc Nephrol, in press</i>	69
Chapter 5	Silencing of Pericyte MicroRNA-132 Reduces Renal Fibrosis and Myofibroblast Proliferation and is Associated with Altered Sirt1 and Cox2 Expression <i>In Preparation</i>	103
Chapter 6	MicroRNA-132 regulates diuresis through vasopressin- and prostaglandin-dependent alteration of Aquaporin-2 localization <i>In Preparation</i>	127
Chapter 7	General Discussion	151
Chapter 8	Summary	163
Chapter 9	Nederlandse samenvatting Curriculum Vitae Dankwoord List of publications	169

Chapter

1

General introduction

Introduction

Kidney disease is a common disorder that affects around 60.000 people in the Netherlands only (in 2011)¹. In the US, up to 10% of the population is affected and this number is rising². In the Netherlands, 15.985 people are dependent on renal replacement therapy, involving either dialysis or, ideally, kidney transplantation. In 2011, 9663 people were living with a kidney transplant while 6322 people were on dialysis, of which 989 undergo peritoneal dialysis and 5333 hemodialysis. Every year, 20% of people that are on dialysis die from complications¹, of which cardiovascular disease is the leading cause of death in patients with chronic kidney disease³. In 2011, 855 kidney transplantations were performed, of which 436 donor kidneys were derived from living donors and 419 kidneys *post mortem*. The number of people that are on the waiting list for a transplant kidney is 883 and the average waiting time for receiving a donor kidney (*post mortem*) is 4 years¹. These numbers indicate the severity of problems caused and number of people affected by kidney disease. It is therefore highly relevant to understand the biological mechanisms that are involved in kidney pathophysiology. This thesis covers several aspects of kidney (dys)function, and in particular its regulation by microRNAs.

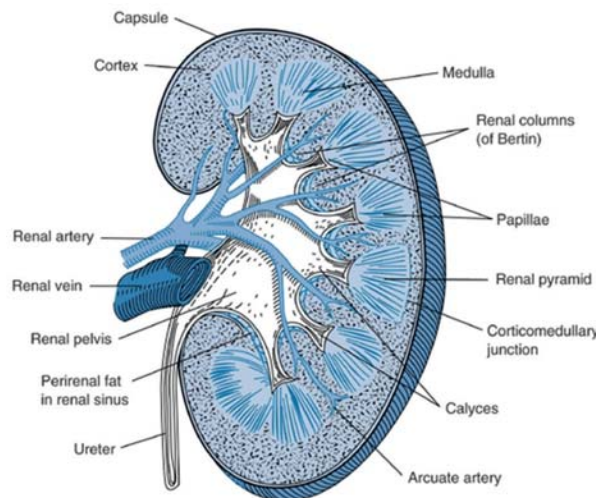


Figure 1. Schematic illustration of a kidney with important anatomic structures highlighted. From: Brenner, B.M. Brenner & Rector's *The Kidney*, Elsevier (2004).

The Kidney

Kidneys are retroperitoneal organs situated in the posterior part of the abdomen on each side of the vertebral column. The right kidney is usually positioned slightly more caudal. In an adult human, the weight of a kidney ranges from 115 to 170 grams and is 11-12 cm. long, 5 to 7.5 cm wide and 2.5 to 3 cm thick. Located on the medial surface is a hilus, through which the renal artery and vein, the lymphatics and a nerve plexus enter the kidney.



The parenchyma consists of the tubular system, the interstitium and the vasculature and can be divided into cortex (outer region) and medulla (inner region) (Figure 1). In humans, the medulla is divided into 8 to 18 striated conical masses, the renal pyramids. In contrast to humans, mice only have one renal pyramid. The base of each pyramid lies on the corticomedullary

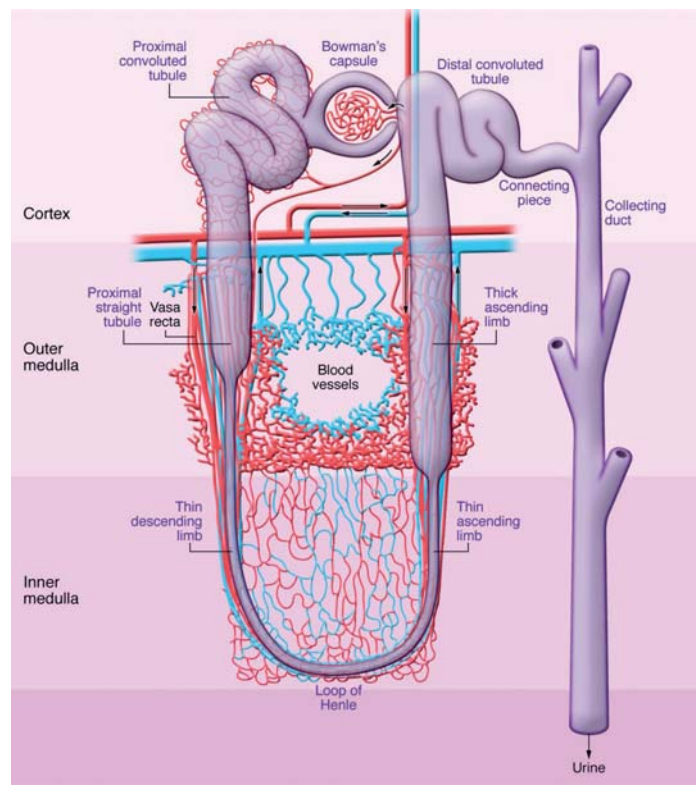


Figure 2. Schematic illustration of a nephron. Adapted from: *cellular pathophysiology of ischemic acute kidney injury*, JV Bonventre and L Yang, *J Clin Invest*, 2011.

boundary and the tip extend towards the renal pelvis, forming a papilla. On the tip of a papilla 10 to 25 small openings can be found that are the ends of the collecting ducts. The cortex is around 1 cm thick and forms a cap over the base of the renal pyramids. At the tips of the pyramids, urine is formed and flows through the ureter to the bladder⁴.

The functional unit of the kidney is the nephron⁵ (Figure 2). The human kidney contains about 0.4 to 1.2×10^6 nephrons^{6,7}. Their main function is to regulate the concentration of water and preservation of soluble substances like sodium by filtering the blood, reabsorbing essential metabolites and excreting the rest as urine. A nephron eliminates waste products from the body, regulates blood pressure, controls levels of electrolytes and metabolites, and regulates blood pH. Its functions are partly regulated by the endocrine system by different hormones while the kidney itself also produces hormones. The nephron consists of the renal corpuscle (glomerulus and Bowman's capsule, Figure 3) connected to the renal tubular system and ending in the collecting duct. In the glomerulus, ultrafiltration takes place. The filtration barrier between the blood and urinary space is composed of a fenestrated endothelium, glomerular basement membrane and the slit pores between the foot processes of the podocytes. In the center of the capillary tuft lies the mesangium, which consists of mesangial cells and extracellular matrix and forms the structural basis of the capillary tuft. Filtration is dependent on blood pressure and velocity, physical-chemical characteristics of compounds in the blood and permeability of the capillary wall. Blood enters the glomerulus through the afferent arteriole while it is leaving via the efferent arteriole. The dynamic interplay between these arterioles forms the basis of the autoregulation of the kidney in a specialized region called the juxtaglomerular apparatus (Figure 3).

This apparatus consists of juxtaglomerular cells, macula densa and extraglomerular mesangial cells⁸. The juxtaglomerular cells (specialized smooth muscle like cells) are situated in the afferent arteriole, right beneath the endothelial cells, and contain the hormone renin^{9,10}. The macula densa consists of epithelial cells from the cortical part of the thick ascending limb. The extraglomerular mesangial cells (or Goormaghtigh or lacis cells⁹) fill up the space between afferent and efferent arteriole and the macula densa¹¹. The relation between these cells, all belonging to the same nephron, is crucial to regulation of the blood volume¹². If the glomerular filtration rate decreases, salt levels in the tubules are lowered. This is registered by the macula densa which stimulates renin secretion by the juxtaglomerular apparatus¹³. Renin activates the renin-angiotensin-aldosterone system (RAAS; Figure 4) that regulates and maintains blood pressure and volume. In addition, the cells of the macula densa sense changes in luminal salt concentrations¹⁴. This initiates the tubuloglomerular feedback response that results in constriction or dilation of the afferent arteriole, thereby controlling the glomerular filtration rate. Secretion of renin is also induced by pressure changes and

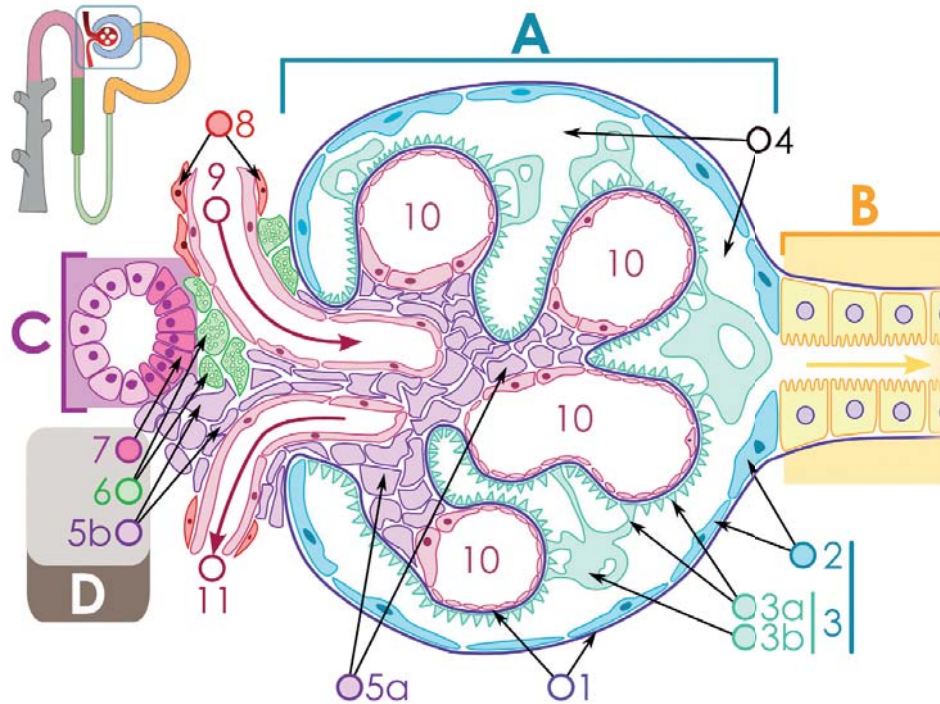


Figure 3. Schematic illustration of the renal corpuscle. *Adapted from: Medical Illustrations, Michal Komorniczak (Poland).*

- | | |
|--------------------------------------|---|
| A – Renal corpuscle | 4. Bowman's space (urinary space) |
| B – Proximal tubule | 5a. Mesangium – Intraglomerular cell |
| C – Distal convoluted tubule | 5b. Mesangium – Extraglomerular cell |
| D – Juxtaglomerular apparatus | 6. Granular cells (Juxtaglomerular cells) |
| 1. Basement membrane (Basal lamina) | 7. Macula densa |
| 2. Bowman's capsule – parietal layer | 8. Myocytes (smooth muscle) |
| 3. Bowman's capsule – visceral layer | 9. Afferent arteriole |
| 3a. Podocyte foot processes | 10. Glomerular capillaries |
| 3b. Podocyte | 11. Efferent arteriole |

under the influence of the sympathetic nerve system and renal prostaglandin production¹³.

In the urinary pole of the glomerulus, the tubular system starts, that extends from the cortex to the medulla and back to the same glomerulus (juxtaglomerular apparatus). In the tubules, water and other solutes are reabsorbed from the ultrafiltrate (pre-urine) into the peritubular capillaries, while some other compounds from these capillaries are secreted into this pre-urine.

The proximal tubule can be divided into an initial convoluted portion (pars convoluta) and a straight part (pars recta). Approximately half of the filtered

salt and water and organic solutes (primarily glucose and amino acids) is reabsorbed here⁴. Fluid reabsorption is coupled to active transport of Na⁺, and little changes occur in the osmolality or Na⁺ concentration of the tubular fluid, indicating that fluid reabsorption is almost iso-osmotic¹⁵.

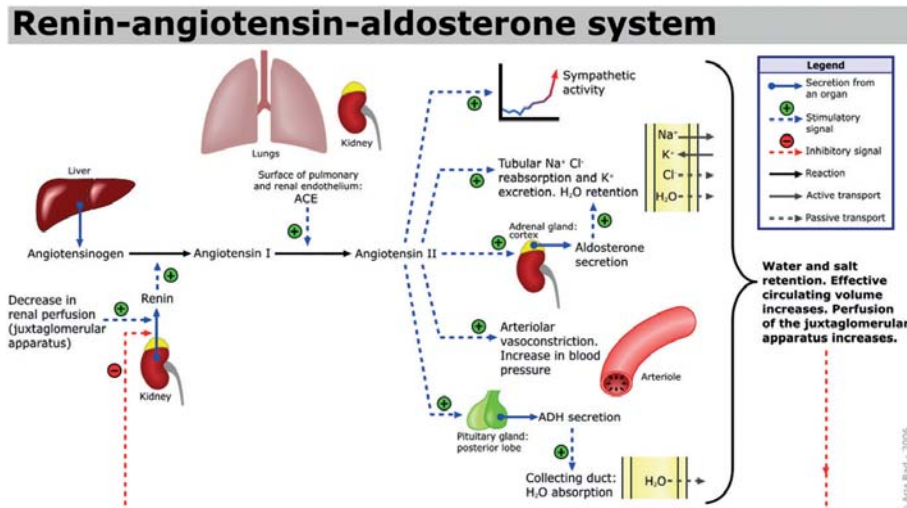


Figure 4. Schematic representation of renin-angiotensin-aldosterone-system.

The loop of Henle is a U-shaped tube that extends from the proximal tubule. It consists of a descending limb and ascending limb. The thin limbs of Henle play an important role in the countercurrent multiplication process that is responsible for the maintenance of a hypertonic medullary interstitium and for the dilution and concentration of the urine^{16,17}. The thin descending limb is permeable to water but has low permeability to salts¹⁸. As the filtrate descends deeper into the hypertonic interstitium of the renal medulla, water is extracted from the tubule fluid by osmosis. Unlike the descending limb, the thin ascending limb is largely impermeable to water, but highly permeable to salts, which causes salts to diffuse out of the tubule.

The loop of Henle is supplied by blood in a series of straight capillaries descending from the cortical efferent arterioles¹⁹. These capillaries (the vasa recta) are highly permeable to water and solutes and easily take up the water and salts that were resorbed by the thin limbs. Due to this, the osmolality of the vasa recta is almost equal to that of the medullary interstitium. Therefore it is essential that the vasa recta has a hairpin turn in the medulla and leaves the medulla at the cortical side. If it would leave at the papillary side, they would wash out the osmotic gradient²⁰.

The hypotonic filtrate is then passed to the distal tubule that comprises the



thick ascending limb, macula densa and distal convoluted tubule. Cells lining the distal tubule have numerous mitochondria to produce energy (ATP) to accommodate active transport, that mainly involves reabsorption of sodium and chloride^{21,22}.

The distal convoluted tubule delivers its filtrate to the collecting duct. The collecting duct system begins in the renal cortex and extends deep into the medulla to end in the tip of the papilla. The epithelium of the collecting duct is relatively impermeable to water in the absence of antidiuretic hormone (ADH or vasopressin). In the presence of ADH, all segments of the collecting duct become water permeable²³. ADH affects the localization of the water channel aquaporin-2²⁴, resulting in the reabsorption of water molecules, while preventing the passage of ions and other solutes. Increased ADH is an indication of dehydration, while sufficient water results in low ADH allowing for diluted urine.

Finally, after passing through the collecting ducts, the urine empties into the urinary bladder via the ureter.

Evolution

The evolution of the nephron is very illustrative for its function and starts with the first invertebrates that lived in salt water. They were iso-osmotic with their environment, in other words, their body fluids have the same salt content, and hence the same osmotic pressure, as the sea water in which they live. Therefore they could easily take up fluid from the sea without compromising their internal milieu. Excretion of waste products was an easy process, as it was removed from the extracellular fluid through simple channels in their skin. When the early vertebrates moved to fresh water, it was necessary to include a water impermeable layer in these channels to prevent dilution by the hypo-osmotic environment. This is where the glomerulus developed, resulting in the ability to filter the excess fluid from the blood that was taken up. In addition, it became essential to retain salts in this fresh water environment. To that end a proximal tubule developed, that could reabsorb salt. Since this tubule is water permeable, this provides a system that could reabsorb fluid in an iso-osmotic manner. However, to be able to produce diluted hypotonic urine, the distal tubule was formed, where salt could be reabsorbed, without the reabsorption of water. This way the fish could excrete its excess water while not losing salts. Millions of years later the vertebrates moved to land. In this environment, conservation of salts was still essential, but the removal of excess fluid became less relevant. On the contrary, the necessity to retain fluid emerged. Since the large glomeruli of fish filtered large amounts of salt and water, and the proximal tubules

were limited to iso-osmotic reabsorption, this was not possible. Therefore glomeruli developed with a smaller capillary tuft to decrease the amount of filtrate. In addition, mechanisms evolved in the tubules that could secrete waste products without the necessity of large amounts of filtrate. Finally, in mammals, a system developed that made concentration of urine possible, the so-called countercurrent exchange. The mammalian nephron contains a loop of Henle, that enables mammals to produce urine that is more concentrated than blood. The longer the loop of Henle, the more concentrated the urine can be^{20,25}.

Nephrogenesis

Mammalian kidney development proceeds through three stages, the pronephros, the mesonephros and the metanephros, that are roughly characterized by mesenchymal-to-epithelial transition of intermediate mesoderm cells^{26,27}. The pronephros arises in the cervical region of the embryo at day 22 of gestation and consists of a few tubular structures that are joined with the pronephric duct^{28,29}. Glomerular structures (glomerula) are also seen, but they are not connected to tubules yet, making it a nonintegrated nephron³⁰. The pronephric duct then extends caudally and degenerates rostrally with the associated pronephric kidney. At day 24 of gestation, the ductal tissue (named Wolffian duct from this point) and its surroundings in the intermediate mesoderm have migrated caudally and now forms the mesonephros. The mesonephric kidney includes about 30 tubules connected to the wolffian duct and their associated glomeruli. The origin of the renal vasculature in glomerulogenesis is uncertain. It has been described to be derived from resident endothelial cells³¹, as well as derived *de novo*³². In other words, it can be the result of angiogenesis or vasculogenesis respectively. Vasculogenesis refers to the *de novo* differentiation and association of cells into blood vessels, when there is no pre-existing capillary network. Angiogenesis involves the formation of new capillaries by sprouting, growth and remodeling of endothelial cells from a pre-existing vascular network^{33,34}. On day 28 of gestation, an outpouching of the wolffian duct develops, the ureteric bud that extends into the caudal region of the intermediate mesoderm (metanephric mesenchyme, Figure 5A). After invading this mesenchymal tissue, the ureteric bud induces the mesenchymal cells that surround it to condense to form a cap³⁵ (Figure 5B). The stroma develops around this mesenchyme and also in between the ureteric branches. This condensate then induces the ureteric bud to branch (Figure 5C) as those branches will eventually form the collecting-duct system. The condensate also forms pretubular aggregates that undergo a mesenchymal-to-epithelial transition and proliferate to form an epithelial

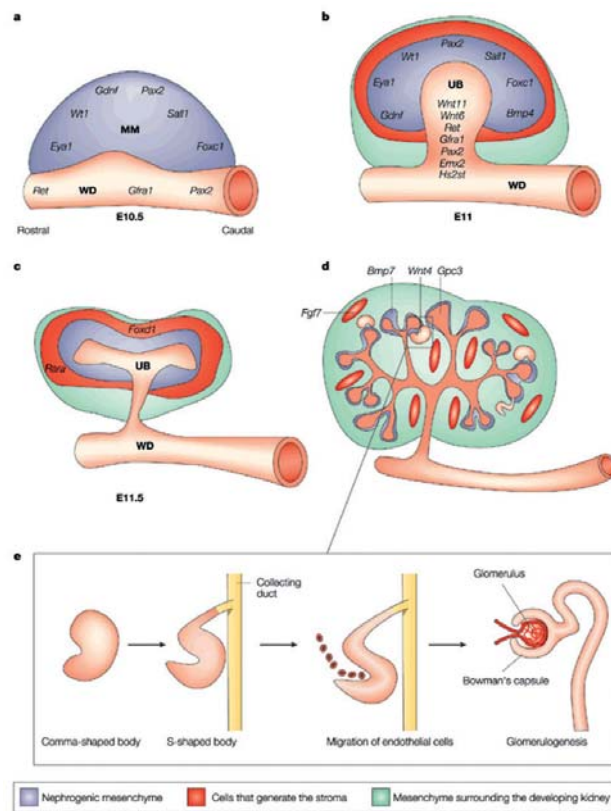


Figure 5. Morphological stages of early kidney development and some of the genes involved in its development.

(A), the kidney starts to develop when the ureteric bud forms at the caudal end of the Wolffian duct (WD). The ureteric bud grows into the metanephric mesenchyme (MM) and (B), induces the mesenchyme that is adjacent to the tips of the ureteric bud (UB) to condense and form the stromal mesenchymal zone. (C), the condensed mesenchyme induces the ureteric bud to branch. (D), in association with ureteric branching morphogenesis, mesenchymal cells are induced in each epithelial-tip region and undergo a mesenchymal-to-epithelial transformation to form the functional unit of the kidney, the nephron. (E), the nephron forms through comma- and S-shaped stages of development. The S-shaped body fuses to a branch of the ureteric tree, which goes on to join the collecting-duct system. Endothelial cells migrate into the assembling nephron to form the glomerulus. *Bmp7*, bone morphogenetic protein 7; *Emx2*, empty spiracles 2; *Eya1*, *Eya1*, eyes absent 1; *Fgf7*, fibroblast growth factor 7; *Foxc1*, forkhead box C1; *Foxd1*, forkhead box D1; *Gdnf1*, glial cell-line-derived neurotrophic factor 1; *Gfra1*, glial cell-linederived neurotrophic factor receptor- α 1; *Gpc3*, glypican-3; *Hs2st*, heparan sulfate 2-O- sulphotransferase 1; *Pax1*, paired-box gene 1; *Rara*, retinoic acid receptor- α ; *Ret*, Ret proto-oncogene; *Sall1*, sal-like 1; *Wnt*, Wingless-related; *Wt1*, Wilms tumour 1. Adapted from: *coordinating early kidney development: lessons from gene targeting*, S. Vaino and Y. Lin, *Nature Review Genetics*, 2002.

tubule that is destined to form the nephron (Figure 5D-E). First, a tubule develops into a comma-shaped body, which then develops into an S-shaped body. The part of the S-shaped body closest to the ureteric bud becomes the distal tubule and fuses with the ureteric bud. The portion of the S-shaped body most distant from the ureteric bud folds and the outer cells become the Bowman capsule while the inner cells give rise to the podocytes. The middle part of the S-shaped body give rise to the proximal tubule and loop of Henle (Figure 5E)³⁶. Figure 5 schematically illustrates nephrogenesis and depicts some of the genes involved.

It has become evident that the basis of eukaryotic complexity is a genetic landscape where parallel systems are involved in fine-tuning gene expression, via RNA-DNA, RNA-RNA, RNA-protein, and DNA-protein interactions. In higher organisms, about 97% of the transcriptional output consists of noncoding RNA (ncRNA) encompassing not only rRNA, tRNA, introns, 5' and 3' untranslated regions, transposable elements, and intergenic regions, but also long-noncoding RNAs (lnc-RNA) and microRNAs (miRNA)³⁷. Gene regulation at the post-transcriptional level by lnc-RNA and miRNA, but also alternative splicing, is increasingly recognized to be of vital importance to (molecular) cell biology and physiology. In this thesis we focused on the role of miRNAs in kidney pathophysiology.

MicroRNAs

MiRNAs are a family of small ~21 nucleotide long non-coding RNAs that regulate gene expression posttranscriptionally in a sequence-specific way³⁸.

Biogenesis

MiRNAs are derived from precursor molecules (pri-miRNAs) that are transcribed from independent genes by RNA polymerase II (canonical processing) or originating from introns of protein coding genes (mirtrons)^{39,40}. Canonical pri-miRNAs are then processed in two steps, catalysed by two RNase III family members with specific dsRNA endonuclease activity, Drosha⁴¹ and Dicer⁴². The first step, taking place in the nucleus, involves processing the pri-miRNA into a ~70 nucleotide hairpin structure (pre-miRNA) by a Drosha-DGCR8 complex⁴¹, where DGCR8 is a dsRNA binding protein (dsRBP). This pre-miRNA is then transported to the cytoplasm by exportin5, a Ran-GTP dependent cargo transporter⁴³. Mirtron pri-miRNAs are a result of splicing and debranching and bypass the Drosha mediated processing step⁴⁴. Pre-miRNAs are then cleaved by Dicer that yields a miRNA/miRNA* duplex⁴².

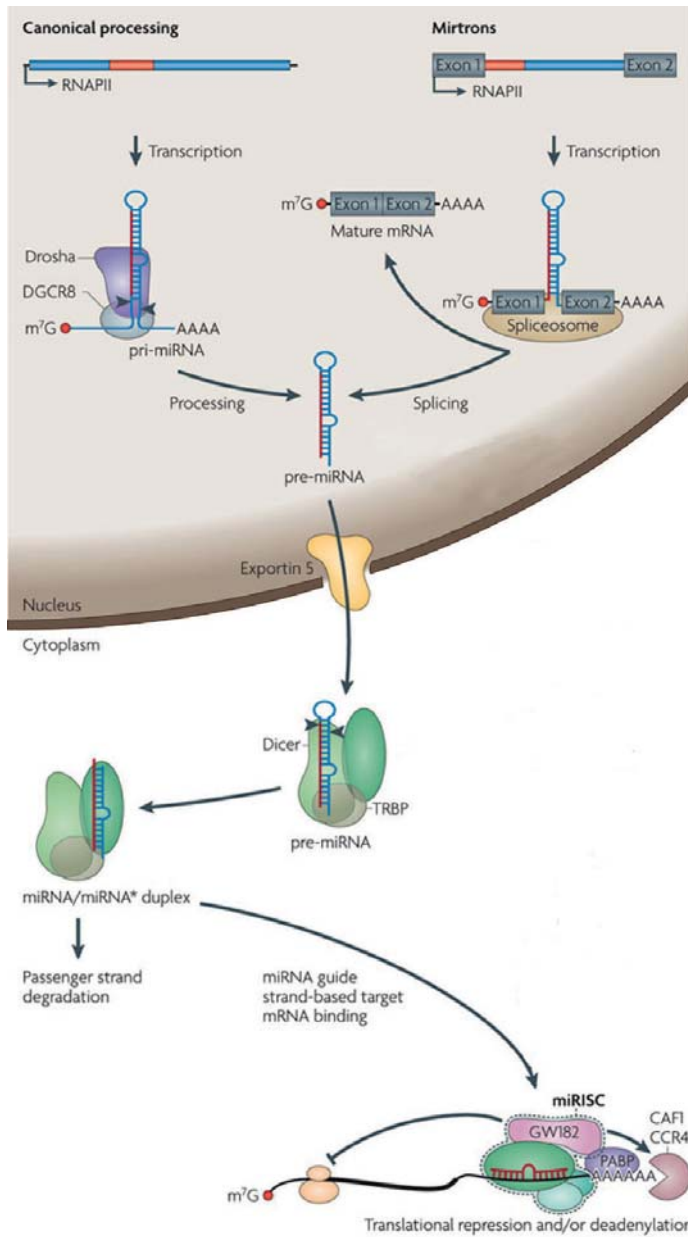


Figure 6. MicroRNA biogenesis.

MicroRNAs (miRNAs) are processed from RNA polymerase II (RNAPII)-specific transcripts of independent genes (canonical processing) or from introns of protein-coding genes (mirtrons). In the canonical pathway, primary precursor (pri-miRNA) processing occurs in two steps, catalysed by two members of the RNase III family of enzymes, Drosha and Dicer, in co-operation with dsRNA-binding protein DGCR8. In the first nuclear step, the Drosha–DGCR8 complex processes pri-miRNA into an ~70-nucleotide precursor hairpin (pre-miRNA), which is exported to the cytoplasm by exportin 5. Pre-miRNAs that originate from very short introns (mirtrons) as a result of splicing and debranching will thereby bypass the Drosha–DGCR8 step. In both cases, cleavage by Dicer in the cytoplasm, assisted by transactivation-responsive (TAR) RNA-binding protein (TRBP), yields a ~20-bp

miRNA/miRNA* duplex. One strand of the miRNA/miRNA* duplex (the guide strand) is preferentially incorporated into a RNA-induced silencing complex (RISC), whereas the other strand (passenger or miRNA*) is released and mostly degraded. Generally, the retained strand is the one that has the less stably base-paired 5' end in the miRNA/miRNA* duplex. GW182, glycine-tryptophan protein of 182 kDa; m7G, 7-methylguanosine-cap; PABP, poly(A) binding protein. *Adapted from: The widespread regulation of microRNA biogenesis, function and decay, Krol et al, Nature Review Genetics, 2010.*

One strand of this duplex (the guide strand) is preferentially incorporated into a RNA induced silencing complex (RISC) and is the mature miRNA. Key components of the RISC are argonaute (AGO) proteins, which directly interact with miRNAs⁴⁵, and glycine-tryptophan protein of 182 kDa (GW182) proteins, which act as downstream effectors in the repression⁴⁶. In general the strand that is preferentially incorporated is the strand with the less stable 5' end as compared to the miRNA* strand. The selective assembly of the mature miRNA into the RISC is thought to reflect the relative ease of unwinding from one end of the miRNA/miRNA* duplex^{47,48}. The passenger strand is mostly degraded, although functional incorporation of passenger strands into RISCs has been reported⁴⁹. The mature miRNAs that are then loaded in the RISC imperfectly base-pair with mostly the 3'UTR of a target gene, thereby affecting protein synthesis. In this base-pairing, it is essential that miRNA nucleotides 2-8 (the seed sequence) are complementary to its target mRNA sequence^{50,51}. Figure 6 schematically illustrates miRNA biogenesis⁵².

Mode of action

Although some reports describe translational activation by miRNAs^{53,54}, virtually all miRNAs are considered to act as inhibitors of protein synthesis. This synthesis is inhibited either by translation inhibition or promoting mRNA decay. Translation inhibition was the explanation that dominated the field the first years after the discovery of miRNAs. However, more and more evidence is emerging that most inhibition of protein synthesis by miRNAs is due to mRNA destabilization. For example, using quantitative mass spectrometry and microarrays, it was determined that although some targets were repressed without detectable changes in mRNA levels, those that were more highly translationally repressed displayed detectable mRNA destabilization and often this was the major component of repression. In addition, they showed that an individual microRNA could directly repress hundreds of genes, albeit to a modest degree making microRNAs fine-tuners of protein output^{55,56}. Another investigation measured mRNA abundance (using microarrays) and translation rate for approximately 8,000 genes after transfection of a microRNA. They found that changes in translation were detectable, but the reduction in mRNA abundance closely matched the reduction in protein level⁵⁷. The most elegant investigation involved ribosome profiling to measure the overall effects of miRNA modulation on protein production and this was compared to simultaneously measured effects on mRNA abundance. For miRNA regulatory interactions, a decrease in mRNA levels accounts for around 84% of the decreased protein production⁵⁸. These results suggest that destabilization of target mRNAs is the predominant reason



for reduced protein output by miRNAs. However, the exact mechanism(s) by which microRNAs exert their function are not well understood⁵⁹. Several mechanisms have been described but the results from studies conducted in different systems have often been contradictory. The discrepancies could be due to technical issues or miRNAs indeed are able to function through several distinct mechanisms⁶⁰. It has been shown though that the miRNA effect starts with translation inhibition at an early step, probably at translation initiation, which is followed by deadenylation of target mRNAs ultimately leading to the decay of mRNAs⁶¹.

microRNAs in the kidney

MicroRNAs are central players in regulatory mechanisms to modulate fundamental cellular processes such as differentiation, proliferation, metabolism, and pathophysiology of many diseases⁶². It has become apparent that miRNAs form an essential part of renal development, maintenance of renal function, and progression of kidney diseases.

The involvement of miRNAs in renal development begins early by its regulation of the nephron progenitors. It has been shown that ablation of Dicer function within these nephron progenitors and the ureteric bud-derived collecting duct system led to an increase in apoptosis and premature termination of nephrogenesis, which ultimately resulted in development of renal cysts⁶³. Dicer, which is central to miRNA function, is thus critical for normal development of the nephrons.

Furthermore, the loss of miRNAs by podocyte-specific knockout of Dicer caused proteinuria soon after birth. This was followed by progression of glomerular and tubular injury and finally resulted in death due to renal failure⁶⁴. This blocking of miRNA function by Dicer ablation resulted in multiple abnormalities in the glomerulus such as podocyte foot process effacement, podocyte apoptosis and depletion, mesangial expansion, capillary dilation, and glomerulosclerosis⁶⁵. Another study specifically deleted Droscha in podocytes, which resulted in proteinuria and collapsing glomerulopathy⁶⁶. In renal disease, several miRNAs have been identified to play an important role. In diabetic nephropathy for instance, which occurs in half of the patients with Diabetes Mellitus type II and is the most significant cause of end stage renal failure⁶⁷, miR-192 function has been shown to be strongly associated with the development of diabetic nephropathy. This is due to the involvement of miR-192 in TGF- β signaling^{68,69}, where decrease in miR-192 levels is directly correlated with tubulointerstitial fibrosis and a low glomerular filtration rate in diabetic individuals⁷⁰. Glomerular and interstitial

fibrosis are the key morphological features of progressive renal disease and are directly related to the development of renal failure⁷¹. Tubulo-interstitial fibrosis involves the recruitment of inflammatory cells, tubular cell loss and the excessive accumulation of myofibroblasts that produce ECM proteins such as fibronectin and collagens, generate high levels of filamentous actin (F-actin) for the formation of stress fibers and acquire a contractile phenotype facilitated by the expression of α -smooth muscle actin (α -SMA).

The miR-200 family provides another example of regulation through its involvement is in renal fibrosis⁷². Loss of expression of miRNAs from this family results in repression of E-cadherin, thereby inducing a profibrotic phenotype of epithelial cells⁷³.

Several additional miRNAs have been identified to play a role in kidney functioning but this knowledge is far from complete. Since miRNAs are recognized as key players of biological processes, this asks for a more detailed understanding of the role of specific miRNAs in kidney health and disease that may ultimately lead to new therapeutic developments.

Scope of thesis

In this thesis we have studied the role of a selection of miRNAs in different (patho-) physiological processes that are essential to our understanding of kidney homeostasis and disease progression.

In **Chapter 2** we describe a role for miR-155 in the process of endothelial to mesenchymal transition (EndoMT). EndoMT has been proposed to be involved in the loss of microvascular capillaries in the pathophysiology of fibrosis and organ failure^{74,75}. In EndoMT, endothelial cells (EC) undergo a mesenchymal transition associated with the dissolution of endothelial tight junctions, reorganization of the cytoskeleton, acquisition of invasive and migratory properties and the production and deposition of extracellular matrix⁷⁶. We show that miR-155 functions as a negative regulator of RhoA signaling in TGF- β -induced EndoMT.

In **Chapters 3 and 4** we focused on Ischemia/reperfusion injury (IRI), which is a central event in clinical conditions such as acute kidney injury and organ transplantation. Emerging evidence suggests that the renal microvascular endothelium of the peritubular network is the primary site of injury in the pathogenesis of ischemia induced renal dysfunction⁷⁷. In addition, microvascular destabilization initiated by the loss of EC-EC interactions and EC-pericyte interactions can lead to significant reductions in peritubular capillary density due to microvascular rarefaction^{78,79}. The resulting loss in



renal perfusion can further exacerbate medullary ischemia and drive the development of interstitial fibrosis by stimulation of pro-fibrinogenic factors such as transforming growth factor- β ⁸⁰. As a consequence, integrity of the peritubular capillary network is also a key determinant for the preservation of renal function. **Chapter 3** focuses on the potential role of miR-126 in the mobilization of vasculogenic progenitor cells upon ischemia by modulating SDF-1 expression. Chapter 3 was focused on the effect of antagonizing miR-126 systemically. In **Chapter 4** however, we overexpressed miR-126 in the hematopoietic compartment and demonstrate that this provides protection against renal ischemia reperfusion injury by promoting vascular integrity.

Chapter 5 details our finding that miR-132 plays an important role in renal fibrosis. Lineage analysis of kidney stroma showed that pericytes, that are known to cover and support capillary walls, are the major source of myofibroblasts⁸¹. We identified miR-132 expression to be increased in these cells in fibrotic kidneys. Silencing miR-132 results in decreased pericyte dedifferentiation and proliferation towards myofibroblasts. In **Chapter 6** another role for miR-132 is discussed. During our experiments described in **Chapter 5** we observed acute weight loss in mice that received antagomir-132. We therefore hypothesized that miR-132 plays a role in water reabsorption. In **Chapter 6** we demonstrate that miR-132 regulates diuresis by altering Aquaporin-2 localization in collecting ducts, which is responsible for the reabsorption of water.

Finally, **Chapters 7-9** provide a general summary of the research presented in this thesis and further discusses the role of miRNAs in kidney health and disease.

References

1. Nierstichting. www.nierstichting.nl. (2011).
2. www.usrds.org. United States Renal Data System.
3. Tonelli, M., et al. Chronic kidney disease and mortality risk: a systematic review. *Journal of the American Society of Nephrology : JASN* 17, 2034-2047 (2006).
4. Brenner, B.M. Brenner & Rector's *The Kidney*, (2004).
5. Braus, H. *Anatomie des Menschen*. (1924).
6. Nyengaard, J.R. & Bendtsen, T.F. Glomerular number and size in relation to age, kidney weight, and body surface in normal man. *The Anatomical record* 232, 194-201 (1992).
7. Oliver, J. *Nephrons and Kidneys: A Quantitative Study of Development and Evolutionary Mammalian Renal Architectonics*. (1968).
8. Barajas, L. Anatomy of the juxtaglomerular apparatus. *The American journal of physiology* 237, F333-343 (1979).
9. Goormaghtigh, N. Facts in favour of an endocrine function of the renal arterioles. *J Pathol* 57, 392 (1945).
10. Edelman, R. & Hartroft, P.M. Localization of renin in juxtaglomerular cells of rabbit and dog through the use of fluorescent-antibody technique. *Circ Res* 9, 1069 (1961).
11. Taugner, R., Schiller, A., Kaissling, B. & Kriz, W. Gap junctional coupling between the JGA and the glomerular tuft. *Cell and tissue research* 186, 279-285 (1978).
12. Schnermann, J. & Briggs, J. The function of the juxtaglomerular apparatus: Control of glomerular hemodynamics and renin secretion. In Seldin, DW et al. : *The kidney: physiology and pathophysiology*, 2nd ed, p1249., (1992).
13. Schnermann, J. Juxtaglomerular cell complex in the regulation of renal salt excretion. *The American journal of physiology* 274, R263-279 (1998).
14. Schlatter, E., Salomonsson, M., Persson, A.E. & Greger, R. Macula densa cells sense luminal NaCl concentration via furosemide sensitive Na⁺2Cl-K⁺ cotransport. *Pflugers Archiv : European journal of physiology* 414, 286-290 (1989).
15. Burg, M. Renal handling of sodium, chloride, water, amino acids, and glucose. In Brenner BM, Rector FC Jr (eds): *The kidney*, Vol I, 3rd ed. p145., (1986).
16. Knepper, M. & Rector, F.C., Jr. Urinary concentration and dilution. In Brenner, BM, Rector FC Jr. (eds): *The kidney* 4th ed. p445., (1991).
17. Hargitay, B. & Kuhn, W. Das Multiplikationsprinzip als Grundlage der Harnkonzentrierung in der Niere. *Z Elektrochem Angew Phys Chemie* 55, 539-558 (1951).
18. Kokko, J.P. & Rector, F.C., Jr. Countercurrent multiplication system without active transport in inner medulla. *Kidney international* 2, 214-223 (1972).
19. Moffat, D.B. & Fourman, J. The Vascular Pattern of the Rat Kidney. *Journal of anatomy* 97, 543-553 (1963).
20. de Jong, P.E., et al. *Klinische nefrologie*, (2005).
21. Hebert, S.C. & Andreoli, T.E. Control of NaCl transport in the thick ascending limb. *The American journal of physiology* 246, F745-756 (1984).
22. Katz, A.I., Doucet, A. & Morel, F. Na-K-ATPase activity along the rabbit, rat, and mouse nephron. *The American journal of physiology* 237, F114-120 (1979).
23. Woodhall, P.B. & Tisher, C.C. Response of the distal tubule and cortical collecting duct to vasopressin in the rat. *The Journal of clinical investigation* 52, 3095-3108 (1973).



24. Deen, P.M., et al. Requirement of human renal water channel aquaporin-2 for vasopressin-dependent concentration of urine. *Science* 264, 92-95 (1994).
25. Smith, H.W. From fish to philosopher: the story of our internal environment, (1959).
26. Larsen, W. Human embryology, (1997).
27. Saxen, L. Organogenesis of the kidney. (1987).
28. Obara-Ishihara, T., Kuhlman, J., Niswander, L. & Herzlinger, D. The surface ectoderm is essential for nephric duct formation in intermediate mesoderm. *Development* 126, 1103-1108 (1999).
29. Mauch, T.J., Yang, G., Wright, M., Smith, D. & Schoenwolf, G.C. Signals from trunk paraxial mesoderm induce pronephros formation in chick intermediate mesoderm. *Developmental biology* 220, 62-75 (2000).
30. Vize, P.D., Seufert, D.W., Carroll, T.J. & Wallingford, J.B. Model systems for the study of kidney development: use of the pronephros in the analysis of organ induction and patterning. *Developmental biology* 188, 189-204 (1997).
31. Ekblom, P., Sariola, H., Karkinen-Jaaskelainen, M. & Saxen, L. The origin of the glomerular endothelium. *Cell differentiation* 11, 35-39 (1982).
32. Hyink, D.P. & Abrahamson, D.R. Origin of the glomerular vasculature in the developing kidney. *Seminars in nephrology* 15, 300-314 (1995).
33. Yancopoulos, G.D., Klagsbrun, M. & Folkman, J. Vasculogenesis, angiogenesis, and growth factors: ephrins enter the fray at the border. *Cell* 93, 661-664 (1998).
34. Risau, W. Differentiation of endothelium. *FASEB journal : official publication of the Federation of American Societies for Experimental Biology* 9, 926-933 (1995).
35. Sariola, H. Nephron induction revisited: from caps to condensates. *Current opinion in nephrology and hypertension* 11, 17-21 (2002).
36. Vainio, S. & Lin, Y. Coordinating early kidney development: lessons from gene targeting. *Nature reviews. Genetics* 3, 533-543 (2002).
37. Sevignani, C., Calin, G.A., Siracusa, L.D. & Croce, C.M. Mammalian microRNAs: a small world for fine-tuning gene expression. *Mamm Genome* 17, 189-202 (2006).
38. He, L. & Hannon, G.J. MicroRNAs: small RNAs with a big role in gene regulation. *Nature reviews. Genetics* 5, 522-531 (2004).
39. Carthew, R.W. & Sontheimer, E.J. Origins and Mechanisms of miRNAs and siRNAs. *Cell* 136, 642-655 (2009).
40. Kim, V.N., Han, J. & Siomi, M.C. Biogenesis of small RNAs in animals. *Nature reviews. Molecular cell biology* 10, 126-139 (2009).
41. Lee, Y., et al. The nuclear RNase III Drosha initiates microRNA processing. *Nature* 425, 415-419 (2003).
42. Hutvagner, G., et al. A cellular function for the RNA-interference enzyme Dicer in the maturation of the let-7 small temporal RNA. *Science* 293, 834-838 (2001).
43. Lund, E., Guttinger, S., Calado, A., Dahlberg, J.E. & Kutay, U. Nuclear export of microRNA precursors. *Science* 303, 95-98 (2004).
44. Ruby, J.G., Jan, C.H. & Bartel, D.P. Intronic microRNA precursors that bypass Drosha processing. *Nature* 448, 83-86 (2007).
45. Hammond, S.M., Boettcher, S., Caudy, A.A., Kobayashi, R. & Hannon, G.J. Argonaute2, a link between genetic and biochemical analyses of RNAi. *Science* 293, 1146-1150 (2001).
46. Eulalio, A., Huntzinger, E. & Izaurralde, E. GW182 interaction with Argonaute is essential for miRNA-mediated translational repression and mRNA decay. *Nature structural & molecular biology* 15, 346-353 (2008).

47. Schwarz, D.S., et al. Asymmetry in the assembly of the RNAi enzyme complex. *Cell* 115, 199-208 (2003).
48. Khvorova, A., Reynolds, A. & Jayasena, S.D. Functional siRNAs and miRNAs exhibit strand bias. *Cell* 115, 209-216 (2003).
49. Ghildiyal, M., Xu, J., Seitz, H., Weng, Z. & Zamore, P.D. Sorting of *Drosophila* small silencing RNAs partitions microRNA* strands into the RNA interference pathway. *Rna* 16, 43-56 (2010).
50. Doench, J.G. & Sharp, P.A. Specificity of microRNA target selection in translational repression. *Genes & development* 18, 504-511 (2004).
51. Lewis, B.P., Burge, C.B. & Bartel, D.P. Conserved seed pairing, often flanked by adenosines, indicates that thousands of human genes are microRNA targets. *Cell* 120, 15-20 (2005).
52. Krol, J., Loedige, I. & Filipowicz, W. The widespread regulation of microRNA biogenesis, function and decay. *Nature reviews. Genetics* 11, 597-610 (2010).
53. Vasudevan, S., Tong, Y. & Steitz, J.A. Switching from repression to activation: microRNAs can up-regulate translation. *Science* 318, 1931-1934 (2007).
54. Henke, J.I., et al. microRNA-122 stimulates translation of hepatitis C virus RNA. *The EMBO journal* 27, 3300-3310 (2008).
55. Baek, D., et al. The impact of microRNAs on protein output. *Nature* 455, 64-71 (2008).
56. Selbach, M., et al. Widespread changes in protein synthesis induced by microRNAs. *Nature* 455, 58-63 (2008).
57. Hendrickson, D.G., et al. Concordant regulation of translation and mRNA abundance for hundreds of targets of a human microRNA. *PLoS biology* 7, e1000238 (2009).
58. Guo, H., Ingolia, N.T., Weissman, J.S. & Bartel, D.P. Mammalian microRNAs predominantly act to decrease target mRNA levels. *Nature* 466, 835-840 (2010).
59. Fabian, M.R., Sonenberg, N. & Filipowicz, W. Regulation of mRNA translation and stability by microRNAs. *Annual review of biochemistry* 79, 351-379 (2010).
60. Wu, L. & Belasco, J.G. Let me count the ways: mechanisms of gene regulation by miRNAs and siRNAs. *Molecular cell* 29, 1-7 (2008).
61. Djuranovic, S., Nahvi, A. & Green, R. miRNA-mediated gene silencing by translational repression followed by mRNA deadenylation and decay. *Science* 336, 237-240 (2012).
62. Chandrasekaran, K., et al. Role of microRNAs in kidney homeostasis and disease. *Kidney international* 81, 617-627 (2012).
63. Nagalakshmi, V.K., et al. Dicer regulates the development of nephrogenic and ureteric compartments in the mammalian kidney. *Kidney international* 79, 317-330 (2011).
64. Ho, J., et al. Podocyte-specific loss of functional microRNAs leads to rapid glomerular and tubular injury. *Journal of the American Society of Nephrology : JASN* 19, 2069-2075 (2008).
65. Shi, S., et al. Podocyte-selective deletion of dicer induces proteinuria and glomerulosclerosis. *Journal of the American Society of Nephrology : JASN* 19, 2159-2169 (2008).
66. Zhdanova, O., et al. The inducible deletion of Droscha and microRNAs in mature podocytes results in a collapsing glomerulopathy. *Kidney international* 80, 719-730 (2011).
67. Ballard, D.J., et al. Epidemiology of persistent proteinuria in type II diabetes mellitus. Population-based study in Rochester, Minnesota. *Diabetes* 37, 405-412 (1988).
68. Kato, M., et al. MicroRNA-192 in diabetic kidney glomeruli and its function in TGF-beta-induced collagen expression via inhibition of E-box repressors. *Proceedings of the National Academy of Sciences of the United States of America* 104, 3432-3437 (2007).
69. Kato, M., et al. A microRNA circuit mediates transforming growth factor-beta1 autoregulation in renal glomerular mesangial cells. *Kidney international* 80, 358-368 (2011).



70. Krupa, A., et al. Loss of MicroRNA-192 promotes fibrogenesis in diabetic nephropathy. *Journal of the American Society of Nephrology : JASN* 21, 438-447 (2010).
71. Hunter, M.G., Hurwitz, S., Bellamy, C.O. & Duffield, J.S. Quantitative morphometry of lupus nephritis: the significance of collagen, tubular space, and inflammatory infiltrate. *Kidney international* 67, 94-102 (2005).
72. Oba, S., et al. miR-200b precursor can ameliorate renal tubulointerstitial fibrosis. *PloS one* 5, e13614 (2010).
73. Gregory, P.A., et al. The miR-200 family and miR-205 regulate epithelial to mesenchymal transition by targeting ZEB1 and SIP1. *Nature cell biology* 10, 593-601 (2008).
74. Bruneau, S., et al. Key Features of the Intra-graft Microenvironment that Determine Long-Term Survival Following Transplantation. *Front Immunol* 3, 54 (2012).
75. Piera-Velazquez, S., Li, Z. & Jimenez, S.A. Role of endothelial-mesenchymal transition (EndoMT) in the pathogenesis of fibrotic disorders. *The American journal of pathology* 179, 1074-1080 (2011).
76. Goumans, M.J., van Zonneveld, A.J. & ten Dijke, P. Transforming growth factor beta-induced endothelial-to-mesenchymal transition: a switch to cardiac fibrosis? *Trends Cardiovasc Med* 18, 293-298 (2008).
77. Bonventre, J.V. & Yang, L. Cellular pathophysiology of ischemic acute kidney injury. *The Journal of clinical investigation* 121, 4210-4221 (2011).
78. Basile, D.P., Donohoe, D., Roethe, K. & Osborn, J.L. Renal ischemic injury results in permanent damage to peritubular capillaries and influences long-term function. *Am J Physiol Renal Physiol* 281, F887-899 (2001).
79. Fligny, C. & Duffield, J.S. Activation of pericytes: recent insights into kidney fibrosis and microvascular rarefaction. *Curr Opin Rheumatol* 25, 78-86 (2013).
80. Spurgeon, K.R., Donohoe, D.L. & Basile, D.P. Transforming growth factor-beta in acute renal failure: receptor expression, effects on proliferation, cellularity, and vascularization after recovery from injury. *Am J Physiol Renal Physiol* 288, F568-577 (2005).
81. Humphreys, B.D., et al. Fate tracing reveals the pericyte and not epithelial origin of myofibroblasts in kidney fibrosis. *The American journal of pathology* 176, 85-97 (2010).

Chapter

2

MicroRNA 2012, 1: 2-10.

MicroRNA-155 functions as a negative regulator of RhoA signaling in TGF- β -induced endothelial to mesenchymal transition

R. Bijkerk¹, R.G. de Bruin¹, C. van Solingen¹, J.M.G.J. Duijs¹, K. Kobayashi², E.P. van der Veer¹, P. ten Dijke², T.J. Rabelink¹, M.J. Goumans² and A.J. van Zonneveld¹.

¹*Department of Nephrology and the Eindhoven Laboratory for Experimental Vascular Medicine,*
²*Department of Molecular Cell Biology and Centre for Biomedical Genetics, Leiden University Medical Center, Leiden, the Netherlands.*

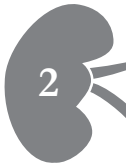
Abstract

Endothelial to mesenchymal transition (EndoMT) has been proposed to be involved in the loss of microvascular capillaries in the pathophysiology of fibrosis and organ failure. In EndoMT, endothelial cells (EC) undergo a mesenchymal transition associated with the loss of cell-cell contacts and the acquisition of a synthetic, contractile phenotype. Here, we sought to identify microRNAs (miRNAs) that could play a central role in regulating EndoMT. In a TGF- β dependent *in vitro* model for EndoMT, we identified miRNAs that were differentially expressed in normoxic and hypoxic conditions. These studies identified miR-155 to be significantly upregulated in EndoMT, an effect that was enhanced under hypoxia, which further augments EndoMT. Silencing of miR-155 directly increased RhoA expression and activity in endothelial cells and affected phosphorylation of downstream LIMK. In contrast, overexpression of miR-155 counteracted RhoA function. Using a selective Rho kinase inhibitor, we could partly suppress EndoMT, strengthening the notion that RhoA plays a central role in EndoMT. Forced overexpression of miR-155 completely suppressed EndoMT, as evidenced by the maintenance of EC characteristics and blocking the acquisition of a mesenchymal phenotype, as compared to control cells. Our data demonstrate that miRNA-155 functions as a negative regulator of RhoA signaling in TGF- β -induced endothelial to mesenchymal transition.

Introduction

Endothelial to mesenchymal transition (EndoMT) is an essential process in embryonic development of the heart valves and involves dedifferentiation of endothelial cells towards a mesenchymal, synthetic phenotype^{1,2}. At the same time, evidence is accumulating that EndoMT can also contribute to the loss of the microvasculature in the adult, limiting the long-term survival of transplanted organs³ and leading to end organ failure in progressive cardiac and renal disease⁴. EndoMT involves the dissolution of endothelial tight junctions, reorganization of the cytoskeleton, acquisition of invasive and migratory properties and the production and deposition of extracellular matrix⁵. These phenotypic features are shared with the pro-fibrotic myofibroblast that drive fibrotic disorders. While myofibroblasts were thought to be derived from resident fibroblasts, epithelial cells or bone marrow-derived cells, evidence is accumulating that EndoMT provides another source of tissue myofibroblasts⁴. A common denominator in chronic diseases associated with the development of cardiac or kidney fibrosis is the reduced bioavailability of nitric oxide (NO)⁶. In mice, long term inhibition of NO synthesis with inhibitors of endothelial nitric oxide synthase (NOS3) leads to induction of TGF- β expression and fibrosis in the kidney and using cell-lineage tracing it was demonstrated that a fraction of the myofibroblasts was derived from endothelial cells (EC)⁷. Likewise, in an experimental model for cardiac fibrosis, it was demonstrated that a major fraction of the myofibroblasts was derived from EC in a TGF- β dependent fashion⁸. These studies strongly suggest that EndoMT may be an early event in the pathogenesis of fibrosis and are consistent with observations that fibrosis starts in the perivascular area⁹. Although the mesenchymal transition of EC to myofibroblastic cells may add to the excessive formation of scar tissue, the associated loss of microvascular EC and capillary density, that eventually leads to a state of chronic ischemia, may act as the real profibrotic switch. The tissue response to hypoxia further upregulates TGF- β expression, promotes the influx of inflammatory cells and thereby exacerbates the fibrotic process.

TGF- β is a well-established regulator of EndoMT⁵. TGF- β can bind to the heteromeric receptor complex of TGF β RI and TGF β RII, which results in the phosphorylation of SMAD2 and SMAD3. The phosphorylated SMAD2/3 complex subsequently associates with SMAD4 and translocates to the nucleus. This complex binds to SMAD-binding DNA elements and also to several regulatory molecules, thereby activating various transcriptional networks^{10,11}.



MicroRNAs (miRNAs) are small ~22 nucleotide regulatory RNAs that function as negative regulators of gene expression¹². Since these molecules play a central role in regulating cellular differentiation, miRNAs may also be involved in EndoMT. Support for this notion can be derived from the fact that miRNAs have been described to regulate TGF- β signaling in epithelial to mesenchymal transition (EMT). Among the best characterized miRNAs, miR-200 has been found to regulate EMT, by targeting the transcriptional E-cadherin suppressors ZEB1 and SIP1, while overexpression of the miR-200 family prevents TGF- β -induced EMT¹³. Furthermore, miR-21 has been shown to be upregulated in EMT¹⁴, and to be essential in cardiac fibrosis¹⁵. More recently, initial evidence detailing a role for miRNAs in EndoMT has come to light, with miR-21 silencing phosphatase and tensin homolog in EC resulting in activation of the Akt-pathway¹⁶.

In the present study, we investigated TGF- β -induced EndoMT in mouse embryonic endothelial cells (MEEC), and determined the miRNA expression profile during this dedifferentiation process. Among the differentially expressed miRNAs, miR-155 was one of the most significantly upregulated miRNAs. While miR-155 is important in regulating diverse processes such as immune regulation and cancer¹⁷, a role for this miR in EndoMT is currently unknown. Ras homolog gene family, member A (RhoA), which is a well-established target of miR-155¹⁸, has been described as a regulator of EMT. In this study, we demonstrated that modulation of miR-155 levels in EC can affect EndoMT via targeting the RhoA pathway.

Materials and Methods

Cell Culture and induction of EndoMT

Generation of mouse embryonic endothelial cells (MEEC) was previously described¹⁹. MEEC were maintained on 1% (w/v) gelatin coating in Dulbecco's modified Eagle medium (Gibco/Invitrogen, Breda, the Netherlands) supplemented with 10% fetal calf serum and 2 mM L-glutamine (Invitrogen). Cells were treated with 2 ng/mL TGF- β 3 (Peprotech, London, UK) for 48 hours, unless indicated otherwise. For the culture of MEEC under hypoxic conditions, hypoxic chambers were flushed with nitrogen, resulting in oxygen levels of <1%. To effectively block RhoA activity, we used the Rho kinase inhibitor Y-27632 (Sigma-Aldrich, Zwijndrecht, the Netherlands) at a final concentration of 3.5 μ g/mL. For the scratch assay, MEEC were scraped in a straight line with a 200 μ L pipette tip. A reference point was marked with a tip marker. Cell migration after 24 hours of incubation was determined by microscopy and expressed as migration distance in μ m.

MiRNA microarray

MEEC were stimulated with TGF- β along with an unstimulated control (n=3). To determine miRNA profiles we used NCode Multi-Species miRNA microarrays V2 (Invitrogen). For this, isolated RNA was poly-A tailed, followed by ligation of the capture sequences. Subsequently, the tagged miRNAs were purified and hybridized to the chips, after which fluorescently-labeled capture reagents were hybridized and signal intensity measured using an array reader. Data analysis was performed using BRB-ArrayTools developed by Dr. Richard Simon and BRB-ArrayTools Development Team. All data were normalized to miR-125b, as we have previously found miR-125b to be unresponsive to TGF- β stimulation in MEEC.

RNA isolation and qRT-PCR analysis

Total RNA from kidneys was isolated using Trizol reagent (Invitrogen). Reverse transcription was performed using a 5 minute 65°C incubation of 250 ng total RNA with dNTPs (Invitrogen) and oligo(dT) (Invitrogen) or using specific Taqman® microRNA probes (Applied Biosystems, Foster City, CA, USA). cDNA was synthesized using a M-MLV First-Strand Synthesis system (Invitrogen). Validation of target genes was performed using SYBR Green Master Mix (Applied Biosystems) and the following primers: Twist (sense): ACGCAGTCGCTGAACGAGGC, Twist (antisense): GTACAGGAAGTCGATGTA-CC, α -SMA (sense): CGTGGCTATTCCTTCGTGAC, α -SMA (antisense): GCGT-



TCGTAGCTCTTCTCC, CD31 (sense): CTCCAACAGAGCCAGCAGTA,
 CD31 (antisense): TCACTTCTTCCGGGGTTCCTTATCTG,
 SDF-1 (sense): CGTGAG-GCCAGGGAAGAGT, SDF-
 1 (antisense): TGATGAGCATGGTGGGTGA, Col1a1
 (sense): TGACTGGAAGAGCGGAGAGT, Col1a1 (antisense):
 GTTCGG-GCTGATGTACCAGT, fibronectin (sense):
 ATGTGGACCCCTCCTGATAGT, fibronectin (antisense):
 GCCCAGTGATTCAGCAAAGG, GAPDH (sense):
 ACT-CCCCTCTTCCACCTTC; GAPDH (antisense):
 CACCACCCTGTTGCTGTAG. Levels of expression were determined by
 normalizing to GAPDH.

Validation of miRNA levels was performed using Taqman® miRassays (Applied Biosystems) according to manufacturer's instructions (Invitrogen), RNU6B was utilized for normalization (sense U6: CTCGCTTCGGCAGCACA and antisense U6: AACGCTTCACGAATTTGCGT). Data were quantitated using the delta delta Ct method.

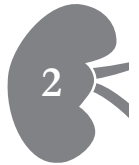
Western Blot

Western blot analyses were performed on cellular lysates harvested in lysis buffer (50 mM Tris-HCl pH7.5, 150 mM NaCl, 1% SDS, 0,5% deoxycholate, 0,5% Triton X-100) containing phosphatase and protease inhibitors. Following quantitation of protein determination, equal amounts of proteins were assessed using SDS-polyacrylamide gels (SDS-PAGE) under reducing conditions. Proteins were transferred to a PVDF membrane (Amersham, 's Hertogenbosch, the Netherlands). Primary antibodies were utilized to detect α -SMA (R&D, Minneapolis, MN, USA), β -actin (Abcam, Cambridge, UK), CD31 (Santa Cruz, Heidelberg, Germany) and RhoA (Cytoskeleton, Denver, Co, USA). Bound primary antibody was labeled with HRP-conjugated secondary antibody in blocking solution. Bound fragments were detected with chemiluminescent reagents (West Dura supersignal; ThermoFisher Scientific, Waltham, MA, USA) and exposed on Hyperfilm ECL (Amersham). Quantitative analysis of the protein bands was performed using ImageJ software and normalized to β -actin.

Antagonism and overexpression of miR-155

Design of Antagomirs

Cholesterol-conjugated RNA analogs, 'antagomirs', (Dharmacon RNA technologies, Lafayette, CO, USA) were synthesized as previously described²⁰. For antagomir-155 the following sequence was used: 5'-a₃c₃cccuaucacaauuagcau₃u₃a₃a₃-Chol-3'. As a control a 'scramblemir' was used,



this RNA analog is constructed from a randomized nucleotide sequence which does not bind to any known microRNAs: 5'-a_su_sgacuaucgcuaaucgc_sa_su_sg_s-Chol-3'. The lower case letters represent 2'-OMe-modified nucleotides; subscript 's' represents phosphorothiate linkage; 'Chol' represents a cholesterol-group linked through a hydroxyprolinol linkage. Antagomir or control scramblemir was added to the medium 16 hours before TGF- β stimulation at a concentration of 5 μ g/mL.

Overexpression of miR-155

To overexpress miR-155, a synthetic pre-miR-155 precursor (Applied Biosystems) was introduced into the cells in a 24-well format with a final concentration of 100 nM. As a control, we used a negative control precursor molecule. Per well, 4 μ L of Lipofectamine 2000 (Invitrogen) was added to facilitate transfection.

Immunocytochemistry

For immunocytochemistry, MEEC were seeded into 4-well chamber slides. At the end of incubation, cells were washed twice with PBS and fixed with 4% paraformaldehyde at room temperature for 5 min. The cells were subsequently washed again, and permeabilized with 0.5% Triton X-100 in PBS for 5 min at room temperature. Cells were then blocked with 10% normal goat serum in PBS for 30 min at room temperature, and incubated for 1 hr with primary antibodies. The following primary antibodies were used: F-actin was visualized with 2 μ g/mL phalloidin-TRITC (Sigma-Aldrich), pLIMK1/pLIMK2 (Cell Signaling Technology, Leiden, the Netherlands), α -SMA (Sigma-Aldrich). Cells were subsequently washed and incubated for 1 hour at room temperature with the appropriate secondary antibodies. The stained cells were covered with Vectashield® mounting medium containing 4',6-diamidino-2-phenylindole (DAPI) (Vector Laboratories, Burlingame, CA, USA). Immunostaining was visualized by fluorescence microscopy (Leica DM1-6000).

RhoA activity assay

RhoA activity was determined using G-lisa (Cytoskeleton). The assay was performed according to the protocol of the manufacturer.

Statistical Analysis

Results are expressed as mean \pm standard error of the mean (SEM). Statistical analysis was performed using Student's t-test. P<0.05 was considered statistically significant (* = >0.05, ** = p<0.01, *** = p<0.001).

Results

TGF- β induces EndoMT in MEEC

We stimulated MEEC with TGF- β to recapitulate EndoMT *in vitro* and assessed whether they displayed mesenchymal characteristics. When MEEC were stimulated with TGF- β for 48 hr they displayed a characteristic morphological transition towards a spindle-like myofibroblast-like phenotype (Figure 1A-B). A hallmark feature of mesenchymal transition is the expression of α -SMA containing stress fibers. Using immune histochemical staining we confirmed this in the TGF- β treated MEEC (Figure 1C-D). Likewise, F-actin containing stress fibers are critical for migration and myofibroblast contraction. When we visualized F-actin by immunostaining with phalloidin we observed marked TGF- β induced stress fiber formation (Figure 1E-F). The TGF- β induced mesenchymal transition of MEEC was associated with

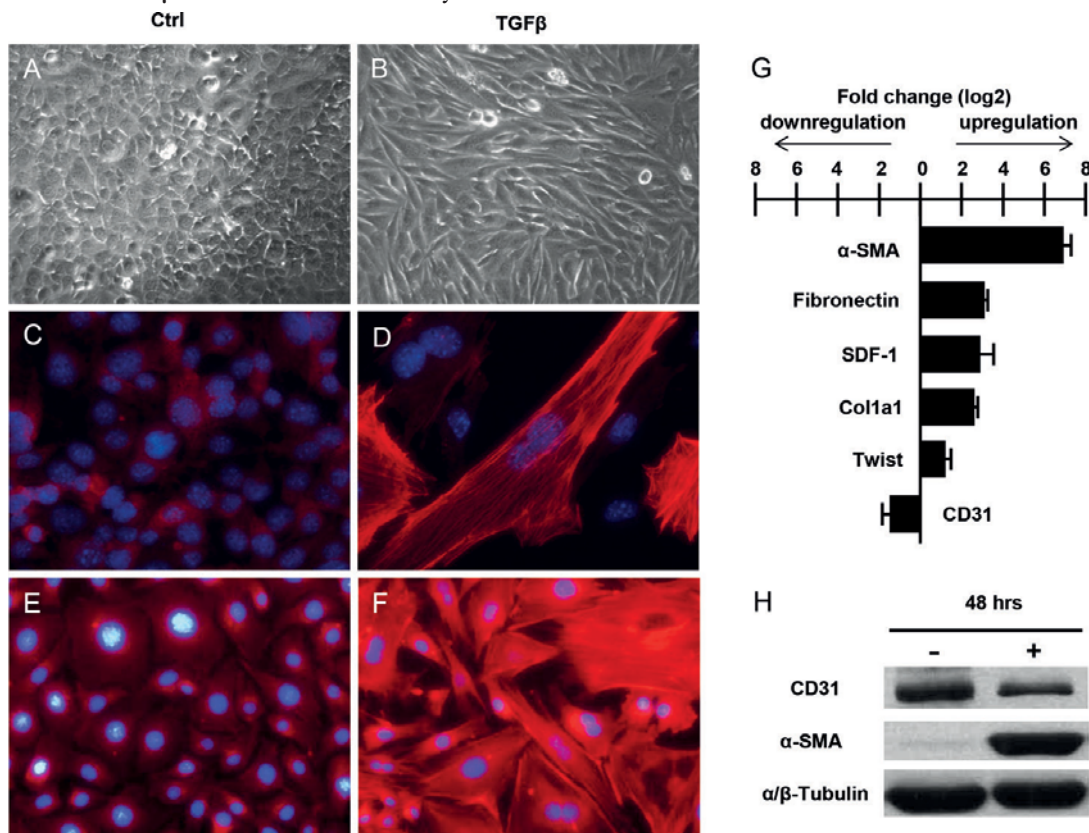
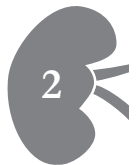


Figure 1. TGF- β induces EndoMT in MEEC. A-B, Representative microscopic images of control MEEC (A) and those stimulated with TGF- β (B) show the morphological transition. C-D, immunofluorescence shows the formation of α -SMA containing stress fibers. E-F, immunofluorescent images show the formation of F-actin containing stress fibers. G, qRT-PCR analysis of EC marker CD31 and myofibroblast markers α -SMA, Fn, col1a1, SDF-1 and Twist. Data is normalized on GAPDH mRNA levels. H, Western Blot shows increased expression of α -SMA and decreased expression of CD31.



a concomitant increase in expression of mRNAs encoding myofibroblast markers α -SMA, fibronectin (Fn), collagen1a1 (col1a1) and Twist²¹ (Figure 1G). Furthermore, stromal cell derived factor-1 mRNA (SDF-1) was up regulated as previously described in EMT²². In contrast, the expression of EC intercellular junction protein CD31 was decreased. Western blot analysis confirmed the observed changes in CD31 and α -SMA mRNA expression at the level of protein expression (Figure 1H).

Hypoxia augments TGF- β induced EndoMT in MEEC

Given that hypoxia is considered to be an HIF-1 α dependent accelerator of EndoMT *in vivo*⁵, we investigated whether hypoxia also augmented EndoMT in MEEC. MEEC were cultured under normoxic and hypoxic conditions (<1% oxygen) in the presence or absence of TGF- β . Following our expectation, hypoxia induced a cellular disorganization that, when combined with TGF- β stimulation resulted in a more profound morphological change towards a myofibroblastic phenotype (Figure 2A-B). Moreover, the combination of hypoxia and TGF- β stimulation led to marked changes in F-actin immunostaining, as evidenced by a highly disorganized staining pattern together with increased stress fiber formation (Figure 2C-D). Further supporting the exacerbation of the myofibroblast phenotype in hypoxia we demonstrated that hypoxic MEEC treated with TGF- β revealed an earlier increase in α -SMA expression (Figure 2I).

Finally, to validate increased production and deposition of extracellular matrix (ECM) under conditions of hypoxia, we performed Sirius Red staining on unstimulated MEEC and MEEC treated with TGF- β for 48 hr. As shown in figure 2J, TGF- β treatment led to an almost two fold increase in ECM production that was even further pronounced in hypoxia (from 4.51 ± 0.20 to 6.42 ± 0.28 , $p < 0.0005$). Together these data confirmed the mesenchymal transition of MEEC following treatment with TGF- β and validated the use of these cells to study mechanisms in EndoMT.

MiRNA expression in TGF- β induced EndoMT

To identify miRNAs that are differentially expressed during EndoMT, we isolated total RNA from MEEC stimulated with TGF- β for 48 hr or unstimulated control cells and processed the samples to determine their miRNA profiles using miRNA microarrays (n=3 per condition). From the 427 miRNAs assessed, 62 miRNAs displayed differential expression during EndoMT. Of these, 51 miRNAs were significantly downregulated during the dedifferentiation process, while 11 miRNAs were upregulated during the conversion to the pro-fibrotic state. Next, we validated the differential

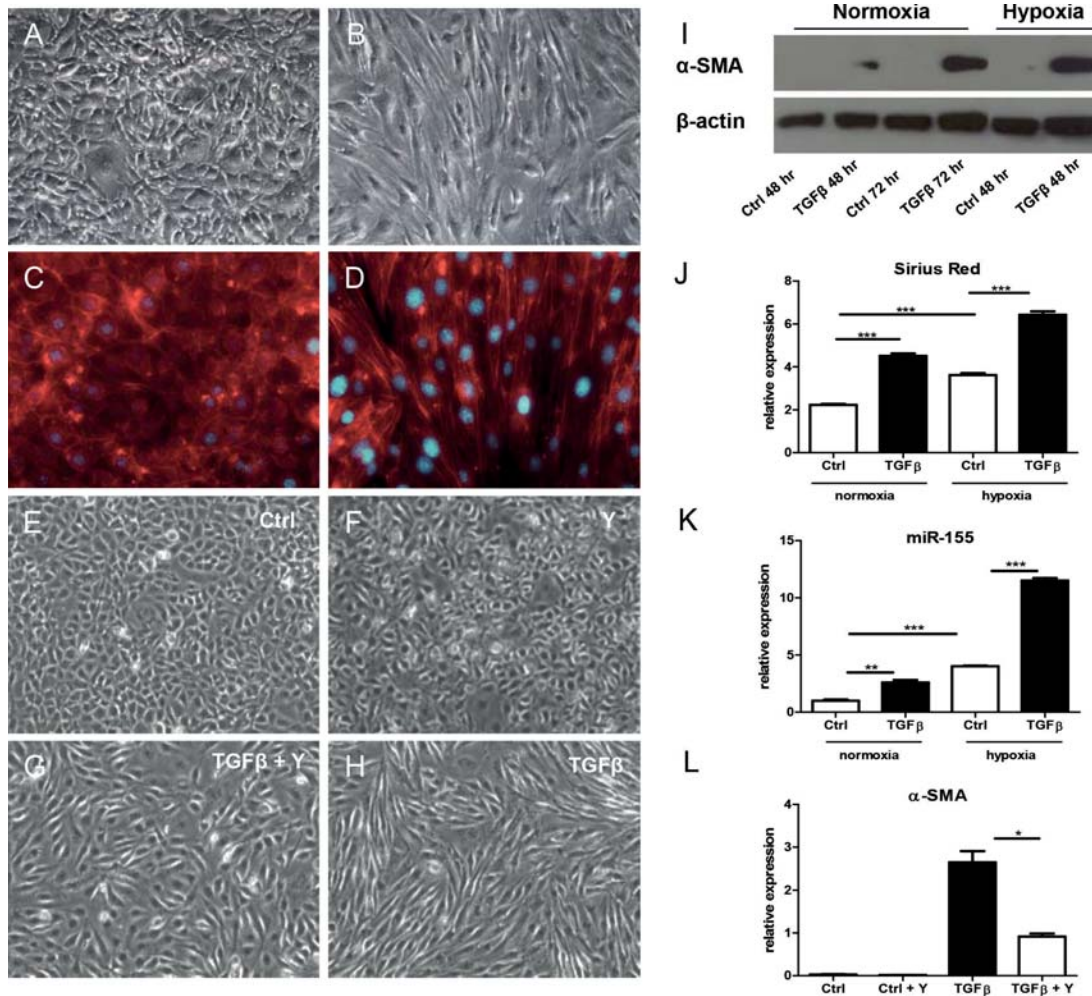


Figure 2. Hypoxia augments, and RhoA is essential for, EndoMT.

A-B, representative microscopic images of cells cultured under hypoxic conditions in the presence or absence of TGF- β . C-D, representative microscopic images of fluorescence of F-actin. E-H, Rho/ROCK inhibitor Y-27632 suppresses EndoMT. Representative microscopic images of unstimulated (E), Y-27632 treated (F), TGF- β and Y-27632 treated (G) and TGF- β treated (H) MEEC. I, Western Blot shows expression of α -SMA in conditions of normoxia and hypoxia. Time points as indicated. J, Sirius Red staining shows that TGF- β stimulation increases extracellular matrix production and is augmented by hypoxia. Expression is relative to cell number. K, qRT-PCR analysis shows that miR-155 expression is increased in EndoMT and augmented by hypoxia. L, qRT-PCR analysis shows reduced α -SMA levels when Y-27632 is added to TGF- β treated cells.

expression of a selection of miRNAs by qPCR and confirmed the differential expression for all tested miRNAs (Table 1).

In our search for miRNAs that regulate EndoMT we selected miR-155 for further study as this miRNA is was one of the few up regulated miRNAs and was previously described to modulate TGF- β -induced EMT through RhoA¹⁸. Given that hypoxia was shown to exacerbate EndoMT, we measured miR-

155 levels both under normoxic and hypoxic conditions in the presence or absence of TGF- β . We found that hypoxia further increased miR-155 levels (Figure 2K), suggesting that TGF- β and hypoxia have a synergistic effect on miR-155 expression levels and that miR-155 expression quantitatively follows EndoMT.



Table 1. Differential miRNA expression in TGF- β induced EndoMT in MEEC. Data is normalized on miR-125b expression, which is the most highly expressed miRNA in MEEC and stable during TGF- β stimulation. Absolute values indicated in first two columns as compared to miR-125b expression level. Third and fourth column show differential expression as determined by respectively microarray and qPCR. – is downregulation, + is upregulation.

miRNA	TGF- β		Fold Change	
	-	+	array	qRT-PCR
miR-125b	1	1	1	1
miR-424	0.13	0.03	-4.3	-2.5
miR-696	0.51	0.21	-2.4	1
miR-93	0.21	0.09	-2.3	n/a
miR-130a	0.19	0.09	-2.0	n/a
miR-15a	0.13	0.07	-1.9	n/a
miR-15b	0.13	0.07	-1.9	n/a
miR-106b	0.16	0.09	-1.8	n/a
miR-22 1	0.14	0.08	-1.8	n/a
miR-20a	0.13	0.08	-1.6	n/a
miR-16	0.34	0.21	-1.6	-2.0
miR-31	0.26	0.18	-1.4	n/a
miR-29a	0.31	0.22	-1.4	-1.5
miR-214	0.06	0.09	+1.5	+2.8
miR-155	0.06	0.08	+1.3	+1.5
miR-199a	0.08	0.10	+1.3	+2.0
miR-199a*	0.09	0.12	+1.3	+2.0
miR-22	0.17	0.22	+1.3	+1.5

Rho/Rock inhibition partly inhibits EndoMT

Since RhoA is a validated target of miR-155 in EMT, we first investigated whether there is also a role for RhoA in EndoMT in MEEC. Using the Rho kinase inhibitor Y-27632 we were able to partly suppress TGF- β induced EndoMT as indicated by a preservation of endothelial cell morphology (Figure

2E-H). In addition, α -SMA mRNA levels were significantly lower (Figure 2L). This indicates that RhoA is essential for full transition of endothelial cells towards a mesenchymal phenotype.

Silencing of miR-155 affects expression of α -SMA

Previously, we demonstrated that antagomirs can be used to specifically silence miRNA expression in EC both *in vitro* as well as *in vivo*²³. To study the effect of miR-155 silencing during EndoMT, we employed an antagomir to miR-155 and a control scramble mir that was designed to lack complementary to the mouse transcriptome. When we assessed the effect of silencing of

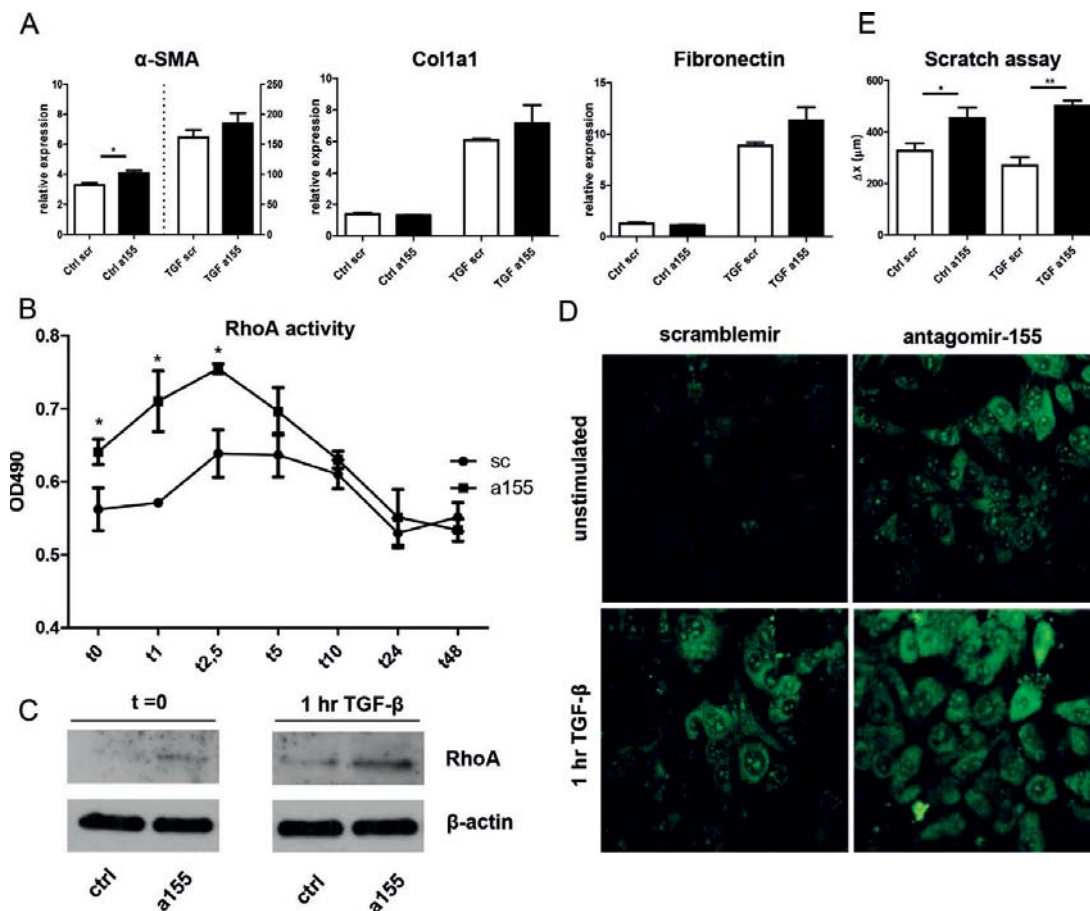
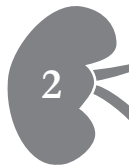


Figure 3. Effect of miR-155 silencing on EndoMT and RhoA signaling.

A, α -SMA, col1a1 and fibronectin mRNA levels, measured by qRT-PCR. TGF- β induced α -SMA levels are plotted on right y-axis. B, RhoA activity at different timepoints after TGF- β stimulation (plotted on x-axis) in antagomir-155 or scramble mir control treated MEEC. C, Western blot for RhoA. Antagomir-155 vs scramble mir control at baseline and 1 hr after TGF- β stimulation. D, representative microscopic images show increased pLIMK expression because of blocking miR-155 in both unstimulated or 1 hr TGF- β stimulated cells. E, increased migratory capacity of MEEC as a result of miR-155 silencing. Migration distance in μ m was measured in a scratch assay.



miR-155 on markers of EndoMT 48 hours after treatment we observed only a minor, not significant trend in the expression of α -SMA, collagen 1a1 and fibronectin mRNA (Figure 3A). Interestingly, in the absence of TGF- β , silencing of miR-155 elevated α -SMA expression (from 3.29 ± 0.29 to 4.07 ± 0.3 , $p < 0.05$) suggesting a repressive role for miR-155 in the basal regulation of cytoskeletal organization.

MiR-155 regulates RhoA expression and activity in MEEC

As the Rho GTPase RhoA is a central regulator of stress fiber formation²⁴ we sought to determine if, similar to what has been described for EMT, miR-155 can also regulate RhoA in EndoMT. Since the conversion of RhoA to the GTP-bound state is known to be a rapid process following stimulation with TGF- β ²⁵, we assessed the dynamics of RhoA activity following TGF- β stimulation in antagomir-155 and scramblemir treated cells. Figure 3B shows that silencing miR-155 indeed leads to a significant upregulation of the activity of RhoA activity in MEEC both before and at 1 and 2.5 hr after TGF- β stimulation. Western blot analyses on baseline lysates or MEEC that were stimulated for 1 hour with TGF- β demonstrated that silencing of miR-155 increases RhoA protein expression concomitant to the increased activity profile (Figure 3C). The reduction of RhoA activity after 24 and 48 hr most likely involves the TGF- β induced increase in miR-155 levels that may exceed the silencing effect of antagomir-155. To further support the effect of miR-155 silencing on RhoA activity we assessed the phosphorylation of LIM kinase (pLIMK), a downstream effector of RhoA dependent stress fiber formation²⁴. MEEC were stimulated with TGF- β in the presence of antagomir-155 or scramblemir and stained for pLIMK at baseline and after 1 hour after stimulation. As shown in figure 3D the expression of pLIMK is increased as a result of miR-155 silencing at both time points again confirming a negative role for miR-155 in RhoA signaling. RhoA has been described to regulate the migration in endothelial cells²⁶. We performed a scratch assay to see if cell migration was also affected by the silencing of mir-155. Twenty four hours after making a scratch, we found that the loss of miR-155 activity has a stimulatory effect on Rho-A dependent migration both in unstimulated as well as in TGF- β stimulated cells (Figure 3E). Our data support a rate limiting role for miR-155 in RhoA activity in MEEC.

Overexpression of miR-155 suppresses features of TGF- β induced EndoMT

Following the above we postulated that overexpression of miR-155 could counteract EndoMT in MEEC. To test this hypothesis we treated MEEC for

16 hr with a synthetic pre-miR-155, and we stimulated the cells with TGF- β for 48 hr to induce EndoMT. Increased levels of miR-155 lead to a virtually complete inhibition of TGF- β -induced EndoMT in MEEC, as evidenced by the maintenance of EC morphology (Figure 4A), while Western blot analysis of lysates harvested from MEEC treated with pre-miR-155 revealed that α -SMA expression remained low while CD31 expression remained high, as compared to scramble miR-treated MEEC (Figure 4B). To confirm that the regulatory role of miR-155 on EndoMT is secondary to inhibition of RhoA expression we also determined RhoA expression at baseline and 1 hr after TGF- β stimulation by Western blot analyses. Indeed, elevation of miR-155 reduces RhoA protein levels compared to the scrambled control pre-miR (Figure 4C). Finally, overexpression of miR-155 was associated with decreased RhoA activity 2.5 hr after TGF- β stimulation (Figure 4D).

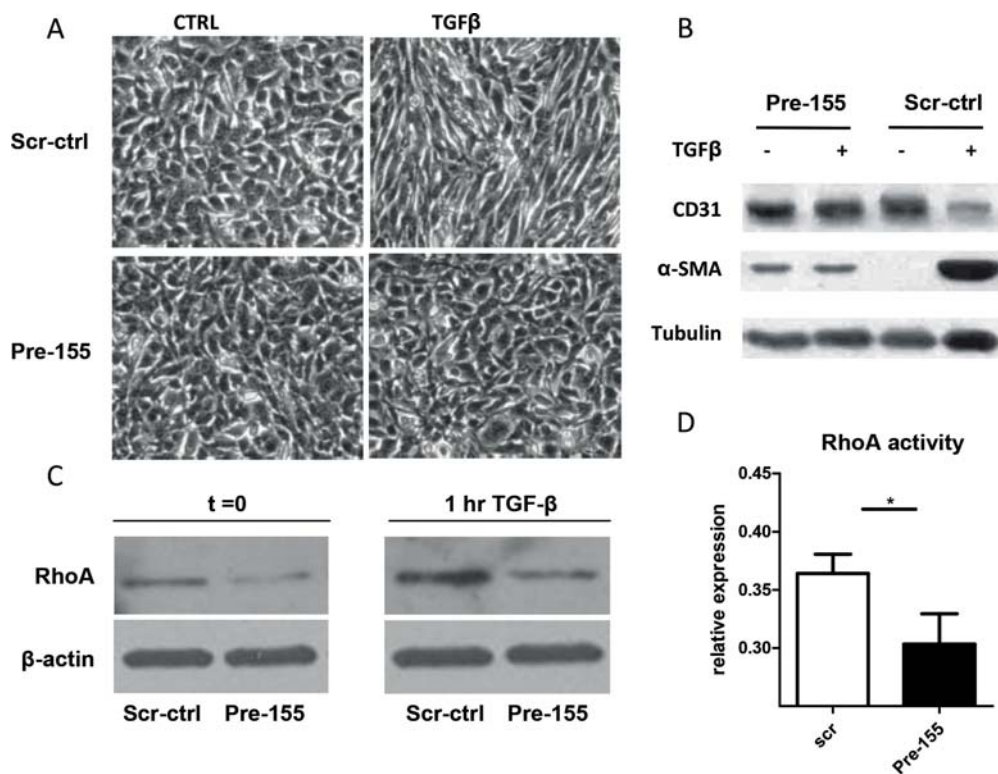


Figure 4. miR-155 overexpression inhibits EndoMT.

A, representative microscopic images of MEEC in the presence or absence of TGF- β , either treated with specific synthetic pre-miR-155 or an unspecific pre-scramblemiR. B, Western blot shows preservation of expression of α -SMA and CD31. Tubulin is used as a loading control. C, RhoA Western blot, pre-miR-155 versus control pre-miR at baseline and 1 hr after TGF- β stimulation. β -actin is used as loading control. D, RhoA activity 2,5 hours after TGF- β stimulation, in the presence of pre-miR-155 or control pre-miR.

Discussion

In this study, we have identified that miR-155 plays a central role in regulating EndoMT. We show that TGF- β stimulation of MEEC results in endothelial to mesenchymal transition and that this mechanism involved the activation of RhoA. Endothelial cell markers are downregulated, and myofibroblast markers are upregulated. In addition to that, stress fiber formation is prominent and an increase in production of extracellular matrix is found. When MEEC are cultured under hypoxic conditions, these features are even stronger.

We profiled TGF- β stimulated MEEC versus control MEEC for miRNAs and found several differentially regulated miRNAs. Overall, we found more miRNAs to be downregulated than up regulated, suggesting a general TGF- β effect on miRNA biosynthesis. This could be true as it has been described that TGF- β dependent SMADs have an effect on miRNA maturation²⁷. Several papers described endothelial cells to contribute to the development of tissue fibrosis through endothelial to mesenchymal transition^{28,29}. The origin of myofibroblasts is controversial though. It has been shown that myofibroblasts in renal fibrotic tissue originate primarily from interstitial, pericyte-like cells³⁰. This could mean that the processes of EMT and EndoMT do not contribute as such to the development of tissue fibrosis. However, the loss of capillaries during fibrosis could, in part, be caused by EndoMT. Furthermore, it is generally accepted that EndoMT is important in embryogenesis, e.g. during formation of the heart.

We showed that miR-155 is important in TGF- β induced EndoMT in MEEC through targeting RhoA. We found the effect on RhoA activity and expression to be an early effect as within a few hours after stimulation with TGF- β in the presence of antagomir-155, and vice versa when miR-155 was over expressed, effects were observed. In addition, in retinal epithelial cells it is described that TGF- β signals to activate RhoA and affects cell migration and α -SMA expression that way³¹. Also in endothelial cells TGF- β is described to activate RhoA, thereby inducing endothelial barrier dysfunction³². By overexpressing miR-155 we inhibit EndoMT as a result of RhoA inhibition, confirming that RhoA in EndoMT can regulate α -SMA expression.

In concordance with upregulation of RhoA activity due to silencing of miR-155 we found increased expression of phosphorylated LIM-kinase, which is phosphorylated by ROCK, the direct target of RhoA²⁴. pLIMK in its turn



phosphorylates cofilin, which then cannot exhibit its actin-depolymerizing activity anymore. So antagomiR-155 contributes to Rho-induced reorganization of the actin cytoskeleton and provides further evidence that miR-155 modulates EndoMT through RhoA regulation. Based on our data and supportive literature we propose a mechanism as illustrated in Figure 5.

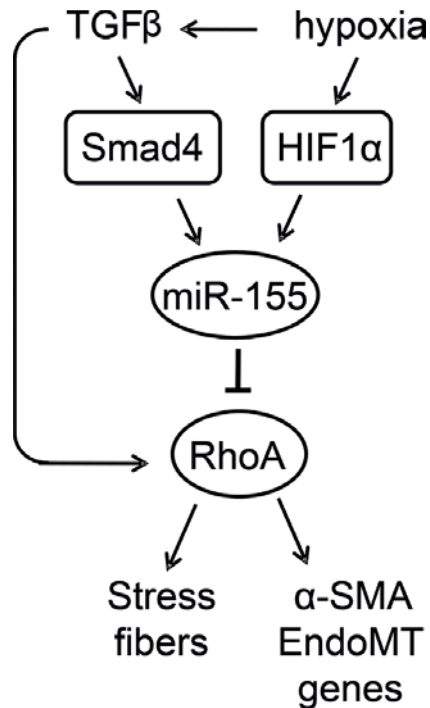


Figure 5. Schematic illustration of miR-155 function in EndoMT.

TGF- β upregulates miR-155 in a SMAD4 dependent manner. In addition, hypoxia upregulates miR-155 through HIF1- α , but also stimulates TGF- β production. TGF- β can stimulate RhoA activity, resulting in stress fiber formation, α -SMA production and induction of other EndoMT related genes. RhoA is suppressed by miR-155, which implies a negative feedback role for miR-155 in RhoA regulation, and therefore EndoMT.

Nevertheless, it is very well possible that miR-155 functions through other targets as well. For example, it has been described that miR-155 targets SMAD5, that inhibits growth-inhibitory effects of TGF- β ³³. This mechanism could also be important in the context of EndoMT as SMAD5 could be counteracting the effects of TGF- β . Another possibly relevant known target includes SMAD2³⁴, that mediates the effect of TGF- β .

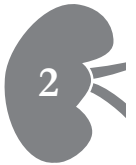
In conclusion, MEEC show to undergo EndoMT after TGF- β stimulation. During this transition miR-155 expression is increased, and is shown to modulate RhoA, and thereby acts as a negative feedback regulator. We showed that over expression of miR-155 can completely inhibit EndoMT and identified miR-155 as a key regulator of EndoMT.

Acknowledgements

This work was supported in part by the Dutch Heart Foundation (NHS grant 2006B145), the Dutch Kidney Foundation (grants C07.2227 and C 09.2329) and a grant from the Netherlands Institute of Regenerative Medicine.

References

1. Markwald, R.R., Fitzharris, T.P. & Manasek, F.J. Structural development of endocardial cushions. *Am J Anat* 148, 85-119 (1977).
2. Nakajima, Y., Yamagishi, T., Hokari, S. & Nakamura, H. Mechanisms involved in valvuloseptal endocardial cushion formation in early cardiogenesis: roles of transforming growth factor (TGF)-beta and bone morphogenetic protein (BMP). *Anat Rec* 258, 119-127 (2000).
3. Bruneau, S., et al. Key Features of the Intragraft Microenvironment that Determine Long-Term Survival Following Transplantation. *Front Immunol* 3, 54 (2012).
4. Piera-Velazquez, S., Li, Z. & Jimenez, S.A. Role of endothelial-mesenchymal transition (EndoMT) in the pathogenesis of fibrotic disorders. *Am J Pathol* 179, 1074-1080 (2011).
5. Goumans, M.J., van Zonneveld, A.J. & ten Dijke, P. Transforming growth factor beta-induced endothelial-to-mesenchymal transition: a switch to cardiac fibrosis? *Trends Cardiovasc Med* 18, 293-298 (2008).
6. Rabelink, T.J., de Boer, H.C. & van Zonneveld, A.J. Endothelial activation and circulating markers of endothelial activation in kidney disease. *Nat Rev Nephrol* 6, 404-414 (2010).
7. O'Riordan, E., et al. Chronic NOS inhibition actuates endothelial-mesenchymal transformation. *Am J Physiol Heart Circ Physiol* 292, H285-294 (2007).
8. Zeisberg, E.M., et al. Endothelial-to-mesenchymal transition contributes to cardiac fibrosis. *Nat Med* 13, 952-961 (2007).
9. Brilla, C.G. & Weber, K.T. Reactive and reparative myocardial fibrosis in arterial hypertension in the rat. *Cardiovasc Res* 26, 671-677 (1992).
10. Zavadil, J. & Bottinger, E.P. TGF-beta and epithelial-to-mesenchymal transitions. *Oncogene* 24, 5764-5774 (2005).
11. ten Dijke, P. & Arthur, H.M. Extracellular control of TGFbeta signalling in vascular development and disease. *Nat Rev Mol Cell Biol* 8, 857-869 (2007).
12. Filipowicz, W., Bhattacharyya, S.N. & Sonenberg, N. Mechanisms of post-transcriptional regulation by microRNAs: are the answers in sight? *Nat Rev Genet* 9, 102-114 (2008).
13. Gregory, P.A., Bracken, C.P., Bert, A.G. & Goodall, G.J. MicroRNAs as regulators of epithelial-mesenchymal transition. *Cell Cycle* 7, 3112-3118 (2008).
14. Zavadil, J., Narasimhan, M., Blumenberg, M. & Schneider, R.J. Transforming growth factor-beta and microRNA:mRNA regulatory networks in epithelial plasticity. *Cells Tissues Organs* 185, 157-161 (2007).
15. Thum, T., et al. MicroRNA-21 contributes to myocardial disease by stimulating MAP kinase signalling in fibroblasts. *Nature* 456, 980-984 (2008).
16. Kumarswamy, R., et al. Transforming growth factor-beta-induced endothelial-to-mesenchymal transition is partly mediated by microRNA-21. *Arterioscler Thromb Vasc Biol* 32, 361-369 (2012).
17. Tili, E., Croce, C.M. & Michaille, J.J. miR-155: on the crosstalk between inflammation and cancer. *Int Rev Immunol* 28, 264-284 (2009).
18. Kong, W., et al. MicroRNA-155 is regulated by the transforming growth factor beta/Smad pathway and contributes to epithelial cell plasticity by targeting RhoA. *Mol Cell Biol* 28, 6773-6784 (2008).
19. Larsson, J., et al. Abnormal angiogenesis but intact hematopoietic potential in TGF-beta type I receptor-deficient mice. *EMBO J* 20, 1663-1673 (2001).
20. Krutzfeldt, J., et al. Silencing of microRNAs in vivo with 'antagomirs'. *Nature* 438, 685-689 (2005).



21. Yang, J., et al. Twist, a master regulator of morphogenesis, plays an essential role in tumor metastasis. *Cell* 117, 927-939 (2004).
22. Taki, M., et al. Up-regulation of stromal cell-derived factor-1alpha and its receptor CXCR4 expression accompanied with epithelial-mesenchymal transition in human oral squamous cell carcinoma. *Oncol Rep* 19, 993-998 (2008).
23. van Solingen, C., et al. Antagomir-mediated silencing of endothelial cell specific microRNA-126 impairs ischemia-induced angiogenesis. *J Cell Mol Med* 13, 1577-1585 (2009).
24. Maekawa, M., et al. Signaling from Rho to the actin cytoskeleton through protein kinases ROCK and LIM-kinase. *Science* 285, 895-898 (1999).
25. Bhowmick, N.A., et al. Transforming growth factor-beta1 mediates epithelial to mesenchymal transdifferentiation through a RhoA-dependent mechanism. *Mol Biol Cell* 12, 27-36 (2001).
26. Zhao, L., et al. The effect of RhoA on human umbilical vein endothelial cell migration and angiogenesis in vitro. *Oncol Rep* 15, 1147-1152 (2006).
27. Davis, B.N., Hilyard, A.C., Lagna, G. & Hata, A. SMAD proteins control DROSHA-mediated microRNA maturation. *Nature* 454, 56-61 (2008).
28. Zeisberg, E.M., Potenta, S.E., Sugimoto, H., Zeisberg, M. & Kalluri, R. Fibroblasts in kidney fibrosis emerge via endothelial-to-mesenchymal transition. *J Am Soc Nephrol* 19, 2282-2287 (2008).
29. Li, J., Qu, X. & Bertram, J.F. Endothelial-myofibroblast transition contributes to the early development of diabetic renal interstitial fibrosis in streptozotocin-induced diabetic mice. *Am J Pathol* 175, 1380-1388 (2009).
30. Humphreys, B.D., et al. Fate tracing reveals the pericyte and not epithelial origin of myofibroblasts in kidney fibrosis. *Am J Pathol* 176, 85-97 (2010).
31. Tsapara, A., et al. The RhoA activator GEF-H1/Lfc is a transforming growth factor-beta target gene and effector that regulates alpha-smooth muscle actin expression and cell migration. *Mol Biol Cell* 21, 860-870 (2010).
32. Lu, Q., et al. Transforming growth factor-beta1-induced endothelial barrier dysfunction involves Smad2-dependent p38 activation and subsequent RhoA activation. *J Appl Physiol* 101, 375-384 (2006).
33. Rai, D., Kim, S.W., McKeller, M.R., Dahia, P.L. & Aguiar, R.C. Targeting of SMAD5 links microRNA-155 to the TGF-beta pathway and lymphomagenesis. *Proc Natl Acad Sci U S A* 107, 3111-3116 (2010).
34. Louafi, F., Martinez-Nunez, R.T. & Sanchez-Elsner, T. MicroRNA-155 targets SMAD2 and modulates the response of macrophages to transforming growth factor- β . *J Biol Chem* 285, 41328-41336 (2010).



Chapter

3

Cardiovasc Res. 2011 Dec 1;92(3):449-55.

MicroRNA-126 modulates endothelial SDF-1 expression and mobilization of Sca-1⁺/Lin⁻ progenitor cells in ischemia

Coen van Solingen^{1,2}, Hetty C. de Boer^{1,2}, Roel Bijkerk^{1,2}, Matthieu Monge¹, Annemarie M. van Oeveren-Rietdijk^{1,2}, Leonard Seghers^{2,3}, Margreet R. de Vries^{2,3}, Eric P. van der Veer^{1,2}, Paul H.A. Quax^{2,3}, Ton J. Rabelink^{1,2} and Anton Jan van Zonneveld^{1,2}

¹Department of Nephrology and the ²Eindhoven Laboratory for Experimental Vascular Medicine, ³Department of Surgery, LUMC, Leiden, the Netherlands.

Abstract

MicroRNA-126 (miR-126), which is enriched in endothelial cells, plays a role in angiogenesis. Based on the seed sequence, miR-126 can also be predicted to regulate vasculogenesis by modulating the endothelial expression of stromal cell-derived factor-1 (SDF-1). Using miR-reporter constructs, we first validated that miR-126 inhibits SDF-1 expression in endothelial cells *in vitro*. Next, we investigated the potential relevance of this observation with respect to the mobilization of progenitor cells. For this, we studied the migration of human CD34⁺ progenitor cells towards chemotactic factors present in endothelial cell-conditioned medium. Antagomir-induced silencing of miR-126 elevated SDF-1 expression by human umbilical vein endothelial cells and enhanced migration of the CD34⁺ cells. In a murine model of hind limb ischemia, a striking increase in the number of circulating Sca-1⁺/Lin⁻ progenitor cells in antagomir-126-treated mice was observed as compared to scramble-mir-treated controls. Immunohistochemical staining of capillaries in the post-ischemic gastrocnemius muscle of miR-126-silenced mice revealed elevated SDF-1 expressing CD31-positive capillaries, whereas a mobilizing effect of miR-126 inhibition was not detected in healthy control animals. MiR-126 can regulate the expression of SDF-1 in endothelial cells. In the context of an ischemic event, systemic silencing of miR-126 leads to the mobilization of Sca-1⁺/Lin⁻ progenitor cells into the peripheral circulation, potentially in response to elevated SDF-1 expression by endothelial cells present in the ischemic tissue.

Introduction

Integrity of the vascular endothelium is central to vascular homeostasis and is determined by the balance between endothelial injury and repair¹. In the context of adverse hemodynamic and metabolic risk factors, endothelial cells (ECs) are damaged and constantly replaced by the proliferation of adjacent mature ECs. In the rat aorta, ECs in areas resistant to atherosclerosis have a low rate of cellular replication and have been estimated to have a lifespan of approximately 12 months. In contrast, EC turnover in lesion-prone sites is accelerated to weeks or less as animals age². To maintain the integrity of the endothelium throughout life, endothelial cells in the arterial wall would therefore have to replicate well over a thousand times. However, primary endothelial cell cultures already become senescent after a limited number of passages due to a progressive shortening of telomeres that takes place upon each cell division. Moreover, telomere erosion is accelerated by chronic exposure of endothelial cells to oxidative stress³. Consequently, it has been suggested that mature ECs are insufficiently capable of repairing the chronically damaged endothelium throughout life. Support for this notion has been provided by several studies identifying a significant contribution by endothelial progenitor cells as an alternative cellular source for re-endothelialization of the damaged artery wall⁴⁻⁶.

Stromal cell derived factor-1 (SDF-1 or CXCL12) has been demonstrated to facilitate the homing of progenitor cells from the peripheral circulation to sites of vascular injury or tissue ischemia. SDF-1 can be actively secreted by injured endothelial cells⁷ or activated platelets⁸, leading to the homing of bone marrow-mobilized progenitor cells to the site of injury^{9,10}. The beneficial role of SDF-1 in recruiting bone marrow cells to ischemic tissue has been established in several animal models to improve recovery after an ischemic event^{7,11-13}. Therefore, SDF-1 is believed to play a central role in regulating both vascular integrity and homeostasis, implicating that its expression should be tightly controlled. Indeed SDF-1 expression is reported to be regulated at multiple levels including transcription and post-translation⁷.

At the post-transcriptional level, SDF-1 expression could be regulated by microRNAs (miRNAs). MiRNAs constitute a class of highly conserved non-coding RNAs that control gene expression by inhibiting the translation of mRNA¹⁴. The ability of miRNAs to regulate multiple targets provides a means for the coordinated control of gene expression and make these molecules especially attractive candidates for regulating cell type-specific differentiation



and modulating cell function¹⁵. In recent years, miRNA expression-profiles of ECs have been analyzed in detail and recent studies demonstrated both pro-angiogenic¹⁶⁻¹⁹ as well as anti-angiogenic functions for endothelial miRNAs^{20,21}.

In silico analyses (<http://www.microrna.org>) for miRNAs targeting the 3' untranslated region (3' UTR) of the SDF-1 mRNA identified miR-126 as a potential post transcriptional regulator of SDF-1 expression. MiR-126 is highly enriched in ECs and has been demonstrated to regulate (ischemia-induced) angiogenesis by blocking the expression of SPRED-1 and PI3KR2²²⁻²⁴. Here, we validated the inhibitory actions of miR-126 on expression and function of SDF-1 in ECs *in vitro*. Furthermore, we demonstrate that antagomir-induced silencing of miR-126 prior to acute ischemia leads to the augmentation of SDF-1 levels in both the circulation and ischemic tissue. This is associated with increased mobilization of bone marrow-derived progenitor cells *in vivo*. Our data demonstrate that endothelial miR-126 can regulate both features of angiogenesis as well as vasculogenesis and suggest a role for miR-126 in the maintenance of endothelial homeostasis.

Materials and Methods

Cells and Cell Culture

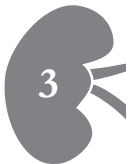
Immortalized human umbilical vein endothelial cells (EC-RF24)²⁵ were cultured in M199 medium (Gibco, Breda, the Netherlands) supplemented with penicillin/streptomycin (Gibco/Invitrogen), 20% fetal calf serum (FCS, Bio Whittaker/Cambrex, Verviers, Belgium), 10 IU/mL heparin (Leo Pharma, Breda, the Netherlands), 2.5% HEPES buffer (Gibco) and 12.5 µg/mL endothelial cell growth supplement (Sigma-Aldrich, St. Louis, MO). Human umbilical vein endothelial cells (HUVEC) were isolated, cultured and characterized as described previously²⁶. In short, ECs were isolated from freshly obtained human umbilical cords by trypsin/EDTA digestion of the interior of the umbilical vein. The cells were cultured in M199 medium supplemented with penicillin/streptomycin, 20% FCS, 10 IU/mL heparin, and 5% bovine pituitary extract (Gibco). CD34⁺ cells were isolated from umbilical cord blood using Ficoll (Amersham, 's-Hertogenbosch, the Netherlands) density gradient centrifugation and positive selection using CD34-MACS microbeads (Miltenyi Biotech, Bergish Gladbach, Germany). Umbilical cord blood and umbilical cords were collected non-identifiable and with informed consent. Since the human tissues were unidentifiable, approval from the university ethics review board was not necessary.

SDF-1 3'UTR Reporter Assays

Synthetic, double-stranded oligonucleotides spanning a 60 base-pair region of the murine 3'UTR of SDF-1 mRNA containing the putative miR-126 binding site with (pSDFmm) or without (pSDF) a C to G mismatch at position 3 of the seed-sequence were cloned into the pMIR-reportTM Expression Reporter Vector System (Applied Biosystems, Amsterdam, the Netherlands; see online publication for oligonucleotide sequences). All plasmids were sequenced to confirm their structure and exclude cloning artefacts. A renilla luciferase expression plasmid (pRL-SV40, Promega, Leiden, the Netherlands) and a plasmid containing a single, perfect match miR-126 binding site served as controls²³.

Design of Antagomirs

Antagomir-126 and a control scramble mir (Dharmacon RNA technologies, Lafayette, CO) were synthesized as previously described²³.



Luciferase Assay

Antagomir-126 or control scramblemir (5 µg/mL) was added to a near confluent layer of fibronectin-adherent EC-RF24 cells. Twenty four hours after antagomir treatment, the EC-RF24 cells were detached by trypsinization and resuspended in 500 µL serum-free Optimem culture medium (Gibco) and 1.5 µg specific pMIR-report and 150 ng pRL-SV40 were added. The cell suspension was chilled for 10 minutes at 4°C and electroporated using the Gene Pulser II (Bio-Rad Laboratories, Veenendaal, the Netherlands). After 10 minutes recovery time at room temperature, 1.5x10E5 cells were plated in a 24-wells plate coated with fibronectin in triplicate. After 24 hours, the firefly-luciferase and renilla-luciferase signals were measured using a Dual-Luciferase® Assay Reporter System (Promega) in a Lumat LB9507 luminometer (EG&G Berthold, Bundoora, Australia).

Western Blot

HUVEC were incubated for 48 hours with 5 µg/mL antagomir-126 or scramblemir. Culture medium was aspirated and cells were washed two times with PBS, cellular lysates were harvested using lysis buffer (50 mM Tris-HCl (pH=7.5), 150 mM NaCl, 1% SDS, 0.5% sodiumdeoxycholate and 0.5% Triton X-100 (Sigma-Aldrich)). Protein levels for SDF-1 and β-actin were assessed by Western blot analysis with chemiluminescence detection. Equal amounts of protein were resolved on 15% SDS-polyacrylamide gels and transferred to PVDF membranes (Millipore, Billerica, MA). SDF-1 was detected using a polyclonal rabbit antibody against human SDF-1 (0.5 ug/mL, Abcam, Cambridge, UK) and for β-actin a polyclonal rabbit antibody against human β-actin (0.1 ug/mL, Abcam) was used. Horseradish peroxidase conjugated goat-anti-rabbit IgG (0.05 ug/mL, DakoCytomation, Enschede, the Netherlands) was used as secondary antibody. Bound fragments were detected with chemiluminescent reagents (Supersignal West Dura Extended Duration Substrate, ThermoScientific) and exposed on Hyperfilm ECL (Amersham). Quantitative analysis of the SDF-1 band intensity on Western blot was performed using imageJ software and normalized for β-actin. The ratio of the SDF-1 band intensity over the β-actin band intensity of the antagomir-126 treated HUVEC was arbitrarily set at 100%.

Migration Assay

HUVEC were incubated in serum-free, cell-specific medium with 0.1% insulin-transferrin-sodium selenite media supplement (ITS, Sigma-Aldrich) containing antagomir-126 or scramblemir (5 µg/mL) at 37°C. After 48 hours, cell supernatants were harvested and placed into the lower compartment of

a transwell system with a pore size of 5 μm (Corning B.V. Life Sciences, Amsterdam, the Netherlands). Human CD34⁺ cells were added to the upper chamber and migration was followed over a period of 4 hours at 37°C. As a positive control 50 ng/mL recombinant human SDF-1 (R&D Systems) was added in the lower compartment. The SDF-1-receptor, CXCR4, was neutralized by incubation of CD34⁺ cells with a blocking antibody against CXCR4 (8 $\mu\text{g}/\text{mL}$, R&D Systems) for 30 minutes at 4°C. After 4h, the cell-suspensions in the lower compartment were harvested, spun down and incubated for 30 minutes at 4°C in FACS buffer (PBS + 1% bovine serum albumin (BSA, Sigma-Aldrich)) with directly conjugated antibodies against human CD34 (PerCP-Cy5, BD Biosciences, Breda, the Netherlands) and human CD133 (APC, Miltenyi Biotec). A fixed number of CD34⁺ cells was fluorescently labeled by incubation with calcein-AM (R&D Systems, Minneapolis, MD) and added prior to FACS analysis.



Hind Limb Ischemia Model

All animal experimental protocols were approved by the animal welfare committee of the Netherlands Organization for Applied Scientific Research (TNO, Leiden, the Netherlands) and conform the Directive 2010/63/EU of the European Parliament. One day prior to surgery, C57BL/6 WT mice (n=6 per group, age=10 weeks, Charles River, Maastricht, the Netherlands) were injected intravenously (200 μL) with antagomir-126 (1.0 mg/animal) or scramblemir (1.0 mg/animal). Before surgery, mice were anesthetized intraperitoneally with a combination of Midazolam (5 mg/kg, Roche Diagnostics, Almere, the Netherlands), Medetomidine (0.5 mg/kg, Orion Corporation, Turku, Finland) and Fentanyl (0.05 mg/kg, Janssen Pharmaceutica, Tilburg, the Netherlands). Ischemia of the left hind limb was induced by electrocoagulation of the left common femoral artery, proximal to the bifurcation of superficial and deep femoral artery, as described²⁷. To sacrifice the mice, blood was withdrawn for FACS-analysis (EDTA-anti-coagulated) by heart puncture and the tibia and femur of both legs were kept for isolation of bone marrow cells. Additionally, the gastrocnemius muscle of both hind limbs was dissected and placed in 4% formaldehyde overnight. After paraffin embedding, 4 μm thick serial cross-sections were made for immunohistochemical analysis.

Whole Blood Analysis

Whole blood was collected by incision of the tail vein or heart puncture and analyzed by semi-automatic hematology analyzer F-820 (Sysmex; Sysmex Corporation, Etten-Leur, the Netherlands), FACS-analysis or ELISA.

Hematological values obtained were white blood cell counts (WBC, $n \times 10^6$ /mL), red blood cell counts (RBC, $n \times 10^9$ /mL), platelets (PLT, $n \times 10^6$ /mL), hematocrit (HCT, %/%) and haemoglobin (HGB, mmol/L). For FACS analysis, we incubated 50 μ L of whole blood for 60 minutes at 4°C with directly conjugated antibodies directed against Sca-1 (FITC, BD-Biosciences), Flk-1 (PE, BD-Pharmingen, San Diego, CA) and a cocktail against lineage-positive cells (APC, BD-Pharmingen). In a separate tube, 50 μ L of whole blood was incubated with an appropriate cocktail of isotype controls, to identify the threshold for lineage-positivity. SDF-1 levels in serum were assessed with ELISA (R&D Systems).

Immunohistochemistry

Four μ m-thick sections of murine gastrocnemius muscle were re-hydrated and incubated with antigen-retrieval buffer (0.1% trypsin/EDTA in PBS). Next, sections were incubated with specific antibodies against murine SDF-1 (rabbit polyclonal IgG, ThermoScientific, Rockford, IL) and murine CD31 (mouse monoclonal IgG2b, Santa Cruz, Heidelberg, Germany) followed by secondary antibodies against goat-anti-rabbit-IgG labeled with Alexa-488 or goat-anti-mouse IgG labeled with Alexa-568 (Molecular Probes). As a negative control, isotype-matched IgGs were used. Images were made using a confocal microscope (Carl Zeiss, Sliedrecht, the Netherlands).

FACS Analysis

All samples obtained for FACS analysis were either immediately analyzed by flow cytometry analysis (FACS LSRII, BD Biosciences) or were fixed in 1% paraformaldehyde and analyzed within 24 hours after preparation. Data were analyzed using FACSDiVa software (BD Biosciences).

Statistical Analysis

Results are expressed as mean \pm standard error of the mean (SEM). Statistical analysis was performed using the Mann-Whitney T-test. $P < 0.05$ was considered statistically significant.

Results

MiR-126 affects the expression and function of SDF-1 in vitro

Using an on line miRNA target search tool ([http:// www.microrna.org](http://www.microrna.org)) we identified a putative miR-126 binding site in the 3'UTR of the SDF-1 mRNA. To assess its functionality, we cloned this binding site into the 3'UTR of a luciferase reporter gene driven by a constitutive promoter (pSDF) and analyzed luciferase expression and of a control plasmid in the human endothelial cell

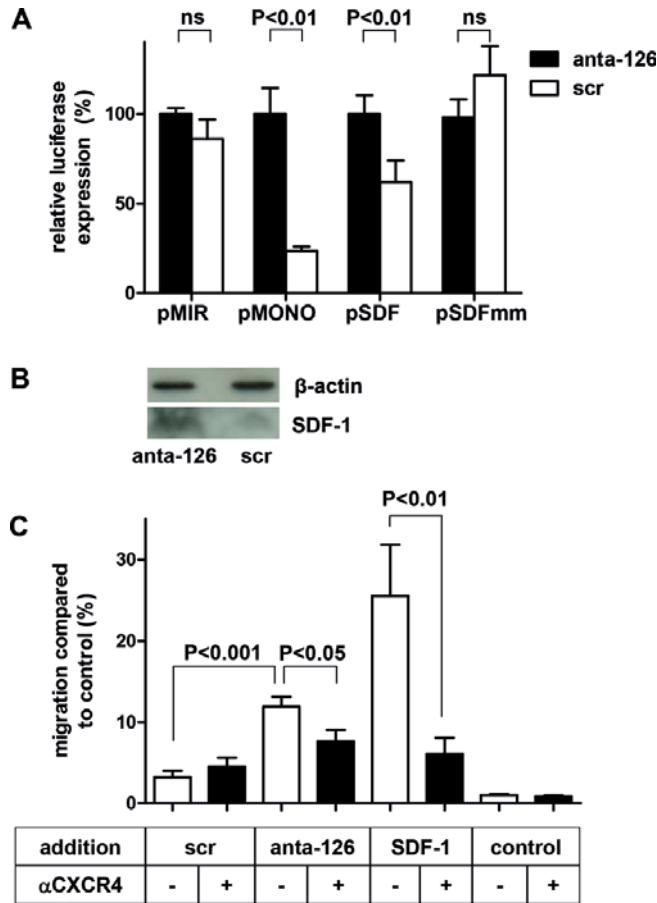


Figure 1. MiR-126 affects the expression and function of SDF-1 in vitro.

A, EC-RF24 were pre-incubated with scrambleir or antagomir-126 and transfected with pMIR as negative control, pMONO as positive control, pSDF with the sequence of the SDF-1 miR-126 binding site or a variant with a single mismatch in the seed sequence (pSDFmmm). Experiments were performed in triplicate and data are expressed as mean values \pm standard error of the mean. B, HUVEC were incubated for 48 hours with antagomir-126 or scrambleir and conditioned cell supernatants subjected to Western blot analysis for SDF-1. C, HUVEC (n=4) were treated with antagomir-126, scrambleir or vehicle and the conditioned media were used to study the chemotactic activity

towards human hematopoietic CD34⁺ cells in vitro. Recombinant SDF-1 was used as positive control and the contribution of the SDF-1 receptor (CXCR4) was studied with the use of a function-blocking antibody (α CXCR4) (n=2).

line EC-RF24. In these miR-126 expressing cells, luciferase expression driven from a reporter construct lacking a miRNA seed sequence (pMIR) was not affected when miR-126 was silenced using an antagomir approach (anta-126). In contrast, a reporter gene carrying a single perfect miR-126 binding site (pMONO) was fully active when miR-126 was silenced but its expression was



strongly reduced in the presence of a control scramblemir (scr). These studies confirm the functionality of miR-126 in EC-RF24 cells. Likewise, the presence of the putative SDF-1 miR-126 binding site in the reporter construct led to a 40% reduction of luciferase-expression in miR-126 expressing cells (Figure 1A, scramble vs. antagomir-126, $P < 0.01$). A single mismatch in the seed sequence of the putative SDF-1 miR-126 binding site (C to G at position 3 of the seed sequence, pSDFmm) alleviated miR-126-dependent repression of reporter gene expression, confirming the presence and specificity of the miR-126 binding site in the 3'UTR of the SDF-1 mRNA. To validate the regulatory effect of miR-126 on endogenous SDF-1 protein expression in endothelial cells, human umbilical vein endothelial cells (HUVEC) were treated with antagomir-126 or scramblemir, after which SDF-1-protein expression was determined by Western blot analysis. A marked increase of SDF-1 protein expression was observed in HUVEC treated with antagomir-126 as compared to scramblemir (Figure 1B).

Next, we assessed the potential of miR-126 to regulate the extent by which endothelial cell-derived SDF-1 attracts progenitor cells. To this end, conditioned medium derived from HUVEC, incubated with antagomir-126 or scramblemir, was applied to the lower compartment of a transwell-system and umbilical cord blood-derived CD34⁺ cells were placed in the upper compartment. As shown in Figure 1C, silencing of miR-126 in HUVEC-enhanced migration of CD34⁺ cells compared to the scramblemir-control ($P < 0.001$). Moreover, neutralization of CXCR4 expressed by the CD34⁺ cells with a function-blocking antibody (α CXCR4, 8 μ g/mL) decreased cell migration towards the conditioned supernatant derived from antagomir-126 treated HUVEC back to the scramble control levels ($P < 0.05$). As a control, maximal cellular migration was observed using medium containing recombinant human SDF-1 (50 ng/mL), which was significantly reduced by α CXCR4 (Figure 1C, $P < 0.01$). These data suggest that suppression of miR-126 in endothelial cells *in vitro* can augment expression of functional SDF-1, leading to elevated progenitor cell migration.

MiR-126 affects progenitor cell mobilization via SDF-1 in vivo

Endothelial miR-126 expression and functionality is conserved in murine EC, both *in vivo*²³ and *in vitro* (data not shown). To investigate the regulatory role of miR-126 on SDF-1-dependent progenitor cell mobilization *in vivo*, we applied single tail vein injections of antagomir-126 or the control scramblemir into wild type (WT) male C57Bl/6 mice (n=6) Ten days after injection, we enumerated the number of circulating Sca-1-positive and lineage-negative

(Sca-1⁺/Lin⁻) cells by FACS analysis. Surprisingly, when we expressed the circulating Sca-1⁺/Lin⁻ cell numbers as a percentage of Lin⁺ leukocytes, we observed a significant decrease in circulating Sca-1⁺/Lin⁻ cells in the mice in which miR-126 had been silenced by antagomir-126 administration as compared to the scramble-mir-treated controls (Figure 2A, P<0.05). This observation could be explained by the fact that antagomir-126 treated mice also displayed a significant increase in total white blood cell (WBC) count (Figure 2B, P<0.01). Such an increase is consistent with reports showing that increased SDF-1 levels in the circulation result in an elevation of WBCs⁹.

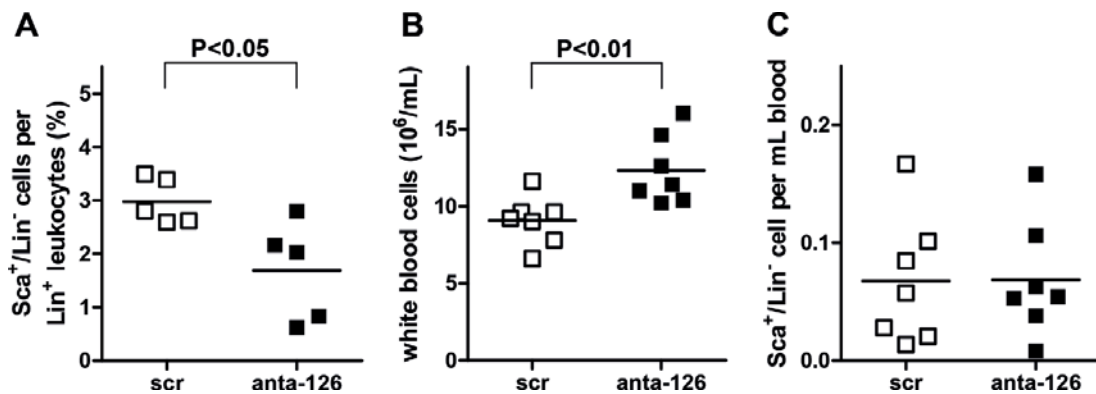


Figure 2. MiR-126 does not solely affect mobilization of Sca-1⁺/Lin⁻ cells in vivo.

A, Ten days after injection of scramble-mir or antagomir-126, Sca-1⁺/Lin⁻ cells in whole blood were analyzed by FACS, expressed as percentage of total Lin⁺ leukocytes. B, Ten days after injection of scramble-mir or antagomir-126, total white blood cell counts per mL was determined. C, Ten days after scramble-mir- or antagomir-126-injection Sca-1⁺/Lin⁻ cells were analyzed by FACS in whole blood expressed as total number in mL blood.

As such, when we expressed the number of circulating Sca-1⁺/Lin⁻ cells per mL blood, the differences between antagomir-126 and scramble-mir-treated animals was lost, indicating that there is no systemic role for miR-126 in Sca-1⁺/Lin⁻ progenitor cell mobilization *in vivo* (Figure 2C).

Ischemic endothelial cells have been established to up regulate SDF-1⁷, which we confirmed *in vitro* in HUVEC under hypoxic conditions (data not shown). We investigated whether an ischemic stimulus in combination with attenuation of miR-126 levels would modulate progenitor cell levels in mice. Therefore, we injected male WT mice (n=6) with either antagomir-126 or scramble-mir and, the next day, this procedure was followed by the induction of unilateral hind limb ischemia (HLI). Ten days after induction of HLI, the animals were sacrificed and serum levels of SDF-1 were assessed by ELISA. Although systemic SDF-1 levels were elevated in antagomir-126-treated mice as compared to controls, no significance was reached (Figure 3A, P=0.19).

Nevertheless, when we examined the *in vivo* mobilization of Sca-1⁺/Lin⁻ cells to the circulation after ischemia, we observed an 8-fold increase of Sca-1⁺/Lin⁻ cells expressed as percentage of total Lin⁺ leukocytes in the blood of

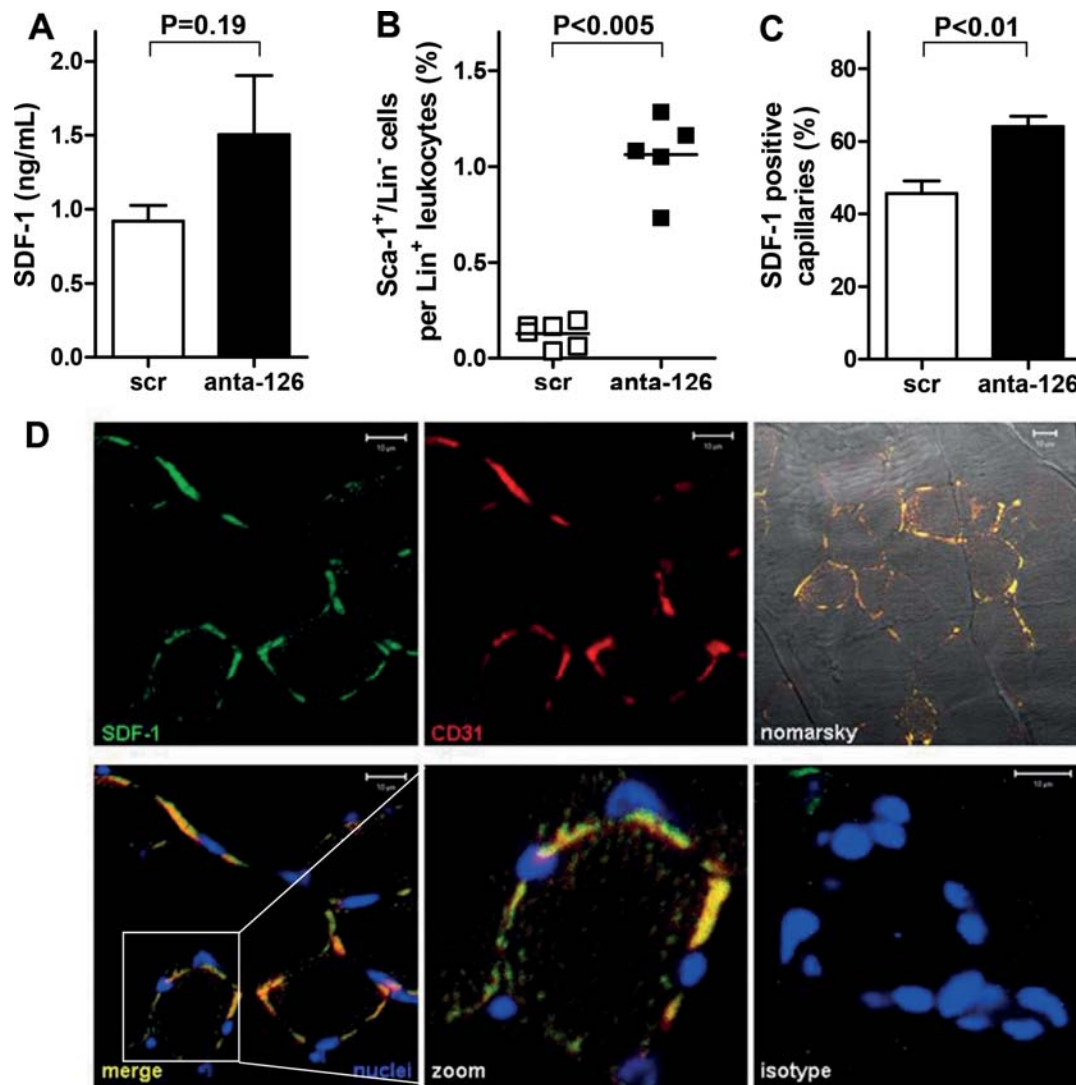
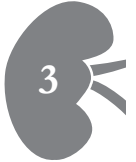


Figure 3. MiR-126 can alter SDF-1-expression and induce progenitor mobilization after ischemic injury in vivo. A, Ten days after HLI antagomir-126-treated mice showed non-significantly elevated levels of SDF-1 in the serum as compared to scramblemir-treated controls (n=6). B, Ten days after HLI and injection of scramblemir or antagomir-126, Sca-1⁺/Lin⁻ cells were measured in whole blood, expressed as percentage of total Lin⁺ leukocytes C, Immunohistochemical micrographs of immunohistochemistry of the gastrocnemius muscle after HLI showed colocalization of SDF-1 and CD31. SDF-1 was visualized with alexa-488 (green) and CD31 with alexa-568 (red). Nuclei were stained with DAPI and shown in blue, Nomarsky contrast images show muscle tissue. Scale bars represent 10 μ m. D, Quantification of microscopic images displayed that antagomir-126-treated mice have increased levels of SDF-1 positive capillaries as percentage of total number of capillaries (n=6).

antagomir-126-treated animals as compared to scramblemir-treated control animals (Figure 3B, $P < 0.005$). The absolute number of Sca-1⁺/Lin⁻ cells per mL blood was raised from 0.24 ± 1.4 in the control group to 2.1 ± 1.4 in the antagomir-126 treated animals. As the observed effects suggested an ischemia-dependent elevation of SDF-1, we next investigated whether the ischemic gastrocnemius muscle could be a potential contributor to the elevated levels of circulating SDF-1. Therefore, we performed both detailed qualitative and quantitative immunohistochemical analysis of SDF-1 expression in relation to CD31-positive capillaries. Indeed, we observed a clear co-localization of SDF-1 and CD31 expression in sections of the ischemic muscle (Figure 3D). Furthermore, the ischemic muscle of antagomir-126-treated animals showed a higher percentage of double-positive capillaries (Figure 3C, $P < 0.01$) as opposed to scramblemir-treated controls. These data imply that the mildly elevated levels of SDF-1 protein in the circulation upon antagomir-126-treatment may be a reflection of the locally enhanced expression of SDF-1 protein in the vessels of ischemic tissue.



Discussion

A function for miR-126 in angiogenic processes in vascular maintenance and during development has been shown in a number of publications demonstrating that loss of miR-126, either in knockout models or mediated by treatment with antagomirs, leads to structural impairment of the vascular bed²²⁻²⁴. In the current study, we provide evidence for a vasculogenic role for miR-126 in regulating the mobilization of endothelial progenitor cells via the release of chemokine SDF-1 from ischemic endothelial cells. *In vitro*, the increased secretion of SDF-1 upon silencing of miR-126 was sufficient to stimulate the migration of human CD34⁺ stem cells. In mice however, systemic silencing with a single tail vein injection of antagomir-126 was not sufficient to raise the levels of circulating murine Sca-1⁺/Lin⁻ progenitor cells. However, in combination with the ligation of the femoral artery, we demonstrated an increase in circulating Sca-1⁺/Lin⁻ cells following miR-126 silencing, strongly suggesting that tissue ischemia is needed to reveal the regulatory role of miR-126 *in vivo*.

Our data suggest that elevated numbers of circulating Sca-1⁺/Lin⁻ cells in the antagomir-treated animals are the result of SDF-1 mediated mobilization of these cells following ischemia. This is supported by the fact that SDF-1-protein expression is also up regulated in the endothelial cells of the ischemic tissue as well as in the peripheral circulation. Nevertheless, definitive proof of a causal role of miR-126 in SDF-1 dependent mobilization of progenitor cells would require an *in vivo* blockade in the SDF-1/CXCR4 axis. For this, inhibitors of the interaction of SDF-1 with CXCR4, such as AMD3100, could be administered to antagomir-126 treated mice and used to alleviate the elevated progenitor cell mobilization following ischemia. This approach is however complicated by the direct effects of these inhibitors on the egress of progenitor cells from the bone marrow which could potentially override the SDF-1 effects elicited by the endothelium in the ischemic tissues in the periphery²⁸. Also, impaired progenitor homing to the ischemic tissue or the spleen cannot be fully excluded²⁹.

An interaction between miR-126 and SDF-1 has previously been shown to increase miR-126 uptake of endothelial cell-derived apoptotic bodies by endothelial cells. This resulted in increased SDF-1 expression through inhibition of Regulator of G-protein signaling 16 (RGS16)³⁰. In contrast, our studies implicate that the abrogation of miR-126 is associated with increased expression of SDF-1, suggesting that miRNAs could serve as a biological

rheostat, with the response magnitude of biological pathways being dependent on the context and source of the external stimulus.

Recently, it has been demonstrated that miRNAs are present in the circulation and that alterations in the profile of plasma or serum miRNAs can be associated with disease states^{31,32}. These early reports mainly displayed a link between circulating miRNAs and cancer, while subsequent studies have also revealed a clear association of circulating miRNAs with cardiovascular disease³³⁻³⁵. Since endothelial injury is considered one of the hallmarks of patients at risk for cardiovascular disease and, upon injury, endothelial cells can secrete miRNA-containing microvesicles³⁶⁻³⁸, it is of interest to address the value of endothelial cell-derived circulating miRNAs as biomarkers for cardiovascular disease. Indeed, two recent clinical studies revealed a decrease in circulating miR-126 levels in patients with coronary artery disease (CAD)³⁹ and diabetes mellitus 2 (DM2)⁴⁰. It was suggested that lowered levels of miR-126 in DM2 patients might be explained by the fact that high glucose levels can lead to a decrease of the miR-126 content in the endothelial particles, while cellular miRNA levels remained unaltered⁴⁰. One may speculate that lowering of circulating miR-126 levels might be a specific signal of the injured

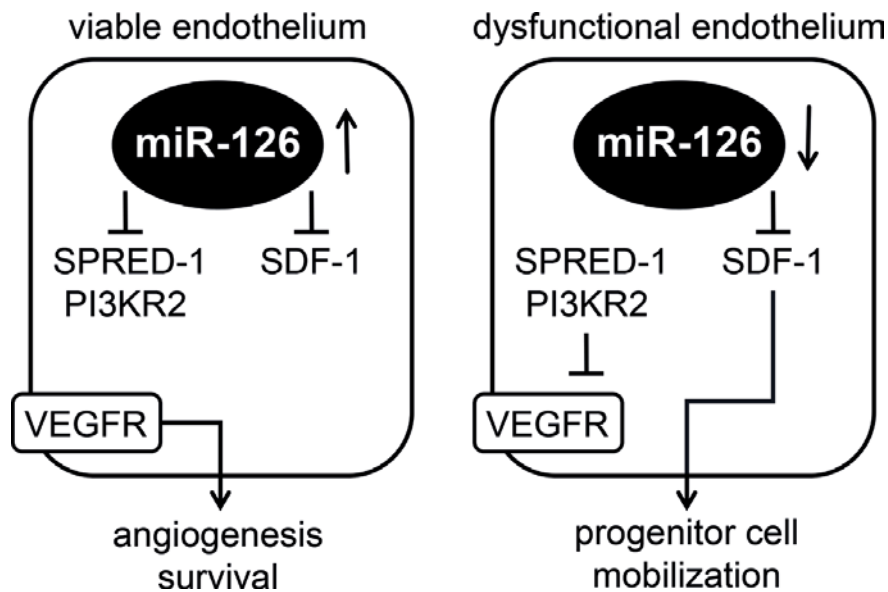


Figure 4. MiR-126 acts as a vasculogenic switch. In viable endothelium miR-126 inhibits the expression of SPRED-1 and PI3KR2 thereby facilitating VEGF-dependent angiogenesis. Furthermore, the expression of SDF-1 and VCAM-1 are inhibited. When miR-126 is lost, SPRED-1 and PI3KR2 are up regulated thereby blocking angiogenesis, at the same time SDF-1 and VCAM-1 levels are up regulated and this elevation subsequently leads to an increased mobilization and adhesion of bone marrow derived progenitors.

endothelium to increase the expression levels of distinct miR-126 targets that are critical for the integrity of the endothelium.

We suggest here that miR-126 functions as a regulator of endothelial homeostasis (Figure 4). In the healthy, viable endothelium, miR-126 is readily expressed and serves to down regulate SPRED-1 and PI3KR2, both of which are inhibitors of angiogenic and cell survival signals in response to vascular endothelial cell growth factor (VEGF)^{22,24}. This condition favors the angiogenic response to injury, as SDF-1 expression is concomitantly repressed by miR-126. On the other hand, under conditions associated with endothelial cell dysfunction or senescence, a decrease in miR-126 levels would inhibit angiogenic and cell survival signals. Furthermore, this condition favors the expression of SDF-1 and VCAM-1⁴¹ of the affected endothelial cells and support re-endothelialization by a vasculogenic response through the recruitment and subsequent adhesion of vascular progenitor cells. As bone marrow-derived CD34⁺ cells were recently demonstrated to represent a more functional EPC population than Sca-1⁺/Lin⁻ progenitor cells, future studies may include these progenitor cell population as well⁴².

Although speculative, our model is supported by the observed decreased levels of circulating miR-126 in DM2 and CAD patients^{39,40} and elevated levels of SDF-1 in patients with acute coronary syndrome (ACS)⁴³. Future studies in patient cohorts will provide insight as to whether the down regulation of circulating miR-126 can be correlated with increased levels of SDF-1.

In conclusion, both *in vitro* and *in vivo*, miR-126 can regulate the expression of SDF-1 in endothelial cells, which may lead to the mobilization of Sca-1⁺/Lin⁻ progenitor cells into the peripheral circulation following conditions of acute ischemia. As the endothelial miR-126 regulates both features of angiogenesis as well as vasculogenesis, a regulatory role for this miRNA in endothelial homeostasis is proposed.

Acknowledgements

CvS is supported by the Netherlands Heart Foundation (grant number 2006B145). MM and RB are supported by the Dutch Kidney Foundation (grant number C08.2282 and C07.2227 respectively). EvdV is supported by the Translational Excellence in Regenerative Medicine (TeRM) Smart Mix Program of the Netherlands Ministry of Economic Affairs and the Netherlands Ministry of Education, Culture and Science. AJvZ is supported by a grant from the Genzyme Renal Innovations Program.

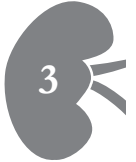
References

1. Rabelink, T.J., de Boer, H.C. & van Zonneveld, A.J. Endothelial activation and circulating markers of endothelial activation in kidney disease. *Nature reviews. Nephrology* 6, 404-414 (2010).
2. Schwartz, S.M. & Benditt, E.P. Clustering of replicating cells in aortic endothelium. *Proceedings of the National Academy of Sciences of the United States of America* 73, 651-653 (1976).
3. Kurz, D.J., et al. Chronic oxidative stress compromises telomere integrity and accelerates the onset of senescence in human endothelial cells. *Journal of cell science* 117, 2417-2426 (2004).
4. Op den Buijs, J., et al. Mathematical modeling of vascular endothelial layer maintenance: the role of endothelial cell division, progenitor cell homing, and telomere shortening. *American journal of physiology. Heart and circulatory physiology* 287, H2651-2658 (2004).
5. Foteinos, G., Hu, Y., Xiao, Q., Metzler, B. & Xu, Q. Rapid endothelial turnover in atherosclerosis-prone areas coincides with stem cell repair in apolipoprotein E-deficient mice. *Circulation* 117, 1856-1863 (2008).
6. Asahara, T., et al. VEGF contributes to postnatal neovascularization by mobilizing bone marrow-derived endothelial progenitor cells. *The EMBO journal* 18, 3964-3972 (1999).
7. Yamaguchi, J., et al. Stromal cell-derived factor-1 effects on ex vivo expanded endothelial progenitor cell recruitment for ischemic neovascularization. *Circulation* 107, 1322-1328 (2003).
8. Massberg, S., et al. Platelets secrete stromal cell-derived factor 1alpha and recruit bone marrow-derived progenitor cells to arterial thrombi in vivo. *The Journal of experimental medicine* 203, 1221-1233 (2006).
9. Hattori, K., Heissig, B. & Rafii, S. The regulation of hematopoietic stem cell and progenitor mobilization by chemokine SDF-1. *Leukemia & lymphoma* 44, 575-582 (2003).
10. de Boer, H.C., et al. Human CD34+/KDR+ cells are generated from circulating CD34+ cells after immobilization on activated platelets. *Arteriosclerosis, thrombosis, and vascular biology* 31, 408-415 (2011).
11. Hiasa, K., et al. Gene transfer of stromal cell-derived factor-1alpha enhances ischemic vasculogenesis and angiogenesis via vascular endothelial growth factor/endothelial nitric oxide synthase-related pathway: next-generation chemokine therapy for therapeutic neovascularization. *Circulation* 109, 2454-2461 (2004).
12. Askari, A.T., et al. Effect of stromal-cell-derived factor 1 on stem-cell homing and tissue regeneration in ischaemic cardiomyopathy. *Lancet* 362, 697-703 (2003).
13. Tepper, O.M., et al. Adult vasculogenesis occurs through in situ recruitment, proliferation, and tubulization of circulating bone marrow-derived cells. *Blood* 105, 1068-1077 (2005).
14. Kloosterman, W.P. & Plasterk, R.H. The diverse functions of microRNAs in animal development and disease. *Developmental cell* 11, 441-450 (2006).
15. Xie, X., et al. Systematic discovery of regulatory motifs in human promoters and 3' UTRs by comparison of several mammals. *Nature* 434, 338-345 (2005).
16. Urbich, C., Kuehbach, A. & Dimmeler, S. Role of microRNAs in vascular diseases, inflammation, and angiogenesis. *Cardiovascular research* 79, 581-588 (2008).
17. Kuehbach, A., Urbich, C., Zeiher, A.M. & Dimmeler, S. Role of Dicer and Drosha for endothelial microRNA expression and angiogenesis. *Circulation research* 101, 59-68 (2007).
18. Fasanaro, P., et al. MicroRNA-210 modulates endothelial cell response to hypoxia and inhibits the receptor tyrosine kinase ligand Ephrin-A3. *The Journal of biological chemistry* 283, 15878-15883 (2008).
19. Chen, Y. & Gorski, D.H. Regulation of angiogenesis through a microRNA (miR-130a) that down-regulates antiangiogenic homeobox genes GAX and HOXA5. *Blood* 111, 1217-1226 (2008).



20. Suarez, Y., Fernandez-Hernando, C., Pober, J.S. & Sessa, W.C. Dicer dependent microRNAs regulate gene expression and functions in human endothelial cells. *Circulation research* 100, 1164-1173 (2007).
21. Poliseno, L., et al. MicroRNAs modulate the angiogenic properties of HUVECs. *Blood* 108, 3068-3071 (2006).
22. Fish, J.E., et al. miR-126 regulates angiogenic signaling and vascular integrity. *Developmental cell* 15, 272-284 (2008).
23. van Solingen, C., et al. Antagomir-mediated silencing of endothelial cell specific microRNA-126 impairs ischemia-induced angiogenesis. *Journal of cellular and molecular medicine* 13, 1577-1585 (2009).
24. Wang, S., et al. The endothelial-specific microRNA miR-126 governs vascular integrity and angiogenesis. *Developmental cell* 15, 261-271 (2008).
25. Fontijn, R., et al. Maintenance of vascular endothelial cell-specific properties after immortalization with an amphotrophic replication-deficient retrovirus containing human papilloma virus 16 E6/E7 DNA. *Experimental cell research* 216, 199-207 (1995).
26. Jaffe, E.A., Nachman, R.L., Becker, C.G. & Minick, C.R. Culture of human endothelial cells derived from umbilical veins. Identification by morphologic and immunologic criteria. *The Journal of clinical investigation* 52, 2745-2756 (1973).
27. van Weel, V., et al. Vascular endothelial growth factor overexpression in ischemic skeletal muscle enhances myoglobin expression in vivo. *Circulation research* 95, 58-66 (2004).
28. Devine, S.M., et al. Rapid mobilization of functional donor hematopoietic cells without G-CSF using AMD3100, an antagonist of the CXCR4/SDF-1 interaction. *Blood* 112, 990-998 (2008).
29. Zhao, X., et al. The spleen recruits endothelial progenitor cell via SDF-1/CXCR4 axis in mice. *J Recept Signal Transduct Res* 30, 246-254 (2010).
30. Zerneck, A., et al. Delivery of microRNA-126 by apoptotic bodies induces CXCL12-dependent vascular protection. *Sci Signal* 2, ra81 (2009).
31. Mitchell, P.S., et al. Circulating microRNAs as stable blood-based markers for cancer detection. *Proceedings of the National Academy of Sciences of the United States of America* 105, 10513-10518 (2008).
32. Lawrie, C.H., et al. Detection of elevated levels of tumour-associated microRNAs in serum of patients with diffuse large B-cell lymphoma. *Br J Haematol* 141, 672-675 (2008).
33. Ji, X., et al. Plasma miR-208 as a biomarker of myocardial injury. *Clin Chem* 55, 1944-1949 (2009).
34. Corsten, M.F., et al. Circulating MicroRNA-208b and MicroRNA-499 reflect myocardial damage in cardiovascular disease. *Circ Cardiovasc Genet* 3, 499-506 (2010).
35. Ai, J., et al. Circulating microRNA-1 as a potential novel biomarker for acute myocardial infarction. *Biochem Biophys Res Commun* 391, 73-77 (2010).
36. Sapet, C., et al. Thrombin-induced endothelial microparticle generation: identification of a novel pathway involving ROCK-II activation by caspase-2. *Blood* 108, 1868-1876 (2006).
37. Combes, V., et al. In vitro generation of endothelial microparticles and possible prothrombotic activity in patients with lupus anticoagulant. *The Journal of clinical investigation* 104, 93-102 (1999).
38. Boulanger, C.M., et al. In vivo shear stress determines circulating levels of endothelial microparticles in end-stage renal disease. *Hypertension* 49, 902-908 (2007).
39. Fichtlscherer, S., et al. Circulating microRNAs in patients with coronary artery disease. *Circulation research* 107, 677-684 (2010).
40. Zampetaki, A., et al. Plasma microRNA profiling reveals loss of endothelial miR-126 and other microRNAs in type 2 diabetes. *Circulation research* 107, 810-817 (2010).

41. Harris, T.A., Yamakuchi, M., Ferlito, M., Mendell, J.T. & Lowenstein, C.J. MicroRNA-126 regulates endothelial expression of vascular cell adhesion molecule 1. *Proceedings of the National Academy of Sciences of the United States of America* 105, 1516-1521 (2008).
42. Yang, J., et al. CD34+ cells represent highly functional endothelial progenitor cells in murine bone marrow. *PLoS One* 6, e20219 (2011).
43. Stellos, K., et al. Expression of stromal-cell-derived factor-1 on circulating platelets is increased in patients with acute coronary syndrome and correlates with the number of CD34+ progenitor cells. *Eur Heart J* 30, 584-593 (2009).



Chapter

4

J Am Soc Nephrol, in press

Hematopoietic microRNA-126 protects against renal ischemia/reperfusion injury by promoting vascular integrity

Roel Bijkerk^{1,2*}, Coen van Solingen^{1,2*}, Hetty C. de Boer^{1,2}, Pieter van der Pol¹, Meriem Khairoun¹, Ruben G. de Bruin^{1,2}, Annemarie M. van Oeveren-Rietdijk^{1,2}, Ellen Liewers¹, Nicole Schlagwein¹, Danielle J. van Gijlswijk¹, Marko K. Roeten^{1,2}, Zeinab Neshati³, Antoine A.F. de Vries³, Mark Rodijk⁴, Karin Pike-Overzet⁴, Yascha W. van den Berg^{2,5}, Henri H. Versteeg^{2,5}, Marlies E.J. Reinders¹, Frank J.T. Staal⁴, Cees van Kooten¹, Ton J. Rabelink^{1,2} and Anton Jan van Zonneveld^{1,2}

¹Department of Nephrology and the ²Eindhoven Laboratory for Experimental Vascular Medicine, ³Department of Cardiology, ⁴Department of Immunohematology and Blood Transfusion, ⁵Department of Thrombosis and Haemostasis, LUMC, Leiden, The Netherlands. *R.B. and C.V.S. contributed equally to this work.

Abstract

Ischemia/reperfusion injury (IRI) is a central phenomenon in kidney transplantation and acute kidney injury. Integrity of the renal peritubular capillary network is an important limiting factor in the recovery from IRI. MicroRNA-126 (miR-126) facilitates vascular regeneration by acting as an angiomiR and by modulating mobilization of hematopoietic stem/progenitor cells. We hypothesized that overexpression of miR-126 in the hematopoietic compartment could protect the kidney against IRI via preservation of microvascular integrity. Here we demonstrate that hematopoietic overexpression of miR-126 increased neovascularization of subcutaneously implanted matrigel plugs in mice confirming its provasculogenic effects. Following renal IRI, mice overexpressing miR-126 display a marked decrease in urea levels, weight loss, fibrotic markers and injury markers such as KIM-1 and NGAL. This protective effect is associated with a higher density of the peritubular capillary network in the corticomedullary junction and increased numbers of bone marrow-derived endothelial cells. Hematopoietic overexpression of miR-126 increases the number of circulating Lin⁻/Sca-1⁺/cKit⁺ hematopoietic stem and progenitor cells. In addition, miR-126 overexpression attenuates CXCR4 expression on Lin⁻/Sca-1⁺/cKit⁺ cells in the bone marrow and increases renal expression of its ligand SDF-1, thus favoring mobilization of Lin⁻/Sca-1⁺/cKit⁺ cells towards the kidney. Taken together, overexpression of miR-126 in the hematopoietic compartment is associated with SDF-1/CXCR4-dependent vasculogenic progenitor cell mobilization and promotes vascular integrity and support recovery of the kidney following IRI.

Introduction

Ischemia/reperfusion injury (IRI) is a central event in clinical conditions such as acute kidney injury and organ transplantation and is strongly associated with delayed graft function and long-term graft survival.¹⁻³ Emerging evidence indicates that the renal microvascular endothelium of the outer medullary peritubular network is the primary site of injury in the pathogenesis of ischemia-induced renal dysfunction.⁴ Following ischemia, perfusion of the peritubular capillary network is rapidly impaired as a consequence of endothelial cell (EC) swelling,⁵ impaired vasorelaxation⁶ and increased leukocyte adhesion.⁷ In addition, microvascular destabilization initiated by the loss of EC-EC⁸ and EC-pericyte interactions can lead to significant reductions in peritubular capillary density due to microvascular rarefaction.^{8,9} The resulting loss in renal perfusion can further exacerbate medullary ischemia and drive the development of interstitial fibrosis by stimulation of pro-fibrogenic factors such as transforming growth factor- β (TGF- β).¹⁰ As a consequence, integrity of the peritubular capillary network is a key determinant for the preservation of renal function. Indeed, clinical biopsy studies have shown an association between loss of tubular structure and function on the one hand and capillary rarefaction on the other.^{11,12}

Due to their limited replicative capacity, renal ECs are thought to be insufficiently capable to completely repair the injured endothelium of the peritubular capillary plexus after IRI.^{13,14} Therefore, current therapeutic strategies to prevent microvascular loss have focused on the prevention of pericyte perturbation to reduce capillary rarefaction,¹⁵⁻¹⁸ However, once rarefaction has occurred, these strategies may fail to induce sufficient revascularization required to reverse renal dysfunction.¹⁹ In search of ways to augment neovascularization in the injured kidney many laboratories have investigated the biology and therapeutic use of circulating vascular progenitor cells originating from the bone marrow (BM) compartment.²⁰ These progenitor cells were shown to incorporate into the injured microvasculature in experimental models for glomerulonephritis,²¹ ischemic nephropathy^{22,23} and interstitial fibrosis.²⁴ This phenomenon has been particularly observed when extensive or repetitive endothelial injury occurs, for example in kidney transplantation.²⁵ Microvascular incorporation of BM-derived progenitor cells has been linked to preservation of the vasculature as they may serve as an alternative cellular source to facilitate re-endothelialization.²⁶ In addition, the CXCR4⁺ fraction of progenitor cells is mobilized to the ischemic kidney by local secretion of the chemokine stromal cell-derived factor-1 (SDF-1)^{23,27}



and has been shown to exert renoprotective effects in a paracrine fashion. PI3K/AKT signaling in progenitor cells plays a critical role in mobilization of progenitors from the BM via the SDF-1/CXCR4 axis²⁸ and their subsequent differentiation towards vascular cells.³⁰ MicroRNA-126 (miR-126) is a key regulator of PI3K/AKT signaling by direct targeting of the negative regulator PI3K regulatory subunit 2 (PI3KR2/p85- β) and targets genes that play key roles in angiogenesis and inflammation.²⁹⁻³¹ In addition, miR-126 was shown to co-regulate the expansion and mobilization of hematopoietic stem/progenitor cells.^{32, 33} We hypothesized that miR-126 overexpression in the hematopoietic compartment of mice can enhance the vasoprotective potential of these progenitors and this will translate to decreased renal injury.

Results

Generation of mice overexpressing miR-126 in the hematopoietic compartment

To investigate the pro-vasculogenic effect of miR-126, we generated mice overexpressing miR-126 in the hematopoietic compartment. To that end, mice were transplanted with lineage-negative enriched CD45.1⁺ BM cells transduced with a lentiviral vector (LV) driving the expression of miR-126 and dsRed under control of a constitutive human U6 and a phosphoglycerate kinase 1 (PGK1) promoter, respectively (Supplementary Figure 1). Eight weeks after transplantation, mice were sacrificed and blood and BM samples were obtained. Smears of peripheral blood (PB) and BM of transduced animals showed dsRed-positivity, confirming the successful transduction of the transplanted BM (Figure 1A). FACS analysis for the expression ratios between congenic markers CD45.1 (donor) and CD45.2 (acceptor) in PB and BM of the transplanted mice demonstrated high levels of chimerism (Figure 1B), as CD45.1 expression in the control group (LV-C) and miR-126 overexpression group (LV-126) was similar to CD45.1 expression in donor mice. Quantitative PCR (qPCR) confirmed a 5.1- (Figure 1C, $P < 0.001$) and 6.0-fold (Figure 1D, $P < 0.05$) higher expression level of miR-126 in BM and PB cells, respectively, in the LV-126 group compared to the LV-C group. Finally, confirming downstream effects of miR-126 over expression, we observed that mRNA levels of 7 out of 9 established miR-126 targets in total BM were reduced in the LV-126 group compared to LV-C controls (Supplementary Figure 2).

Hematopoietic overexpression of miR-126 increases neovascularization of subcutaneously implanted angiogenic matrigel plugs in mice

To assess the impact of hematopoietic overexpression of miR-126 on vasculogenesis, we performed *in vivo*, angiogenic matrigel plug assays. Therefore, 7 weeks after BM transplantation, matrigel plugs enriched with recombinant pro-angiogenic factors SDF-1 and vascular endothelial growth factor (VEGF), were subcutaneously implanted in the flanks of LV-126 and LV-C mice. After 7 days, the skin was opened to visualize the neovasculature of the implants by a sidestream dark field camera. Movies (Figure 2B) confirmed the ingrowth of functional neovasculature with active flow of red blood cells. To quantify the extent of neovascularization, microscopic images were taken from both sides of the angiogenic plugs. Figure 2A shows a panel of representative microphotographs, with arrowheads indicating the blood-filled microvascular structures that had formed in the matrigel plugs following



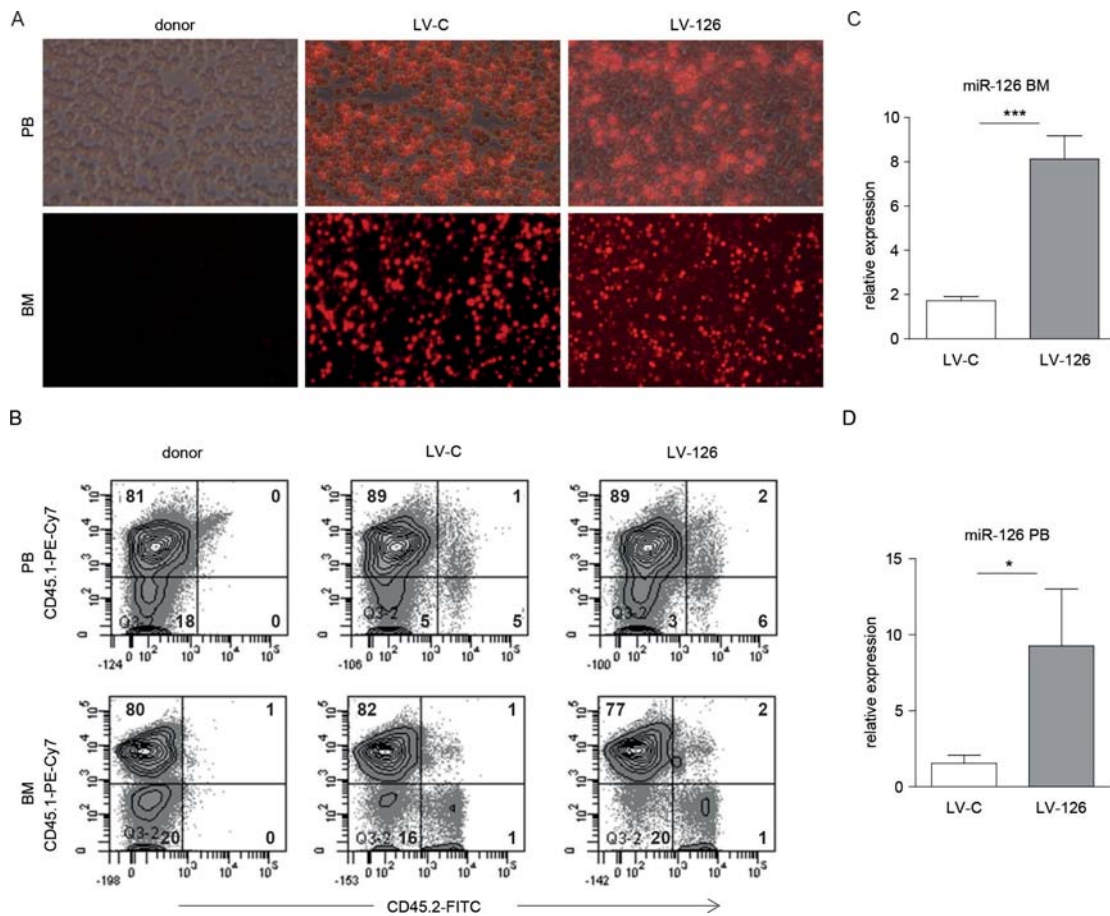


Figure 1. Overexpression of miR-126 and BM transplantation in vivo. (A) Microscopic images of peripheral blood (PB) and bone marrow (BM) smears show dsRed⁺ cells in animals transplanted with either LV-C or LV-126 when compared to cells of non-transplanted animals (donor). (B) Representative FACS plots demonstrate successful chimerism in PB and BM by CD45.1 (donor) and CD45.2 (acceptor) levels. Numbers represent percentage of cells in corresponding quadrant. qRT-PCR demonstrates significant upregulation of miR-126 levels in BM (C) and PB (D) of LV-126 mice when compared to LV-C mice.

implantation. Using these photographs we counted the number of vessels per matrigel implant and observed a nearly significant increase in the number of vessels in the LV-126 mice as compared to the LV-C animals (Figure 2C, $n=10$, $P=0.053$). Moreover, quantification of the total microvascular surface area revealed a significant increase (40%) in vascularization in the LV-126 mice (Figure 2D, $P<0.02$), which correlated directly with the levels of miR-126 expression in the BM of the mice (Figure 2E, $P=0.05$, $r^2 = 0.20$). Immunohistological analyses of the vascularized matrigel plugs (Figure 2F-G) demonstrated stabilized, maturing vessels and a profound infiltration of BM-derived, dsRed⁺ cells that overlap with staining for murine EC antigen-32

(MECA32) or von Willebrand Factor (vWF)(Figure 2F and Supplementary Figure 3A). Around the newly formed blood vessels, cells positive for platelet derived growth factor receptor β (PDGFR β) and neural/glial antigen 2 (NG2)(Figure 2G and Supplementary Figure 3B) were detected, which were also positive for dsRed, suggesting a BM origin.

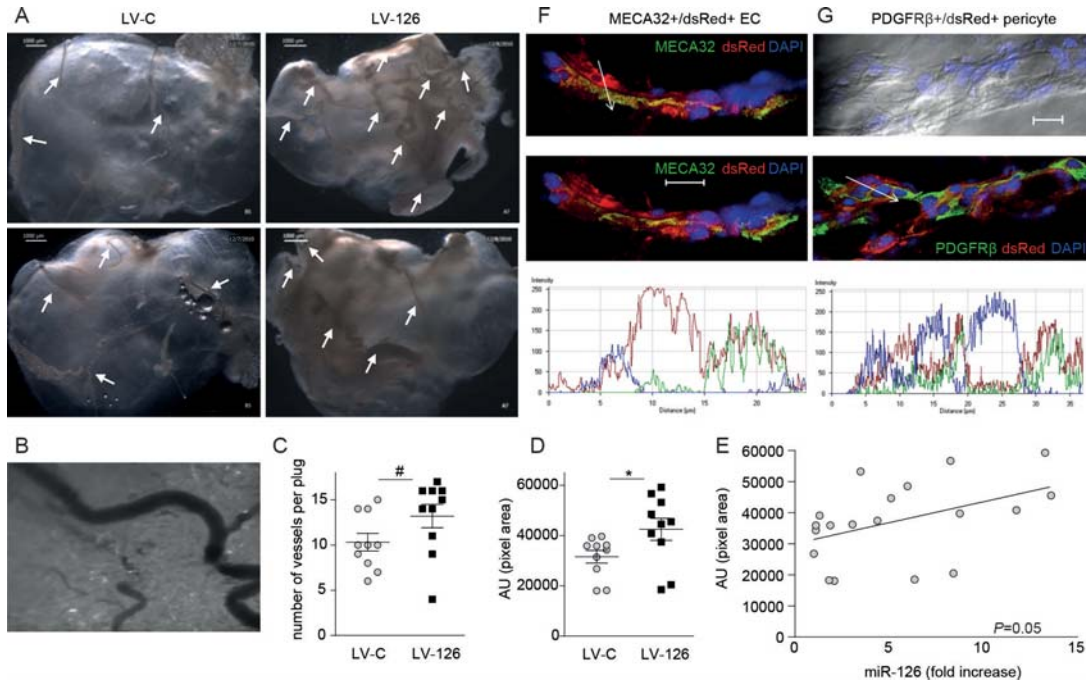


Figure 2. Overexpression of miR-126 in BM cells leads to increased neovascularization in subcutaneously implanted matrigel plugs. (A) Representative microscopic images of both sides of matrigel plugs seven days after implantation in LV-C mice (left micrographs) and LV-126 mice (right micrographs). Arrowheads point to neovascularization. (B) A movie still displaying the presence of red blood cells in the neovasculature of the matrigel plugs. (C) Quantification of the number of vessels per plug shows increased vascularization in animals transplanted with LV-126 BM with borderline significance ($P=0.053$). (D) Vessels were ‘digitalized’ and the total length (in pixel area) was quantified. LV-126 animals demonstrated a significantly higher vessel surface area as compared to LV-C animals. (E) Total surface area of plug-vessels correlates significantly with the expression levels of miR-126 in the BM ($P=0.05$). (F-G) Representative confocal images of a vessel and corresponding cross sectional profiles of fluorescent labels (colors correspond to images) stained for MECA32+/dsRed+ EC in 2 different planes (F) and stained for PDGFR β +/dsRed+ pericytes (G). * $P<0.01$, # $P<0.10$.

Our data indicate that overexpression of miR-126 in the hematopoietic compartment stimulates neovasculation of implanted matrigel plugs that possibly involves both BM-derived EC as well as BM-derived perivascular cells.

MiR-126 overexpression in the hematopoietic compartment protects against renal IRI

Given the observed pro-vasculogenic effects in mice overexpressing miR-126 in the hematopoietic compartment we hypothesized that these mice would be less susceptible to IRI due to an improved capacity to maintain renal microvascular integrity. To investigate this hypothesis, 8 weeks after BM transplantation, LV-126 and LV-C mice were subjected to bilateral renal ischemia and were sacrificed 3 days or 3 weeks after the procedure. Renal IRI resulted in extensive renal dysfunction in the LV-C mice as shown by increased blood levels of urea (Figure 3A). In contrast, mice overexpressing miR-126 were protected against renal dysfunction, with a moderate elevation in urea levels as compared to control mice. At 72 h after reperfusion this deterioration of renal function in the LV-C mice was accompanied by a significantly lower weight than the LV-126 mice (Figure 3B) and significantly lower mRNA levels of the tubular injury markers kidney injury molecule-1 (KIM-1) and neutrophil gelatinase-associated lipocalin (NGAL), pro-inflammatory markers interleukin-6 (IL-6) and chemokine (C-C motif) ligand 2 (CCL2), and upregulation of anti-inflammatory cytokine interleukin-10 (IL-10) (Figure 3C). In addition, analyses of post-IRI, H&E stained kidney sections revealed that mice in the LV-126 group displayed significantly less acute tubular necrosis (ATN) and tubular cast formation (rating 0-3) compared to the LV-C mice (Figure 3E). Direct immunohistochemical staining confirmed a markedly lower expression of tubular injury marker KIM-1 (2.6-fold) in the LV-126 group (Figure 3F, $P < 0.001$). Tubular injury after reperfusion was accompanied by extensive infiltration of CD45⁺ leukocytes (Figure 3G). However, overexpression of miR-126 did not reduce the total number of infiltrating leukocytes, neither did it affect the total number of F4/80⁺ macrophages (Figure 3H). In contrast, we did find a decrease in the presence of Gr1⁺ granulocyte count as a result of overexpression of miR-126 (Figure 3I). As miR-126 has been described to positively regulate mast cell proliferation and cytokine production,³⁴ we stained the sections with toluidine blue to determine the mast cell content of the kidneys, but could not observe any positive mast cell staining in the kidneys of either group (data not shown).

To determine whether the early protective effects observed in the LV-126 group also have beneficial effects on the longer-term fibrotic complications of IRI³⁵ we measured gene expression levels of fibrosis markers Collagen-1 α 1 (Col1 α 1), Collagen-3 α 1 (Col3 α 1) and TGF- β , and of the myofibroblast marker α -smooth muscle actin (α -SMA) in mice that were sacrificed 3 weeks after reperfusion. Indeed, we confirmed that expression of each of these

markers was significantly reduced in the kidneys from the LV-126 group compared to those of the LV-C mice (Figure 3D).

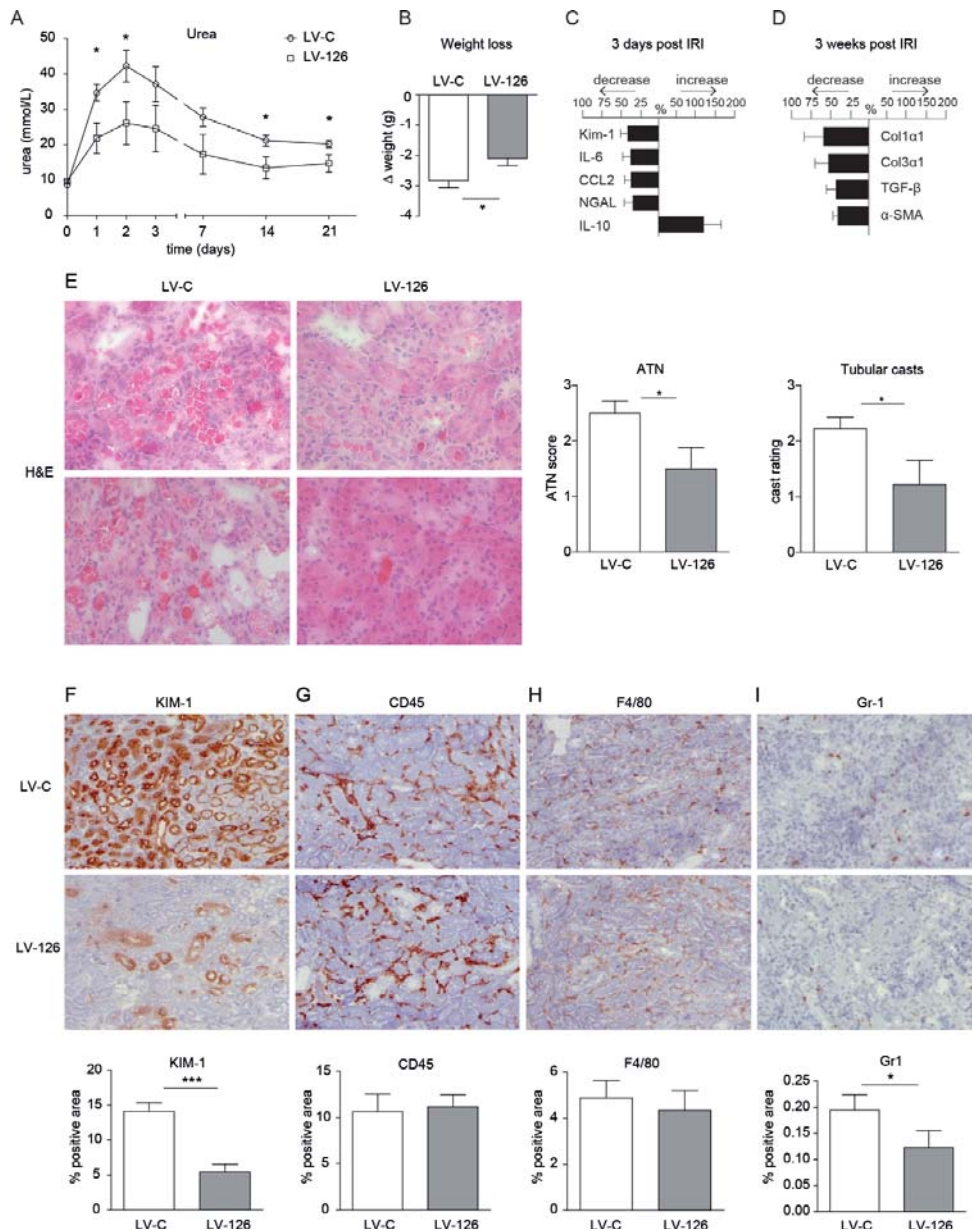


Figure 3. miR-126 protects against renal IRI. (A) miR-126 overexpression results in decreased blood urea levels after IRI. (B) miR-126 overexpression results in less weight loss 3 days after IRI. qRT-PCR analysis normalized on GAPDH mRNA levels of renal gene expression in LV-126 and LV-C mice of (C) KIM-1, NGAL, CCL2, IL-6 and IL-10 3 days after injury and (D) -SMA, col1a1, col3a1 and TGF-β 3 weeks after injury. Increase or decrease is relative to LV-C group. (E) Representative images of H&E staining on LV-C and LV-126 kidney sections. Graphs show quantification of ATN and cast score. (F-I) Representative images of staining for tubular damage (E, KIM-1), leukocytes (F, CD45), macrophages (G, F4/80) and neutrophils (H, Gr-1) 3 days after IRI. Graphs below images show quantification of staining results for all mice (n=10 per group).

Hematopoietic overexpression of miR-126 preserves capillary density after IRI and is associated with increased numbers of BM-derived peritubular capillary EC

To determine the impact of hematopoietic miR-126 overexpression on renal vascular integrity after IRI, we assessed the density of the peritubular capillary network by staining for MECA32 before and after IR. We focused on the corticomedullary junction since it is known that this region is disproportionately damaged by IRI.⁴ As shown in Figure 4A and 4E we observed that the density of MECA32⁺ peritubular capillaries in the LV-C mice was markedly decreased three days post-IR, while microvascular density was virtually maintained in the LV-126 mice (Figure 4G). Since both the control- and miR-126 viral vectors carried the dsRed reporter gene, BM-derived cells could be identified based on their dsRed positivity. Notably, a 2.2-fold increase was observed in the number of dsRed⁺ BM-derived cells in the kidneys of the LV-126 mice as compared to the LV-C group (Figure 4B and 4H). Importantly, this increase was IR-dependent, as the number of dsRed⁺ cells in the LV-126 mice in the non-IR group was comparable to that of the LV-C mice (Figure 4F-H). Since no differences were observed in the numbers of infiltrated CD45 leukocytes or the macrophage content between the two experimental IRI groups, we sought to determine the cell type that could be responsible for the increase in dsRed⁺ cells. Based on the interstitial localization of the dsRed⁺ cells we could exclude that they were tubular epithelial cells. Double staining of kidneys for dsRed and the endothelial marker CD31 demonstrated that a major fraction of the BM-derived dsRed⁺ cells were ECs (Figure 4C). Quantification of these BM-derived capillary EC (CD31⁺/dsRed⁺) showed a significant 2.0-fold increase ($P=0.04$) in the LV-126 group compared to the control group (Figure 4D).

Confocal imaging confirmed the presence of BM-derived ECs as we readily detected numerous dsRed⁺ cells co-staining for MECA32 integrated into networks of MECA32⁺/dsRed⁺ ECs (Figure 4I-K). In concordance with the results of the matrigel plug assay, also in the kidney we observed co-localization of dsRed and PDGFR β (Supplementary Figure 4). DsRed⁺CD31⁺ cells were also found in the endothelium of the larger vessels (Supplementary Figure 5A) and at a lower rate in the glomeruli of the LV-126 mice (Supplementary Figure 5B). We conclude that overexpression of miR-126 in the hematopoietic compartment aids to preserve the integrity of the renal microvasculature following IRI and associates with an increased incorporation of BM-derived cells into the vasculature.

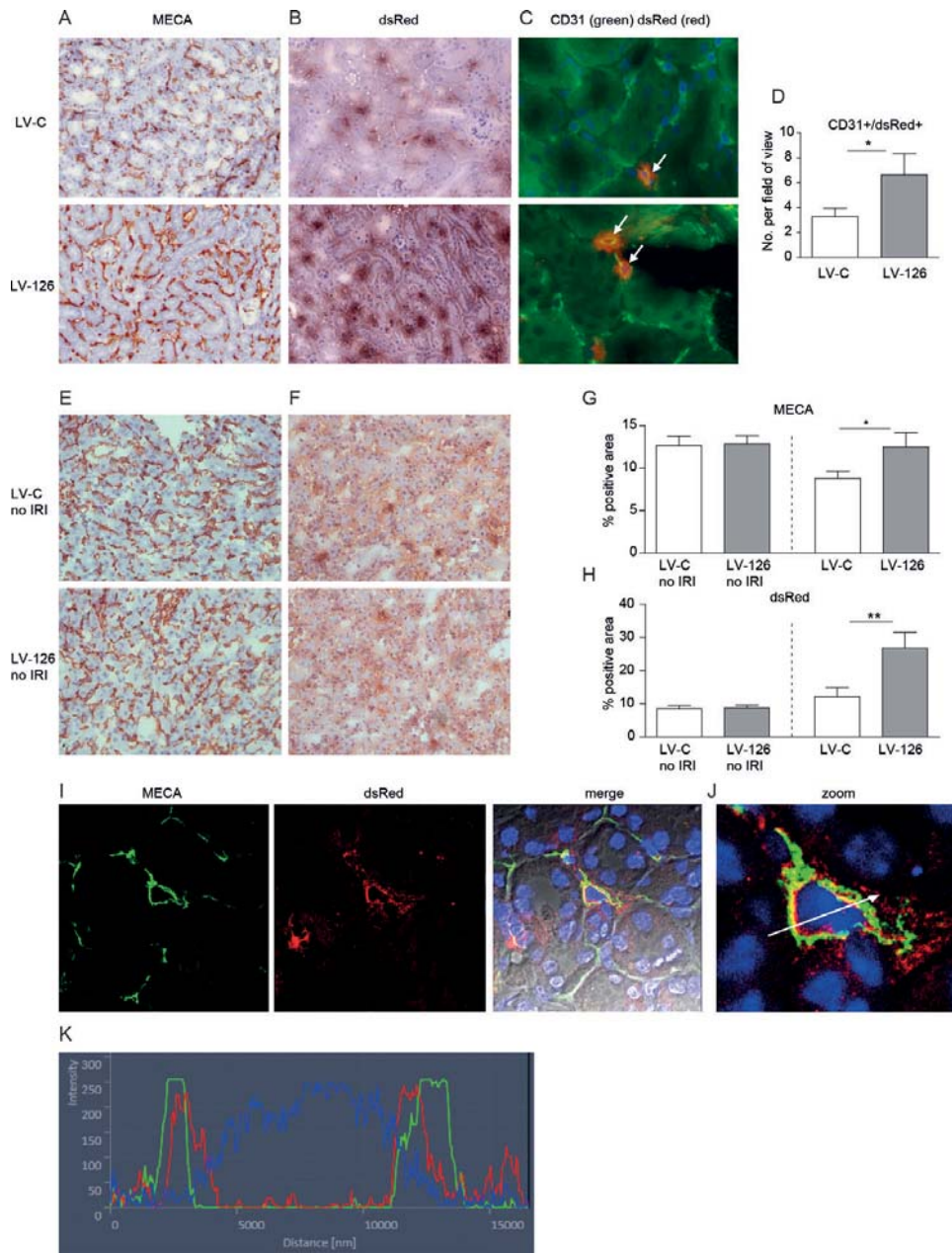


Figure 4. MiR-126 preserves capillary density by increasing incorporation of BM-derived EC. (A) Representative microscopic images and (G) quantification of MECA32 staining in corticomedullary junctions show higher capillary density in mice that overexpress miR-126 3 days after IRI. (B) Representative microscopic images and (H) quantification of dsRed staining in the kidney show increased dsRed signal in LV-126 mice. (C) Representative images showing CD31+/dsRed+ cells as indicated by arrows and (D) quantification shows higher numbers of BM-derived EC in the miR-126 group. (EF) Representative microscopic images and (GH) quantification of MECA32 and dsRed staining in corticomedullary junctions of non-ischemic kidney shows no differences as a result of miR-126 overexpression. (I) Confocal images confirm dsRed-positive ECs by MECA staining. (J) Zoomed image of dsRed+ EC and corresponding cross sectional profile of fluorescent labels (K, colors correspond to images) shows overlap of MECA32 and dsRed.

LV-126 mice display increased hematopoietic stem- and progenitor cell numbers in the circulation following IRI

After having shown the provasculogenic effects of BM miR-126 overexpression in the matrigel plug assay and in the kidney after IRI, we assessed the impact of miR-126 overexpression on the hematopoietic system itself. Therefore, a detailed comparison was performed of the composition of cells in the BM and in the circulation in LV-126 and LV-C mice (Supplementary Table 1 and 2). Little to no differences were observed in the number of white blood cells (WBCs), red blood cells (RBC), platelets (plt), hemoglobin (Hgb) or hematocrit (Hct) content between the two experimental groups in blood samples collected before and 4 and 8 weeks after BM transplantation. Also, no substantial differences were found in absolute numbers of T-cells, B-cells, NK-cells, plasmacytoid dendritic cells (pDCs), neutrophils or eosinophils. Since circulating myeloid cells are known to display pro-angiogenic properties³⁶ and we previously demonstrated that pro-angiogenic cells could be cultured from a BM-derived immature, CD31⁺/Ly6C^{hi} myeloid progenitor cell fraction³⁷, the monocytic cells were further subdivided into Ly6C^{hi}, Ly6C^{med} and Ly6C^{lo} fractions but again, no significant differences could be observed between the experimental groups. Next, we assessed the impact of overexpression of miR-126 on the number of Lin⁻/Sca-1⁺/cKit⁺ (LSK) and Lin⁻/Sca-1⁺/Flk⁺ (LSF) hematopoietic stem/progenitor cells in PB and BM, before (pre-IRI) and 3 days after kidney IRI. While the absolute numbers of circulating LSK (Figure 5A) or LSF cells (Figure 5B) before kidney IRI did not differ significantly between the experimental groups, three days after IRI, the LSK and LSF cells in PB were induced 2.5- and 1.5-fold respectively ($P < 0.05$ for both). Concomitant with their elevation in the circulation, BM-levels of the LSK and LSF cells were decreased, supporting enhanced mobilization of these cells from BM to the periphery after overexpression of miR-126.

Correlation analysis (Table 1) revealed a strong positive correlation between the expression level of miR-126 in the BM and LSK cell number in PB. The number of LSK cells correlated positively with capillary density (MECA staining) in the kidney, while strong negative correlations were observed with renal injury markers (urea, KIM-1, NGAL) further supporting that miR-126 is the driver of the observed protective effects.

CXCR4/SDF-1 signaling is affected in LV-126 mice after IRI

Since the mobilization of LSK and LSF cells was markedly increased in the LV-126 mice we sought to determine whether overexpression of miR-126 in the hematopoietic compartment was also associated with a shift in the balance between BM and peripheral SDF-1/CXCR4 signaling. As CXCR4

expression retains hematopoietic stem and progenitor cells in the BM and its inhibition can be employed to mobilize these cells from the BM,³⁸ we measured CXCR4 expression on BM-LSK cells using flow cytometry. Indeed, CXCR4 expression was selectively reduced on BM-LSK cells in the LV-126 group, while Lin⁺ cells showed an elevated expression of CXCR4

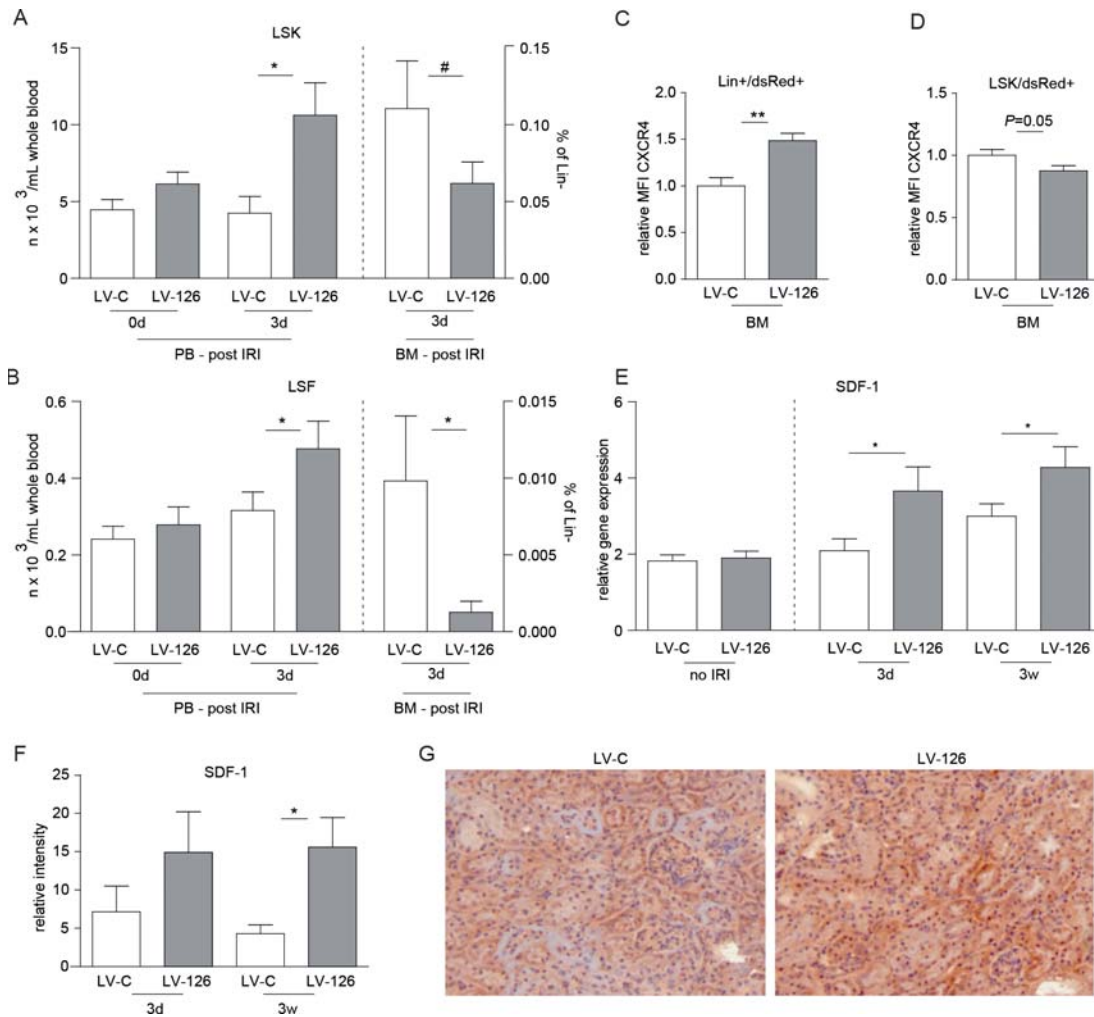


Figure 5. Overexpression of miR-126 results in increased hematopoietic stem/progenitor cell levels in PB and altered CXCR4/SDF-1 signaling. (A) FACS analysis of Lin⁻/Sca-1⁺/cKit⁺ (LSK) and (B) Lin⁻/Sca-1⁺/Flk⁺ (LSF) cells in PB and BM shows an increase of these circulating cells after injury after miR-126 overexpression. (C) FACS analysis on dsRed⁺/Lin⁺ cells shows an increased mean fluorescence intensity (MFI) for CXCR4 in LV-126 group, while (D) the dsRed⁺ LSK cells shows a decreased MFI for CXCR4 in LV-126 group. (E) qRT-PCR in kidneys shows increased SDF-1 mRNA levels in response to miR-126 overexpression in BM, while in non-ischemic kidneys this increase is absent. (F) Quantification and (G) representative microscopic images (3 days post IRI) of SDF-1 staining in kidney sections show increased SDF-1 expression in miR-126 overexpressing mice.

Table 1. Statistical analysis between different research indices. p=propability values; r= Spearman correlation coefficient. Values in bold are considered statistically significant (p<0.05).

	correlation	miR-126	LSK	LSF	urea	MECA	Kim1	Kim1	NGAL	dsRed
material		BM	PB	PB	serum	kidney	kidney	kidney	kidney	kidney
method		PCR	FACS	FACS		IHC	PCR	IHC	IHC	IHC
miR-126	p r		0.007 0.65	0.34 0.26	0.46 -0.20	0.53 0.20	0.65 -0.12	0.15 -0.38	0.36 -0.24	0.02 0.58
LSK PB	p r	0.007 0.65		0.004 0.64	0.020 -0.54	0.008 0.68	0.03 -0.52	0.04 -0.50	0.04 -0.50	0.03 0.51
LSF PB	p r	0.34 0.26	0.004 0.64		0.003 -0.66	0.001 0.77	0.0005 -0.74	0.03 -0.51	0.001 -0.73	0.76 0.08
MECA	p r	0.53 0.20	0.008 0.68	0.001 0.77	0.009 -0.67		0.002 -0.75	0.02 -0.61	0.001 -0.77	0.96 -0.02

(Figure 5C-D). This relative loss of CXCR4 expression on LSK cells in miR-126 overexpressing BM (Figure 5D) may cause the selective mobilization of these cells to the periphery (Figure 5A). On the other hand, recruitment of hematopoietic stem and progenitor cells to ischemic tissue is dependent on SDF-1 expression at the site of injury.^{27, 39} As shown in Figure 5, in the tubuli of post-ischemic kidneys of LV-126 mice, both SDF-1 mRNA (5E) and protein expression (5F-G) were increased as compared to the LV-C mice both 3 days as well as 3 weeks after IRI, while SDF-1 mRNA expression levels were not changed in non-ischemic kidneys.

Discussion

Here we describe that overexpression of miR-126 in the hematopoietic compartment augments neovascularization in subcutaneously implanted matrigel plugs and protects the kidney from IRI. Protection of the kidney and vascular integrity correlated significantly with the levels of circulating vascular progenitor cells. In its turn, mobilization of LSK cells and the integration of dsRed⁺ cells in the renal microvascular network in the LV-126 mice were directly related to BM miR-126 expression levels. Therefore, our data support a direct causal role for miR-126 augmented vasculogenesis leading to the preservation of renal function following IRI.

One mechanism by which miR-126 augments vasculogenesis is by selectively enhancing the mobilization of potentially vasculogenic stem and progenitor cells. Elevated SDF-1 expression by the kidney following IRI is known to be a main driver of the homing of BM-derived progenitor cells to the injured kidney by altering the balance of SDF-1 expression from the BM to the periphery.^{27, 39, 40} However, it has been demonstrated that plasma elevation of SDF-1 also mobilizes Lin⁺ leukocytes.⁴¹ In our study, detailed flow cytometric analyses of the circulating hematopoietic cells in the LV-126 mice demonstrated selective mobilization of LSK and LSF cells in response to elevated SDF-1 expression by the ischemic kidney. A possible explanation for this observation could be that, in the BM, only the LSK cells displayed lower CXCR4 expression while the lineage-positive leukocytes expressed increased levels of CXCR4 and therefore would have a higher propensity to be retained in the BM.³⁸

Several studies have described a regulatory role for miR-126 in SDF-1/CXCR4 signaling. MiR-126 was shown to target SDF-1 directly^{33, 42} but also indirectly via targeting regulator of G protein signaling 16 (RGS16), a negative regulator of CXCR4 function. Silencing of RGS16 is thought to stimulate an autoregulatory feedback loop that increases the production of SDF-1.⁴³ Silencing of RGS16 by miR-126 could provide a mechanism for the elevated renal epithelial SDF-1 expression by the LV-126 mice. Although speculative, miR-126 could be increased in the tubular epithelial cells by lateral transfer through the fusion of miR-126 rich, blood cell derived microvesicles as it was recently described that injection of endothelial progenitor cell (EPC)-derived miR-126 rich microparticles exerted a protective effect in IRI.⁴⁴ Alternatively, the increased number of BM-derived EC that line the microvascular network of the kidney of the LV-126 mice could serve as a source of miR-126 via the production of microparticles,⁴⁵ as it was recently shown that, under certain



conditions, such particles can cross the tubular basement membrane.⁴⁶ In addition, activated platelets may be involved as miR-126 is among the most abundant miRNAs in platelets^{47,48} and they could serve as transporter of miR-126 to the site of injury⁴⁹. As EPCs can take up platelets and their molecular content⁵⁰, platelets could also add to EPC function through miR-126 transfer. Furthermore, platelets have been shown to constitute a rich source of local SDF-1 deposition themselves⁵¹.

We propose that preservation of the capillary density in the LV-126 kidneys following IR is a major contributor to the protected kidney function in the LV-126 mice. As this maintenance of vascular integrity after IR is associated with an enhanced incorporation of BM-derived dsRed⁺ endothelial cells and pericytes we propose that overexpression of miR-126 in the hematopoietic compartment improves microvascular repair as compensation for the loss of capillaries. In addition, BM-derived EC and/or perivascular cells that had already been incorporated into the kidneys prior to IRI, could be more resistant to injury due to miR-126 dependent enhancement of pro-survival AKT signaling^{30,31} and therefore add to the protection after IRI.

Next to the effects on their mobilization, hematopoietic overexpression of miR-126 could also have direct beneficial effects on the function of vasculogenic stem and progenitor cells via its actions on AKT signaling.^{29-31,52} For instance, it was recently shown in preeclampsia that miR-126 modulates the proangiogenic properties of EPC through targeting PI3KR2,⁵³ which also appears to be affected in our study (Supplementary Figure 2). Augmenting AKT signaling in vascular progenitor cells could be particularly relevant in kidney disease as most patients are characterized by a state of EPC dysfunction.^{54,55} In addition, kidney graft function and the use of immunosuppressants were shown to directly affect EPC number and survival.⁵⁶⁻⁵⁸

In addition to BM-derived EC, we observed dsRed⁺ cells expressing the pericyte marker PDGFR β in the matrigel plug. Furthermore, a subpopulation of dsRed⁺ cells in the kidney were shown to be most likely pericytes. This suggests that also pericytes originated from BM. Support for this notion is emerging in literature, where the role of BM-derived pericytes is increasingly discussed.^{59,60}

Taken together, we demonstrate that enhancing the vasculogenic potential by overexpression of miR-126 in the hematopoietic compartment protects the kidney from IRI further confirming the critical role of EC integrity in the progression of kidney disease. Therefore, strategies aimed at improvement of the endogenous vasculogenic potential such as described in this study would not only enhance the mobilization of the vasculogenic progenitors to the injured kidney but may also correct EPC dysfunction in renal disease.



Materials and Methods

Mice

C57BL/6J wild type (WT; CD45.2⁺) and B6.SJL-Ptprca Pepcb/BoyCrl (CD45.1⁺) mice were obtained from Charles River (Maastricht, the Netherlands). All animal experimental protocols were approved by the animal welfare committee of the Leiden University Medical Center.

Lentiviral vectors

Stable expression of miR-126 in BM-derived Lin⁻ cells was accomplished using the vesicular stomatitis virus (VSV) G protein-pseudotyped self-inactivating human immunodeficiency virus type 1 (HIV1)-based vector LV.hU6.miRNA-126.hPGK1.DsRed.T4. In the shuttle plasmid for generating this vector, the coding sequence of murine miRNA-126 is preceded by the human U6 gene promoter and followed by a reporter gene cassette consisting of the human phosphoglycerate kinase 1 (hPGK1) gene promoter and the coding sequence of a rapidly maturing variant of the red fluorescent protein of *Discosoma spec.* (Supplementary Figure 1A).⁶¹ The shuttle plasmid encoding the control vector LV.hPGK1.DsRed.T4 has the same genetic makeup as LV.hU6.miRNA-126.hPGK1.DsRed.T4 except for the absence of the human U6 gene promoter and murine miRNA-126-coding sequence (Supplementary Figure 1A). LV particles were produced in 293T cells with the aid of the packaging plasmids psPAX2 (Addgene, Cambridge, MA, USA) and pLP/VSVG (Invitrogen, Breda, the Netherlands) essentially as previously described.⁶² At 48 h after the start of the transfection, the culture fluid was collected and freed of cellular debris by centrifugation at room temperature for 10 min at 825×g followed by filtration through a 0.45-μm pore-sized cellulose acetate filter (Pall, Port Washington, NY, USA). To concentrate the LV particles, 5 ml of 20% (wt/vol) sucrose (Merck, Whitehouse Station, NJ, USA) in phosphate-buffered saline (PBS) was carefully layered under 30 ml of the cleared culture medium, which was then centrifuged for 2 h at 15,000 rotations per minute for 2 h at 10°C in an SW28 rotor (Beckman Coulter, Woerden, the Netherlands). Next, the supernatant was discarded and the pellet containing the LV particles was suspended in 500 μl of PBS-1% bovine serum albumin (BSA; Sigma-Aldrich, St. Louis, MO, USA) by gentle rocking overnight at 4°C.

Transduction and transplantation of BM cells

BM cells were isolated from the femora and tibia of CD45.1⁺ mice and were enriched for Lin⁻ cells using a Lineage Cell Depletion Kit (Miltenyi

Biotec, Bergish Gladbach, Germany). Following isolation, Lin⁻ cells (80-90% purity, Supplementary Figure 1B) were grown in StemSpan-SFEM (Stemcell Technologies Inc, Vancouver, BC, Canada) supplemented with 50 ng/mL recombinant mouse stem cell factor (rmSCF), 10 ng/mL recombinant mouse thrombopoietin (rmTPO) and 50 ng/mL recombinant mouse fms-related tyrosine kinase 3 ligand (rmFLT3-L) (all from R&D Systems, Minneapolis, MN, USA). After 24 h the cells were transduced with either LV.hU6.miRNA-126.hPGK1.DsRed.T4 or LV.hPGK1.DsRed.T4 by spin oculation in the presence of 4 µg/mL proteamine sulphate (Sigma Aldrich, St Louis, MO, USA) and maintained for another 24 h in supplemented StemSpan-SFEM. Transduced CD45.1 donor cells (300.000/mouse) were combined with supportive spleen cells (500.000/mouse) and injected into the tail vein of lethally irradiated (8 Gy) male C57BL/6J, CD45.2 acceptor mice.

Matrigel plug assay

Seven weeks after transplantation, mice were injected subcutaneously into the flank with 0.5 mL ice-cold matrigel (BD Biosciences, Breda, the Netherlands) supplemented with 100 ng/mL recombinant mouse SDF-1 (Invitrogen) and 50 ng/mL recombinant mouse VEGF (Invitrogen). After 7 days, the skin was opened to monitor the vasculature of the implants with a Sidestream Dark Field (SDF)-camera. Subsequently, implants were extracted, imaged with a Leica DMI6000microscope (Leica Microsystems, Rijswijk, the Netherlands) fixed in 4% paraformaldehyde and snap frozen at -80°C. From all microscopic images of the matrigel implants the number of visual vessels were counted on both sides of the implants. To obtain the total length of the vessels, pictures were digitalized and the total pixel area of the vessels was calculated using ImageJ software (National Institutes of Health, Bethesda, Maryland, USA).

Mouse model for ischemia reperfusion injury

Eight weeks after transplantation the renal artery and vein of mice were clamped bilaterally for 15 minutes using surgical clamps (S&T, Neuhausen, Switzerland) followed by reperfusion as described previously.⁶³ Kidney function was determined by measuring urea in serum samples using standard auto-analyzer methods by our hospital research services. Kidneys were recovered either 72 hours or 3 weeks after reperfusion for immunohistological analyses and assessment of gene expression.

Immunohistology

Sections (4 µm) of snap-frozen kidneys were air-dried and acetone-fixed. Twenty µm sections of matrigel plugs were fixed with methanol on a glass



slide and subsequently blocked with 2% fetal calf serum (FCS, Bio Whittaker/Cambrex, Verviers, Belgium), 3% bovine serum albumin (BSA, Sigma Aldrich) in PBS. For stainings involving horseradish peroxidase (HRP)-conjugated secondary antibodies, endogenous peroxidase was blocked with H₂O₂. Sections were then incubated with specific antibodies directed against murine KIM-1 (R&D systems), F4/80 (Abcam, Cambridge, UK), CD45 (Abcam), Gr-1 (a kind gift of G. Kraal, Vrije Universiteit Medisch Centrum, Amsterdam, the Netherlands), dsRed (LSBio, Seattle, WA, USA), MECA32 (Becton Dickinson, Franklin Lakes, New Jersey, USA), CD31 (FITC, Becton Dickinson), NG2 (Millipore), PDGFR β (Abcam), SDF-1 (eBioscience, San Diego, CA, USA), vWF (Dako, Glostrup, Denmark), followed by appropriate secondary antibodies that were HRP-conjugated (Jackson Immunoresearch, Westgrove, PA, USA) or labeled with Alexa-488 or Alexa-568 (Molecular Probes). As negative control, isotype-matched IgGs were used. HRP-based stainings were visualized using Nova RED (Vector Labs, Peterborough, UK) and counterstained with hematoxylin. Mast cells were stained by toluidine blue (Sigma-Aldrich). Quantification of immunohistological staining results (expressed in pixels) was performed using image J software. Fluorescent micrographs were made using fluorescence microscopy (LSM 700, Zeiss, Germany) or confocal laser scanning microscopy (LSM 510, Zeiss). Quantification of CD31⁺dsRed⁺ double stained cells was performed in a blinded manner by manual counting. H&E staining was performed on snap-frozen kidney sections by standard methods. Histological evaluations for acute tubular necrosis and tubular cast formation were performed in a blinded manner by two independent observers.

RNA isolation and qRT-PCR analysis

Total RNA was isolated from kidney sections using Trizol reagent (Invitrogen). Reverse transcription was performed using a 5-minute 65°C incubation of 250 ng total RNA with dNTPs (Invitrogen) and oligo(dT) (Invitrogen) or using specific Taqman[®] microRNA probes (miR-126, Applied Biosystems, Bleiswijk, the Netherlands). For mRNA detection, cDNA was synthesized using a M-MLV First-Strand Synthesis system (Invitrogen) and validation was carried out using SYBR Green Master Mix (Applied Biosystems). Primer sequences can be found in Supplementary Table 3. Levels of expression were determined by normalizing to GAPDH. Validation of miR-levels was performed using Taqman[®] miR assays (Applied Biosystems). MiR-levels were normalized on RNU6B levels obtained from the same RNA. Results were normalized using Gene Expression Analysis for iCycler IQ[®] RT-PCR Detection System (Bio-Rad Laboratories, Veenendaal, the Netherlands).

Flow cytometry and blood and bone marrow analysis

Whole blood was collected by incision of the tail vein or heart puncture and analyzed using a semi-automatic hematology analyzer (Sysmex F-280; Sysmex Corporation, Etten-Leur, the Netherlands), microscope (LSM 700, Leica) and flow cytometry (FACS, LSR II, BD Biosciences). Hematological values obtained included white blood cell counts (WBC, $n \times 10^6/\text{mL}$), red blood cell counts (RBC, $n \times 10^9/\text{mL}$), platelets (Plt, $n \times 10^6/\text{mL}$), hematocrit (Hct, %/%) and haemoglobin (Hgb, mmol/L). For microscopic images a smear was made from PB or BM and images were made using a fluorescence microscope. For FACS analysis, we incubated 35 μL of whole blood or 10^6 BM cells for 30 minutes at 4°C with directly conjugated antibodies against CD45.1-PE-Cy7 (BD), CD45.2-APC-Cy7 (BD), B220-APC-Cy7 (eBioscience), CD11b-APC (Biolegend, San Diego, CA, USA), Ly6G-PE (BD), CD115-PerCP-Cy5.5 (R&D Systems) and Ly6C-FITC (Bioconnect, Huissen, The Netherlands). A separate sample was prepared for incubation with Sca-1-FITC (BD), CD117-PerCP-Cy5.5 (BD) and a cocktail against lineage-positive cells (APC-conjugated, BD). Likewise, samples were prepared for these markers in combination with staining for CXCR4 (MBL international, Woburn, MA, USA). After labeling, cell suspensions were washed with PBS containing 1% BSA (Sigma-Aldrich) and 0.01% sodium azide. Erythrocytes were removed by addition of lysis buffer (0.155 M NH_4Cl , 0.01 M KHCO_3 , 0.1 mM EDTA) and finally, cells were fixed with 1% paraformaldehyde. In a separate tube the sample was incubated with an appropriate cocktail of isotype controls. Data were analyzed using FACS-Diva software (BD Biosciences). The gating strategy for peripheral blood subpopulations is described in detail in Supplementary Figure 6.

Statistical Analysis

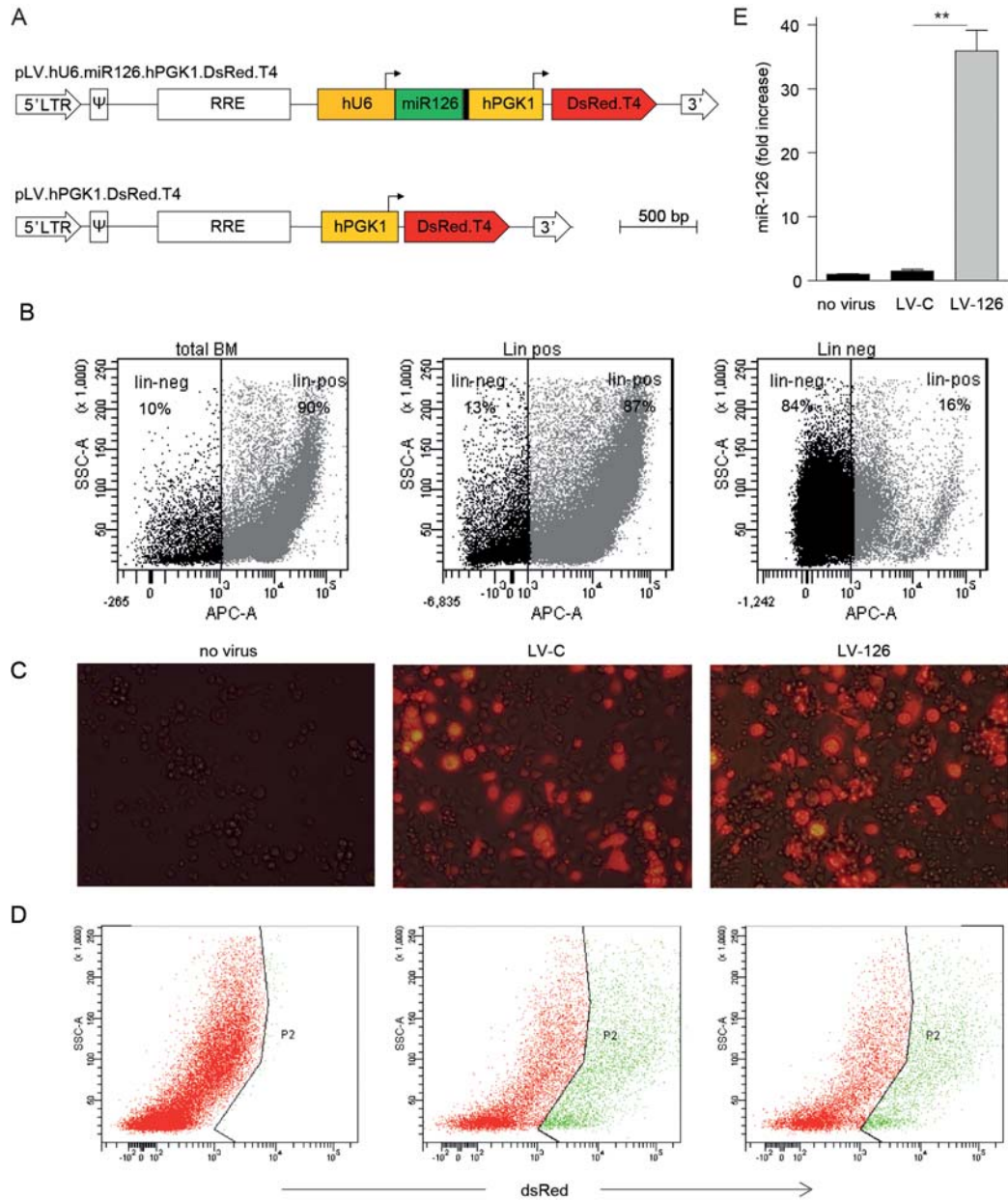
Results are expressed as mean \pm standard error of the mean (SEM) unless stated otherwise. Statistical analysis was performed using students t-test. For correlation analysis Spearman's rank correlation coefficient was used. $P < 0.05$ was considered statistically significant. Asterisks and hashtags were used to indicate levels of significance as follows: *, $P < 0.05$, **, $P > 0.01$, ***, $P < 0.001$ and #; $P < 0.10$.

Acknowledgements

We would like to thank Martijn H. Brugman and Kim J.M. Janssen for technical support. This work was supported by grants from the Dutch Heart Foundation (NHS 2006B145), Dutch Kidney Foundation (C07.2227 and C09.2329), Genzyme Renal Innovations Program and the Netherlands Institute of Regenerative Medicine.



Supplementary Files



Supplementary Figure 1.



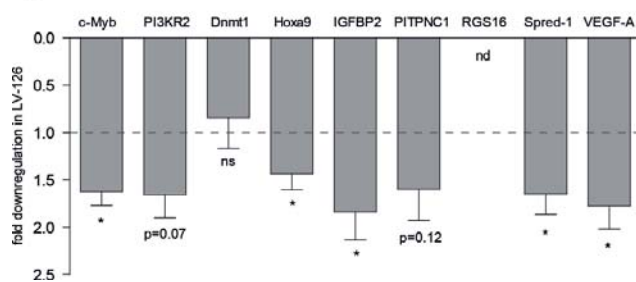
Supplementary Figure 1. Overexpression of miR-126 in Lin- bone marrow cells in vitro. (A) Schematic representation of the lentiviral miR-126 expression vector (pLV.hU6.miR126.hPGK1.DsRed.T4) (LV-126, upper scheme) and its control (pLV.hPGK1.DsRed.T4) (LV-C, lower scheme). A 445 bp PCR fragment (forward primer (Sal1): 5'-AAAAAAGTCGACGCGGAAGGCGGTGGGGACTCCC-3', reverse primer (BstB1): 5'-AAAAAATTCGAA CCAGAAGACTCAGGCCCCAGGC-3') containing the precursor RNA hairpin for miR-126 flanked on both side by 180 nucleotides, was cloned downstream of the constitutive U6 promoter into the Sal1 and BstB1 cloning sites of vector pLV.hU6.hPGK1.DsRed.T4. Both vectors contain the dsRED reporter gene behind a PGK promoter to allow tracing of transduced cells. 5' LTR, chimeric 5' long terminal repeat containing the U3 region of Rous sarcoma virus coupled to the R and U5 regions of human immunodeficiency virus type 1 (HIV1); Ψ , HIV1 packaging signal; RRE, HIV1 Rev-responsive element; cPPT, HIV1 central polypurine tract and termination site; hU6, human U6 gene promoter; miR126, coding sequence of mouse miR-126; black box, RNA polymerase III transcriptional terminator, hPGK1, human phosphoglycerate kinase 1 gene promoter; DsRed.T4, coding sequence of a rapidly maturing variant of the Discosoma spec. red fluorescent protein61; 3' LTR, 3' HIV1 long terminal repeat containing a deletion in the U3 region to render the LV self-inactivating. (B) FACS plots showing APC-labeled Lin+ BM cells, before (left panel) and after negative selection for Lin+- cells (middle panel) and Lin- cells. (C) Fluorescent microscopy of Lin- cells, 2 days after transduction, shows a high number of fluorescent dsRed+ cells validating efficient transduction of the cells by both LC-V and LV-126. Non-transduced cells (no virus) are shown in the left panel as control. (D) FACS analysis of cells 5 days post transduction display an efficiency of about 30% for both constructs (P2 gate=green). (E) Quantitative rtPCR analysis (qPCR) five days after transduction showed a ~20-fold increase (n=3, P<0.005) in miR-126 expression levels in cells transduced with the LV-126 construct as compared to the LV-C construct and non-transduced BM cells (no virus).

A

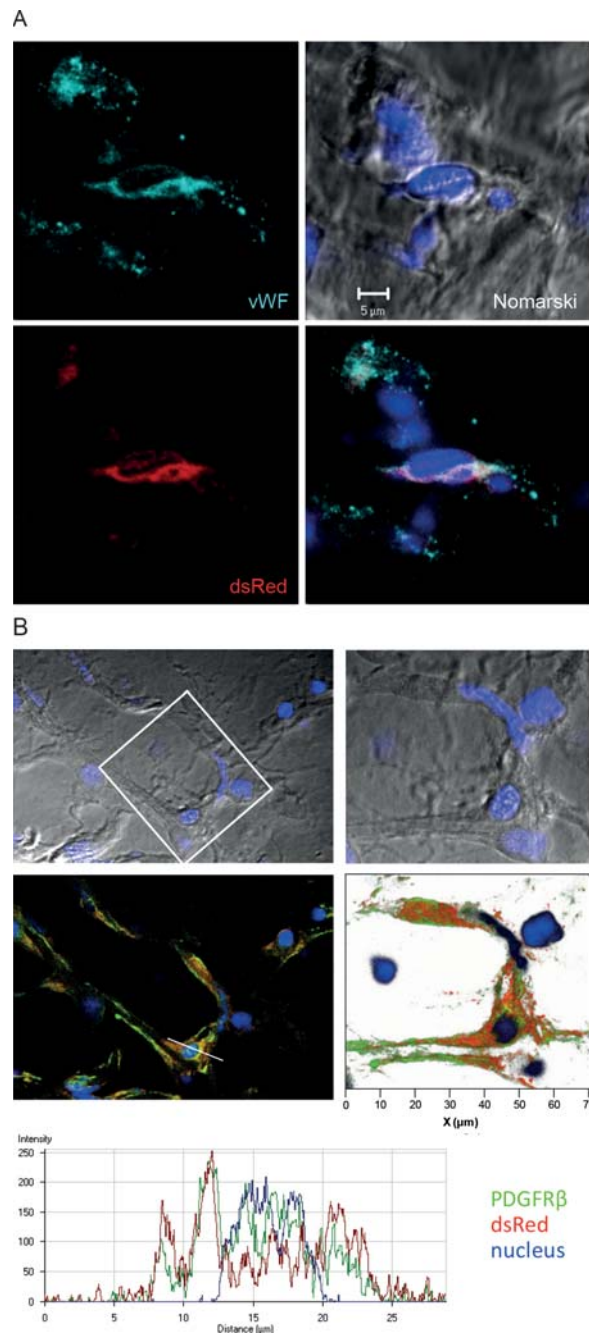
Cell type/tissue	Target protein	Process	References
Endothelium, Hematopoietic stem cells, breast cancer	PI3KR2	vascular development, angiogenesis	1-3
Endothelium	RGS16	atherosclerosis, Sca1 ⁺ incorporation	4
CD4 ⁺ T cells	Dnmt1	DNA methylation	5
Hematopoietic stem cells	Hoxa9, c-Myb	hematopoietic development, erythropoiesis	6, 7
Breast cancer	IGFBP2, PITPNC1	Suppression of metastatic angiogenesis	8
Breast and lung cancer	VEGF-A	Tumor growth	3, 9
Endothelium and mast cells	Spred-1	vascular development, angiogenesis, endothelial progenitor cell outgrowth	1, 10, 11

Supplementary Figure 2. Down regulation of established miR-126 targets. (A) overview of the selected miR-126 targets including details on proposed functions and relevant tissues. (B) qRT-PCR for established miR-126 targets in bone marrow (BM) shows downregulation in LV-126 mice as compared to LV-C mice. Of note, 1-fold means no difference, ns = not significant and RGS16 gene expression was not detectable (nd).

B

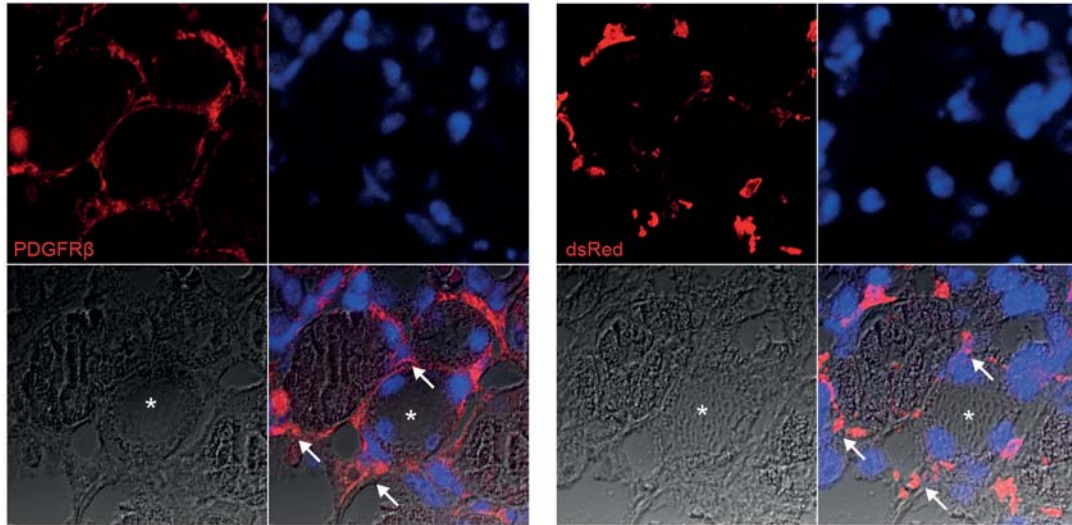


1. Fish JE, Santoro MM, Morton SU, Yu S, Yeh RF, Wythe JD, Ivey KN, Bruneau BG, Stainier DY, Srivastava D. miR-126 regulates angiogenic signaling and vascular integrity. *DevCell* 15: 272-284, 2008.
2. Huang F, Fang ZF, Hu XQ, Tang L, Zhou SH, Huang JP. Overexpression of miR-126 promotes the differentiation of mesenchymal stem cells toward endothelial cells via activation of PI3K/Akt and MAPK/ERK pathways and release of paracrine factors. *Biol Chem* 394: 1223-1233, 2013.
3. Zhu N, Zhang D, Xie H, Zhou Z, Chen H, Hu T, Bai Y, Shen Y, Yuan W, Jing Q, Qin Y. Endothelial-specific intron-derived miR-126 is down-regulated in human breast cancer and targets both VEGFA and PIK3R2. *MolCell Biochem* 351: 157-164, 2011.
4. Zernecke A, Bidzhikov K, Noels H, Shagdarsuren E, Gan L, Denecke B, Hristov M, Koppel T, Jahantigh MN, Lutgens E, Wang S, Olson EN, Schober A, Weber C. Delivery of microRNA-126 by apoptotic bodies induces CXCL12-dependent vascular protection. *SciSignal* 2: ra81, 2009.
5. Zhao S, Wang Y, Liang Y, Zhao M, Long H, Ding S, Yin H, Lu Q. MicroRNA-126 regulates DNA methylation in CD4⁺ T cells and contributes to systemic lupus erythematosus by targeting DNA methyltransferase 1. *Arthritis Rheum* 63: 1376-1386, 2011.
6. Shen WF, Hu YL, Uttarwar L, Passegue E, Largman C. MicroRNA-126 regulates HOXA9 by binding to the homeobox. *MolCell Biol* 28: 4609-4619, 2008.
7. Grabher C, Payne EM, Johnston AB, Bolli N, Lechman E, Dick JE, Kanki JP, Look AT. Zebrafish microRNA-126 determines hematopoietic cell fate through c-Myb. *Leukemia* 25: 506-514, 2011.
8. Png KJ, Halberg N, Yoshida M, Tavazoie SF. A microRNA regulon that mediates endothelial recruitment and metastasis by cancer cells. *Nature* 481: 190-194, 2012.
9. Liu B, Peng XC, Zheng XL, Wang J, Qin YW. MiR-126 restoration down-regulate VEGF and inhibit the growth of lung cancer cell lines in vitro and in vivo. *Lung Cancer* 66: 169-175, 2009.
10. Wang S, Aurora AB, Johnson BA, Qi X, McAnally J, Hill JA, Richardson JA, Bassel-Duby R, Olson EN. The endothelial-specific microRNA miR-126 governs vascular integrity and angiogenesis. *Dev Cell* 15: 261-271, 2008.
11. Meng S, Cao JT, Zhang B, Zhou Q, Shen CX, Wang CQ. Downregulation of microRNA-126 in endothelial progenitor cells from diabetes patients, impairs their functional properties, via target gene Spred-1. *J Mol Cell Cardiol* 53: 64-72, 2012.



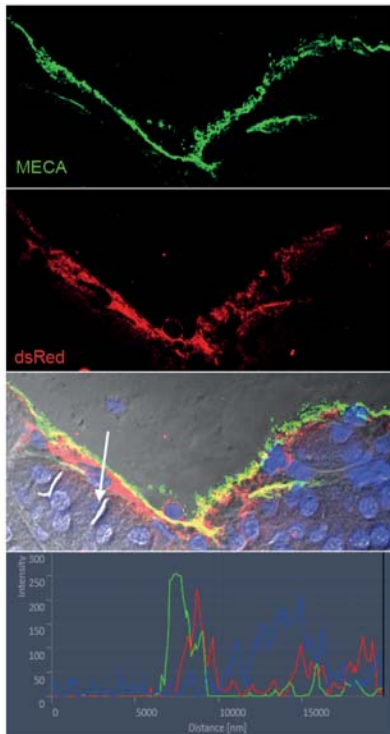
Supplementary Figure 3. DsRed+ endothelial cells and pericytes in vascular structures in matrigel. (A) Representative confocal images of a vessel stained for EC (vWF, green) and dsRed (red). (B) Representative confocal images of a zoomed region and corresponding cross sectional profiles of fluorescent labels (colors correspond to images) stained for PDGFRβ+/dsRed+ pericytes in LV-126 mouse. Right panels show zoom of region indicated by white square.



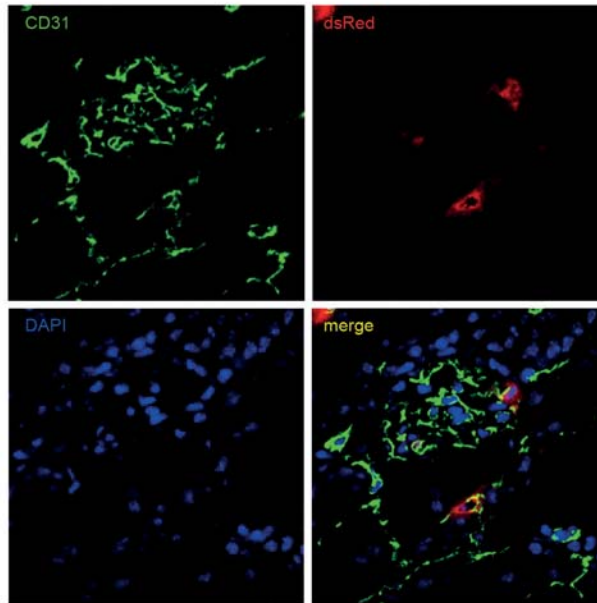


Supplementary Figure 4. Representative confocal images of sequential kidney sections of LV-126 mice showing structures positive for both PDGFR β and dsRed (arrows). * represents corresponding tubuli.

A



B



Supplementary Figure 5. DsRed-positive ECs in a large vessel and in a glomerulus. (A) representative confocal images of dsRed-positive ECs lining a large blood vessel and a cross sectional profile of fluorescent labels (colors correspond to images) shows overlap of MECA32 and dsRed. (B) Representative confocal images show a dsRed-positive glomerular CD31+ EC.

Supplementary Table 1. Hematological indices (Sysmex) and FACS analysis of whole blood. Values are expressed as mean numbers \pm standard deviation of CD45.1 positive (donor derived) cells. Values in bold are significantly different (* p<0.05) between the LV-control and LV-126 group.

PB	Pre BMT	Post BMT & pre IRI					Post IRI							
		4w	4w	4w	8w	8w	3d	3d	3d	3w	3w			
Sysmex	baseline													
WBC	$10^9/L$	LV-C	LV-126	LV-C	LV-126	LV-C	LV-126	LV-C	LV-126	LV-C	LV-126	LV-C	LV-126	LV-126
		7.4 \pm 3.7	7.6 \pm 3.0	14.2 \pm 3.4	15.3 \pm 4.3	8.5 \pm 1.6	9.3 \pm 2.5	9.3 \pm 2.5	12.5 \pm 4.1	12.5 \pm 4.1	14.6 \pm 3.2	12.5 \pm 4.1	14.6 \pm 3.2	14.6 \pm 3.2
RBC	$10^{12}/L$	9.5 \pm 0.6	9.8 \pm 0.5	9.8 \pm 0.8	10.0 \pm 0.8	6.9 \pm 1.5	7.4 \pm 1.3	7.4 \pm 1.3	6.7 \pm 1.3	6.7 \pm 1.3	7.7 \pm 2.9	6.7 \pm 1.3	7.7 \pm 2.9	7.7 \pm 2.9
Plt	$10^9/L$	420 \pm 192	504 \pm 185	682 \pm 158	714 \pm 237	660 \pm 287	712 \pm 440	712 \pm 440	328 \pm 266	328 \pm 266	391 \pm 286	328 \pm 266	391 \pm 286	391 \pm 286
Hgb	mmol/L	9.0 \pm 0.5	9.2 \pm 0.5	9.5 \pm 0.6	9.5 \pm 0.5	6.6 \pm 1.4	7.0 \pm 1.1	7.0 \pm 1.1	7.5 \pm 1.5	7.5 \pm 1.5	8.4 \pm 1.2	7.5 \pm 1.5	8.4 \pm 1.2	8.4 \pm 1.2
Hct	L/L	0.49 \pm 0.04	0.50 \pm 0.02	0.51 \pm 0.04	0.51 \pm 0.04	0.34 \pm 0.07	0.36 \pm 0.07	0.36 \pm 0.07	0.31 \pm 0.06	0.31 \pm 0.06	0.36 \pm 0.14	0.31 \pm 0.06	0.36 \pm 0.14	0.36 \pm 0.14
FACS														
CD45.1+ WBCs	$10^6/mL$	6.1 \pm 3.4	5.9 \pm 2.5	11.4 \pm 4.7	13.3 \pm 4.2	7.6 \pm 1.4	7.7 \pm 2.3	7.7 \pm 2.3	10.5 \pm 3.5	10.5 \pm 3.5	12.6 \pm 3.2	10.5 \pm 3.5	12.6 \pm 3.2	12.6 \pm 3.2
T-cells	$10^6/mL$	0.29 \pm 0.15	0.32 \pm 0.28	1.19 \pm 0.46	1.38 \pm 0.59	1.07 \pm 0.29	1.09 \pm 0.22	1.09 \pm 0.22	1.08 \pm 0.35	1.08 \pm 0.35	1.40 \pm 0.22	1.08 \pm 0.35	1.40 \pm 0.22	1.40 \pm 0.22
B-cells	$10^6/mL$	2.5 \pm 1.5	1.9 \pm 1.1	5.8 \pm 2.7	6.7 \pm 2.6	2.8 \pm 0.9	3.3 \pm 1.2	3.3 \pm 1.2	4.5 \pm 1.8	4.5 \pm 1.8	5.3 \pm 1.7	4.5 \pm 1.8	5.3 \pm 1.7	5.3 \pm 1.7
NK-cells	$10^6/mL$	0.00 \pm 0.00	0.14 \pm 0.09	0.24 \pm 0.13	0.22 \pm 0.09	0.11 \pm 0.05	0.10 \pm 0.05	0.10 \pm 0.05	0.24 \pm 0.13	0.24 \pm 0.13	0.30 \pm 0.16	0.24 \pm 0.13	0.30 \pm 0.16	0.30 \pm 0.16
pDC	$10^6/mL$	0.03 \pm 0.02	0.05 \pm 0.03*	0.12 \pm 0.05	0.15 \pm 0.07	0.05 \pm 0.02	0.05 \pm 0.02	0.05 \pm 0.02	0.10 \pm 0.03*	0.10 \pm 0.03*	0.16 \pm 0.06*	0.10 \pm 0.03*	0.16 \pm 0.06*	0.16 \pm 0.06*
Neutrophils	$10^6/mL$	0.0 \pm 0.0	2.1 \pm 1.7	1.8 \pm 0.8	2.3 \pm 1.4	2.2 \pm 0.6	1.7 \pm 0.9	1.7 \pm 0.9	2.5 \pm 0.9	2.5 \pm 0.9	3.1 \pm 1.7	2.5 \pm 0.9	3.1 \pm 1.7	3.1 \pm 1.7
Eosinophils	$10^6/mL$	0.02 \pm 0.01	0.25 \pm 0.20	0.42 \pm 0.21	0.50 \pm 0.23	0.59 \pm 0.23	0.489 \pm 0.32	0.489 \pm 0.32	0.38 \pm 0.21	0.38 \pm 0.21	0.37 \pm 0.19	0.38 \pm 0.21	0.37 \pm 0.19	0.37 \pm 0.19
Monocytes	$10^6/mL$	0.04 \pm 0.02	0.53 \pm 0.35	0.86 \pm 0.37	0.93 \pm 0.38	0.27 \pm 0.16	0.28 \pm 0.14	0.28 \pm 0.14	0.78 \pm 0.26	0.78 \pm 0.26	0.81 \pm 0.38	0.78 \pm 0.26	0.81 \pm 0.38	0.81 \pm 0.38
- Ly6C ^{hi}		0.03 \pm 0.02	0.33 \pm 0.24	0.42 \pm 0.22	0.47 \pm 0.20	0.09 \pm 0.11	0.08 \pm 0.07	0.08 \pm 0.07	0.45 \pm 0.14	0.45 \pm 0.14	0.49 \pm 0.26	0.45 \pm 0.14	0.49 \pm 0.26	0.49 \pm 0.26
- Ly6C ^{med}		0.00 \pm 0.00	0.07 \pm 0.05	0.10 \pm 0.05	0.12 \pm 0.06	0.01 \pm 0.01	0.02 \pm 0.01	0.02 \pm 0.01	0.10 \pm 0.03	0.10 \pm 0.03	0.11 \pm 0.07	0.10 \pm 0.03	0.11 \pm 0.07	0.11 \pm 0.07
- Ly6C ^{lo}		0.01 \pm 0.00	0.13 \pm 0.08	0.34 \pm 0.14	0.33 \pm 0.15	0.17 \pm 0.07	0.18 \pm 0.07	0.18 \pm 0.07	0.23 \pm 0.11	0.23 \pm 0.11	0.19 \pm 0.08	0.23 \pm 0.11	0.19 \pm 0.08	0.19 \pm 0.08

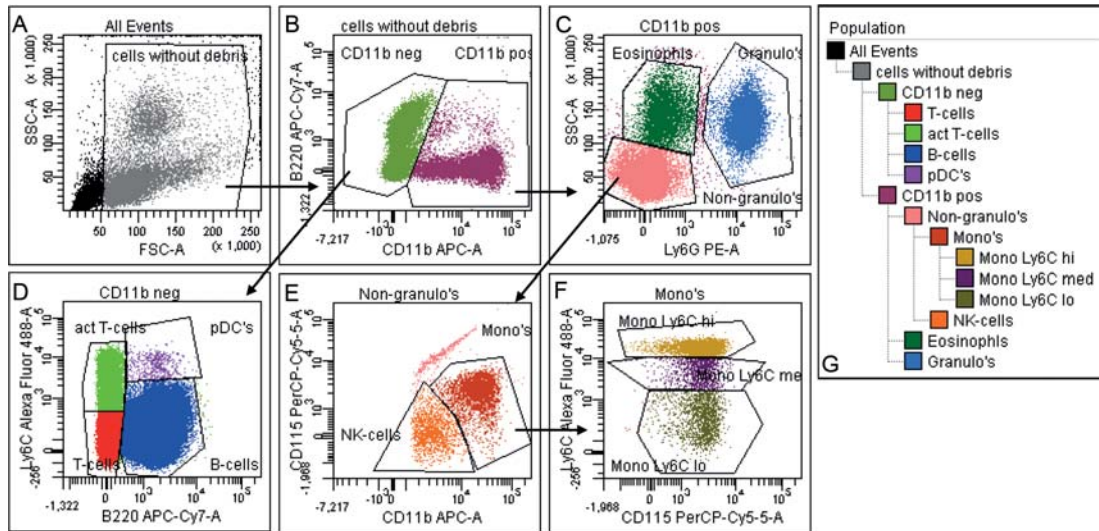


Supplementary Table 2. FACS analysis of bone marrow. Values are expressed as mean percentages \pm standard deviation of CD45.1-positive (donor derived) cells. Values in bold are significantly different (* $p < 0.05$. *** $p < 0.001$) between the LV-control and LV-126 group.

BM		LV-C	LV-126	LV-C	LV-126
		3d post IRI	3d post IRI	3w post IRI	3w post IRI
CD45.1+ WBCs	(n x 10 ⁶ /mL)	81.6 \pm 6.9	73.0 \pm 15.2	82.6 \pm 5.0	84.9 \pm 5.5
T-cells	(n x 10 ⁶ /mL)	2.7 \pm 0.5	2.7 \pm 1.2	2.0 \pm 0.8	1.6 \pm 0.6
B-cells	(n x 10 ⁶ /mL)	8.5 \pm 2.9	7.3 \pm 2.6	6.2 \pm 2.4	5.3 \pm 1.7
NK-cells	(n x 10 ⁶ /mL)	2.5 \pm 1.0	2.2 \pm 1.1	3.0 \pm 0.5*	2.0 \pm 1.2*
pDC	(n x 10 ⁶ /mL)	1.4 \pm 0.6*	0.8 \pm 0.2*	0.7 \pm 0.3	0.6 \pm 0.1
Neutrophils	(n x 10 ⁶ /mL)	33.9 \pm 5.3	30.7 \pm 5.8	45.8 \pm 9.6*	55.5 \pm 4.6*
Eosinophils	(n x 10 ⁶ /mL)	4.9 \pm 1.4	4.8 \pm 3.2	1.9 \pm 0.8	1.2 \pm 0.7
Monocytes (all)	(n x 10 ⁶ /mL)	23.6 \pm 2.2*	20.4 \pm 2.6*	18.3 \pm 2.6	12.7 \pm 7.1
- Ly6C ^{hi}		2.8 \pm 1.8	3.0 \pm 2.1	0.6 \pm 0.4	0.4 \pm 0.3
- Ly6C ^{med}		20.6 \pm 1.3***	15.0 \pm 3.8***	16.7 \pm 2.4	11.4 \pm 6.3
- Ly6C ^{lo}		0.6 \pm 0.3	0.6 \pm 0.3	0.7 \pm 0.4	0.5 \pm 0.3

Supplementary Table 3. Primers for qRT-PCR analysis.

Target Gene	Forward primer	Reverse primer
α -SMA	CGTGGCTATTCTTCGTGAC	GCGTTCGTAGCTCTCTCC
Col1 α 1	TGACTGGAAGAGCGGAGAGT	GTTCCGGCTGATGTACCAGT
CCL2	GCACCAGCCAACCTCTCAC	CTTCTTGGGGTCAGCACAG
IL-10	AATAAGAGCAAGGCAGTGGAG	CCCTGGATCAGATTAGAGAGC
TGF- β	GCAACATGTGGAACCTACCAGAA	GACGTCAAAAGACAGCCACTCA
Col3 α 1	TCCCTTGGAAATCTGTGAATC	TGAGTCGAATTGGGGAGAAT
Kim-1	GGGCTTCTATGTTGGCATC	TGTCCTCAGCTCGGGAATG
NGAL	GTTTCACCCGCTTGCCAAG	CCACACTCACCACCCATTC
IL-6	ACAAAGCCAGAGTCCTTCAG	TGGTCTTGGTCTTAGCC
SDF-1	CGTGAGGCCAGGGAAGAGT	TGATGAGCATGGTGGGTTGA
GAPDH	ACTCCCACTCTCCACCTTC	CACCACCCTGTGCTGTAG
U6	CTCGCTTCGGCAGCACA	AACGCTCACGAATTTGCGT
PI3KR2	GGATGCCCTGGCTTCAACGA	CTGGGAGTATGTGGCCTGACT
c-Myb	GAGCACCAACTGTCTCG	CACCAGGGGCTGTCTTAG
DNMT1	AAGAATGGTGTGTCTACCGAC	CATCCAGGTTGCTCCCTTG
IGFBP2	CAGACGCTACGCTGCTATCC	CCCTCAGAGTGGTCGTCATCA
PITPNC1	CAACCCATCATGTGCTCTAC	CCCGAACATCATCCATTGTCAT
Hoxa9	TGGCCGAACACCCCG	CACCAAAACCCGCGC
RGS16	CGAGTGGGCCAGTAAGCATAA	CGAAAGACTCTCTCCATCCAG
VEGF-A	GTACCTCCACCATGCCAAGT	GCATTCACATCTGCTGTGCT
Spred -1	GATGAGCGAGGAGACGGCGAC	GTCTCTGAGTCTCTCCACGGA



Supplementary Figure 6. Gating strategy for flow cytometry analysis. A gate is drawn on all cells in a FCS/SSC plot (A) to exclude debris. Of the cells gated in plot A, the expression of CD11b (X-axis) and B220 (Y-axis) is shown in plot B, on which gates are placed on the CD11b-neg cells and the CD11-pos cells. The CD11-pos cells are selected in plot C, showing expression of Ly6G (X-axis) and side scatter (SSC, Y-axis), in which Ly6G-pos/SSC-hi cells represent neutrophilic granulocytes, Ly6G-neg/SSC-hi cells represent eosinophilic granulocytes and the Ly6G-neg/SSC-lo cells represent the non-granulocytic cells. These latter cells are selected in plot E, showing their expression of CD11b (X-axis) and CD115 (Y-axis): CD11b-hi/CD115-hi cells represent the monocytes and the CD11b-dim/CD115-neg cells represent NK cells. The monocytes gated in plot E are selected in plot F, showing their expression of CD115 (X-axis) and Ly6C (Y-axis): Ly6C-hi cells represent the pro-inflammatory monocytes, Ly6C-med cells represent the intermediate monocyte population and Ly6C-lo cells represent the anti-inflammatory, pro-angiogenic/repair-associated monocytes. The CD11b-neg cells gated in plot B are selected in plot D and show their expression of the B-cell marker B220 (X-axis) and Ly6C (Y-axis): B220-neg/Ly6C-neg cells represent the T-cells, B220-pos/Ly6C-neg cells are B-cells, B220-neg/Ly6C-pos cells are activated T-cells and B220-pos/Ly6C-pos cells are plasmacytoid dendritic cells (pDCs). All cells were analyzed within the CD45.1 group as these cells represent the donor cells.



References

1. Perico N, Cattaneo D, Sayegh MH, Remuzzi G. Delayed graft function in kidney transplantation. *Lancet* 364: 1814-1827, 2004.
2. Pagtalunan ME, Olson JL, Tilney NL, Meyer TW. Late consequences of acute ischemic injury to a solitary kidney. *J Am Soc Nephrol* 10: 366-373, 1999.
3. Sharfuddin AA, Molitoris BA. Pathophysiology of ischemic acute kidney injury. *Nat Rev Nephrol* 7: 189-200, 2011.
4. Bonventre JV, Yang L. Cellular pathophysiology of ischemic acute kidney injury. *J Clin Invest* 121: 4210-4221, 2011.
5. Flores J, DiBona DR, Beck CH, Leaf A. The role of cell swelling in ischemic renal damage and the protective effect of hypertonic solute. *J Clin Invest* 51: 118-126, 1972.
6. Lieberthal W, Wolf EF, Rennke HG, Valeri CR, Levinson NG. Renal ischemia and reperfusion impair endothelium-dependent vascular relaxation. *Am J Physiol* 256: F894-900, 1989.
7. Kelly KJ, Williams WW, Jr., Colvin RB, Bonventre JV. Antibody to intercellular adhesion molecule 1 protects the kidney against ischemic injury. *Proc Natl Acad Sci U S A* 91: 812-816, 1994.
8. Basile DP, Donohoe D, Roethe K, Osborn JL. Renal ischemic injury results in permanent damage to peritubular capillaries and influences long-term function. *Am J Physiol Renal Physiol* 281: F887-899, 2001.
9. Fligny C, Duffield JS. Activation of pericytes: recent insights into kidney fibrosis and microvascular rarefaction. *Curr Opin Rheumatol* 25: 78-86, 2013.
10. Spurgeon KR, Donohoe DL, Basile DP. Transforming growth factor-beta in acute renal failure: receptor expression, effects on proliferation, cellularity, and vascularization after recovery from injury. *Am J Physiol Renal Physiol* 288: F568-577, 2005.
11. Ishii Y, Sawada T, Kubota K, Fuchinoue S, Teraoka S, Shimizu A. Injury and progressive loss of peritubular capillaries in the development of chronic allograft nephropathy. *Kidney Int* 67: 321-332, 2005.
12. Namikoshi T, Satoh M, Horike H, Fujimoto S, Arakawa S, Sasaki T, Kashihara N. Implication of peritubular capillary loss and altered expression of vascular endothelial growth factor in IgA nephropathy. *Nephron Physiol* 102: p9-16, 2006.
13. Basile DP, Friedrich JL, Spahic J, Knipe N, Mang H, Leonard EC, Changizi-Ashtiyani S, Bacallao RL, Molitoris BA, Sutton TA. Impaired endothelial proliferation and mesenchymal transition contribute to vascular rarefaction following acute kidney injury. *Am J Physiol Renal Physiol* 300: F721-733, 2011.
14. Rabelink TJ, de Boer HC, van Zonneveld AJ. Endothelial activation and circulating markers of endothelial activation in kidney disease. *Nat Rev Nephrol* 6: 404-414, 2010.
15. Jung YJ, Kim DH, Lee AS, Lee S, Kang KP, Lee SY, Jang KY, Sung MJ, Park SK, Kim W. Peritubular capillary preservation with COMP-angiopoietin-1 decreases ischemia-reperfusion-induced acute kidney injury. *Am J Physiol Renal Physiol* 297: F952-960, 2009.
16. Lin SL, Chang FC, Schrimpf C, Chen YT, Wu CF, Wu VC, Chiang WC, Kuhnert F, Kuo CJ, Chen YM, Wu KD, Tsai TJ, Duffield JS. Targeting endothelium-pericyte cross talk by inhibiting VEGF receptor signaling attenuates kidney microvascular rarefaction and fibrosis. *Am J Pathol* 178: 911-923, 2011.
17. Long DA, Price KL, Ioffe E, Gannon CM, Gnudi L, White KE, Yancopoulos GD, Rudge JS, Woolf AS. Angiopoietin-1 therapy enhances fibrosis and inflammation following folic acid-induced acute renal injury. *Kidney Int* 74: 300-309, 2008.

18. Schrimpf C, Xin C, Campanholle G, Gill SE, Stallcup W, Lin SL, Davis GE, Gharib SA, Humphreys BD, Duffield JS. Pericyte TIMP3 and ADAMTS1 modulate vascular stability after kidney injury. *J Am Soc Nephrol* 23: 868-883, 2012.
19. Long DA, Norman JT, Fine LG. Restoring the renal microvasculature to treat chronic kidney disease. *Nat Rev Nephrol* 8: 244-250, 2012.
20. Becherucci F, Mazzinghi B, Ronconi E, Peired A, Lazzeri E, Sagrinati C, Romagnani P, Lasagni L. The role of endothelial progenitor cells in acute kidney injury. *Blood Purif* 27: 261-270, 2009.
21. Rookmaaker MB, Smits AM, Tolboom H, Van 't Wout K, Martens AC, Goldschmeding R, Joles JA, Van Zonneveld AJ, Grone HJ, Rabelink TJ, Verhaar MC. Bone-marrow-derived cells contribute to glomerular endothelial repair in experimental glomerulonephritis. *Am J Pathol* 163: 553-562, 2003.
22. Li B, Cohen A, Hudson TE, Motlagh D, Amrani DL, Duffield JS. Mobilized human hematopoietic stem/progenitor cells promote kidney repair after ischemia/reperfusion injury. *Circulation* 121: 2211-2220, 2010.
23. Patschan D, Krupinca K, Patschan S, Zhang Z, Hamby C, Goligorsky MS. Dynamics of mobilization and homing of endothelial progenitor cells after acute renal ischemia: modulation by ischemic preconditioning. *Am J Physiol Renal Physiol* 291: F176-185, 2006.
24. Li J, Deane JA, Campanale NV, Bertram JF, Ricardo SD. The contribution of bone marrow-derived cells to the development of renal interstitial fibrosis. *Stem Cells* 25: 697-706, 2007.
25. Lagaaï EL, Cramer-Knijnenburg GF, van Kemenade FJ, van Es LA, Bruijn JA, van Krieken JH. Endothelial cell chimerism after renal transplantation and vascular rejection. *Lancet* 357: 33-37, 2001.
26. Asahara T, Murohara T, Sullivan A, Silver M, van der Zee R, Li T, Witzenbichler B, Schatteman G, Isner JM. Isolation of putative progenitor endothelial cells for angiogenesis. *Science* 275: 964-967, 1997.
27. Tögel F, Isaac J, Hu Z, Weiss K, Westenfelder C. Renal SDF-1 signals mobilization and homing of CXCR4-positive cells to the kidney after ischemic injury. *Kidney Int* 67: 1772-1784, 2005.
28. Zheng H, Fu G, Dai T, Huang H. Migration of endothelial progenitor cells mediated by stromal cell-derived factor-1 α /CXCR4 via PI3K/Akt/eNOS signal transduction pathway. *J Cardiovasc Pharmacol* 50: 274-280, 2007.
29. Asgeirsdottir SA, van Solingen C, Kurniati NF, Zwiers PJ, Heeringa P, van Meurs M, Satchell SC, Saleem MA, Mathieson PW, Banas B, Kamps JA, Rabelink TJ, van Zonneveld AJ, Molema G. MicroRNA-126 contributes to renal microvascular heterogeneity of VCAM-1 protein expression in acute inflammation. *Am J Physiol Renal Physiol* 302: F1630-1639, 2012.
30. Fish JE, Santoro MM, Morton SU, Yu S, Yeh RF, Wythe JD, Ivey KN, Bruneau BG, Stainier DY, Srivastava D. miR-126 regulates angiogenic signaling and vascular integrity. *Dev Cell* 15: 272-284, 2008.
31. Harris TA, Yamakuchi M, Ferlito M, Mendell JT, Lowenstein CJ. MicroRNA-126 regulates endothelial expression of vascular cell adhesion molecule 1. *Proc Natl Acad Sci U S A* 105: 1516-1521, 2008.
32. Salvucci O, Jiang K, Gasperini P, Maric D, Zhu J, Sakakibara S, Espigol-Frigole G, Wang S, Tosato G. MicroRNA126 contributes to granulocyte colony-stimulating factor-induced hematopoietic progenitor cell mobilization by reducing the expression of vascular cell adhesion molecule 1. *Haematologica* 97: 818-826, 2012.
33. van Solingen C, de Boer HC, Bijkerk R, Monge M, van Oeveren-Rietdijk AM, Seghers L, de Vries MR, van der Veer EP, Quax PH, Rabelink TJ, van Zonneveld AJ. MicroRNA-126 modulates endothelial SDF-1 expression and mobilization of Sca-1(+)/Lin(-) progenitor cells in ischaemia. *Cardiovasc Res* 92: 449-455, 2011.



34. Ishizaki T, Tamiya T, Taniguchi K, Morita R, Kato R, Okamoto F, Saeki K, Nomura M, Nojima Y, Yoshimura A. miR126 positively regulates mast cell proliferation and cytokine production through suppressing Spred1. *Genes Cells* 16: 803-814, 2011.
35. Kim J, Seok YM, Jung KJ, Park KM. Reactive oxygen species/oxidative stress contributes to progression of kidney fibrosis following transient ischemic injury in mice. *Am J Physiol Renal Physiol* 297: F461-470, 2009.
36. Yoder MC. Endothelial progenitor cell: a blood cell by many other names may serve similar functions. *J Mol Med (Berl)* 91: 285-295, 2013.
37. Loomans CJ, Wan H, de Crom R, van Haperen R, de Boer HC, Leenen PJ, Drexhage HA, Rabelink TJ, van Zonneveld AJ, Staal FJ. Angiogenic murine endothelial progenitor cells are derived from a myeloid bone marrow fraction and can be identified by endothelial NO synthase expression. *Arterioscler Thromb Vasc Biol* 26: 1760-1767, 2006.
38. Broxmeyer HE, Orschell CM, Clapp DW, Hangoc G, Cooper S, Plett PA, Liles WC, Li X, Graham-Evans B, Campbell TB, Calandra G, Bridger G, Dale DC, Srouf EF. Rapid mobilization of murine and human hematopoietic stem and progenitor cells with AMD3100, a CXCR4 antagonist. *J Exp Med* 201: 1307-1318, 2005.
39. Ceradini DJ, Kulkarni AR, Callaghan MJ, Tepper OM, Bastidas N, Kleinman ME, Capla JM, Galiano RD, Levine JP, Gurtner GC. Progenitor cell trafficking is regulated by hypoxic gradients through HIF-1 induction of SDF-1. *Nat Med* 10: 858-864, 2004.
40. Hattori K, Heissig B, Rafii S. The regulation of hematopoietic stem cell and progenitor mobilization by chemokine SDF-1. *Leuk Lymphoma* 44: 575-582, 2003.
41. Hattori K, Heissig B, Tashiro K, Honjo T, Tateno M, Shieh JH, Hackett NR, Quitoriano MS, Crystal RG, Rafii S, Moore MA. Plasma elevation of stromal cell-derived factor-1 induces mobilization of mature and immature hematopoietic progenitor and stem cells. *Blood* 97: 3354-3360, 2001.
42. Zhang Y, Yang P, Sun T, Li D, Xu X, Rui Y, Li C, Chong M, Ibrahim T, Mercatali L, Amadori D, Lu X, Xie D, Li QJ, Wang XF. miR-126 and miR-126(*) repress recruitment of mesenchymal stem cells and inflammatory monocytes to inhibit breast cancer metastasis. *Nat Cell Biol* 15: 284-294, 2013.
43. Zernecke A, Bidzhekov K, Noels H, Shagdarsuren E, Gan L, Denecke B, Hristov M, Koppel T, Jahantigh MN, Lutgens E, Wang S, Olson EN, Schober A, Weber C. Delivery of microRNA-126 by apoptotic bodies induces CXCL12-dependent vascular protection. *Sci Signal* 2: ra81, 2009.
44. Cantaluppi V, Gatti S, Medica D, Figliolini F, Bruno S, Deregibus MC, Sordi A, Biancone L, Tetta C, Camussi G. Microvesicles derived from endothelial progenitor cells protect the kidney from ischemia-reperfusion injury by microRNA-dependent reprogramming of resident renal cells. *Kidney Int* 82: 412-427, 2012.
45. Zhou J, Li JY, Nguyen P, Wang KC, Weiss A, Kuo YC, Chiu JJ, Shyy JY, Chien S. Regulation of Vascular Smooth Muscle Cell Turnover by Endothelial Cell-secreted MicroRNA-126: Role of Shear Stress. *Circ Res*, 2013.
46. Borges FT, Melo SA, Ozdemir BC, Kato N, Revuelta I, Miller CA, Gattone VH, 2nd, LeBleu VS, Kalluri R. TGF-beta1-containing exosomes from injured epithelial cells activate fibroblasts to initiate tissue regenerative responses and fibrosis. *J Am Soc Nephrol* 24: 385-392, 2013.
47. de Boer HC, van Solingen C, Prins J, Duijs JM, Huisman MV, Rabelink TJ, van Zonneveld AJ. Aspirin treatment hampers the use of plasma microRNA-126 as a biomarker for the progression of vascular disease. *Eur Heart J*, 2013.
48. Nagalla S, Shaw C, Kong X, Kondkar AA, Edelstein LC, Ma L, Chen J, McKnight GS, Lopez JA, Yang L, Jin Y, Bray MS, Leal SM, Dong JF, Bray PF. Platelet microRNA-mRNA coexpression profiles correlate with platelet reactivity. *Blood* 117: 5189-5197, 2011.

49. Zampetaki A, Willeit P, Tilling L, Drozdov I, Prokopi M, Renard JM, Mayr A, Weger S, Schett G, Shah A, Boulanger CM, Willeit J, Chowienczyk PJ, Kiechl S, Mayr M. Prospective Study on Circulating MicroRNAs and Risk of Myocardial Infarction. *J Am Coll Cardiol* 60: 290-299, 2012.
50. Bitzer M, Ben-Dov IZ, Thum T. Microparticles and microRNAs of endothelial progenitor cells ameliorate acute kidney injury. *Kidney Int* 82: 375-377, 2012.
51. Massberg S, Konrad I, Schurzinger K, Lorenz M, Schneider S, Zohlhoefer D, Hoppe K, Schiemann M, Kennerknecht E, Sauer S, Schulz C, Kerstan S, Rudelius M, Seidl S, Sorge F, Langer H, Peluso M, Goyal P, Vestweber D, Emambokus NR, Busch DH, Frampton J, Gawaz M. Platelets secrete stromal cell-derived factor 1alpha and recruit bone marrow-derived progenitor cells to arterial thrombi in vivo. *J Exp Med* 203: 1221-1233, 2006.
52. Dimmeler S, Aicher A, Vasa M, Mildner-Rihm C, Adler K, Tiemann M, Rutten H, Fichtlscherer S, Martin H, Zeiher AM. HMG-CoA reductase inhibitors (statins) increase endothelial progenitor cells via the PI 3-kinase/Akt pathway. *J Clin Invest* 108: 391-397, 2001.
53. Yan T, Liu Y, Cui K, Hu B, Wang F, Zou L. MiR-126 regulates EPCs function: implications for a role of miR-126 in preeclampsia. *J Cell Biochem*, 2013.
54. Goligorsky MS, Yasuda K, Ratliff B. Dysfunctional endothelial progenitor cells in chronic kidney disease. *J Am Soc Nephrol* 21: 911-919, 2010.
55. Reinders ME, Rabelink TJ, Briscoe DM. Angiogenesis and endothelial cell repair in renal disease and allograft rejection. *J Am Soc Nephrol* 17: 932-942, 2006.
56. Davies WR, Wang S, Oi K, Bailey KR, Tazelaar HD, Caplice NM, McGregor CG. Cyclosporine decreases vascular progenitor cell numbers after cardiac transplantation and attenuates progenitor cell growth in vitro. *J Heart Lung Transplant* 24: 1868-1877, 2005.
57. de Groot K, Bahlmann FH, Bahlmann E, Menne J, Haller H, Fliser D. Kidney graft function determines endothelial progenitor cell number in renal transplant recipients. *Transplantation* 79: 941-945, 2005.
58. Imanishi T, Kobayashi K, Kuki S, Takahashi C, Akasaka T. Sirolimus accelerates senescence of endothelial progenitor cells through telomerase inactivation. *Atherosclerosis* 189: 288-296, 2006.
59. Dar A, Domev H, Ben-Yosef O, Tzukerman M, Zeevi-Levin N, Novak A, Germanguz I, Amit M, Itskovitz-Eldor J. Multipotent vasculogenic pericytes from human pluripotent stem cells promote recovery of murine ischemic limb. *Circulation* 125: 87-99, 2012.
60. Tigges U, Hyer EG, Scharf J, Stallcup WB. FGF2-dependent neovascularization of subcutaneous Matrigel plugs is initiated by bone marrow-derived pericytes and macrophages. *Development* 135: 523-532, 2008.
61. Bevis BJ, Glick BS. Rapidly maturing variants of the Discosoma red fluorescent protein (DsRed). *Nat Biotechnol* 20: 83-87, 2002.
62. Ramkisoensing AA, Pijnappels DA, Swildens J, Goumans MJ, Fibbe WE, Schali J, de Vries AA, Atsma DE. Gap junctional coupling with cardiomyocytes is necessary but not sufficient for cardiomyogenic differentiation of cocultured human mesenchymal stem cells. *Stem Cells* 30: 1236-1245, 2012.
63. de Vries DK, Lindeman JH, Tsikas D, de Heer E, Roos A, de Fijter JW, Baranski AG, van Pelt J, Schaapherder AF. Early renal ischemia-reperfusion injury in humans is dominated by IL-6 release from the allograft. *Am J Transplant* 9: 1574-1584, 2009.



Chapter

5

In preparation

Silencing of Pericyte MicroRNA-132 Reduces Renal Fibrosis and Myofibroblast Proliferation and is Associated with Altered Sirt1 and Cox2 Expression

R. Bijkerk^{1,2}, C. van Solingen¹, R.G. de Bruin¹, J.M.G.J. Duijs¹, T.J. Rabelink¹, B.D. Humphreys² and A.J. van Zonneveld¹

¹Department of Nephrology and the Einthoven Laboratory for Experimental Vascular Medicine, Leiden University Medical Center (LUMC), Leiden. ²Renal Division, Department of Medicine, Brigham & Women's Hospital and Harvard Medical School, Boston, Massachusetts, USA.

Abstract

Lineage analysis has shown that during nephrogenesis, FoxD1-positive mesenchymal cells give rise to adult interstitial pericytes. These FoxD1-derivative interstitial cells expand and differentiate into smooth muscle actin (α -SMA) positive myofibroblasts during renal fibrosis, accounting for a large majority of myofibroblasts. MicroRNAs (miRNAs) involved in this differentiation could serve as a target to decrease myofibroblast formation in fibrotic kidney disease. To identify miRNAs differentially expressed in myofibroblasts we induced fibrosis in FoxD1-GC;Z/Red mice by unilateral ureteric obstruction (UUO). Subsequently, dsRed positive cells were isolated using FACS sorting and used for miRNA profiling. MiR-132 was amongst the most highly upregulated miRNAs in the dsRed positive cells in the fibrotic kidney. In vitro we demonstrated that silencing miR-132 results in reduction of myofibroblast marker α -SMA, reduced proliferation and increased levels of its established target Sirt1 and downstream Cox2. In vivo silencing of miR-132 by antagomirs directed to miR-132 in the UUO model resulted in a 35% decrease in collagen deposition and decreased tubular apoptosis after 10 days as compared to scramble mir controls, while no difference was observed yet after 5 days. IHC analysis demonstrated that the number of interstitial α -SMA positive cells was similarly decreased, which could be confirmed by both western blot and qRT-PCR analyses. No difference was observed in capillary density. Furthermore, we demonstrated that miR-132 silencing is associated with decreased Sirt1 and Cox2 expression and decreases the number of proliferating interstitial cells. Silencing miR-132 protects counteracts the progression of renal fibrosis, decreases myofibroblast proliferation and is associated with strongly altered Sirt1 and Cox2 levels.

Introduction

Pericytes are stromal cells that are known to cover and support capillary walls. Lineage tracing of pericyte cell fate using FoxD1-Cre;Rosa26R mice demonstrated that these perivascular cells are the major source of α -SMA positive myofibroblasts in mouse models of renal fibrosis^{1,2}.

MicroRNAs (miRNAs) are small ~22 nt RNAs and constitute a class of highly conserved non-coding RNAs that control gene expression by inhibiting the translation of mRNA³. MiRNAs are able to regulate multiple targets and thereby provide a means for the coordinated control of gene expression. As a consequence, these molecules are attractive candidates for regulating cell type-specific differentiation and modulating cell function⁴.

Several reports already established a role for miRNAs in the development of tissue fibrosis. In the failing heart miR-21 levels are increased in fibroblasts and *in vivo* silencing of miR-21 by antagomirs reduces cardiac ERK-MAP kinase activity and interstitial fibrosis⁵. Likewise, miR-133⁶ and cardiac specific miR-208⁷ have been involved in the pathogenesis of fibrosis in the heart. In addition, members of the miR-29 family have been described in fibrosis. In a myocardial infarction model it was shown that members of the miR-29 family are down regulated and miR-29 silencing with anti-miRs *in vitro* and *in vivo* induced the expression of collagens, whereas over expression of miR-29 in fibroblasts reduced collagen expression⁸. Also in the liver members of the miR-29 family were shown to be downregulated in fibrosis⁹. In kidneys from rats, knockdown of miR-29b resulted in upregulation of several collagen genes¹⁰.

In the kidney, several miRNAs (miR-21, -214, -324-3p, 382) are now recognized to be important mediators in the development of renal fibrosis¹¹⁻¹⁵. Also miR-192 is involved as a tight association was demonstrated of miR-192 expression in the kidney with both activation of TGF-beta/Smad signaling^{16,17}, as well as with tubulo-interstitial fibrosis and low estimated glomerular filtration rate (GFR) in diabetic nephropathy patients¹⁸.

As pericytes are considered to be the main source of myofibroblasts, we aimed to identify miRNAs that play an important role in the process of myofibroblast formation from pericytes in renal fibrosis. To this end, we used a FoxD1-GC;DsRed mouse model to genetically label pericytes and subsequently isolated these cells through FACS-sorting from healthy kidneys



and fibrotic kidneys that were exposed to unilateral ureter obstruction (UUO). Following miRNA profiling of the isolated cells we found miR-132 to be dramatically increased. Since miR-132 has been described to directly target NAD-dependent deacetylase Sirt1¹⁹ and Sirt1 is known to protect against renal fibrosis²⁰ we further investigated the role of this miRNA in renal fibrosis and related its expression to SIRT1 activity. We demonstrated that silencing of miR-132 reduces the fibrotic response in a UUO model of renal fibrosis predominantly by decreasing the proliferative capacity of pericyte-derived myofibroblasts.

Results

Accumulation of FoxD1-derivative interstitial cells in UUO in mice

To follow the fate of pericytes in the pathogenesis of fibrosis we used a genetic mouse model expressing a GFP-Cre (GC) fusion protein driven by the FoxD1 promoter (*FoxD1-GC*). In *FoxD1-GC; R26R* adult mouse, perivascular interstitial cells can be identified in kidney sections following LacZ staining. As shown in figure 1A and confirming previous studies¹, 10 days after UUO we observed a marked expansion of LacZ positive pericyte-derived myofibroblasts exclusively in the interstitium of the fibrotic kidneys. To allow for cell sorting of kidney cell suspension using FACS sorting of fluorescently labeled pericyte derived cells we subsequently crossed the FoxD1-GC strain with the Z/Red (dsRed) reporter line, which shows a virtually identical expression profile as the FoxD1-GC;R26R strain (Figure 1B). Fibrosis was induced in these FoxD1-GC;Z/Red mice by unilateral ureteric obstruction (UUO) and FoxD1-derivative interstitial cells (dsRed positive) were isolated using FACS sorting from fibrotic kidneys (UUO) vs. contralateral kidneys (CLK). As expected, we observed a marked increase in dsRed positive cells in the kidney after UUO, confirming a marked expansion of in dsRed positive pericyte-derived cells (Figure 1C).



Differential miRNA expression in FoxD1-derivative interstitial cells in fibrosis

To identify miRNAs that are involved in the myofibroblastic response of pericytes in fibrotic kidney disease, we profiled miRNAs from FoxD1-derivative interstitial cells isolated from fibrotic and contralateral control kidneys. This provides a unique miRNA profile of a restricted cell population within an *in vivo* renal injury setting (Figure 1D). As shown in table 1 we found some miRNAs that were previously found to be differentially expressed in fibrosis by profiling miRNAs from whole kidneys, like miR-21^{5,14} and miR-214¹¹. In addition, we found miR-29 family members to be down regulated, which are known to target collagens¹⁰. In contrast to previous studies, our approach allowed the identification of miRNAs differentially expressed in pericyte-derive myofibroblasts. Among these, miR-132 stood out as its expression was increased ~21-fold in the myofibroblast compared fractions compared to that of the pericyte control cell suspensions. Also, when validating the upregulation of this miRNA in total kidney (UUO versus CLK; Figure 1E), we observed a 3-4 fold upregulation. To further assess the association of increased miR-132 expression in renal injury we sought to determine if miR-132 would also be differentially regulated in a different renal injury model.

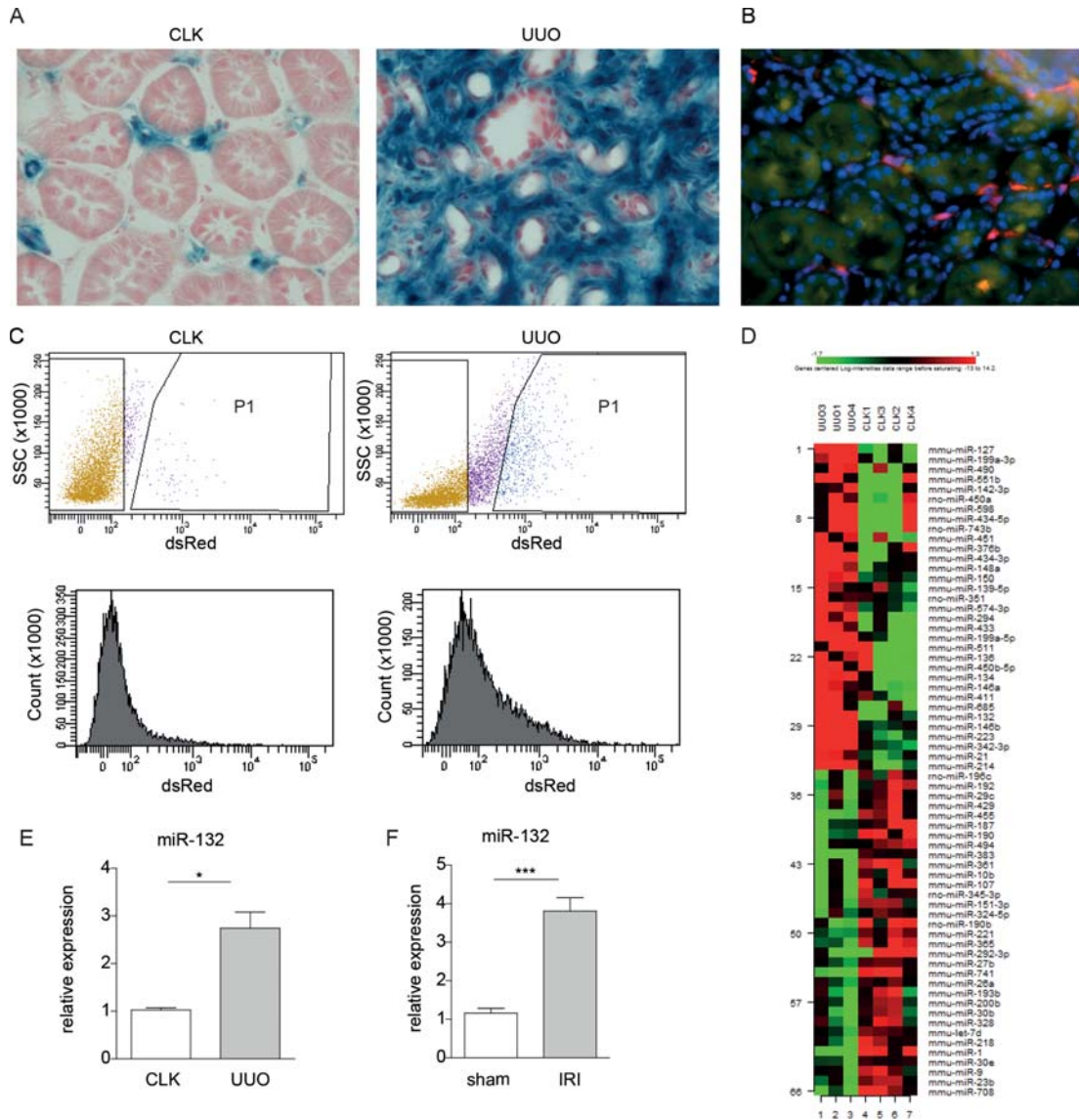


Figure 1. Differential miRNA expression in FoxD1-derivative interstitial cells during fibrosis. A, FoxD1-GC;R26R mice show typical localization of FoxD1 positive cells in mouse kidney visualized by galactosidase expression (LacZ), representing pericytes. UUO induces expansion of FoxD1-derivative myofibroblasts in the interstitium. B, FoxD1-GC;Z/Red mice show similar pericyte specific labeling as compared to FoxD1-GC;R26R mice. C, FACS plots of sorted cells from CLK and UUO kidney. Gated population (P1) represents sorted cell population that are markedly increased after UUO as depicted in the histograms. D, heatmap representing differentially expressed miRNAs with fold change more than 1.3 and p-values lower than 0.17. Red indicates high expression, green low expression. E, qRT-PCR quantification of miR-132 expression in total RNA from UUO kidneys compared to CLK. F, qRT-PCR for miR-132 in total kidney RNA obtained 3 days after renal ischemia reperfusion injury as compared to kidneys from sham operated mice.

Table 1. Differential miRNA expression. Top 20 differentially expressed miRNAs based on p-value. Mean of intensities represents absolute expression level of the miRNA. A positive fold change indicates upregulation in UUO versus healthy kidney. FDR is false detection ratio.

Parametric p-value	FDR	Mean of intensities in CLK	Mean of intensities in UUO	Fold-change	Description
8,80E-06	0,00222	125167,44	1405838,75	11,2	mmu-miR-146b
0,000 5411	0,0668	300290,57	4273538,8	14,3	mmu-miR-223
0,0007948	0,0668	111408,45	658123,93	5,9	mmu-miR-342-3p
0,0036602	0,169	462549,95	3083917,85	6,7	mmu-miR-150
0,0042723	0,169	45198,89	179091	4,0	mmu-miR-574-3p
0,0045003	0,169	382274,52	153939,05	-2,48	mmu-miR-221
0,004864	0,169	81697,22	12130,35	-6,73	mmu-miR-455
0,0054653	0,169	38732,3	828418,64	21,3	mmu-miR-132
0,0060219	0,169	2663,3	244306,59	90,9	mmu-miR-214
0,0078164	0,197	343928,67	176584,64	-1,95	mmu-miR-27b
0,0108911	0,25	166,11	2,42	-68,56	mmu-miR-741
0,0137817	0,274	582439,88	1837951,1	3,1	mmu-miR-21
0,0148108	0,274	1,78	308,9	175,4	mmu-miR-199a-5p
0,0152064	0,274	1099753,64	4653872,5	4,2	mmu-miR-146a
0,019057 5	0,307	37212,5	4528,03	-8,22	mmu-miR-708
0,0202887	0,307	729981,29	177074,88	-4,12	mmu-miR-365
0,0207106	0,307	12843,49	295,09	-43,52	mmu-miR-383
0,0290634	0,398	45829,84	1348570,58	29,4	mmu-miR-685
0,0300052	0,398	5,89	3216,63	555,6	mmu-miR-134
0,0391934	0,443	3,89	338,65	90,9	mmu-miR-294



Therefore, we induced ischemia-reperfusion injury in mice, isolated RNA from the kidneys 3 days after injury and measured miR-132 levels. Indeed, also in this renal injury model we found an over three fold upregulation of miR-132 (Figure 1F).

Silencing miR-132 affects Sirt1, Cox2 and α -SMA expression in vitro

MiR-132 has been described to directly target Sirt1¹⁹ and thereby attenuate renal fibrosis through protection from oxidative injury by increasing Cox2 expression²⁰. Therefore we assessed whether miR-132 could also play a role in the differentiation of pericytes towards myofibroblasts in renal fibrosis through targeting Sirt1.

Previously we demonstrated that antagomirs can be used to specifically silence miRNA expression both *in vitro* as well as *in vivo*²¹. Here, we employed an antagomir directed to miR-132 to study the effect of miR-132 in renal fibrosis. First, we investigated the role of miR-132 in regulating Sirt1 and Cox2

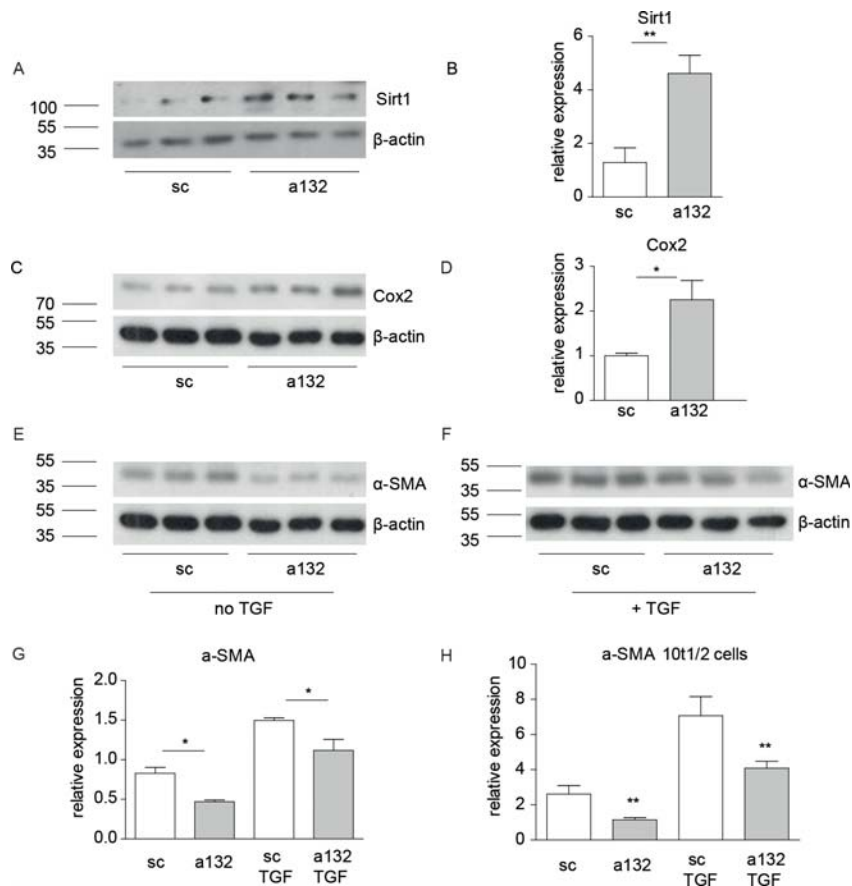


Figure 2. In vitro silencing of miR-132 results in increased Sirt1 and Cox2 expression, while α -SMA is decreased. A, western blot for Sirt1 on NIH3T3 cells treated with antagomir-132 or the scramblemir control. B, Bar graph shows quantification of Sirt1 western blots. C, western blot for Cox on NIH3T3 cells treated with antagomir-132/scramblemir. D, Bar graph shows quantification of Cox2 western blots. All results are normalized on β -actin levels. E and F, western blot for α -SMA of TGF- β stimulated NIH3T3 cells treated with antagomir-132 or the scramblemir control. G, Bar graph shows quantification of α -SMA western blots. Results are normalized on β -actin levels. H, qPCR for α -SMA RNA expression in TGF- β stimulated C3H10T1/3 cells treated with antagomir-132 or the scramblemir control.

expression *in vitro*. When pericyte-like mouse fibroblast cell line (NIH3T3 cells) were cultured in the presence of antagomir-132 for 48 hours both Sirt1 and Cox2 protein expression were increased over two fold as determined by western blot, indicating that antagomir-132 indeed is able to positively affect these proteins (Figure 2A-D).

Cells were then stimulated with TGF- β to induce differentiation towards myofibroblasts. This was evidenced by a change in morphology (elongation; data not shown) and an increase in α -SMA protein expression. The addition of antagomir-132 led to abrogation of this transition as illustrated by a

decrease in morphological alteration (data not shown) and decreased α -SMA protein expression (Figure 2E-G). Note that baseline α -SMA levels are already lowered due to antagomir-132. To confirm this ‘anti-fibrotic’ effect of antagomir-132, we repeated the experiment on pericyte-like mesenchymal C3H/10T1/2 cells and stimulated them with TGF- β to induce myofibroblast formation. This resulted in increased α -SMA gene expression, which was again decreased when cultured with antagomir-132 (Figure 2H), thereby validating the potential anti-fibrotic role of antagomir-132.

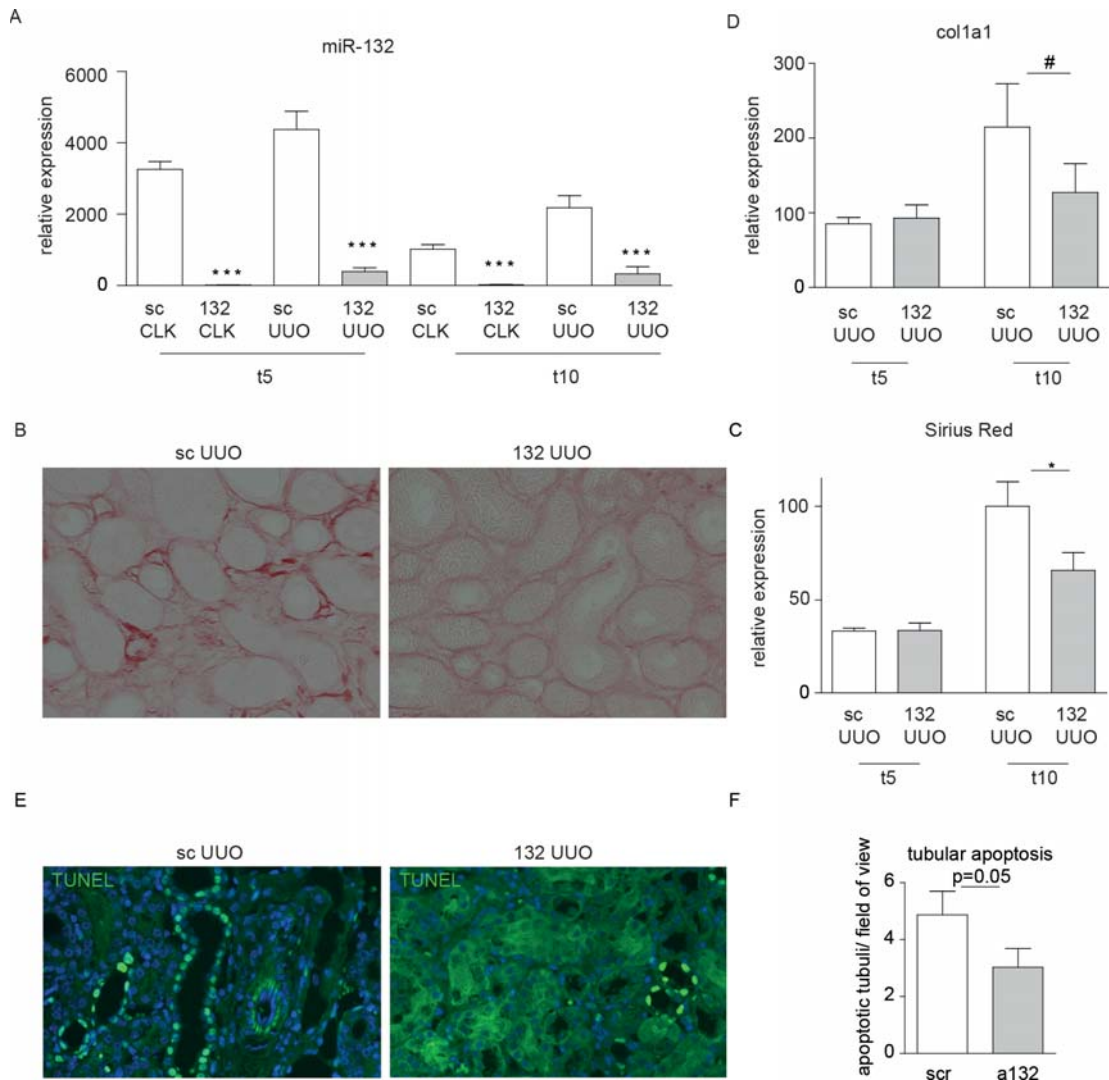


Figure 3. Silencing of miR-132 results in decreased collagen deposition. A, qRT-PCR for miR-132 in total kidney shows silencing of miR-132. B and C, representative microscopic images of Sirius Red staining of UUO kidneys from scramblemir (B) and antagomir-132 (C) treated mice. D, quantification of Sirius Red staining at day 5 and day 10 shows decreased collagen levels at day 10. E, qRT-PCR for collagen1 α 1. (E and F), representative microscopic images of TUNEL staining (E) and quantification of tubuli containing apoptotic cells (F).

Silencing miR-132 suppresses collagen deposition in vivo

Given the antifibrotic effects of miR-132 silencing in vitro, we next investigated the effect of miR-132 silencing in a mouse model of renal fibrosis. Balb/c mice WT mice were administrated with antagomir-132 or scrambled control antagomirs (n=7 per group, 40 mg/kg), exposed to UUO and sacrificed 5 and 10 days after the procedure. Antagomir silencing of miR-132 expression in the treated kidneys was confirmed by q-RT-PCR and was found to be almost complete, although in the fibrotic kidneys a low level of expression was retained.

To determine the effect of miR-132 silencing on fibrosis we performed picosirius red staining to quantify the collagen content in the kidneys. While no difference in kidney collagen content was observed 5 days after UUO, 10 days after UUO we did observe a significant protective effect of miR-132 silencing amounting to a ~25% reduction in collagen deposition (Figure 3A, $p < 0.05$). This result was consistent with the reduction of collagen-1 α 1 gene expression that was not different 5 days after UUO but significantly reduced in the antagomir-132 treated mice 10 days after UUO (Figure 3D, $P = 0.09$). In concordance with the reduced fibrosis, we found a nearly significant reduction in the number of apoptotic tubular epithelial cells, as determined by TUNEL staining, in the antagomir-132 treated cells (Figure 3EF).

Silencing miR-132 reduces the myofibroblast formation 10 days after UUO

To assess the effect of antagomir-132 silencing on UUO induced myofibroblast formation we stained the kidney sections for α -smooth muscle actin (α -SMA). We observed a marked reduction in the number of cells staining positive for α -SMA in kidneys from the mice treated with antagomir-132 as compared to the kidneys of scramblemir-treated mice 10 days after UUO (Figure 4, $p < 0.05$). To validate this finding we determined total α -SMA protein expression in these kidneys by western blot. This confirmed the decrease in α -SMA expression in the antagomir-132 treated group at 10 days after surgery (Figure 4CD, $p < 0.0005$). Also the α -SMA mRNA levels were consistent with the downregulation of the gene 10 days after UUO (Figure 4E, $p < 0.05$). Again no differences in α -SMA expression were observed 5 days after UUO. Since the α -SMA staining directly correlates to the number of FoxD1-derivative interstitial cells¹ we conclude that, following UUO, silencing of miR-132 impacts on the differentiation and/or proliferation of pericytes towards myofibroblasts.

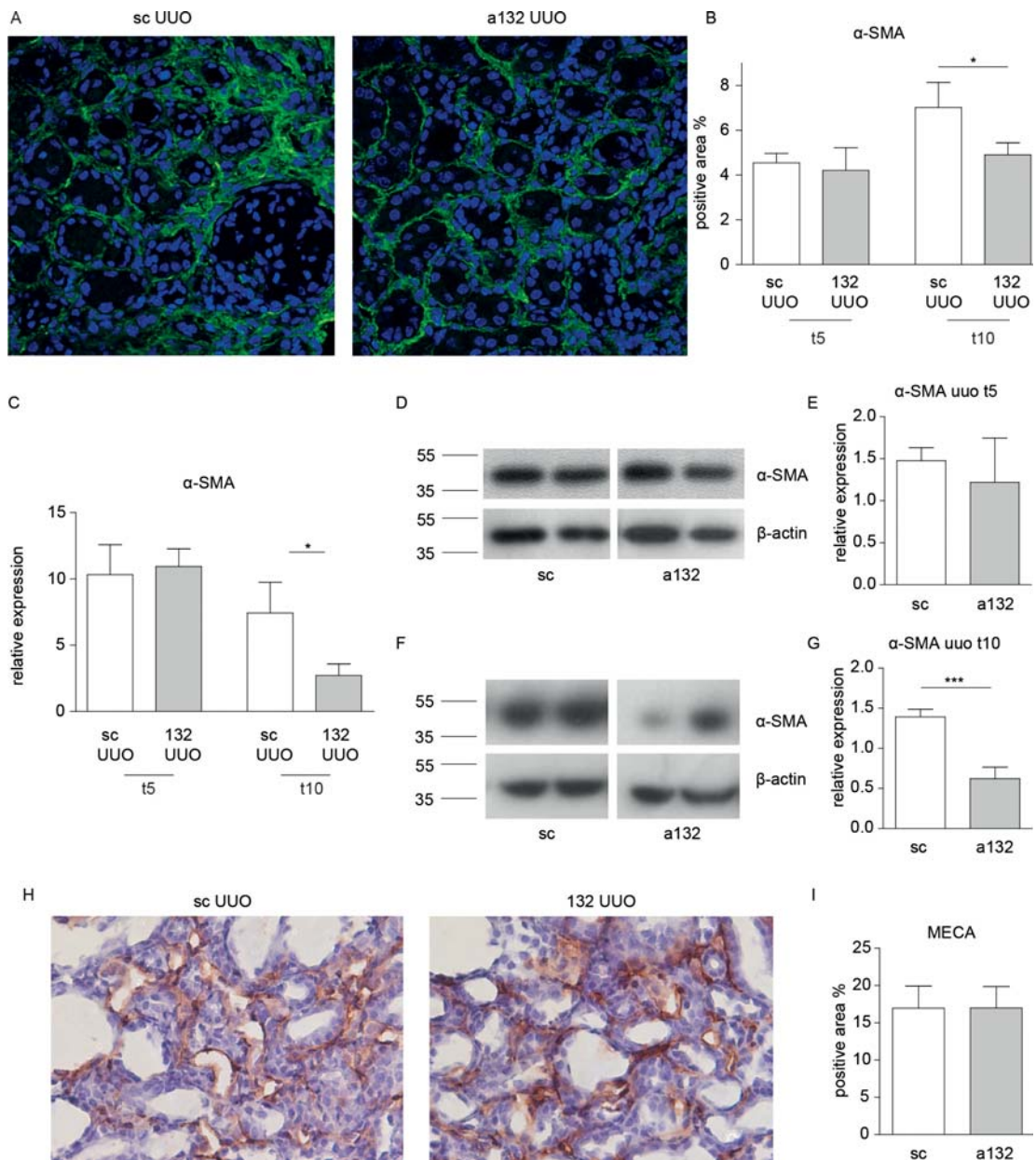


Figure 4. Silencing of miR-132 reduces α -SMA levels 10 days after UOU. A, representative microscopic images of immunofluorescent staining for α -SMA show decreased α -SMA staining in kidneys from mice treated with antagomir-132. B, bar graph shows quantification of α -SMA staining. C, qPCR for α -SMA. D-G, representative duplicate western blots and quantification for α -SMA, normalized by β -actin, in UOU kidneys after 5 days (D and E) and 10 days (F and G). H, no differences in capillary density as illustrated by representative microscopic images of staining for MECA on kidney sections. I, bar graph shows quantification of MECA staining.

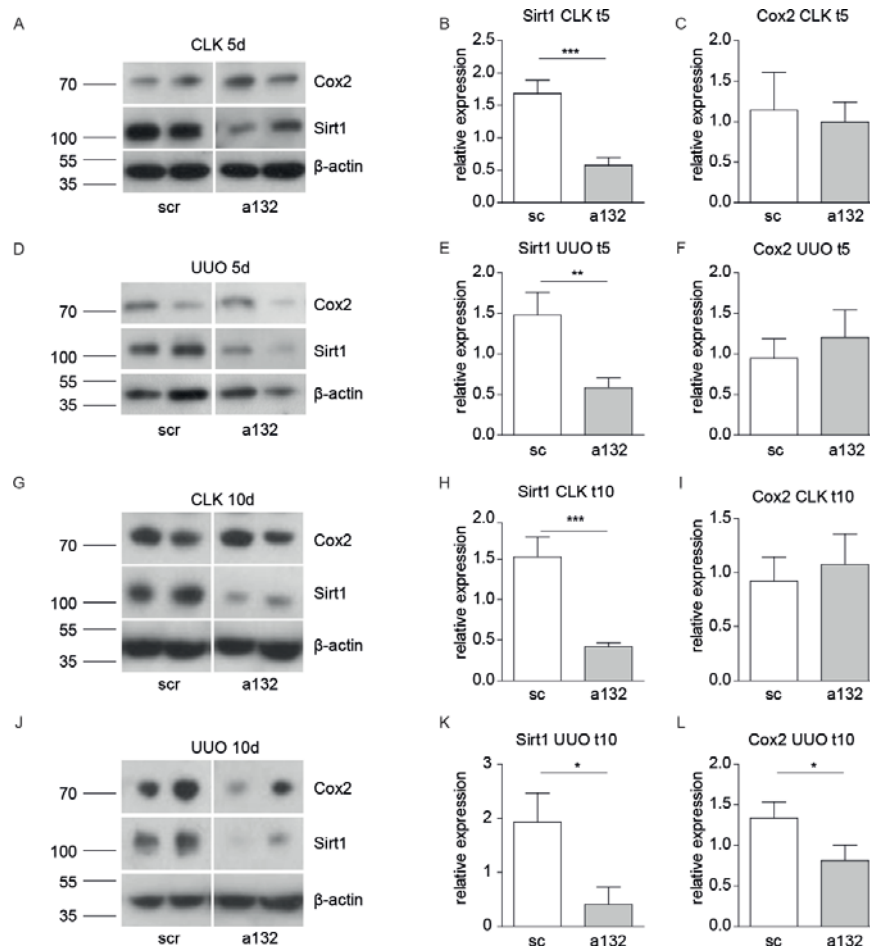


Figure 5. Reduced Sirt1 and Cox2 expression in UUUO kidneys of antagomir-132 treated mice. A-L, Western Blot quantification of Sirt1 and Cox2 expression in UUUO and control kidneys treated with antagomir-132 or control scramblemir. Bar graphs depict quantified, β -actin normalized Sirt1 and Cox2 expression levels in the treated kidneys.

No difference in capillary density

As the loss of pericytes may be associated with loss of the peritubular capillary network we sought to determine the capillary density in both treatment groups. To that end, we stained whole kidney sections with mouse endothelial cell antigen (MECA). In contrast to our expectation, we did not observe a difference in capillary density between antagomir-132 and scramblemir treated mice 10 days after UUUO (Figure 4HI).

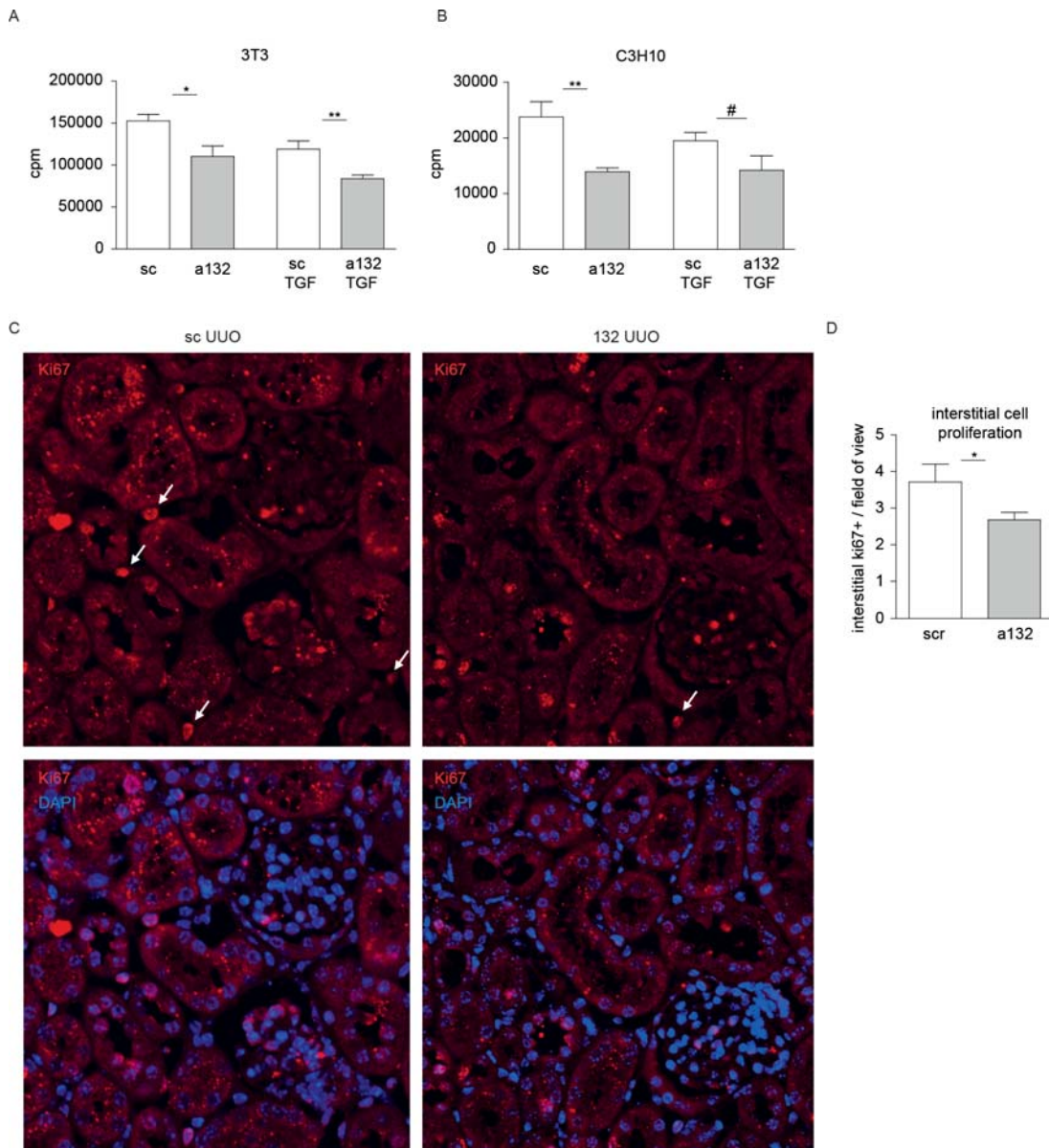


Figure 6. Silencing miR-132 reduces (myo)fibroblast proliferation. Thymidine incorporation proliferations assays demonstrate decreased proliferation of NIH3T3 cells (A) and C3H/10T1/2 cells (B) treated with antagomir-132. Cpm is counts per minute. (C and D), representative microscopic images of Ki67 staining (C) and quantification of Ki67 positive interstitial cells (D) 10 days after UUO in kidneys of mice treated with antagomir-132 or the scramble control.

Antagomir-132 decreases levels of Sirt1 and Cox2 in vivo

Following the above, we investigated whether the antifibrotic effects of miR-132 silencing were associated with increased expression of Sirt1 and Cox2. However, in contrast to the effects we observed with myofibroblast formation *in vitro*, miR-132 silencing in UUO kidneys and control kidneys



significantly decreased Sirt1 levels at both timepoints of sacrifice (Figure 5). Cox2 expression was only reduced in the obstructed kidney at day 10 (Figure 5L). This decrease follows the pattern we observed for fibrotic markers that also were decreased only at this time point. Western blot on pooled kidney lysates for each group confirms these findings (Supplementary Figure 1).

Silencing of miR-132 inhibits proliferation of (myo)fibroblasts

As we observed differences in fibrosis only after 10 days, we sought to determine whether miR-132 silencing would affect (myo)fibroblast proliferation. NIH3T3 and C3H/10T1/2 cells were cultured with or without TGF- β and treated with antagomir-132 or scramblemir and proliferation was quantified using the thymidine incorporation assay. Proliferation of both cell lines was significantly reduced when miR-132 was silenced (Figure 6AB). Subsequently we analyzed the number of interstitial proliferating cells in kidney sections from fibrotic kidneys that received either antagomir-132 or scramblemir. Indeed, a decreased number of proliferating cells was observed in the interstitium of antagomir-132 treated kidneys, further supporting a role for miR-132 in (myo)fibroblast proliferation.

Discussion

When mouse kidneys are exposed to UUO, miR-132 expression is strongly increased in the pericyte-derivative myofibroblasts that accumulate during the fibrotic response. As silencing of this microRNA resulted in a decreased fibrotic phenotype of the kidneys 10 days after UUO we conclude that miR-132 plays a rate limiting role in this model of kidney fibrosis. Our data support a facilitary role for miR-132 in the proliferation of myofibroblasts. As myofibroblasts are also the major contributors to the excessive production of extra cellular matrix proteins, silencing of miR-132 leads to a reduction in the myofibroblastic response as well as to a reduced buildup of collagen-rich scar tissue.

In recent studies aimed at the identification of miRNAs that are involved in the pathogenesis of kidney fibrosis miR-132 was not listed as significantly upregulated in kidneys following UUO, while other common fibrotic miRNAs (mir-21, mir-214, miR-29) were included¹⁴. We strongly believe this illustrates the value of our approach to use lineage tracing to assess cell type specific miRNA responses that may be masked by the response or influx of numerous other cell types when total kidney RNA preparations are used to identify differentially expressed miRNAs. This is clearly illustrated by the fact that we showed a 21 fold upregulation of miR-132 in the selected FoxD1-derivative cells in obstructed kidneys versus contralateral kidneys while in the RNA preparations from total kidneys miR-132 levels were only 3 fold enriched. Likewise we clearly confirmed suppression of Sirt1 expression by miR-132 *in vitro*, while SIRT1 protein expression in lysates of whole kidneys that were treated with antagomir-132 expression was markedly reduced. Since in this case our measurement involved whole kidney analysis, it is still possible that in the FoxD1-derivative cells Sirt1 is negatively regulated by miR-132 and the observed decrease is due to the response of other cell types. Although Sirt1 is upregulated in the fibrotic kidney (Supplementary Figure 1), the reduction in SIRT1 expression in the whole kidney extracts is not the result of the reduced fibrotic response in this treatment group as Sirt1 expression is also reduced in the treated contralateral kidneys. Clearly other indirect miR-132 dependent effects may be operational.

The finding that fibrosis is reduced at day 10 only is in concordance with the finding that Cox2 expression is also reduced only in that particular situation. It has been described that Cox2 plays a role in fibroblast differentiation²², so the lower Cox2 levels might be involved in the reduction of number of



myofibroblasts. It is more likely however that lower Cox2 levels just reflect the decrease in fibrosis as Cox2 is strongly increased during fibrosis (see also Supplementary Figure 1).

It was unexpected that although we observe reduced fibrosis due to miR-132 silencing, this is a 'long-term' effect as after 5 days we did not observe this protective effect. The fact there is no difference in capillary density is also surprising, as peritubular capillary rarefaction is a typical feature of renal fibrosis²³. In addition, it seems plausible that pericyte to myofibroblast transition could result in detachment of pericytes from the microvascular interface leaving unstable capillaries that would result in rarefaction². These findings suggest an initial phase where pericytes detach from the vessels and transform into myofibroblasts, followed by a proliferation phase of these cells. As we did not observe differences in capillary density, and found the protective effect to take place in a later phase, this suggests miR-132 is not involved in the initial, but in the later proliferating phase. This is supported by the fact that we identified antagomir-132 to be able to suppress proliferation of two different pericyte-like cell lines *in vitro*. In addition, miR-132 silencing has been described to be anti-proliferative in endothelial cells²⁴ and in saphenous vein-derived pericyte progenitor cells (SVPs)²⁵. However, the latter paper also described that SVPs reduce interstitial fibrosis after myocardial infarction, while this inhibition of fibrosis and reduced cardiac fibroblast proliferation and differentiation into myofibroblasts was abrogated by transfection of SVPs with anti-miR-132. These data suggest a dynamic role for miR-132, dependent on source, location and environment.

Taken together, we have demonstrated differential expression of miRNAs in FoxD1-derivative interstitial cells in fibrotic kidneys and show that silencing of miR-132 protects against renal fibrosis. This protection is correlated with a decrease in renal Sirt1 levels and our data suggest an important role for miR-132 in the proliferation of myofibroblasts in renal fibrosis.

Materials and Methods

Cell Culture

The cell lines C3H/10T1/2 and NIH3T3 (mouse fibroblast) were obtained from ATCC (American Type Culture Collection, Manassas, VA). Both cell lines were maintained in Dulbecco's modified Eagle medium (Gibco/Invitrogen, Breda, the Netherlands) supplemented with 10% fetal calf serum (Bio Whittaker/Cambrex, Verviers, Belgium) and 1x L-glutamin (Invitrogen) with a final concentration of 2 mM and were incubated at 37 °C in 5% CO₂. Cells were treated with 10 ng/mL TGF- β 1 (R&D) for 48 hours unless otherwise indicated. Antagomir-132 or scramblemir was added in a concentration of 5 μ g/mL.

Animal experiments

All animal experimental protocols were approved by the animal welfare committee of the veterinary authorities of the Leiden University Medical Center or protocols overseen by Animal Resources and Comparative Medicine at Harvard University.

Bilateral Ischemia Reperfusion Injury of the Kidneys

C57BL/6 WT mice (n=5 per group, age=10 weeks, Charles River, Maastricht, the Netherlands) were used. Before surgery, mice were anesthetized and the core body temperature was maintained at 37 °C. Via flank incisions the renal artery and vein were identified and bilaterally clamped for 25 minutes using surgical clamps (S&T, Neuhausen, Switzerland). In the sham-group identical surgical procedures were used, except that clips were not applied. After removing the clamps, color change indicating proper reflow was confirmed. After 72 hours the mice were anesthetized and euthanized. Kidneys were removed and RNA was isolated as described elsewhere.

Unilateral Ureteral Obstruction (UUO)

For miRNA profiling of FoxD1-derivative cells, 8 week old FoxD1-GC;Z/Red mice were used. For antagomir studies, 8 week old Balb/c mice WT mice (Jackson Laboratories, Bar Harbor, ME, USA) were used. Unilateral ureteral obstruction (UUO) was performed through a left flank incision under general anesthesia. The ureter was identified and ligated twice at the level of the lower pole of the kidney with two separate silk ties. Antagomir or control scramblemir was administrated i.v. at a dose of 40 mg/kg bodyweight 24 hours before surgery.



Profiling microRNAs by TaqMan® Array MicroRNA Cards

For miRNA cDNA synthesis, total RNA was reverse transcribed using the miRNA reverse transcription kit (Applied Biosystems, Foster City, CA, USA) in combination with the stem-loop Megaplex Human primer pools A V2.1 (Applied Biosystems) according to manufacturer's instructions. For each cDNA sample, 384 microRNAs including 6 controls (RNU44, RNU48, 4*U6), were profiled using TaqMan® Array MicroRNA Human Card A V2.0 (Applied Biosystems) according to manufacturer's instructions. All arrays were run on a 7900HT Fast Real-Time PCR System (Applied Biosystems) and default thermal-cycling conditions. For each array the obtained Ct-values were converted to relative quantities normalized to RNU48.

RNA isolation and qRT-PCR analysis

Total RNA from kidneys was isolated using Trizol reagent (Invitrogen, Breda, The Netherlands). Reverse transcription was performed using a 5 minute 65°C incubation of 250 ng total RNA with dNTPs (Invitrogen) and oligo(dT) (Invitrogen) or using specific Taqman® microRNA probes (miR-132, Applied Biosystems). cDNA was synthesized using a M-MLV First-Strand Synthesis system (Invitrogen). Validation of mRNA levels was carried out using SYBR Green Master Mix (Applied Biosystems). Primer sequences of target genes are as follows: α -SMA (sense) CGTGGCTATTCCTTCGTGAC; α -SMA (antisense): GCGTTCGTAGCTCTTCTCC; Col1 α 1 (sense): TGACTGGAAGAGCGGAGAGT; Col1 α 1 (antisense): GTTCGGGCTGATGTACCAGT; GAPDH (sense): ACTCCCACTCTTCCACCTTC; GAPDH (antisense): CACCACCCTGTTGCTGTAG. Levels of expression were determined by normalizing to GAPDH. Validation of miRNA levels was performed using Taqman® miR assays (Applied Biosystems). MiRNA levels were normalized on RNU6B levels obtained from the same RNA. The following primers were used for PCR: U6 (sense) CTCGCTTCGGCAGCACA and U6 (antisense) AACGCTTCACGAATTTGCGT. Results were normalized using Gene Expression Analysis for iCycler IQ® RT-PCR Detection System (Bio-Rad Laboratories, Veenendaal, The Netherlands).

Western Blot

Cells or tissues collected for Western Blot were lysed in RIPA buffer (50mM Tris-HCl pH7.5, 150 mM NaCl, 0.1% SDS, 0.5% sodium deoxycholate, 1mM EDTA, 1% Triton X-100) containing phosphatase and protease inhibitors. Equal amounts of proteins (~20 ug) were prepared in sodium dodecyl sulfate (SDS) sample buffer and boiled for 5 min at 95°C before

loading onto 10% sodium dodecyl sulfate-polyacrylamide (SDS-PAGE) gradient gels, and electrophoresis was carried out under reducing conditions. Proteins were then transferred to nitrocellulose membranes (Amersham, 's Hertogenbosch, the Netherlands) that were blocked overnight with PBS with 0.1% Tween 20 containing 5% nonfat powdered milk and incubated with the primary antibody in this blocking solution for 1 h at room temperature. The blots were subsequently washed in PBS-Tween and then incubated with an appropriate HRP-conjugated secondary antibody in blocking solution. Primary antibodies against the following proteins were used: α -SMA (0.25 ug/mL, R&D, Minneapolis, MN, USA), β -actin (0.1 ug/mL, Abcam, Cambridge, UK), Sirt-1 (1 ug/mL, Abcam) and Cox2 (0.1 ug/mL, Abcam). Horseradish peroxidase conjugated goat-anti-rabbit IgG or goat-anti-mouse IgG (0.05 ug/mL, DakoCytomation, Enschede, The Netherlands) was used as secondary antibody. Bound fragments were detected with chemiluminescent reagents (Supersignal West Dura Extended Duration Substrate; ThermoFisher Scientific, Waltham, MA, USA) and exposed on Hyperfilm ECL (Amersham). Quantitative analysis of the protein bands intensity on Western blot was performed using imageJ software and normalized for β -actin.

Design of Antagomirs

Cholesterol-conjugated RNA analogs, 'antagomirs', (Dharmacon RNA technologies, Lafayette, CO, USA) were synthesized as previously described²⁶. For antagomir-132 the following sequence was used: 5'-c_sg_sacc_sauggc_suguagac_sug_su_sa_s-Chol-3'. As a control a 'scramblemir' was used, this RNA analog is constructed from a randomized nucleotide sequence which does not bind to any known microRNAs: 5'-a_su_sgac_suac_sgc_suauuc_sgc_sa_su_sg_s-Chol-3'. The lower case letters represent 2'-OMe-modified nucleotides; subscript 's' represents phosphorothiate linkage; 'Chol' represents a cholesterol-group linked through a hydroxyprolinol linkage.

Immunohistochemistry

Mice were anesthetized, sacrificed, and immediately perfused via the left ventricle with ice-cold PBS for 2 minutes. Kidneys were sagittally sectioned and half was fixed in 10% neutral buffered formalin at 4°C for 12 hours, processed, embedded in paraffin wax, sectioned, and stained with picrosirius red as follows: the kidney sections were deparaffinized with xylene and then re-hydrated in water through graded ethanol. The slides were then incubated for 5 minutes in 0.2% phosphomolybdic acid (Sigma, St. Louis, MO, USA) to reduce background. The sections were incubated in picrosirius red for three hours followed by a two washes with acidified water. The sections were then



dehydrated and mounted in permount mounting medium (Fisher Scientific, Landsmeer, the Netherlands). Images of complete sections were obtained using a Panoramic Midi slide scanner (3DHitech, Budapest, Hungary). The area of collagen deposition, stained red by picosirius red staining, was measured using ImageJ software; whole sections were analyzed. For ki67 staining, after de-paraffinization, sections were subjected to heat-induced antigen retrieval using citrate buffer (10mM, pH 6.0) in a microwave for 20 min. Next, sections were incubated overnight at 4°C with an antibody against Ki67 (Santa Cruz Biotechnology, Santa Cruz, CA, USA) followed by an appropriate secondary antibody labeled with Alexa-488 (Molecular Probes). Apoptotic cells were counted after being identified by the terminal deoxynucleotidyl-transferase-mediated deoxyuridine 5-triphosphate nick end labeling (TUNEL) assay (Roche, Mannheim, Germany).

Other halves of the kidney were fixed in 4% PFA for 1 hour at 4°C, cryopreserved in 20% sucrose, and frozen. 5 µm sections were stained for α-SMA using mouse fluorescein isothiocyanate-conjugated antibody (Sigma). For MECA32, first endogenous peroxidase was blocked with H₂O₂. Sections were then incubated with a specific antibody against MECA32 (Becton Dickinson, Franklin Lakes, New Jersey, USA), followed by horseradish peroxidase (HRP)-conjugated appropriate secondary antibodies (Jackson ImmunoResearch, Westgrove, PA, USA). As a negative control, isotype-matched IgG was used. The staining was visualized using Nova RED (Vector Labs, Peterborough, UK) and counterstained with hematoxylin. Quantification of immunohistochemistry was performed Using image J software, whole sections were analyzed.

FACS sorting

Kidneys were homogenized using a gentleMACS dissociator (Miltenyi Biotec, Bergish Gladbach, Germany) in combination with enzymatic digestion using Liberase (Roche). The obtained cell suspension was sorted using the FACS Aria II (BD Biosciences, Franklin lakes, NJ, USA).

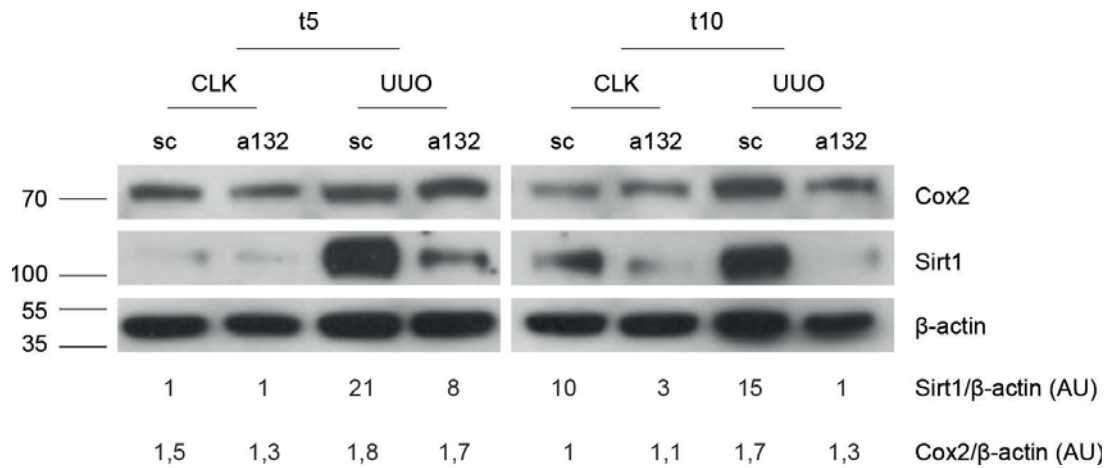
Proliferation assay

Proliferation was measured by the addition of ³H-thymidine (0.5 µCi/well; Amersham Biosciences, The Netherlands) 16 hours before cell lysis. The amount of ³H-thymidine incorporation was measured using a liquid scintillation analyzer (Tri-Carb 2900R). Responses are expressed as mean counts per minute of triplicate cultures.

Statistical Analysis

Results are expressed as mean \pm standard error of the mean (SEM). Statistical analysis was performed using student's T-test. $P < 0.05$ were considered statistically significant.

Supplementary Files



Supplementary Figure 1. Western blot on pooled kidney lysates confirm decrease in Sirt1 due to miR-132 inhibition. Cox2 is only decreased 10 days after UUO. Note that UUO itself results in increased Sirt1 and Cox levels. Below the western blot, Sirt1 or Cox2 over β -actin ratios are indicated.



References

1. Humphreys, B.D., et al. Fate tracing reveals the pericyte and not epithelial origin of myofibroblasts in kidney fibrosis. *Am J Pathol* 176, 85-97 (2010).
2. Schrimpf, C. & Duffield, J.S. Mechanisms of fibrosis: the role of the pericyte. *Curr Opin Nephrol Hypertens* 20, 297-305 (2011).
3. Xie, X., et al. Systematic discovery of regulatory motifs in human promoters and 3' UTRs by comparison of several mammals. *Nature* 434, 338-345 (2005).
4. Kloosterman, W.P. & Plasterk, R.H. The diverse functions of microRNAs in animal development and disease. *Dev Cell* 11, 441-450 (2006).
5. Thum, T., et al. MicroRNA-21 contributes to myocardial disease by stimulating MAP kinase signalling in fibroblasts. *Nature* 456, 980-984 (2008).
6. Matkovich, S.J., et al. MicroRNA-133a protects against myocardial fibrosis and modulates electrical repolarization without affecting hypertrophy in pressure-overloaded adult hearts. *Circ Res* 106, 166-175 (2010).
7. van Rooij, E., et al. Control of stress-dependent cardiac growth and gene expression by a microRNA. *Science* 316, 575-579 (2007).
8. van Rooij, E., et al. Dysregulation of microRNAs after myocardial infarction reveals a role of miR-29 in cardiac fibrosis. *Proc Natl Acad Sci U S A* 105, 13027-13032 (2008).
9. Roderburg, C., et al. Micro-RNA profiling reveals a role for miR-29 in human and murine liver fibrosis. *Hepatology* 53, 209-218 (2011).
10. Liu, Y., et al. Renal medullary microRNAs in Dahl salt-sensitive rats: miR-29b regulates several collagens and related genes. *Hypertension* 55, 974-982 (2010).
11. Denby, L., et al. miR-21 and miR-214 are consistently modulated during renal injury in rodent models. *Am J Pathol* 179, 661-672 (2011).
12. Macconi, D., et al. MicroRNA-324-3p promotes renal fibrosis and is a target of ACE inhibition. *J Am Soc Nephrol* 23, 1496-1505 (2012).
13. Kriegel, A.J., Liu, Y., Cohen, B., Usa, K. & Liang, M. MiR-382 targeting of kallikrein 5 contributes to renal inner medullary interstitial fibrosis. *Physiol Genomics* 44, 259-267 (2012).
14. Zarjou, A., Yang, S., Abraham, E., Agarwal, A. & Liu, G. Identification of a microRNA signature in renal fibrosis: Role of miR-21. *Am J Physiol Renal Physiol* (2011).
15. Zhong, X., Chung, A.C., Chen, H.Y., Meng, X.M. & Lan, H.Y. Smad3-mediated upregulation of miR-21 promotes renal fibrosis. *J Am Soc Nephrol* 22, 1668-1681 (2011).
16. Chung, A.C., Huang, X.R., Meng, X. & Lan, H.Y. miR-192 mediates TGF-beta/Smad3-driven renal fibrosis. *J Am Soc Nephrol* 21, 1317-1325 (2010).
17. Kato, M., et al. MicroRNA-192 in diabetic kidney glomeruli and its function in TGF-beta-induced collagen expression via inhibition of E-box repressors. *Proc Natl Acad Sci U S A* 104, 3432-3437 (2007).
18. Krupa, A., et al. Loss of MicroRNA-192 promotes fibrogenesis in diabetic nephropathy. *J Am Soc Nephrol* 21, 438-447 (2010).
19. Strum, J.C., et al. MicroRNA 132 regulates nutritional stress-induced chemokine production through repression of SirT1. *Mol Endocrinol* 23, 1876-1884 (2009).
20. He, W., et al. Sirt1 activation protects the mouse renal medulla from oxidative injury. *J Clin Invest* 120, 1056-1068 (2010).
21. van Solingen, C., et al. Antagomir-mediated silencing of endothelial cell specific microRNA-126 impairs ischemia-induced angiogenesis. *J Cell Mol Med* 13, 1577-1585 (2009).

22. Frungieri, M.B., Weidinger, S., Meineke, V., Kohn, F.M. & Mayerhofer, A. Proliferative action of mast-cell tryptase is mediated by PAR2, COX2, prostaglandins, and PPARgamma : Possible relevance to human fibrotic disorders. *Proc Natl Acad Sci U S A* 99, 15072-15077 (2002).
23. Ishii, Y., et al. Injury and progressive loss of peritubular capillaries in the development of chronic allograft nephropathy. *Kidney Int* 67, 321-332 (2005).
24. Anand, S., et al. MicroRNA-132-mediated loss of p120RasGAP activates the endothelium to facilitate pathological angiogenesis. *Nature medicine* 16, 909-914 (2010).
25. Katare, R., et al. Transplantation of human pericyte progenitor cells improves the repair of infarcted heart through activation of an angiogenic program involving micro-RNA-132. *Circ Res* 109, 894-906 (2011).
26. Krutzfeldt, J., et al. Silencing of microRNAs in vivo with 'antagomirs'. *Nature* 438, 685-689 (2005).



Chapter

6

In preparation

MicroRNA-132 regulates diuresis through vasopressin- and prostaglandin-dependent alteration of Aquaporin-2 localization

R. Bijkerk^{1,3}, C. Trimpert², C. van Solingen¹, R.G. de Bruin¹, T.J. Rabelink¹, B.D. Humphreys³, P.M.T. Deen² and A.J. van Zonneveld¹.

¹Department of Nephrology and the Einthoven Laboratory for Experimental Vascular Medicine, Leiden University Medical Center, Leiden, the Netherlands. ²Department of Physiology, Radboud University Nijmegen Medical Centre, Nijmegen, the Netherlands.

³Renal Division, Department of Medicine, Brigham & Women's Hospital and Harvard Medical School, Boston, Massachusetts, USA.

Abstract

The collecting duct (CD) principal cells of our kidneys are critical in the maintenance of blood water levels, as binding of vasopressin (AVP) to its V2-receptor and the subsequent translocation of aquaporin-2 (AQP2) water channels to the apical membrane fine-tunes water balance. Cyclooxygenase-2 (Cox2) produces prostaglandins such as PGE2 that counteract renal AVP action by inducing internalization and lysosomal degradation of AQP2. A role for microRNAs (miRNAs) in the regulation of water and electrolyte balance remains unexplored. We identified miR-132 as a potential post-transcriptional regulator of Cox2 expression and investigated the role of this miR132 in diuresis *in vitro* and *in vivo*. Silencing of miR-132 in cultured collecting duct cells as well as in fibroblast cells resulted in the upregulation of Cox2 expression and altered AQP2 expression in collecting duct cells. Silencing of miR-132 in mice caused severe weight loss as a result of acute diuresis characterized by increased plasma osmolality and decreased urine osmolality. In addition, urinary PGE2 levels were elevated and hypothalamic AVP mRNA expression and blood AVP levels were not increased, despite the increased blood osmolality. This resulted in less translocation of AQP2 to the apical membrane in CD cells. Taken together, Silencing of miR-132 causes acute diuresis. Our data indicate that this is the result of a Cox2-dependent decrease in AVP synthesis/release and increase in renal PGE2 counteracting renal AVP-stimulated water reabsorption through AQP2. This is the first demonstration of water balance regulation by a miRNA.

Introduction

For our body, replenishment of water losses by an equivalent intake is essential to maintain our volume and osmo balance, as excessive water retention leads to acute or chronic hyponatremia coinciding with brain edema or osteoporosis, whereas overhydration and dehydration are fundamental to hypertension and hypotension, respectively. The collecting duct principal cells of our kidneys are critical in these regulatory processes. In states of hypovolemia or hypernatremia, the anti-diuretic hormone vasopressin is produced within the hypothalamic paraventricular (PVN) and supraoptic (SON) neurons¹. AVP is then processed, stored, and secreted into the circulation by the posterior pituitary. Upon binding to its type-2 receptor (V2R) in renal collecting duct principal cells, AVP induces a cAMP signaling cascade and activation of protein kinase A (PKA), which results in translocation of AQP2 to the apical membrane, rendering these cells water permeable²⁻⁴. Driven by the transcellular osmotic gradient, water will enter the cells through AQP2 and will leave the cells via AQP3 or AQP4, which are present in the basolateral membrane, resulting in concentrated urine¹. Upon correction of blood tonicity or volume, blood vasopressin levels will drop and AQP2 is internalized again⁵. Besides this short-term effect, vasopressin regulates AQP2 expression on the long term by increasing its transcription via activation of and promoter binding by the cyclic AMP responsive element binding protein (CREB)^{6,7}. Lack of functional V2R or AQP2 results in X-linked or autosomal nephrogenic diabetes insipidus (NDI), respectively, disorders characterized by polyuria and polydipsia due to unresponsive to vasopressin⁸, and which reveals the essential role of the V2R and AQP2 in principal collecting duct cells in this process.

AVP dependent regulation of water homeostasis can be modulated by endocrine factors such as ANG II, catecholamines, as well as prostaglandins (PGs), metabolites of the cyclooxygenase (Cox) pathway⁹. Accordingly, renal prostaglandin E₂ (PGE₂) is known to counteract renal vasopressin action¹⁰, by inducing the internalization and lysosomal degradation of AQP2¹¹. In addition, NSAIDs transiently enhance urine concentration¹². On the other hand, recent studies showed that inhibition of Cox by indomethacin reduced renal AQP2 expression in rats, implying that PGs may actually help maintain AQP2 levels¹³. Finally, PGE₂ could affect central vasopressin levels, as PGE₂ has been reported to reduce central AVP production and release¹⁴.



Several studies have assessed the expression of microRNAs (miRNAs) in the kidney^{15,16}. MiRNAs are a class of super-regulatory molecules, which control the expression of sets of genes that are often functionally related at the post-transcriptional level¹⁷. Following several impressive examples for a pivotal role for miRNAs in cardiovascular development and hematopoiesis¹⁸, there is no doubt that miRNAs will also regulate pivotal functions in renal electrolyte homeostasis. Indeed, functional involvement of miRNAs in kidney regulatory processes was shown by several recent papers. For instance, Cre-mediated deletion of dicer from uretic buds and its descendents, including collecting duct epithelium and urothelium, by using Hox7B-CRE mice resulted in severe hydronephrosis¹⁹. Importantly, most mice had focal microscopic tubular cysts originating from the collecting duct, indicating that preventing pre-miRNA dicing, and thus regulation by miRNAs in these segments, especially affects the renal collecting duct. Also, based on *in vitro* analysis, miR-192 has been suggested to have a role in aldosteron-mediated sodium and potassium balance²⁰ and miR-200b and miR-717 were associated with alterations in renal tonicity²¹. However, experimental *in vivo* analysis of, the role of miRNAs in maintaining the body's water and electrolyte balance has virtually remained unexplored.

In the present study, we aimed to identify a role for miRNAs in prostaglandin dependent regulation of water homeostasis. We found that miR-132 can directly target Cox2 and silencing of miR-132 in mice revealed a severe weight loss, polyuria, and internalization of AQP2 from the plasma membrane, suggesting the first identification of a miRNA regulating principal cell water transport.

Materials and Methods

Mice

Male balb/c mice were used (n=10 per group, age=8 weeks, Charles River Nederland, Maastricht, the Netherlands). 24 hours before i.v. tail injection of 40 mg/kg bodyweight of antagomir-132 or control scramblemir, mice were housed in metabolic cages until day of sacrifice. Standard chow diet and drinking water were provided *ad libitum*. Following antagomir injection, 24-hours urine was collected during the days indicated. Mice were anesthetized with isoflurane and blood was drawn by cardiac puncture. Kidney and hypothalamus were removed and samples for RNA and protein (kidney only) analysis were frozen in liquid N₂. The samples for immunocytochemistry were fixed in 10% neutral buffered formalin at 4°C for 12 hours, processed, embedded in paraffin wax and sectioned. All tissues were stored at -80°C. Blood plasma was obtained by centrifugation (15 min at 150 g at room temperature, no brake). The animal experiments and protocols were approved by the animal welfare committee of the veterinary authorities of the Leiden University Medical Center.

Cell culture

The cell lines NIH3T3 (3T3) and mIMCD3 (IMCD) were obtained from ATCC (American Type Culture Collection, Manassas, VA). 3T3 cells were maintained in Dulbecco's modified Eagle medium (DMEM, Gibco/Invitrogen, Breda, the Netherlands), and IMCD cells in DMEM/HAM-F12 medium. Both media were supplemented with 10% fetal calf serum (Bio Whittaker/Cambrex, Verviers, Belgium) and 1x L-glutamin (Invitrogen) at a final concentration of 2 mM. Mouse cortical collecting duct (mpkCCD) cells (clone 11) were grown as previously described²² in a modified defined medium (DMEM:Ham's F12 1:1 vol/vol; 60 nM sodium selenate, 5 µg/ml transferrin, 2mMglutamine, 50 nM dexamethasone, 1 nM triiodothyronine, 10 ng/ml epidermal growth factor, 5 µg/ml insulin, 20 mM D-glucose, 2% fetal calf serum and 20 mM HEPES (pH 7.4).

Antagomir design

Cholesterol-conjugated RNA analogs, 'antagomirs', (Thermo Scientific, Waltham, MA, USA) were synthesized as previously described²³. For antagomir-132 the following sequence was used: 5'-c_sg_sacc_sauggc_suguagac_sug_su_sa_s-Chol-3'. As a control a 'scramblemir' was used, this RNA analog is constructed from a randomized nucleotide sequence which does not bind to any known microRNAs: 5'-a_su_sgac_su_sauc_sg_sc_su_sauc_sgc_sa_su_sg_s-



Chol-3'. The lower case letters represent 2'-OMe-modified nucleotides; subscript 's' represents phosphorothiate linkage; 'Chol' represents a cholesterol-group linked through a hydroxyprolinol linkage.

Plasma and urine assays

Multistix 8 SG (Siemens, country etc) were used to qualitatively determine specific gravity in urine. Plasma and urine osmolality were determined using a freezing point depression osmometer. Urinary AVP levels were determined on 10x diluted 24-hrs urine samples using an enzymatic AVP immunoassay (Cayman Chemical, Ann Arbor, MI, USA), according to the protocol of the manufacturer. Plasma and urine PGE2 levels were determined using an enzymatic PGE immunoassay (Cayman Chemical), according to the protocol of the manufacturer. Blood samples were supplemented with indomethacin directly after drawing blood, to prevent *ex vivo* formation of prostaglandins that have the potential to interfere with the assay.

Cox2 3'UTR miR-132 reporter assay

A synthetic, double-stranded oligonucleotide spanning a 60 bp region of the murine 3' UTR of Cox2 mRNA containing the putative miR-132 binding site (Supplementary material) was cloned downstream of the firefly luciferase reporter gene in the pMIR-reportTM Expression Reporter Vector System (Applied Biosystems, Amsterdam, the Netherlands), thereby generating pMIR-132-report. The same construct lacking the miRNA sequence (pMIR132-reportNC) served as a negative control. Sequence analysis confirmed proper cloning and sequence of the inserts. A renilla luciferase expression plasmid (pRL-SV40, Promega, Leiden, the Netherlands) served as a transfection efficiency control. Antagomir-132 or control scramblemir (5 mg/mL) was added to a near confluent layer of IMCD cells. Twenty-four hours after antagomir treatment, IMCD cells were trypsinized, resuspended in 500 mL serum-free Optimem culture medium (Gibco), and 1.5 µg pMIR-132-report or pMIR-132-reportNC, together with 150 ng pRL-SV40 were added. The cell suspension was chilled for 10 min at 4°C and electroporated using the Gene Pulser II (Bio-Rad Laboratories, Veenendaal, the Netherlands). After 10 min recovery time at room temperature, 1.5×10^5 cells were plated in a 24-wells plate in triplicate. After 24 h, the firefly-luciferase and renilla-luciferase signals were measured using a Dual-Luciferase Assay Reporter System (Promega) in a Lumat LB9507 luminometer (EG&G Berthold, Bundoora, Australia).

Western Blot

Western blot analyses were performed on cellular lysates harvested in lysis buffer (50 mM Tris-HCl pH7.5, 150 mM NaCl, 1% SDS, 0.5% deoxycholate, 0.5%

Triton X-100) containing protease inhibitors (Complete protease inhibitor cocktail, Roche, Basel, Switzerland). Protein equivalents were separated using SDS-polyacrylamide gels (SDS-PAGE) under reducing conditions and transferred to a nitrocellulose membrane (Bio-Rad Laboratories, Veenendaal, The Netherlands). Primary antibodies were utilized to detect β -actin, AQP2 and Cox2 (Abcam, Cambridge, UK), AQP2-pS256 and AQP2-pS261 antibodies were kindly provided by Dr. Jason Hoffert, University of Aarhus, Aarhus, Denmark and Dr. Knepper respectively^{24,25}. Bound primary antibody was labeled with HRP-conjugated secondary antibody in blocking solution. Bound fragments were detected with chemiluminescent reagents (West Dura supersignal; ThermoFisher Scientific, Waltham, MA, USA) and exposed on Hyperfilm ECL (Amersham). Quantitative analysis of the protein bands was performed using ImageJ software and normalized to β -actin.

RNA isolation and qRT-PCR analysis

Total RNA was isolated from kidney and hypothalamus using Trizol reagent (Invitrogen). Validation of miR-132 expression was performed using Taqman® miR assays (Applied Biosystems, Foster City, CA, USA) according to manufacturer's instructions. RNU6B was utilized for normalization (sense U6: CTCGCTTCGGCAGCACA and antisense U6: AACGCTTCACGAATTTGCGT). To quantify mRNA levels, 250 ng total RNA was reverse transcribed using oligo(dT) primers and M-MLV First-Strand Synthesis system (Invitrogen) according to the manufacturers protocol. Quantitative PCR of target genes was done using SYBR Green Master Mix (Applied Biosystems). Used primer sequences of target genes were: AVP (sense): CTCTCCGCTTGTTCCTGAG; AVP (antisense): GCAGATGCTTGGTCCGAAG; NHE3 (sense): TACATGGCCGGGCTTTCGACC; NHE3 (antisense): GAGGACTTTGCTGAGGAACTTCCGG; NKCC2 (sense): GGCTTGATCTTTGCTTTTGC; NKCC2 (antisense): CCATCATTGAATCGCTCTCC; NCC (sense): CTTCGGCCACTGGCATTCTG; NCC (antisense): GATGGCAAGGTAGGAGATGG; ENaC (sense): ACCAGGCCCCCTGCAATCAG; ENaC (antisense): CGCAGTGTGAGGGACAAACCATTTG ; GAPDH (sense): ACTCCCCTCTTCCACCTTC; GAPDH (antisense): CACCACCCTGTTGCTGTAG. Levels of expression were normalized to GAPDH and quantified using the delta delta Ct method.



Immunohistochemistry

Paraffin-embedded kidneys were sectioned at 4 μm . After de-paraffinization, they were subjected to heat-induced antigen retrieval method using citrate buffer (10mM, pH 6.0) in a microwave for 20 min. Next, sections were incubated with a specific antibody against murine AQP2 (Abcam) or Cox2 (Abcam) followed by an appropriate secondary antibody labeled with Alexa-568 (Molecular Probes). Images were made using a confocal microscope (Carl Zeiss, Sliedrecht, the Netherlands).

In Situ Hybridization

In situ hybridization for miR-132 was performed by Bioneer (Denmark) as previously described²⁶.

Results

miR-132 directly targets Cox2

PGE₂, produced by Cox2, is known to counteract vasopressin-induced renal water reabsorption in collecting duct by inducing the internalization and lysosomal degradation of AQP2. To potentially identify miRNAs involved in this process, we used online available algorithms (www.microrna.org) and identified miR-132 as a potential post-transcriptional regulator of Cox2. To confirm functional inhibition of Cox2 mRNA by this microRNA, we cloned part of the 3'UTR of murine COX2 in a luciferase construct and introduced this construct in the mIMCD3 (IMCD) collecting duct cell line. Following transfection with antagomir-132 or the scramble mir control, we found increased luciferase expression in the presence of antagomir-132 as compared to control scramble mir, illustrating that miR-132 can directly bind and regulate Cox2 mRNA expression (Figure 1A). As miRNAs are mainly negative gene regulators, we next investigated whether silencing of miR-132 in collecting duct cells would lead to a de-repression of Cox2 expression. To that end, we used the mpkCCD collecting duct cell line that is known to induce AQP2 expression after dDAVP stimulation²². Indeed, both in the absence and presence of dDAVP silencing of miR-132 led to a modest but significant increase in Cox2 expression as compared to scramble mir controls (Figure 1BC).

Next to renal collecting duct cells, renal interstitial cells have also been reported to express Cox2 and may thus be under regulation of miR-132. To test this, we used 3T3 cells as an *in vitro* model for renal interstitial cells and cultured them in the presence of antagomir-132 or scramble mir. Indeed, also in these cells we found a significant 2-fold increase in Cox2 expression in cells treated with antagomir-132 as compared to the scramble mir (Figure 1DE).

Blocking miR-132 results in increased AQP2 expression in vitro

Since miR-132 targets Cox2 and Cox2-produced prostaglandins reduce dDAVP-induced AQP2 abundance, silencing miR-132 was anticipated to decrease AQP2 abundance. To test this, we cultured mpkCCD cells in the presence of dDAVP to induce AQP2 expression, and blocked miR-132 by adding antagomir-132. Surprisingly, subsequent western blot analysis showed increased levels of AQP2 with miR-132 silencing (Figure 1FG). This indicates that in this collecting duct cell line, miR-132 dependent AQP2 regulation does not involve direct Cox2 mediated signaling. How miR-132 mediates the increase in AQP2 expression in mpkCCD cells needs further investigation.



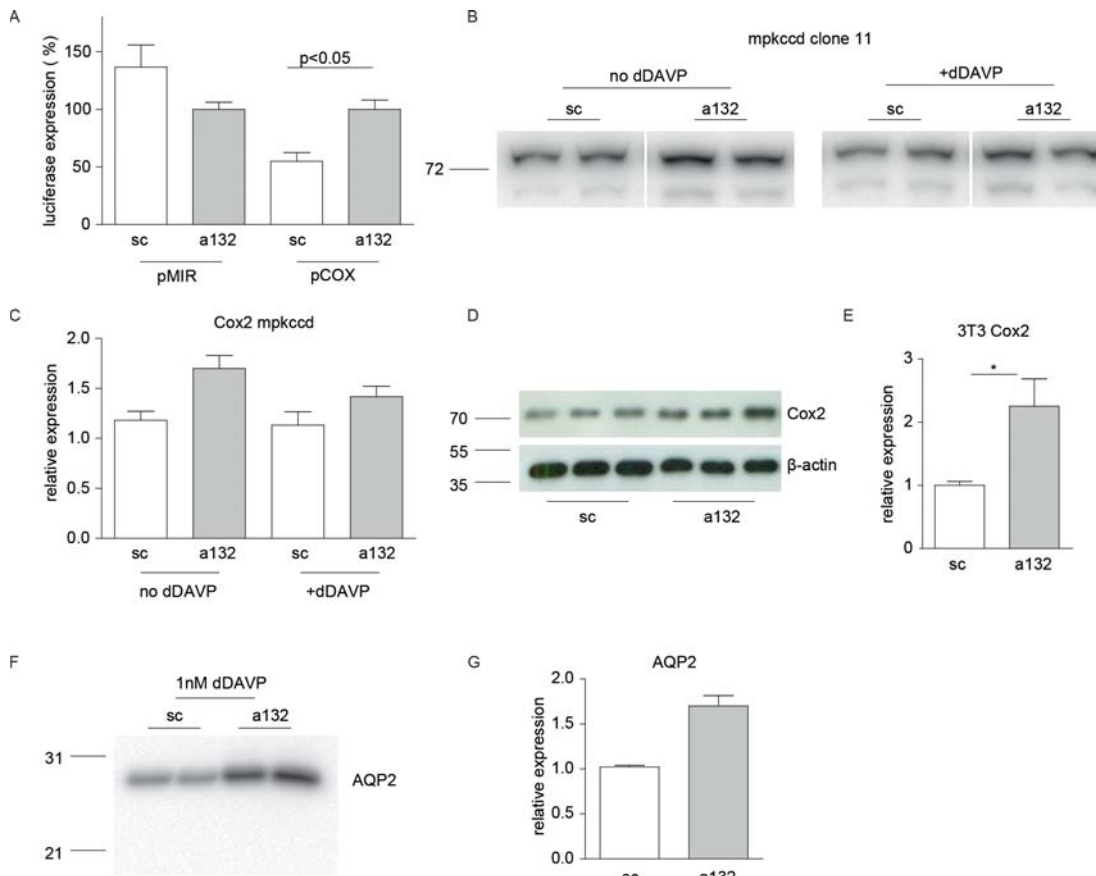


Figure 1. miR-132 targets Cox2 and affects AQP2 expression in vitro. A, luciferase assay confirms functional, 3'UTR-dependent repression of Cox2 expression by miR-132. B-C, representative western blot for Cox2 in mpkccd (B) and 3T3 (D) cells and corresponding quantification (C and E) shows increased Cox2 expression following miR-132 silencing. F and G, representative western blot (F) for AQP2 and quantification (G) in mpkccd cells after dDAVP stimulation illustrates miR-132 dependent regulation.

MiR-132 silencing in mice results in weight loss and diuresis

As, *in vivo*, the Cox2 expressing target cell for miR-132 could be different from the collecting duct cell or, because miR-132 action might be influenced by systemic factors, we next sought to determine the effect of silencing miR-132 on water homeostasis in mice. To keep track of physiological parameters, we housed the mice in metabolic cages to collect 24-hours urine following injection of antagomir-132 or control scramblemir. Mice were sacrificed either 1 day or 3 days after injection, blood was collected and kidneys and hypothalami were isolated. To validate *in vivo* miR-132 silencing we quantified miR-132 expression by qRT-PCR and observed an almost 1000 fold downregulation of miR-132 in total kidney tissue at both 1- and 3 days after administration (Figure 2A). To get insight in the regional expression of

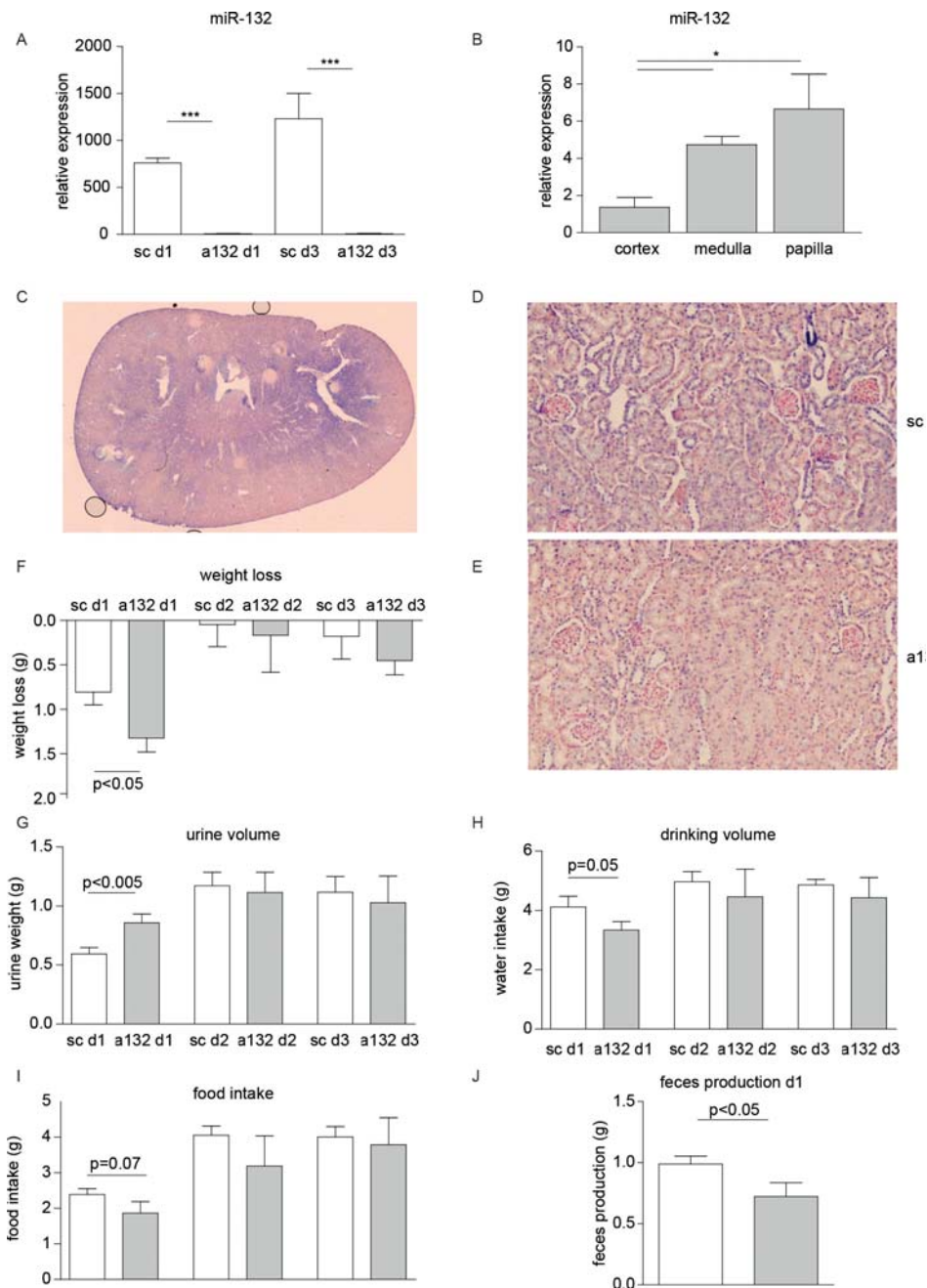


Figure 2. Silencing of miR-132 induces diuresis. A, antagomir-132 successfully knocked down miR-132 in vivo in the kidney determined by qRT-PCR. B, qRT-PCR for miR-132 in dissected kidneys shows higher miR-132 levels in medullary regions. C, representative whole mount image of in situ hybridization (ISH) for miR-132 confirms highest miR-132 expression in medulla. D, representative microscopic images of ISH illustrate predominant tubular epithelial localization of miR-132 and (E) knockdown by antagomir-132. F, miR-132 silencing results in weight loss 1 day after injection as compared to scramble mir control. G, antagomir-132 treatment results in diuresis 1 day after injection. H-J, antagomir-132 treatments results in a trend towards less water (H) and food (I) intake 1 day after injection, as well as reduced feces production (J).



miR-132 in the untreated kidney we dissected cortex, medulla and papilla and subsequent qRT-PCR analysis demonstrated that miR-132 expression displays a regional increase from cortex to papilla (Figure 2B). Although expression was found throughout the entire kidney, *in situ* hybridization (ISH) confirmed abundant medullary expression of miR-132 (Figure 2C) with highest levels in distal tubular epithelial cells (Figure 2D). Also some vascular smooth muscle cells clearly stained positive (Supplementary Figure 1). ISH of kidneys of antagomir-132 treated mice validated miR-132 silencing as miR-132 staining was markedly reduced (Figure 2DE).

Physiological parameters also revealed striking effects of miR-132 silencing. As early as 24 hours after injection, mice injected with antagomir-132 lost 0.5 gram more body weight than scramblemir-injected mice, which corresponds to 2-2.5% of their total body weight (Figure 2F).

Importantly, and in line with the significant weight loss, at 24-hours post-injection, urine and drinking volumes of mice treated with antagomir-132 were significantly higher and lower, respectively, as compared to the volumes of control mice (Figure 2GH). This suggests miR-132 silencing affects thirst sensation which, in combination with polyuria, resulted in even more dehydration explaining the observed weight loss. Antagomir-132 treated mice showed a trend towards decreased food intake, which corresponded to a reduced feces production (Figure 2IJ).

As we observed antagomir-132 induced polyuria (Figure 3A), we sought to determine if urine and plasma osmolality were changed. As shown in Figure 3B we found an increase in plasma osmolality associated with a decrease in urine osmolality. In concordance, we observed a decrease in specific gravity of these urines, assessed qualitatively using urine strips (data not shown). As sodium is considered to be the main determinant of plasma osmolality, we measured sodium levels in plasma but, surprisingly did not find an increase in sodium concentration (Figure 3C). Urinary sodium did show a trend towards increased levels (figure 3D), suggesting miR-132 silencing partly hampers active sodium reabsorption.

Silencing of miR-132 abrogates apical localization of AQP2 in collecting duct cells

Given the increased fractional excretion of water in the antagomir-132 treated mice, we next quantified AQP2 protein expression by western blot. However, we found no significant reduction in total AQP2 expression in mice that were injected with antagomir-132 compared to the scramblemir treated controls (Figure 4AB). In contrast, when we investigated the cellular localization of AQP2 using immunofluorescent staining we observed a striking difference

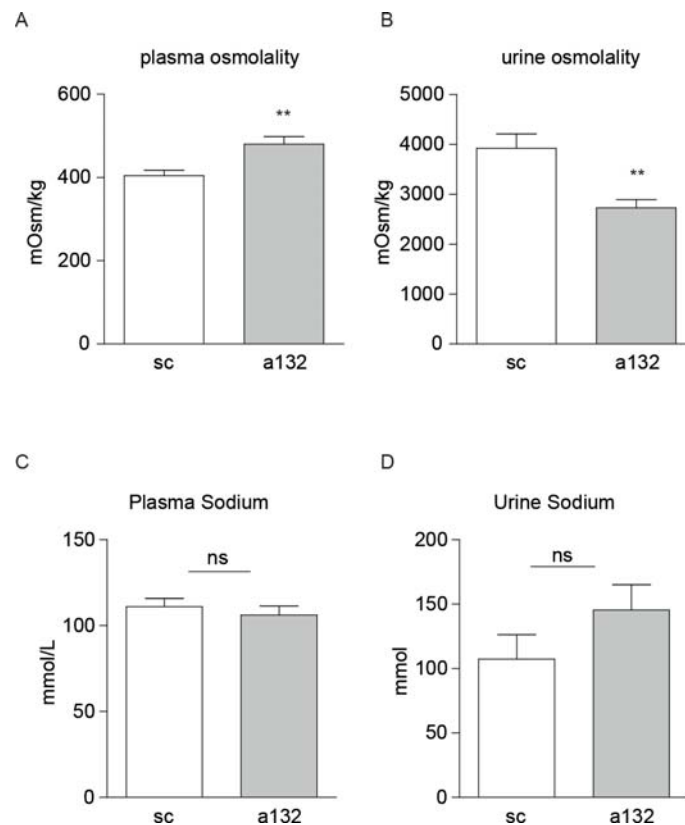


Figure 3. Blocking miR-132 results in a strong change in osmolality while not in sodium levels. A and B, plasma osmolality (A) increased after miR-132 silencing, while urine osmolality decreased (B). C and D, plasma (C) and urine (D) sodium levels were not significantly altered, although urinary sodium showed a trend towards increased levels.



between both treatment groups. In kidney sections from control mice, a clear apical staining is observed whereas in antagomir-132 treated mice however, AQP2 is mainly located intra-cellularly (Figure 4C). Subsequently, we sought to determine if S256 and S261 phosphorylation of AQP2 had been affected as this has been described to be involved in the localization of AQP2²⁷. As shown in Figure 4C-E, no differences were observed.

MiR-132 silencing suppresses sodium-hydrogen exchanger 3 (NHE3) gene expression

Unexpectedly, despite the increased osmolality we did not measure a difference in plasma sodium levels. However, urinary sodium showed a trend towards increased levels, suggesting antagomir-132 partly inhibits active sodium reabsorption. Therefore we investigated gene expression of four main sodium transporters along the tubular system, sodium-hydrogen exchanger 3 (NHE3), sodium-chloride symporter (NCC), Na-K-Cl cotransporter

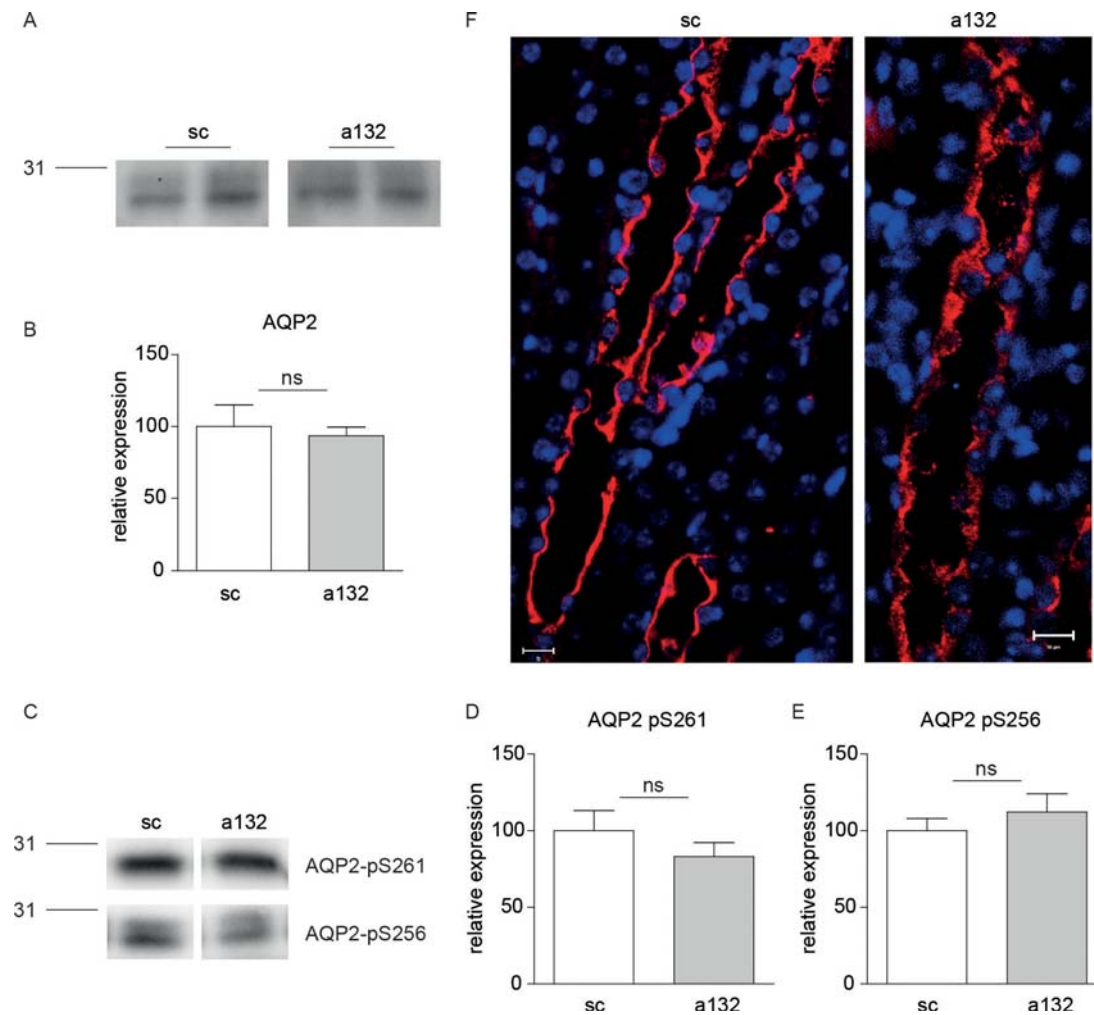


Figure 4. miR-132 silencing results in altered AQP2 localization. A and B, representative western blot for AQP2 (A) and quantification (B) shows no differences in expression. C-E, representative western blots for phosphorylated AQP2 variants AQP2-pS261 and AQP2-pS256 (C) and quantification (D and E) indicate no differences in phosphorylation. F, representative microscopic images of AQP2 staining reveals different localization of AQP2. Blocking miR-132 results in less apical AQP2 staining.

(NKCC2) and the amiloride-sensitive epithelial sodium channel (ENaC). Interestingly, a striking decrease in NHE3 was found (Supplementary Figure 2).

Silencing of miR-132 increases urinary PGE levels

Since we demonstrated that miR-132 could directly target Cox2, we hypothesized that silencing of miR-132 should result in a de-repression of Cox2 expression and increased production of PGE2. Therefore we determined renal prostaglandin production (which is also used as a measure

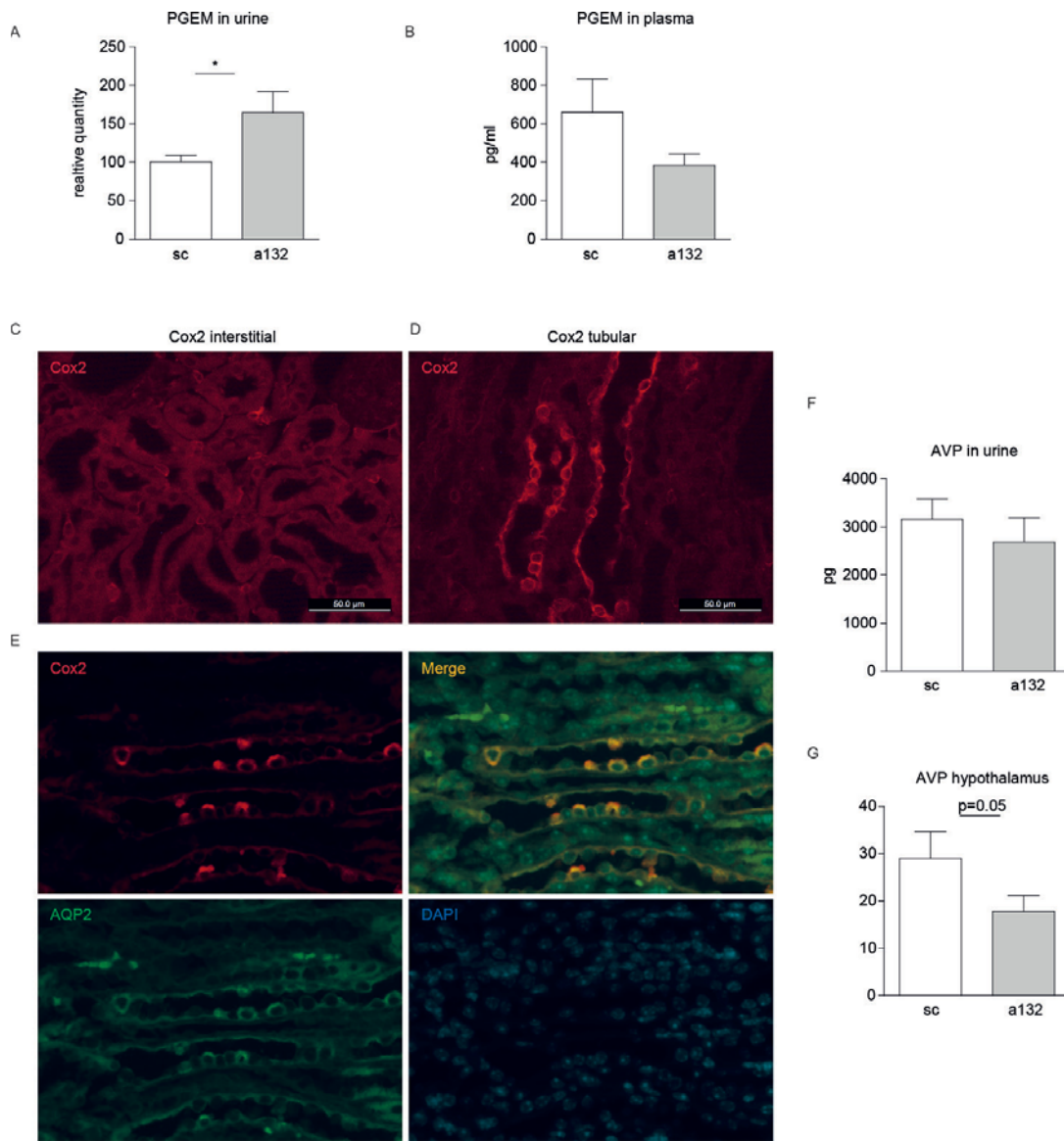


Figure 5. Increased renal PGE2 production while no increase in AVP. A, urinary PGE2 levels increased due to miR-132 silencing. B, Plasma PGE2 levels were not significantly altered but showed a trend towards reduced levels. C and D, representative microscopic images of renal Cox2 shows interstitial (C) and tubular epithelial (D) cell positive staining. E, representative microscopic images of double staining for Cox2 and AQP2 shows colocalization in collecting ducts. F, AVP levels in urine, reflecting plasma AVP, did not alter due to miR-132 silencing, despite increases plasma osmolality. G, pituitary AVP gene expression is decreased due to blocking miR-132.

for Cox2 activity) by measuring this in the urine, as urinary PGE2 excretion is mainly derived from medullary synthesis²⁸. Indeed, we found significantly increased PGE2 levels in urine of mice treated with antagomir-132 (Figure 5A). In contrast, circulating PGE2 levels had a tendency to be decreased

(Figure 5B). To determine where miR-132 could affect Cox2 we performed a staining to assess where Cox2 is expressed. Although some controversy exists about the location of constitutive Cox2 expression, we found it to be expressed in interstitial cells, cortical tubular structures (based on morphology predominantly distal, data not shown) and in specific medullary tubular epithelial structures (Figure 5C-D). The latter we identified to be collecting ducts as determined by co-staining with AQP2 (Figure 5E). This pattern highly corresponds to miR-132 localization, consistent with a functional link between the miR and Cox2.

MiR-132 blocking attenuates hypertonicity-induced increase in blood AVP levels

In normal physiology increased plasma osmolality stimulates drinking and secretion of AVP, resulting in increased renal water reabsorption, more concentrated urine, and less concentrated blood plasma. We assessed vasopressin levels in the urine, which reflects AVP levels in the blood²⁹, and surprisingly found no increase in AVP levels (Figure 5F). In fact, we see a trend towards decreased levels of vasopressin. Alternatively, or additionally, the observed effect of increased diuresis, may be due to reduced central vasopressin production and release, possible through PGE2 as well, as PGE2 has been implied in central AVP production and release¹⁴. To assess this hypothesis we excised the hypothalamus of the animals and determined AVP gene expression by qPCR. We found decreased levels of AVP gene expression in the hypothalamus in mice that received antagomir-132 (Figure 5G). These data suggest that silencing of miR-132 has a central effect on AVP production providing an additional explanation for the (trend towards) lower urinary AVP levels.

Discussion

In this study we identified a novel regulatory role for miR-132 in diuresis by affecting the translocation of AQP2 to the apical membrane in principal collecting duct cells. Silencing of miR-132 results in less AQP2 mediated water reabsorption and therefore in polyuria. This finding is accompanied by increased plasma osmolality and decreased urine osmolality. The effects we observed seem to be acute, as they are present within 24 hours after injection of antagomir-132, while 48 hours after injection, no further weight loss or polyuria is found. This suggests the body responds to this interference in homeostatic conditions by a feedback mechanism, which seems appropriate as regulation of water and electrolyte balance is tightly controlled. Antagomir-132 treated mice showed a trend towards decreased food intake that corresponded with reduced feces production which is therefore no contributor to weight loss. However, these observations suggest the mice display signs of malaise.

We identified Cox2 to be a novel direct target of miR-132 and show in collecting duct (mpkccd) cells as well as in interstitial (fibroblast) cells (NIH3T3) that blocking miR-132 results in increased Cox2 levels. *In vivo*, this is illustrated by increased renal PGE2 production as demonstrated by PGE2 levels in the urine. However, plasma PGE2 levels are decreased, suggesting that miR-132 can have ambiguous effects, depending on the site of action.

We found miR-132 expression predominantly in tubular structures, with highest levels in the renal medulla and more distant regions of the tubule. In addition, we observed most Cox2 expression in distant regions of the tubule, mainly in collecting ducts, although contradictory findings have been reported on this subject^{30,31}. As we demonstrated that Cox2 is a direct target of miR-132, this suggests its regulation could be mainly taking place here. This would mean that PGE2 is produced in the same cells as they target. However, also (cortical) interstitial cells are expressing Cox2, and as we have shown in 3T3 cells, silencing miR-132 in interstitial cells resulted in a firm increase in Cox2 expression. To elucidate the exact site of action of miR-132 and its target(s) involved in diuresis further investigations are necessary.

The increased renal PGE2 levels can explain the decrease in AQP2 translocation and subsequent increased diuresis as it is known to counteract AVP induced AQP2 translocation^{10,11}. In addition, AVP levels in the urine, reflecting AVP levels in the circulation²⁹ were slightly decreased, possibly due to decreased AVP production in the hypothalamus as we show that



hypothalamic AVP gene expression is decreased as a result of antagonizing miR-132. These decreased levels could again be explained by an alteration in PGE2 levels¹⁴ although the exact mechanism needs further investigation. In addition, to clarify the role of central AVP production on the observed phenomena in this study, one needs to investigate the effect of antagomir-132 while also providing synthetic dDAVP to the mice, which could rescue the phenotype if it was completely due to central AVP interference.

It has been well established that AVP also has long term effects in principal collecting duct cells by activating transcription of AQP2 via activation of and promoter binding by the cyclic AMP responsive element binding protein (CREB)^{6,7}. CREB itself is known to regulate transcription of miR-132³², providing a potential feedback loop in signaling. Furthermore, miR-132 can target p300³³, which is a transcriptional co-activator that can act in concert with CREB. In addition, promoter activity of Cox2 is dependent on CREB/p300 transcription factors^{34,35}. These factors are adding additional layers of possible autoregulation within water maintenance. Besides, this might explain the *in vitro* discrepancies we found with AQP2 expression. On the other hand, it has been shown that inhibition of Cox2 by indomethacin reduced renal AQP2 expression in rats, implying that prostaglandins may actually help maintain AQP2 levels¹³, which might also explain our *in vitro* observations.

We observed an increase in plasma osmolality suggesting the mice are hypovolemic. This would normally be accompanied by decreased blood pressure and subsequent activation of the RAAS pathway. Angiotensin II, that will be increased due to RAAS activation, is known to exert a dipsogenic effect³⁶. The dipsogenic action of angiotensin II is thought to be mediated by the subfornical organ (SFO), because the SFO contains a high concentration of the angiotensin AT1 receptor³⁷ and ablation of the SFO completely abolished the dipsogenic response to angiotensin II³⁸. However, we surprisingly found the polyuric mice to drink less. It could be expected therefore that angiotensin II signaling is disturbed. Indeed, a crosstalk between miR-132 and angiotensin II has been described³⁹. Furthermore it was shown that miR-132 can directly target Angiotensin II type 1 Receptor (AT1R)⁴⁰. These data suggest that also angiotensin II signaling is disturbed in these mice by silencing miR-132. Interestingly, NHE3 is also known to be regulated by angiotensin II⁴¹, so disturbed angiotensin II signaling could also reduce NHE3 expression, which is what we observed.

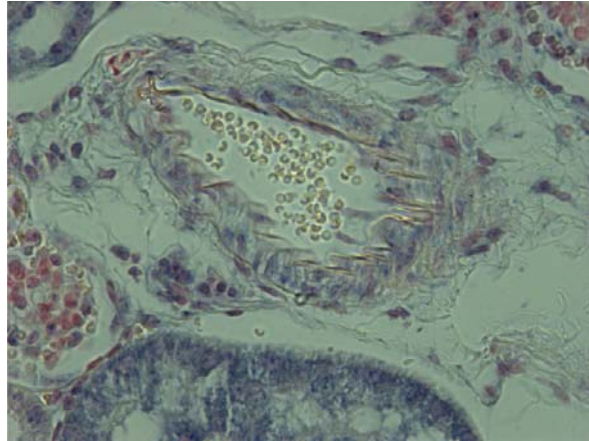
Some neurons in the above mentioned SFO are osmoreceptors, being sensitive to the osmotic pressure of the blood. These neurons project to

the supraoptic nucleus and paraventricular nucleus to regulate the activity of vasopressin-secreting neurons. AVP levels are known to be subject to circadian regulations. Also CREB mediated miR-132 expression is circadian-regulated, in the suprachiasmatic nucleus (SCN), where it is important for proper clock-resetting responses to light⁴². Furthermore, AVP plays an important role in nocturnal enuresis. It is therefore that DDAVP is used as a drug to treat nocturnal enuresis, although this phenomenon is not mediated by the V2R and does not involve AQP2^{43,44}. It would be plausible however for miR-132 to play a role in this regulation as it is involved in diuresis. Interestingly, a comprehensive miRNA sequencing study indicated miR-132 to be highly enriched in the pituitary¹⁵, suggesting antagomir-132 could strongly affect the above mentioned processes at this site.

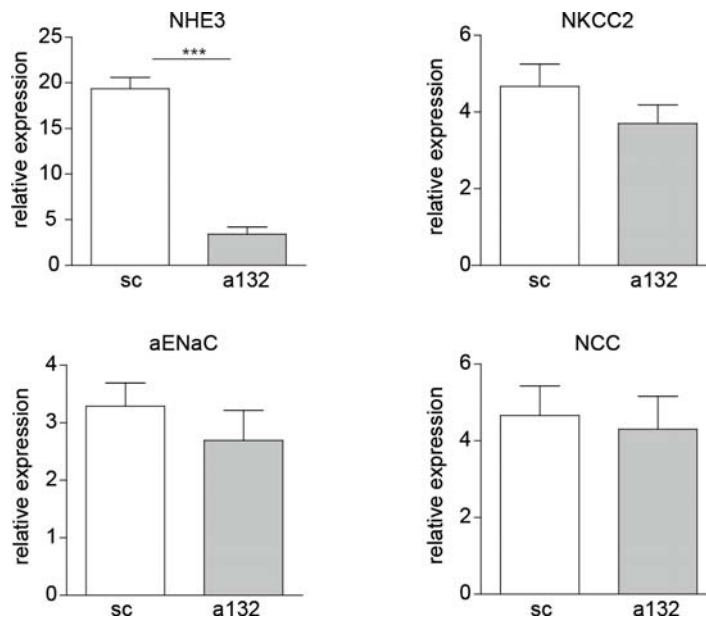
Taken together, it is evident that miR-132 plays a central role in physiology, specifically in water and volume balance regulation. It is therefore likely that miR-132 expression is crucial to associated disorders like hypertension, edema, Diabetes Insipidus and syndrome of inappropriate antidiuretic hormone hypersecretion (SIADH). This makes miR-132 a very attractive candidate for future therapeutics and further investigation in physiological processes.



Supplementary Files



Supplementary figure 1. In situ hybridization (ISH) shows miR-132 is present in vascular smooth muscle cells.



Supplementary figure 2. qRT-PCR of 4 main sodium transporters along the tubular system reveals a strong decrease in NHE3 expression due to miR-132 silencing.

References

1. Sinke, A.P. & Deen, P.M. The physiological implication of novel proteins in systemic osmoregulation. *FASEB journal : official publication of the Federation of American Societies for Experimental Biology* 25, 3279-3289 (2011).
2. Nielsen, S., et al. Vasopressin increases water permeability of kidney collecting duct by inducing translocation of aquaporin-CD water channels to plasma membrane. *Proceedings of the National Academy of Sciences of the United States of America* 92, 1013-1017 (1995).
3. Nielsen, S., DiGiovanni, S.R., Christensen, E.I., Knepper, M.A. & Harris, H.W. Cellular and subcellular immunolocalization of vasopressin-regulated water channel in rat kidney. *Proceedings of the National Academy of Sciences of the United States of America* 90, 11663-11667 (1993).
4. Fushimi, K., et al. Cloning and expression of apical membrane water channel of rat kidney collecting tubule. *Nature* 361, 549-552 (1993).
5. Nonoguchi, H., et al. Immunohistochemical localization of V2 vasopressin receptor along the nephron and functional role of luminal V2 receptor in terminal inner medullary collecting ducts. *The Journal of clinical investigation* 96, 1768-1778 (1995).
6. Matsumura, Y., Uchida, S., Rai, T., Sasaki, S. & Marumo, F. Transcriptional regulation of aquaporin-2 water channel gene by cAMP. *Journal of the American Society of Nephrology : JASN* 8, 861-867 (1997).
7. Yasui, M., Zelenin, S.M., Celsi, G. & Aperia, A. Adenylate cyclase-coupled vasopressin receptor activates AQP2 promoter via a dual effect on CRE and AP1 elements. *The American journal of physiology* 272, F443-450 (1997).
8. Robben, J.H., Knoers, N.V. & Deen, P.M. Cell biological aspects of the vasopressin type-2 receptor and aquaporin 2 water channel in nephrogenic diabetes insipidus. *American journal of physiology. Renal physiology* 291, F257-270 (2006).
9. Antunes-Rodrigues, J., de Castro, M., Elias, L.L., Valenca, M.M. & McCann, S.M. Neuroendocrine control of body fluid metabolism. *Physiological reviews* 84, 169-208 (2004).
10. Hebert, R.L., Jacobson, H.R. & Breyer, M.D. PGE2 inhibits AVP-induced water flow in cortical collecting ducts by protein kinase C activation. *The American journal of physiology* 259, F318-325 (1990).
11. Breyer, M.D. & Breyer, R.M. Prostaglandin E receptors and the kidney. *American journal of physiology. Renal physiology* 279, F12-23 (2000).
12. Anderson, R.J., Berl, T., McDonald, K.D. & Schrier, R.W. Evidence for an in vivo antagonism between vasopressin and prostaglandin in the mammalian kidney. *The Journal of clinical investigation* 56, 420-426 (1975).
13. Kim, S.W., et al. Indomethacin enhances shuttling of aquaporin-2 despite decreased abundance in rat kidney. *Journal of the American Society of Nephrology : JASN* 15, 2998-3005 (2004).
14. Kennedy, C.R., et al. Urine concentrating defect in prostaglandin EP1-deficient mice. *American journal of physiology. Renal physiology* 292, F868-875 (2007).
15. Landgraf, P., et al. A mammalian microRNA expression atlas based on small RNA library sequencing. *Cell* 129, 1401-1414 (2007).
16. Chandrasekaran, K., et al. Role of microRNAs in kidney homeostasis and disease. *Kidney international* 81, 617-627 (2012).
17. Xie, X., et al. Systematic discovery of regulatory motifs in human promoters and 3' UTRs by comparison of several mammals. *Nature* 434, 338-345 (2005).
18. Small, E.M. & Olson, E.N. Pervasive roles of microRNAs in cardiovascular biology. *Nature* 469, 336-342 (2011).



19. Pastorelli, L.M., et al. Genetic analyses reveal a requirement for Dicer1 in the mouse urogenital tract. *Mammalian genome : official journal of the International Mammalian Genome Society* 20, 140-151 (2009).
20. Elvira-Matelot, E., et al. Regulation of WNK1 expression by miR-192 and aldosterone. *Journal of the American Society of Nephrology : JASN* 21, 1724-1731 (2010).
21. Huang, W., et al. Tonicity-responsive microRNAs contribute to the maximal induction of osmoregulatory transcription factor OREBP in response to high-NaCl hypertonicity. *Nucleic acids research* 39, 475-485 (2011).
22. Boone, M., Kortenoeven, M., Robben, J.H. & Deen, P.M. Effect of the cGMP pathway on AQP2 expression and translocation: potential implications for nephrogenic diabetes insipidus. *Nephrol Dial Transplant* 25, 48-54 (2010).
23. Krutzfeldt, J., et al. Silencing of microRNAs in vivo with 'antagomirs'. *Nature* 438, 685-689 (2005).
24. Hoffert, J.D., et al. Dynamics of aquaporin-2 serine-261 phosphorylation in response to short-term vasopressin treatment in collecting duct. *American journal of physiology. Renal physiology* 292, F691-700 (2007).
25. Nishimoto, G., et al. Arginine vasopressin stimulates phosphorylation of aquaporin-2 in rat renal tissue. *The American journal of physiology* 276, F254-259 (1999).
26. Nielsen, B.S., et al. High levels of microRNA-21 in the stroma of colorectal cancers predict short disease-free survival in stage II colon cancer patients. *Clinical & experimental metastasis* 28, 27-38 (2011).
27. Tamma, G., Robben, J.H., Trimpert, C., Boone, M. & Deen, P.M. Regulation of AQP2 localization by S256 and S261 phosphorylation and ubiquitination. *Am J Physiol Cell Physiol* 300, C636-646 (2011).
28. Lote, C.J. & Haylor, J. Eicosanoids in renal function. *Prostaglandins, leukotrienes, and essential fatty acids* 36, 203-217 (1989).
29. Moses, A.M. & Steciak, E. Urinary and metabolic clearances of arginine vasopressin in normal subjects. *The American journal of physiology* 251, R365-370 (1986).
30. Breyer, M.D. & Harris, R.C. Cyclooxygenase 2 and the kidney. *Current opinion in nephrology and hypertension* 10, 89-98 (2001).
31. Yang, T., et al. Regulation of cyclooxygenase expression in the kidney by dietary salt intake. *The American journal of physiology* 274, F481-489 (1998).
32. Vo, N., et al. A cAMP-response element binding protein-induced microRNA regulates neuronal morphogenesis. *Proceedings of the National Academy of Sciences of the United States of America* 102, 16426-16431 (2005).
33. Lagos, D., et al. miR-132 regulates antiviral innate immunity through suppression of the p300 transcriptional co-activator. *Nature cell biology* 12, 513-519 (2010).
34. Deng, W.G., Zhu, Y. & Wu, K.K. Role of p300 and PCAF in regulating cyclooxygenase-2 promoter activation by inflammatory mediators. *Blood* 103, 2135-2142 (2004).
35. Ramsay, R.G., Ciznadija, D., Vanevski, M. & Mantamadiotis, T. Transcriptional regulation of cyclo-oxygenase expression: three pillars of control. *International journal of immunopathology and pharmacology* 16, 59-67 (2003).
36. Fitzsimons, J.T. Angiotensin, thirst, and sodium appetite. *Physiological reviews* 78, 583-686 (1998).
37. Allen, A.M., et al. Angiotensin receptors in the nervous system. *Brain research bulletin* 47, 17-28 (1998).
38. Simpson, J.B. & Routtenberg, A. Subfornical organ: a dipsogenic site of action of angiotensin II. *Science* 201, 379-381 (1978).

39. Jin, W., et al. Small RNA sequencing reveals microRNAs that modulate angiotensin II effects in vascular smooth muscle cells. *The Journal of biological chemistry* 287, 15672-15683 (2012).
40. Elton, T.S., et al. MiR-132 Regulates Angiotensin II Type 1 Receptor Expression Through a Protein Coding Region Binding Site. *Circulation* 118, S_513 (2008).
41. Houillier, P., et al. Signaling pathways in the biphasic effect of angiotensin II on apical Na/H antiport activity in proximal tubule. *Kidney international* 50, 1496-1505 (1996).
42. Cheng, H.Y., et al. microRNA modulation of circadian-clock period and entrainment. *Neuron* 54, 813-829 (2007).
43. Muller, D., Marr, N., Ankermann, T., Eggert, P. & Deen, P.M. Desmopressin for nocturnal enuresis in nephrogenic diabetes insipidus. *Lancet* 359, 495-497 (2002).
44. Robben, J.H., et al. Relief of nocturnal enuresis by desmopressin is kidney and vasopressin type 2 receptor independent. *Journal of the American Society of Nephrology : JASN* 18, 1534-1539 (2007).



Chapter

7

General discussion

General Discussion

Chronic kidney diseases occur when disorders such as diabetes, chronic inflammation or toxic substances eventually lead to kidney failure and fibrosis deteriorating the structure of the organ. Patients with failing kidneys require dialysis or kidney transplantation, procedures that are either not successful in the long term (dialysis), or not always available (transplantation). As microRNAs (miRNAs) have been shown to be important in virtually all biological processes, it is no longer the question *if* miRNAs are involved in renal injury and repair but, instead, the focus is now on *what* critical pathways they modulate. Moreover, the fact that miRNAs can coordinate multiple genes, that are often functionally related, makes them attractive targets for intervention. In this thesis, we have provided compelling evidence for a regulatory role of miRNA-155, -126 and -132 in the pathophysiology of the kidney.

In **Chapter 2** we describe that miR-155 plays a rate-limiting role in endothelial to mesenchymal transition (EndoMT). EndoMT was originally recognized as a process in the developing embryo. Endothelial cells (ECs), lining the endocardium can dedifferentiate to cellularize the endocardial cushions in the development of functional heart valves¹. This process is reminiscent to the formation of the tubular system in the kidney through mesenchymal to epithelial transitions during nephrogenesis^{2,3} as described in the introduction of this thesis. During EndoMT, ECs lose their expression of endothelial cell markers, delaminate from the surrounding monolayer, and migrate into the cardiac jelly⁴. TGF- β signaling has been described to drive this process^{5,6}. Next to the physiological role of EndoMT in embryogenesis, ECs that undergo EndoMT develop into myofibroblast-like cells and are thought to contribute to the development of renal fibrosis⁷⁻⁹. The analogue of EndoMT for epithelial cells, epithelial to mesenchymal transition (EMT), has even more often been described as a source of profibrotic myofibroblasts¹⁰. However, the exact origin of myofibroblasts has long been the subject of controversy. Genetic labeling studies in murine models of kidney fibrosis clearly demonstrated that no double-staining of labeled tubular epithelial cells with markers of activated fibroblast such as α -SMA and FSP-1 occurs, thus defying the existence of EMT¹¹. The evidence for endothelial-to-mesenchymal transformation is built on genetic labeling of endothelial cells using ambiguous markers like Tie-2⁷. Here clear double-staining of Tie-2 labeled cells and myofibroblast markers has been demonstrated. However Tie-2 is also expressed on myeloid cells and notably on pericytes. It is therefore very intriguing that studies

using sophisticated models of cell fate tracing demonstrated that pericytes and perivascular fibroblasts and not epithelial cells are the primary source of myofibroblasts in kidney fibrosis^{11,12}. This could mean that the processes of EMT and EndoMT do not contribute quantitatively to the development of tissue fibrosis. However, a change in phenotype of these cells could be profibrotic through other mechanisms. For instance, EndoMT results in the loss of capillaries. Along the same lines, loss of pericyte–endothelial cross-talk in response to renal injury causes microvascular rarefaction and interstitial fibrosis, emphasizing the role of both the pericyte and the endothelial cell in this process¹³. The detachment of pericytes from endothelium under pathological conditions and differentiation into myofibroblasts leads to pericyte deficiency at the microvascular interstitial interface, resulting in unstable microvasculature and hence rarefaction, ultimately leading to nephron ischemia and loss¹⁴.

As pericytes were demonstrated to constitute the primary source of myofibroblasts in kidney fibrosis, we investigated whether pericyte miRNAs play a rate-limiting role in myofibroblast formation. In **Chapter 5**, we used the same FoxD1-based murine lineage tracing model that was used to demonstrate the dominant role of pericytes in myofibroblast formation¹¹, and applied the ureter obstruction model to induce renal fibrosis. Following FACS sorting to isolate (differentiated) pericytes we showed a 21-fold upregulation of miR-132 in these FoxD1-derivative interstitial cells in obstructed kidneys versus contralateral kidneys. In total kidney extracts, we only found a 3-fold increase. This suggests that the increase in miR-132 is pericyte-myofibroblast specific. Silencing of miR-132 in this renal fibrosis model using antagomir-based inhibition resulted in attenuation of renal fibrosis as demonstrated by decreased collagen deposition and α -SMA expression. The number of α -SMA positive cells was decreased, suggesting less differentiation towards myofibroblasts by pericytes since it has been shown that virtually 100% of α -SMA positive interstitial cells are coming from FoxD1-positive progenitors¹¹. In addition, *in vitro* antagonism of miR-132 in 3T3 mouse fibroblasts strongly decreased proliferation as determined by a thymidine incorporation assay, supporting an anti-proliferative role of miR-132 in pericytes/myofibroblasts.

Antagomir-based inhibition of miRNA function was used throughout this thesis. **Chapters 2, 3, 5 and 6** describe studies that involve miRNA silencing through intravenous injections of antagomirs, chemically modified cholesterol conjugated antisense oligonucleotides, which bind to its complementary miRNA, thereby blocking its function¹⁵. Antagomir administration almost



completely abrogates miRNA expression as demonstrated for example in **Chapters 5**, where, as long as ten days after injection this inhibition was observed. The data described in this thesis illustrates the potential therapeutic use of antagomir-based approaches for silencing of miRNAs. Indeed, a similar chemistry for antagonizing miRNA function is now investigated in humans in a phase II clinical trial for treating Hepatitis C¹⁶. Results of this study so far demonstrated that the drug was safe and well tolerated and resulted in decreased viral titers¹⁷. However, only few miRNAs are as tissue specific as miR-122 is for the liver¹⁸, as most miRNAs are present in multiple cell types and tissues¹⁹ and mostly have several targets and can affect very different pathways^{20,21}. This makes the use of miRNA inhibitors challenging, as it could theoretically have multiple off-target effects. On the other hand, miRNAs could coordinately target multiple related genes within a certain pathway²², thereby making them potentially even more attractive candidates to therapeutically target.

That miRNAs can have pleiotropic effects is demonstrated in this thesis. First, in **Chapters 3 and 4**, we describe an increase in circulating hematopoietic progenitor cells that results from both systemic silencing of miR-126 (**Chapter 3**) as well as from overexpression in the hematopoietic compartment (**Chapter 4**). This indicates that a single miRNA can work in opposite ways depending on cell type and the micro-environmental context and suggests that miR-126 could serve as a biological switch, with the response magnitude of biological pathways being dependent on cell type, the context and source of the external stimulus, and underlines the importance of miR-126 in vascular homeostasis. A striking example of the pleiotropic actions of miRNAs is presented in **Chapter 5 and 7**. MiR-132 has been described to be present in pericytes and to be upregulated in these cells during renal fibrosis. When we silenced this miRNA using antagomir-132 we could suppress the formation of myofibroblasts and reduce the development of renal fibrosis. In **Chapter 6**, using the same antagomir-132, we observed a completely different role for this miRNA. Here, we describe miR-132 to play an essential role in Aquaporin-2 mediated water reabsorption in the collecting duct through a prostaglandin-E2 and vasopressin dependent mechanism. This illustrates the difficulties that can be encountered using miRNA based therapeutics, as antagomir-132 used to suppress fibrosis development, could concomitantly affect water reabsorption and thereby have harmful side-effects. In fact, in our fibrosis study described in **Chapter 5** we observed weight loss 24 hour after injection of the antagomir-132, while scramble-mir-treated mice did not lose weight. This is probably due to the polyuretic effects of miR-132

described in **Chapter 6**. Although hypothetical at this point, in both chapters, Cox2 can be a target of mir-132 that contributes to the observed findings. As described above, in **Chapter 6** miR-132 silencing increased Cox2 levels and elevated renal prostaglandin-E2 levels and potentially explain the observed polyuretic effects. In **Chapter 5**, augmented prostaglandin-E2 levels due to Cox2 increase in interstitial cells could reduce renal fibrosis by protecting these cells against apoptosis and oxidative stress²³.

In **Chapters 3 and 4** we focus on the role of miR-126 in vascular homeostasis. We previously collected data supporting a role for miR-126 in the angiogenic response induced by ischemia using a murine unilateral hind limb ischemia model²⁴. Using this model we were able to assess the hypoxia induced angiogenic response in the gastrocnemius calf muscle²⁵ and found that the mice treated with antagomir-126 showed a strongly reduced capillary density in this muscle as compared to the scramblemir-treated control mice. However, *in vitro* experiments to assess the effects of antagomir-126 silencing in human umbilical vein endothelial cells (HUVEC) revealed functional impairments. The effects of miR-126 on angiogenesis likely involve mechanisms operational in and on endothelial cells in the *in vivo* context, possibly through its interaction with pericytes, as results described in **Chapter 4** suggest that miR-126 also influences pericyte incorporation in the vasculature.

Other groups also showed that targeted deletion of miR-126 in mice and zebrafish impairs angiogenesis, likely through upregulation of Sprouty-related EVH1 domain-containing protein (Sprd-1) and phosphoinositol-3 kinase regulatory subunit 2 (PIK3R2) expression^{26,27}, which are actively involved in the negative regulation of vascular endothelial growth factor (VEGF) receptor and CXCR4 signaling²⁸ and are both predicted targets of miR-126²⁹. Consequently, low levels of miR-126 would be associated with elevated levels of Sprd-1 or PIK3R2 and repressed angiogenic signaling, which makes them likely targets to be associated with the decreased ischemia-induced angiogenesis as demonstrated in our studies. This mechanism could also apply to our findings in **Chapter 4**. Here we demonstrate that the angiogenic potential of miR-126 may reach beyond its presence in endothelial cells, as miR-126 was previously considered to be endothelial cell specific^{30,31}. Recently, miR-126 has also been identified in platelets, epithelial cells and hematopoietic cells³²⁻³⁴. We over-expressed miR-126, together with a dsRed gene, in bone marrow cells and subsequently performed bone marrow transplantation. Following the restoration of the hematopoietic system, we induced renal ischemia reperfusion injury, and in separate mice we inserted angiogenic matrigel plugs supplemented with SDF-1 and VEGF in the flank



of mice. We demonstrate a protective role for miR-126 in renal ischemia reperfusion injury and improvement in capillary density in the kidney. In combination with higher numbers of bone marrow derived endothelial cells, as determined by dsRed and CD31 co-staining, this suggests protection of renal function through increased vasculogenesis or preserved vascular integrity by endothelial progenitor cells (EPC). Interestingly, it is known that circulating EPC are markedly reduced in renal failure³⁵ and kidney graft function was shown to determine EPC number in renal transplant recipients³⁶. Of particular interest is that immunosuppressants, already at sub-clinical concentrations, appear to induce rapid cell death of EPC in early stages of their differentiation^{37,38}. Another important player in our study could be the vesicles derived from EPCs that have been shown to protect against renal IRI through transfer of miR-126³⁹. Therefore, overexpression of miR-126 in the hematopoietic compartment could potentially contribute to protection against renal IRI by transfer of miR-126 via microvesicles. Together these observations emphasize that augmenting microvascular endothelial repair through miR-126 modulation may well have therapeutic implications in renal disease.

To validate the role of hematopoietic miR-126 in vascular integrity, we performed a matrigel assay to determine whether miR-126 could contribute to neovascularization. We found an almost two fold increase in vascularization of the plugs. This confirms the angiogenic role of miR-126 we described previously²⁴. Furthermore, MECA32+dsRed+ cells were incorporated in the vasculature, again implying a role for EPCs. This data supports our findings from the IRI experiment that hematopoietic miR-126 functions, at least partly, by stimulating vascularization.

The observed increase in vascularization of the matrigel plug however, could also be due to increased recruitment of leukocyte subsets. For instance, extravasation of monocytes into a foreign body can result in differentiation into macrophages that then can support angiogenesis^{40,41}. Subsequently, macrophages can contribute to angiogenesis by producing angiogenic factors like VEGF and TGF- β ^{42,43} or facilitating anastomosis of the forming vessels⁴⁴.

In addition to bone marrow-derived EC, in the matrigel plug we observed double staining for dsRed and pericyte marker NG-2. This suggests that also pericytes could originate from bone marrow. Support for this notion is emerging in literature, where the role of bone marrow derived pericytes is increasingly discussed^{45,46}.

In our study described in **Chapter 4**, detailed flow cytometric analyses of the circulating hematopoietic cells in the mice that overexpressed miR-126 in the hematopoietic compartment, demonstrated selective mobilization of Lin-/Sca-1+/cKit+ (LSK) and Lin-/Sca-1+/Flk+ (LSF) cells in response to elevated SDF-1 expression by the ischemic kidney. SDF-1 expression is induced after renal IRI⁴⁷ and can augment the homing of bone marrow-mobilized progenitor cells to sites of injury⁴⁸⁻⁵⁰. A possible explanation for this selective mobilization could be that, in the BM, only the LSK cells displayed lower CXCR4 expression while the lineage-positive leukocytes expressed increased levels of CXCR4 and therefore would have a higher propensity to be retained in the BM⁵¹. Several studies have described a regulatory role for miR-126 in SDF-1/CXCR4 signaling. MiR-126 was shown to target SDF-1 directly^{52,53} but also indirectly via targeting regulator of G protein signaling 16 (RGS16), a negative regulator of CXCR4 function⁵⁴. Silencing of RGS16 is thought to stimulate an autoregulatory feedback loop that increases the production of SDF-1. Silencing of RGS16 by miR-126 could provide a mechanism for the elevated renal epithelial SDF-1 expression observed in mice that overexpressed miR-126.

In conclusion, the data described in this thesis illustrates the importance of miRNAs in (renal) biology. It also demonstrates the dynamic interplay between different miRNAs within the vascular system. Specifically, we describe roles for miR-155, miR-126 and miR-132 in vascular stability and differentiation of cells of the vascular system, i.e. endothelial cells and pericytes. MiR-126 is involved in neovascularization and maintaining vascular integrity, while miR-155 plays a role in differentiation of endothelial cells towards a mesenchymal-like cell, thereby potentially leaving the capillaries unstable. The same is true for miR-132, but then at the level of pericytes. The differentiation of these cells can result in detachment from the capillary thereby destabilizing it. In addition, it is reported that miR-132 in pericyte progenitor cells plays an important role in angiogenesis in the context of cardiac fibrosis⁵⁵. Also, tumor endothelial cells were described to contain high levels of miR-132 which is involved in pathological (tumor) angiogenesis⁵⁶. This emphasizes again the spectrum of activities of a single miRNA. These data show that all three miRNAs are involved in renal (patho)physiology and maintaining vascular integrity and further emphasizes the importance of the cellular context of miRNA function.



Future perspectives/Considerations

As has been shown in this thesis, miRNAs can have pleiotropic effects. To fully understand a single miRNA's diverse functions, one needs to comprehensively study a miRNA of interest in several models, different (micro)environments and a variety of cell and organ types. For example, profiling can be done on total kidney tissue from injury models but the interplay of so many different cell types including the inflammatory cells make it essential to employ models of lineage tracing to reveal the true role of the individual players as its roles may be contradictory in different cells types. On the other hand, to fully understand a biological process, one also needs to study the interplay of different miRNAs involved in the same process. Although the studies described in this thesis provide an important step towards better understanding, extensive follow up research is needed to fully comprehend renal miRNA biology.

Furthermore, we can learn from other organs. For example, in animal models of cardiac fibrosis loss of miR-29a function in fibroblasts was related to the excessive production of extracellular matrix proteins⁵⁷. Also, upregulation of miR-21 in fibroblasts of the failing heart appears to enhance fibroblast survival and cardiac fibrosis⁵⁸. In fact, also in renal fibrosis models, these miRNAs have been shown to be important modulators of fibrosis^{59,60}.

In addition, the mechanisms underlying the regulation of miRNA expression itself need more investigation. If we can identify how miRNA expression is controlled, this provides us with the opportunity to take over control and modulate this expression.

In conclusion, identifying the role of miRNA involvement in all aspects and layers of modulation within renal functioning is a vast task and challenge, but one that will lead to the generation of novel therapeutic approaches to maintain and improve renal function after injury.

References

1. Markwald, R.R., Fitzharris, T.P. & Manasek, F.J. Structural development of endocardial cushions. *Am J Anat* 148, 85-119 (1977).
2. Larsen, W. *Human embryology*, (1997).
3. Saxen, L. *Organogenesis of the kidney*. (1987).
4. Markwald, R., Eisenberg, C., Eisenberg, L., Trusk, T. & Sugi, Y. Epithelial-mesenchymal transformations in early avian heart development. *Acta anatomica* 156, 173-186 (1996).
5. Goumans, M.J., van Zonneveld, A.J. & ten Dijke, P. Transforming growth factor beta-induced endothelial-to-mesenchymal transition: a switch to cardiac fibrosis? *Trends in cardiovascular medicine* 18, 293-298 (2008).
6. Nakajima, Y., Yamagishi, T., Hokari, S. & Nakamura, H. Mechanisms involved in valvuloseptal endocardial cushion formation in early cardiogenesis: roles of transforming growth factor (TGF)-beta and bone morphogenetic protein (BMP). *Anat Rec* 258, 119-127 (2000).
7. Li, J., Qu, X. & Bertram, J.F. Endothelial-myofibroblast transition contributes to the early development of diabetic renal interstitial fibrosis in streptozotocin-induced diabetic mice. *The American journal of pathology* 175, 1380-1388 (2009).
8. Zeisberg, E.M., Potenta, S.E., Sugimoto, H., Zeisberg, M. & Kalluri, R. Fibroblasts in kidney fibrosis emerge via endothelial-to-mesenchymal transition. *J Am Soc Nephrol* 19, 2282-2287 (2008).
9. Li, J. & Bertram, J.F. Review: Endothelial-myofibroblast transition, a new player in diabetic renal fibrosis. *Nephrology* 15, 507-512 (2010).
10. Kalluri, R. & Neilson, E.G. Epithelial-mesenchymal transition and its implications for fibrosis. *The Journal of clinical investigation* 112, 1776-1784 (2003).
11. Humphreys, B.D., et al. Fate tracing reveals the pericyte and not epithelial origin of myofibroblasts in kidney fibrosis. *The American journal of pathology* 176, 85-97 (2010).
12. Lin, S.L., Kisseleva, T., Brenner, D.A. & Duffield, J.S. Pericytes and perivascular fibroblasts are the primary source of collagen-producing cells in obstructive fibrosis of the kidney. *The American journal of pathology* 173, 1617-1627 (2008).
13. Lin, S.L., et al. Targeting endothelium-pericyte cross talk by inhibiting VEGF receptor signaling attenuates kidney microvascular rarefaction and fibrosis. *The American journal of pathology* 178, 911-923 (2011).
14. Schimpf, C. & Duffield, J.S. Mechanisms of fibrosis: the role of the pericyte. *Current opinion in nephrology and hypertension* 20, 297-305 (2011).
15. Krutzfeldt, J., et al. Silencing of microRNAs in vivo with 'antagomirs'. *Nature* 438, 685-689 (2005).
16. Miravirsen, Santaris Pharma, clinicaltrials.gov. (2012).
17. Reesink, H.W., et al. Final Results: Randomized, Double-Blind, Placebo-Controlled Safety, Anti-Viral Proof-of-Concept Study of Miravirsen, an Oligonucleotide Targeting miR-122, in Treatment-Naive Patients with Genotype 1 Chronic HCV Infection. *International Liver Congress* (2012).
18. Jopling, C. Liver-specific microRNA-122: Biogenesis and function. *RNA biology* 9, 137-142 (2012).
19. Landgraf, P., et al. A mammalian microRNA expression atlas based on small RNA library sequencing. *Cell* 129, 1401-1414 (2007).
20. Baek, D., et al. The impact of microRNAs on protein output. *Nature* 455, 64-71 (2008).
21. Selbach, M., et al. Widespread changes in protein synthesis induced by microRNAs. *Nature* 455, 58-63 (2008).



22. Png, K.J., Halberg, N., Yoshida, M. & Tavazoie, S.F. A microRNA regulon that mediates endothelial recruitment and metastasis by cancer cells. *Nature* 481, 190-194 (2012).
23. He, W., et al. Sirt1 activation protects the mouse renal medulla from oxidative injury. *The Journal of clinical investigation* 120, 1056-1068 (2010).
24. van Solingen, C., et al. Antagomir-mediated silencing of endothelial cell specific microRNA-126 impairs ischemia-induced angiogenesis. *Journal of cellular and molecular medicine* 13, 1577-1585 (2009).
25. Madeddu, P., et al. Murine models of myocardial and limb ischemia: diagnostic end-points and relevance to clinical problems. *Vascular pharmacology* 45, 281-301 (2006).
26. Fish, J.E., et al. miR-126 regulates angiogenic signaling and vascular integrity. *Developmental cell* 15, 272-284 (2008).
27. Wang, S., et al. The endothelial-specific microRNA miR-126 governs vascular integrity and angiogenesis. *Developmental cell* 15, 261-271 (2008).
28. Jiang, B.H., Zheng, J.Z., Aoki, M. & Vogt, P.K. Phosphatidylinositol 3-kinase signaling mediates angiogenesis and expression of vascular endothelial growth factor in endothelial cells. *Proceedings of the National Academy of Sciences of the United States of America* 97, 1749-1753 (2000).
29. <http://www.targetscan.org>.
30. Berezikov, E., et al. Many novel mammalian microRNA candidates identified by extensive cloning and RAKE analysis. *Genome research* 16, 1289-1298 (2006).
31. Harris, T.A., Yamakuchi, M., Ferlito, M., Mendell, J.T. & Lowenstein, C.J. MicroRNA-126 regulates endothelial expression of vascular cell adhesion molecule 1. *Proceedings of the National Academy of Sciences of the United States of America* 105, 1516-1521 (2008).
32. Edelstein, L.C. & Bray, P.F. MicroRNAs in platelet production and activation. *Blood* 117, 5289-5296 (2011).
33. Mattes, J., Collison, A., Plank, M., Phipps, S. & Foster, P.S. Antagonism of microRNA-126 suppresses the effector function of TH2 cells and the development of allergic airways disease. *Proceedings of the National Academy of Sciences of the United States of America* 106, 18704-18709 (2009).
34. Shen, W.F., Hu, Y.L., Uttarwar, L., Passegue, E. & Largman, C. MicroRNA-126 regulates HOXA9 by binding to the homeobox. *Molecular and cellular biology* 28, 4609-4619 (2008).
35. de Groot, K., et al. Uremia causes endothelial progenitor cell deficiency. *Kidney Int* 66, 641-646 (2004).
36. de Groot, K., et al. Kidney graft function determines endothelial progenitor cell number in renal transplant recipients. *Transplantation* 79, 941-945 (2005).
37. Davies, W.R., et al. Cyclosporine decreases vascular progenitor cell numbers after cardiac transplantation and attenuates progenitor cell growth in vitro. *J Heart Lung Transplant* 24, 1868-1877 (2005).
38. Imanishi, T., Kobayashi, K., Kuki, S., Takahashi, C. & Akasaka, T. Sirolimus accelerates senescence of endothelial progenitor cells through telomerase inactivation. *Atherosclerosis* 189, 288-296 (2006).
39. Cantaluppi, V., et al. Microvesicles derived from endothelial progenitor cells protect the kidney from ischemia-reperfusion injury by microRNA-dependent reprogramming of resident renal cells. *Kidney Int* 82, 412-427 (2012).
40. Barleon, B., et al. Migration of human monocytes in response to vascular endothelial growth factor (VEGF) is mediated via the VEGF receptor flt-1. *Blood* 87, 3336-3343 (1996).
41. Murdoch, C., Giannoudis, A. & Lewis, C.E. Mechanisms regulating the recruitment of macrophages into hypoxic areas of tumors and other ischemic tissues. *Blood* 104, 2224-2234 (2004).

42. Grunewald, M., et al. VEGF-induced adult neovascularization: recruitment, retention, and role of accessory cells. *Cell* 124, 175-189 (2006).
43. Plaks, V., et al. Uterine DCs are crucial for decidua formation during embryo implantation in mice. *J Clin Invest* 118, 3954-3965 (2008).
44. Fantin, A., et al. Tissue macrophages act as cellular chaperones for vascular anastomosis downstream of VEGF-mediated endothelial tip cell induction. *Blood* 116, 829-840 (2010).
45. Tigges, U., Hyer, E.G., Scharf, J. & Stallcup, W.B. FGF2-dependent neovascularization of subcutaneous Matrigel plugs is initiated by bone marrow-derived pericytes and macrophages. *Development* 135, 523-532 (2008).
46. Dar, A., et al. Multipotent vasculogenic pericytes from human pluripotent stem cells promote recovery of murine ischemic limb. *Circulation* 125, 87-99 (2012).
47. Stokman, G., et al. SDF-1 provides morphological and functional protection against renal ischaemia/reperfusion injury. *Nephrology, dialysis, transplantation : official publication of the European Dialysis and Transplant Association - European Renal Association* 25, 3852-3859 (2010).
48. Hattori, K., Heissig, B. & Rafii, S. The regulation of hematopoietic stem cell and progenitor mobilization by chemokine SDF-1. *Leuk Lymphoma* 44, 575-582 (2003).
49. Ceradini, D.J., et al. Progenitor cell trafficking is regulated by hypoxic gradients through HIF-1 induction of SDF-1. *Nat Med* 10, 858-864 (2004).
50. Togel, F., Isaac, J., Hu, Z., Weiss, K. & Westenfelder, C. Renal SDF-1 signals mobilization and homing of CXCR4-positive cells to the kidney after ischemic injury. *Kidney Int* 67, 1772-1784 (2005).
51. Broxmeyer, H.E., et al. Rapid mobilization of murine and human hematopoietic stem and progenitor cells with AMD3100, a CXCR4 antagonist. *The Journal of experimental medicine* 201, 1307-1318 (2005).
52. van Solingen, C., et al. MicroRNA-126 modulates endothelial SDF-1 expression and mobilization of Sca-1(+)/Lin(-) progenitor cells in ischaemia. *Cardiovascular research* 92, 449-455 (2011).
53. Zhang, Y., et al. miR-126 and miR-126* repress recruitment of mesenchymal stem cells and inflammatory monocytes to inhibit breast cancer metastasis. *Nature cell biology* 15, 284-294 (2013).
54. Zerneck, A., et al. Delivery of microRNA-126 by apoptotic bodies induces CXCL12-dependent vascular protection. *Sci Signal* 2, ra81 (2009).
55. Katare, R., et al. Transplantation of human pericyte progenitor cells improves the repair of infarcted heart through activation of an angiogenic program involving micro-RNA-132. *Circ Res* 109, 894-906 (2011).
56. Anand, S., et al. MicroRNA-132-mediated loss of p120RasGAP activates the endothelium to facilitate pathological angiogenesis. *Nat Med* 16, 909-914 (2010).
57. van Rooij, E., et al. Dysregulation of microRNAs after myocardial infarction reveals a role of miR-29 in cardiac fibrosis. *Proceedings of the National Academy of Sciences of the United States of America* 105, 13027-13032 (2008).
58. Thum, T., et al. MicroRNA-21 contributes to myocardial disease by stimulating MAP kinase signalling in fibroblasts. *Nature* 456, 980-984 (2008).
59. Chau, B.N., et al. MicroRNA-21 promotes fibrosis of the kidney by silencing metabolic pathways. *Sci Transl Med* 4, 121ra118 (2012).
60. Wang, B., et al. Suppression of microRNA-29 expression by TGF-beta1 promotes collagen expression and renal fibrosis. *J Am Soc Nephrol* 23, 252-265 (2012).



Chapter

8

Summary

Summary

Kidney disease is a common disorder that affects up to 10% of the population and this number is rapidly rising. Chronic kidney diseases occur when disorders such as diabetes, hypertension, inflammation or toxic substances eventually lead to kidney failure. The patient then requires dialysis or kidney transplantation, procedures that are either not successful in the long term (dialysis), or not always available (transplantation). As MicroRNAs (miRNAs) seem to be important in virtually all biological processes it is no longer a question if miRNAs are involved in renal injury and repair but what critical pathways they modulate. Therefore, miRNAs could serve as attractive targets for intervention. In this thesis, studies are described in which roles of miRNA-155, -126 and -132 in the context of kidney functioning are investigated.

Chapter 1 provides a general background on the prevalence of kidney disease and describes the kidney and its function. In addition, evolution and nephrogenesis of the kidney is discussed, providing background for studies described in this thesis. Furthermore, the biogenesis, function and mode of action of miRNAs is described, followed by a short overview of the relevance of miRNAs for kidney functioning.

In **Chapter 2** we investigated the role of miRNAs, miR-155 in particular, in endothelial to mesenchymal transition (EndoMT), which has been proposed to be involved in the loss of microvascular capillaries in the pathophysiology of fibrosis and organ failure. In EndoMT, endothelial cells (EC) undergo a mesenchymal transition associated with the loss of cell-cell contacts and the acquisition of a synthetic, contractile phenotype. In a TGF- β dependent *in vitro* model for EndoMT, we identified miRNAs that were differentially expressed in normoxic and hypoxic conditions. These studies identified miR-155 to be significantly upregulated in EndoMT, an effect that was enhanced under hypoxia, which further augments EndoMT. Silencing of miR-155 directly increased RhoA expression and activity in endothelial cells and affected phosphorylation of downstream LIMK. In contrast, overexpression of miR-155 counteracted RhoA function. Using a selective Rho kinase inhibitor, we could partly suppress EndoMT, strengthening the notion that RhoA plays a central role in EndoMT. Forced overexpression of miR-155 completely suppressed EndoMT, as evidenced by the maintenance of EC characteristics and blocking the acquisition of a mesenchymal phenotype, as compared to control cells. Our data demonstrate that miRNA-155 functions as a negative

regulator of RhoA signaling in TGF- β -induced endothelial to mesenchymal transition.

We previously showed that miR-126 plays a role in angiogenesis. Based on the seed sequence, miR-126 can also be predicted to regulate vasculogenesis by modulating the endothelial expression of stromal cell-derived factor-1 (SDF-1). In **Chapter 3** this was investigated. Using miR-reporter constructs, we first validated that miR-126 inhibits SDF-1 expression in endothelial cells *in vitro*. Next, we investigated the potential relevance of this observation with respect to the mobilization of progenitor cells. For this, we studied the migration of human CD34⁺ progenitor cells towards chemotactic factors present in endothelial cell-conditioned medium. Antagomir-induced silencing of miR-126 elevated SDF-1 expression by human umbilical vein endothelial cells and enhanced migration of the CD34⁺ cells. In a murine model of hind limb ischemia, a striking increase in the number of circulating Sca-1⁺/Lin⁻ progenitor cells in antagomir-126-treated mice was observed as compared to scramble-mir-treated controls. Immunohistochemical staining of capillaries in the post-ischemic gastrocnemius muscle of miR-126-silenced mice revealed elevated SDF-1 expressing CD31-positive capillaries, whereas a mobilizing effect of miR-126 inhibition was not detected in healthy control animals. In conclusion, miR-126 can regulate the expression of SDF-1 in endothelial cells. In the context of an ischemic event, systemic silencing of miR-126 leads to the mobilization of Sca-1⁺/Lin⁻ progenitor cells into the peripheral circulation, potentially in response to elevated SDF-1 expression by endothelial cells present in the ischemic tissue.

Ischemia/reperfusion injury (IRI) is a central phenomenon in kidney transplantation. Managing the effects of renal IRI is crucial to short- and long-term graft survival following kidney transplantation. The peritubular capillary network may well be the rate limiting factor in the recovery of IRI. Following our findings that microRNA-126 plays a central role in maintaining vascular integrity, in **Chapter 4** we investigated if overexpression of microRNA-126 in bone marrow cells can aid in the recovery after IRI. Using a lentiviral construct we overexpressed miR-126 in bone marrow cells. Subsequently these cells were injected into lethally irradiated mice. Eight weeks after reconstitution of the bone marrow the mice underwent renal bilateral IRI. We found functional protection against IRI as a result of overexpression of miR-126 as demonstrated by decreased urea levels. In addition, damage markers Kim-1 and NGAL were decreased. This protection was associated with increased capillary density and increased influx of bone marrow derived



cells. We demonstrated that an elevated amount of endothelial cells was bone marrow derived that matched the observation of increased circulating hematopoietic stem and progenitor cells. We show that miR-126 attenuated CXCR4 expression on these cells, suggesting these cells would have a lower propensity to be retained in the BM. We confirmed the vascular role of hematopoietic miR-126 in a matrigel assay, where we show that overexpression of miR-126 results in increased neovascularization.

These findings suggest that over expression of miR-126 in the hematopoietic compartment protects against renal ischemia/reperfusion injury through stimulation of hematopoietic progenitor cell mobilization that leads to an improvement of the renal microvasculature.

In **Chapter 5** we investigated the role of miRNAs in fibrosis with a focus on the formation of myofibroblasts. Lineage analysis has shown that during nephrogenesis, FoxD1-positive mesenchymal cells give rise to adult interstitial pericytes. These FoxD1-derivative interstitial cells expand and differentiate into smooth muscle actin (α -SMA) positive myofibroblasts during renal fibrosis, accounting for a large majority of myofibroblasts, which are responsible for scar formation in fibrotic kidney disease. MicroRNAs (miRNAs) involved in this differentiation could serve as a target to decrease myofibroblast formation in fibrotic kidney disease. To identify differentially expressed microRNAs, renal fibrosis was induced in FoxD1-GC;Z/Red mice by unilateral ureteric obstruction (UVO) and miRNAs were profiled in FoxD1-derivative interstitial cells (dsRed positive) that were isolated using FACS sorting from fibrotic versus healthy kidneys. MiR-132 was amongst the most highly up regulated microRNAs in these cells in fibrotic kidneys. *In vitro* we demonstrated that silencing miR-132 results in reduction of myofibroblast marker α -SMA and increased levels of its established target Sirt1 and downstream Cox2.

In vivo silencing of miR-132 in the UVO induced fibrosis model resulted in a ~35% decrease in renal collagen deposition after 10 days as compared to scramble mir controls, while no difference was observed yet after 5 days. In addition, immunohistochemical analyses demonstrate that the number of interstitial α -SMA positive cells is similarly decreased, which is confirmed by both western blot and qRT-PCR analyses. However, no difference is observed in capillary density. Surprisingly, silencing miR-132 is associated with reduced levels of Sirt-1, indicating this is not the responsible mechanism.

However, we demonstrated that miR-132 silencing has anti-proliferative effects, suggesting miR-132 plays an important role in the proliferation of myofibroblasts.

In **Chapter 6** we describe a role for miR-132 in diuresis. The collecting duct principal cells of our kidneys are critical in this maintenance of blood water levels, as binding of vasopressin (anti-diuretic hormone) to its V2-receptor and the subsequent translocation of AQP2 water channels to the apical membrane fine-tunes the water balance. Cyclooxygenase-2 (Cox2) produces prostaglandins such as PGE2, which are known to counteract renal vasopressin action in principal cells by inducing the internalization and lysosomal degradation of Aquaporin-2. Using miR-reporter constructs we identified microRNA-132 to directly target Cox2. Silencing of miR-132 *in vitro* in collecting duct cells as well as in fibroblast cells resulted in upregulation of Cox2 expression. Silencing of miR-132 *in vivo* in mice resulted in increased renal PGE2 production, as determined by urinary PGE2 levels, in combination with an attenuated AVP response. Subsequently, translocation of AQP2 to the apical membrane in collecting duct cells was disturbed. This ultimately led to acute diuresis and severe weight loss. These data demonstrate an essential role for miR-132 in water homeostasis.

Finally, in **Chapter 7**, all studies described in this thesis are discussed and put in perspective with respect to present knowledge.



Chapter

9

Nederlandse samenvatting

Curriculum Vitae

Dankwoord

List of publications

Samenvatting

Nierziekten zijn een veel voorkomende aandoening welke tot 10% van de bevolking treft en dit aantal is snel groeiend. Chronisch nierfalen treedt op wanneer aandoening als diabetes, hoge bloeddruk, ontstekingen of toxische substanties op den duur tot nierschade leiden. De patient heeft dan niervervangende therapie nodig in de vorm van dialyse of niertransplantatie, procedures die niet succesvol zijn op lange termijn (dialyse) of niet altijd beschikbaar (transplantatie). Omdat microRNAs (miRNAs), die betrokken zijn in posttranscriptionele genregulatie, belangrijk lijken te zijn in praktisch alle biologische processen is het niet langer de vraag of miRNAs betrokken zijn bij nierschade en herstel, maar actueel is welke essentiële processen ze moduleren. Om deze reden zouden miRNAs interessante targets voor therapeutische interventie kunnen zijn. In dit proefschrift zijn studies beschreven die een rol voor miR-155, -126 and -132 beschrijven in de context van nierfunctie.

Hoofdstuk 1 geeft algemene achtergrondinformatie met betrekking tot de prevalentie van nierziekten en het functioneren van de nier in het algemeen. Ook wordt de evolutie en nefrogenese van de nier beschreven, welke als achtergrond dienen voor studies die beschreven zijn in dit proefschrift. Daarnaast wordt de biogenese van miRNAs samengevat gevolgd door een beschrijving van de werking van miRNAs en een korte overview van de relevantie van miRNAs in nierfunctie.

In **Hoofdstuk 2** hebben we de rol van miRNAs, met name miR-155, onderzocht in endotheel-mesenchymale transitie (EndoMT), waarvan wordt gedacht dat het betrokken kan zijn bij het verlies van microvasculaire capillairen in de pathofysiologie van fibrose en orgaanfalen. In EndoMT, endotheelcellen (EC) ondergaan een mesenchymale transitie geassocieerd met het verlies van cel-cel contacten en het verkrijgen van een 'synthetisch', contractiel fenotype. In een TGF- β afhankelijk *in vitro* model voor EndoMT hebben we miRNAs geïdentificeerd die differentieel tot expressie kwamen onder normoxische en hypoxische condities. Hierbij werd miR-155 geïdentificeerd als significant opgereguleerd in EndoMT, een effect dat toenam bij hypoxia, wat zelf bijdraagt aan EndoMT. Het blokkeren van miR-155 verhoogde RhoA expressie en activiteit in EC en had invloed op fosforylering van downstream LIMK. MiR-155 overexpressie leidde tot vermindering van RhoA functie. Gebruik makend van een Rho kinase inhibitor konden we EndoMT gedeeltelijk onderdrukken, wat benadrukt dat RhoA een centrale rol speelt

in EndoMT. Overexpressie van miR-155 leidde kon het volledige EndoMT proces blokkeren in vergelijking tot controle cellen, zoals blijkt uit het behoud van EC karakteristieken en de afwezigheid van een mesenchymaal fenotype. Deze data demonstreren dat miR-155 als een negatieve regulator functioneert van RhoA in TGF- β geïnduceerde endotheel-mesenchymale transitive.

Gebaseerd op de ‘seed sequence’ kan voorspeld worden dat miR-126 naast angiogenese (zoals we eerder aangetoond hebben) ook in arteriogenese een rol speelt door middel van regulatie van de expressie van stromal cell-derived factor-1 (SDF-1). In **Hoofdstuk 3** werd dit onderzocht. Door middel van miR-reporter constructen hebben we gevalideerd dat miR-126 in EC *in vitro* inderdaad SDF-1 expressie inhibeert. Vervolgens onderzochten we de potentiële relevantie hiervan voor de mobilizatie van progenitor cellen. Daarvoor bekeken we de migratie van humane CD34+ progenitor cellen naar chemotactische factoren in endotheel cel-geconditioneerd medium. Antagomir-geïnduceerd inhiberen van miR-126 verhoogde SDF-1 expressie in ‘human umbilical vein endothelial cells’ en stimuleerde migratie van de CD34+ cellen. In het eerder genoemde muismodel voor ischemie in de achterpoot konden we een sterke toename in circulerende Sca-1+/Lin- progenitor cellen waarnemen in antagomir-126 behandelde muizen in vergelijking tot scramble-mir behandelde controle muizen. Immunohistochemische kleuring van de capillairen in de post-ischemische kuitpomp toonden een verhoging aan van SDF-1 expresserende CD31-positieve capillairen als gevolg van miR-126 inhibitie, terwijl in gezonde controle muizen dit mobilizatie effect door middel van miR-126 inhibitie niet kon worden aangetoond. Kortom, miR-126 kan SDF-1 expressie reguleren in EC. In de context van een ischemisch event leidt systemische miR-126 inhibitie tot mobilizatie van Sca-1+/Lin- progenitor cellen naar de perifere circulatie, potentieel ten gevolge van verhoogde SDF-1 expressie door endotheel cellen die aanwezig zijn in ischemisch weefsel.

Ischemie/reperfusie schade (IRI) is een centraal fenomeen in niertransplantatie. Het managen van de effecten van nier IRI is cruciaal voor korte- en lange termijn overleving van de getransplanteerde nier na transplantatie. Het peritubulaire capillaire netwerk zou zeer goed de centrale factor kunnen zijn in het herstel na IRI. Naar aanleiding van onze eerdere bevindingen dat miR-126 een centrale rol speelt in vasculaire integriteit, hebben we in **Hoofdstuk 4** onderzocht of overexpressie van miR-126 in beenmerg cellen kan helpen bij het herstel na IRI. Met behulp van een lentiviraal construct hebben we miR-126 tot overexpressie gebracht in beenmerg cellen. Vervolgens werden deze



cellen geïnjecteerd in lethaal bestraalde muizen. Acht weken na reconstitutie van het beenmerg ondergingen de muizen bilaterale nier IRI. We vonden functionele bescherming tegen IRI door overexpressie van miR-126 zoals aangetoond met verlaagde ureum levels. Bovendien waren schademarkers Kim-1 en NGAL lager. Deze bescherming was geassocieerd met verhoogde capillaire dichtheid en een toegenomen influx van beenmerg afkomstige cellen. We demonstreerden dat een verhoogd aantal endotheel cellen afkomstig zijn uit het beenmerg, een observatie kloppend met de verhoging in circulerende hematopoietische stam- en progenitorcellen. We hebben aangetoond dat miR-126 CXCR4 expressie verlaagt op deze cellen, welke een stimulus is om in het beenmerg te blijven, waardoor deze cellen dus makkelijker migreren uit het beenmerg. We bevestigden de vasculaire rol van hematopoietische miR-126 in een matrigel assay, waarin overexpressie van miR-126 resulteerde in verhoogde neovascularizatie. Deze bevindingen suggereren dat overexpressie van miR-126 in het hematopoietische compartiment beschermt tegen nier ischemie/reperfusie schade door stimulatie van hematopoietische progenitor cel mobilizatie wat leidt tot een verbetering van de microvasculatuur in de nier.

In **Hoofdstuk 5** onderzochten we de rol van miRNAs in fibrose met een focus op de formatie van myofibroblasten. Lineage analyse heeft aangetoond dat, tijdens nefrogenese, FoxD1-positieve mesenchymale cellen uitgroeien tot volwassen interstitiele pericyten. Deze FoxD1-afkomstige interstitiele cellen delen tot en differentieren naar smooth muscle actin (α -SMA) positieve myofibroblasten tijdens nierfibrose en nemen daarmee een grote meerderheid van de myofibroblasten voor hun rekening, welke verantwoordelijk zijn voor littekenweefselvorming in fibrotische nierziekten. MiRNAs betrokken bij deze differentiatie zouden als target kunnen dienen om myofibroblast formatie tegen te gaan. Om differentieel tot expressie komende miRNAs te identificeren hebben we nierfibrose geïnduceerd in FoxD1-GC;Z/Red muizen door middel van unilaterale ureter obstructie (UUO), waarna miRNAs geprofiled zijn in FoxD1-afkomstige interstitiele cellen (dsRed positief) die geïsoleerd waren met FACS sorting uit zowel fibrotische als gezonde nieren. MiR-132 was één van de meest opgereguleerde miRNAs in deze cellen in fibrotische nieren. *In vitro* hebben we aangetoond dat miR-132 inhibitie resulteert in reductie van myofibroblast marker α -SMA en verhoging van bekend target Sirt1 en downstream cyclooxygenase-2 (Cox2). *In vivo* miR-132 inhibitie in het UUO nierfibrose model leidde na 10 dagen tot een ~35% verlaging van collageen depositie in vergelijking tot scramble mir controles, terwijl er nog geen verschil waargenomen werd na 5 dagen. Daarnaast demonstreren

immunohistochemische analyses dat het aantal α -SMA positieve cellen vergelijkbaar afneemt, wat bevestigd wordt door zowel western blot als qRT-PCR analyses. Echter, geen verschil in capillaire dichtheid werd waargenomen en verrassenderwijs was miR-132 inhibitie geassocieerd met verlaagde Sirt1 levels. We hebben echter wel aangetoond dat het remmen van miR-132 anti-proliferatieve effecten heeft wat suggereert dat miR-132 een belangrijke rol speelt in de proliferatie van myofibroblasten.

In **Hoofdstuk 6** beschrijven we een rol voor miR-132 in water reabsorptie. De collecting duct cellen van onze nieren zijn kritiek in deze reabsorptie en homeostase van waterlevels in het bloed, daar het binden van vasopressine (anti-diuretisch hormoon) aan de V2-receptor en de daaropvolgende translocatie van Aquaporin-2 (AQP2) waterkanaaltjes naar het apicale membraan de waterbalans fine-tunen. Cox2 produceert prostaglandines zoals PGE2, waarvan bekend is dat deze de vasopressine functie in collecting duct cellen tegenwerkt door het induceren van internalizatie en lysosomale degradatie van AQP2. Gebruik makend van miR-reporter constructen hebben we Cox2 geïdentificeerd als directe target van miR-132. Remmen *in vitro* van miR-132 in zowel collecting duct cellen als fibroblasten resulteerde in opregulatie van Cox2. MiR-132 inhibitie *in vivo* in muizen leidde tot een verhoging in PGE2 productie door de nier, zoals aangetoond door verhoogde PGE2 levels in de urine, in combinatie met een onderdrukte AVP respons. Daaruitvolgend was translocatie van AQP2 naar het apicale membraan in collecting duct cellen verstoord. Dit resulteerde uiteindelijk in acute diurese en gewichtsverlies. Deze data demonstreert een essentiële rol voor miR-132 in de waterhuishouding.

Tenslotte geeft **Hoofdstuk 7** een beschouwing van alle studies beschreven in dit proefschrift en plaatst deze in een breder perspectief met betrekking tot de huidige kennis.



Curriculum Vitae

De schrijver van het proefschrift, Roel Bijkerk, werd geboren op 18 maart 1983 te Maassluis. In 2001 behaalde hij het VWO diploma aan het C.S.G. Aquamarijn te Vlaardingen. In datzelfde jaar begon hij met de studie Life Science & Technology aan de Universiteit Leiden en de Technische Universiteit Delft. Tijdens deze studie verrichte hij een Bachelor onderzoeksstage op de afdeling Nierziekten van het LUMC te Leiden onder supervisie van Dr. B. Oortwijn. Tijdens deze stage deed hij onderzoek naar het effect van IgA depositie op mesangiumcellen in het kader van IgA nefropathie. De Master onderzoeksstage tijdens deze opleiding verrichtte hij op de R&D sectie van de biologie afdeling van het Nederlands Forensisch Instituut onder supervisie van Dr. W.J.F. de Leeuw. Het onderwerp van deze stage betrof de ontwikkeling van nieuwe detectie methoden voor minimale biologische sporen in forensische context. De studie Life Science & Technology werd afgesloten in 2006 met de Master “Cell Diagnostics”. Aansluitend werkte hij korte tijd bij het Nederlands Forensisch Instituut als Research Assistant waar hij zich bezig hield met het opzetten en implementeren van een verbeterde DNA-analyse techniek voor genotypering in forensische context. Na vervolgens enkele maanden rond de wereld te hebben gereisd, begon hij in 2007 aan een nierstichting-gefinancierd promotieonderzoek getiteld “Exploring the role of microRNAs in renal endothelial regeneration” op de afdeling Nierziekten van het LUMC onder supervisie van Prof. Dr. A.J. van Zonneveld en Prof. Dr. T.J. Rabelink. In het kader van dit promotieonderzoek heeft hij een jaar binnen de Renal Division van het Brigham and Women’s Hospital, Harvard Medical School in Boston, Massachusetts, USA gewerkt in de onderzoeksgroep van Dr. B.D. Humphreys. De resultaten van het promotieonderzoek zijn beschreven in dit proefschrift. Vanaf 2012 verricht hij postdoctoraal onderzoek op een beurs van de Netherlands Institute for Regenerative Medicine (NIRM) met als onderwerp “Exploring endothelial to mesenchymal transition in innovative mouse models for renal fibrosis” in de onderzoeksgroep van Prof. Dr. A.J. van Zonneveld.



Dankwoord

In de zomer van 2007 tijdens een concert van Guus Meeuwis kreeg ik het goede nieuws te horen dat ik mocht beginnen aan het promotieonderzoek beschreven in dit proefschrift. Nu dit tot een goed einde is gebracht zou ik graag een aantal mensen willen bedanken.

Anton Jan en Ton, mijn promotores, allereerst wil ik natuurlijk jullie bedanken. Anton Jan, jouw enthousiasme voor het onderzoek is uniek en aanstekelijk. Ik heb veel kunnen leren van jouw enorme schat aan kennis en had me geen fijnere begeleider kunnen voorstellen. Ton, ik wil jou met name bedanken voor de mogelijkheid om een jaar naar Boston te gaan om daar het onderzoek naar een hoger niveau te tillen en mij als wetenschapper verder te ontwikkelen.

Ben, I would like to thank you for your hospitality (both in and outside the lab) and for providing me with the opportunity to do research in your lab for a year. It was a great experience, you taught me a lot and I think this research will result in high impact publications. Also the members of the lab in Boston: Steve, Derek, Ivica, Rado, Matt, Jie, Fengfeng, Nilka, Claudia and all the others, thanks for your help and friendship.

PCR, Pieter, Coen, Roel. De 3 musketiers van de afdeling nierziekten. Coen en Pieter, paranimfen, we hebben gezamenlijk gestreden voor die doctors titel sinds we tegelijkertijd begonnen aan de opleiding Life Science & Technology. Coen, m'n labmaatje. Jij stelde me voor aan Anton Jan en was daardoor mede verantwoordelijk voor mijn avontuur op de afdeling nierziekten. We hebben veel onderzoek samen gedaan en we zijn een perfect en efficiënt team. En naast veel gezelligheid, ook altijd goede discussies. Bedankt voor een mooie tijd. Pieter, samen veel in de trein, interessante congressen, nooit een saaie dag. En ook wij gingen uiteindelijk nauw samenwerken, en je ziet wat voor mooie paper er uitkomt! Bedankt voor een mooie tijd.

Mijn dank gaat ook uit naar alle collega's van het 'vasculaire nefrologie lab', bedankt voor alle hulp door de jaren heen. Specifiek wil ik nog Ruben bedanken, naast dat je een gezellige gozer bent en heel plezierig in de omgang, stond je altijd klaar om mij uit de brand te helpen. En Eric, zoals jou is er geen ander. We konden eindeloos discussieren over bijvoorbeeld het goed of kwaad van perfectionisme. Bedankt voor jouw betrokkenheid. Hetty, de nuchtere, kritische persoon van onze groep. Bedankt voor al je hulp en het

laten zien hoe je goed wetenschap moet bedrijven. Martijn, altijd gezellig en behulpzaam, bedankt. Janine, een tijdje mijn roommate toen je ons lab kwam versterken, bedankt. Jac, jij hebt veel werk verzet voor alle microRNA projecten en verder was je onnavolgbaar, bedankt. Marko, Annemarie, Marina, Matthieu, Carolien, Chun Yu, Margien (Peggy), Bernard, bedankt.

Verder wil ik natuurlijk ook iedereen van het gehele nierziekten lab (Rianne, Sandra, Nicole, Ellen, Danielle, Cees, en alle anderen) bedanken voor de hulp en ook voor het creëren van een sfeer waardoor het elke dag een plezier is om op het lab te zijn. Hetzelfde geldt natuurlijk voor alle collega's van het Eindhoven lab.

Daarnaast was het erg plezierig samenwerken met de afdelingen Moleculaire Celbiologie (Peter ten Dijke, Marie Jose Goumans), Immunohematologie en Bloedtransfusie (Frank Staal), en Cardiologie (Twan de Vries) van het LUMC, en met de afdeling Fysiologie (Peter Deen, Christiane Trimpert) van het Radboud Universitair Medisch Centrum in Nijmegen.

Pa en Ma, ook jullie wil ik bedanken voor de steun in al mijn keuzes en mij altijd het gevoel te geven trots te zijn! Tenslotte wil ik mijn lieve eega bedanken; Corinne, poekie, bedankt voor al je steun, bedankt voor jouw opoffering om samen het Boston avontuur aan te gaan. En samen met onze lieve Tara gaan we een mooie tijd tegemoet.



List of publications

Bijkerk R, de Bruin RG, van Solingen C, Duijs JMGJ, Roeten MK, van der Veer EP, ten Dijke P, de Boer HC, Rabelink TJ, Goumans MJ, van Zonneveld AJ. miR-155 functions as a suppressor of endothelial to mesenchymal transition through RhoA regulation. *MicroRNA*, 2012.

Bijkerk R, van Solingen C, de Boer HC, van der Pol P, Khairoun M, de Bruin RG, van Oeveren-Rietdijk AM, Lievers E, Schlagwein N, van Gijlswijk DJ, Roeten MK, Neshati Z, de Vries AAF, Rodijk M, Pike-Overzet K, van den Berg YW, Versteeg HH, Reinders MEJ, Staal FJT, van Kooten C, Rabelink TJ, van Zonneveld AJ. Hematopoietic microRNA-126 protects against renal ischemia/reperfusion injury by promoting vascular integrity. *J Am Soc Nephrol*. 2013, in press.

van der Veer E, de Bruin RG, Kraaijeveld A, de Vries MR, Bot I, Pera T, Segers FM, van Gils JM, Trompet S, Roeten M, Beckers C, van Santbrink PJ, Janssen A, van Solingen C, Swildens J, de Boer HC, Peters EH, **Bijkerk R**, Rousch M, Doop M, Schalijs M, van der Wal AC, Richard S, Van Berkel TJ, Pickering JG, Hiemstra PS, Goumans MJ, Rabelink TJ, de Vries AA, Quax PH, Jukema JW, Biessen EA, van Zonneveld AJ. The RNA-binding protein Quaking is a critical regulator of vascular smooth muscle cell phenotype. *Circ Res*. 2013.

van Solingen C, **Bijkerk R**, de Boer HC, Rabelink TJ, van Zonneveld AJ. The role of microRNA-126 in vascular homeostasis. *Curr Vasc Pharmacol*. 2013

van Solingen C, de Boer HC, **Bijkerk R**, Monge M, van Oeveren-Rietdijk AM, Seghers L, de Vries MR, van der Veer EP, Quax PH, Rabelink TJ, van Zonneveld AJ. MicroRNA-126 modulates endothelial SDF-1 expression and mobilization of Sca-1⁺/Lin⁻ progenitor cells in ischemia. *Cardiovasc Res*. 2011.

van Solingen C, Seghers L, **Bijkerk R**, Duijs JMGJ, Roeten MK, van Oeveren-Rietdijk AM, Baelde HJ, Monge M, Vos JB, de Boer HC, Quax PHA, Rabelink TJ, van Zonneveld AJ. Antagomir-Mediated Silencing of Endothelial Cell Specific MicroRNA-126 Impairs Ischemia-Induced Angiogenesis. *J Cell Mol Med*. 2008.

Bijkerk R, Khairoun M, Duijs JMGJ, ter Horst CJH, de Vries APJ, de Koning EJP, de Fijter JW, Rabelink TJ, van Zonneveld AJ, Reinders MEJ. Circulating MicroRNAs Correlate with Diabetic Nephropathy and Systemic Microvascular Damage and Normalize after Simultaneous Pancreas-Kidney Transplantation. Submitted.

Bijkerk R, van Solingen C, Duijs JMGJ, Rabelink TJ, Humphreys BD, van Zonneveld AJ. Silencing of Pericyte MicroRNA-132 Reduces Renal Fibrosis and Myofibroblast Proliferation and is Associated with altered Sirt1 and Cox2 expression. In preparation.

Bijkerk R, Trimpert C, van Solingen C, Rabelink TJ, Humphreys BD, Deen PMT, van Zonneveld AJ. MicroRNA-132 regulates diuresis through vasopressin- and prostaglandin-dependent alteration of Aquaporin-2 localization. In preparation.



